UNIVERSITÉ DE SHERBROOKE

Faculté de génie

Département de génie mécanique

AMÉLIORATION ÉNERGÉTIQUE DU PROCÉDÉ DE CAPTAGE DE CO_2 EN POSTCOMBUSTION AU MOYEN DES ÉJECTEURS

ENERGY IMPROVEMENTS IN THE POST-COMBUSTION CO_2 CAPTURE PROCESS BY MEANS OF EJECTORS

Thèse de doctorat
Spécialité : génie mécanique

Doctoral Thesis
Specialty: Mechanical Engineering

J. Christopher Reddick

Jury:
Mikhail SORIN (supervisor/directeur)
Zine AIDOUN (co-supervisor/co-directeur)
Hachimi FELLOUAH
Nicolas GALANIS
Roberto SUNYE

Sherbrooke (Québec) Canada February 2017

To my mother and father,

Barbara and Jim Reddick.

To my wife Helene,

To our children:

Kathleen, Michael, Joanne and Barbara

RÉSUMÉ

Le but principal de ce projet doctoral est de déterminer le potentiel d'amélioration de l'efficacité énergétique du système de captage de carbone dans les stations thermiques de production d'électricité, par l'intégration optimale des éjecteurs monophasiques. Il s'agit du système de captage postcombustion du dioxyde de carbone (CO_2) par absorption/désorption utilisant la monoéthanolamine (MEA). Les éjecteurs intégrés utilisent des rejets thermiques de 100 °C qu'on retrouve dans les stations thermiques de production d'électricité. La revalorisation de ces rejets permet la substitution partielle de vapeur de turbine à coût élevé, qui serait autrement prise de la centrale thermique. Le deuxième objectif de la thèse est d'évaluer expérimentalement la performance d'un éjecteur à vapeur où le fluide secondaire de l'éjecteur est un mélange de vapeur d'eau et d'un gaz non-condensable, dans le cas présent, le CO_2.

Deux tuyères d'éjecteur à vapeur, d'un diamètre de 4.60 mm et 4.23 mm, ont été évaluées sur une plage de niveaux de CO_2 dans le fluide secondaire, jusqu'à environ 40% en masse. La pression primaire était maintenue à 450 kPa avec une surchauffe à 10 °C et la pression secondaire était de 70 kPa. On a constaté que la pression critique ne changeait pas à mesure que la fraction massique de CO_2 dans le fluide secondaire augmentait. Cependant, le rapport d'entraînement a augmenté de façon linéaire sur la plage expérimentale. Une amélioration de 23% du rapport d'entraînement par rapport à la vapeur pure a été observée lorsque le fluide secondaire contient 42% de CO_2 par masse. Ce comportement contraste nettement avec le comportement observé expérimentalement d'un éjecteur à vapeur pure, où une augmentation du rapport d'entraînement se produit au détriment d'une diminution de la pression critique.

Trois articles détaillés ont été publiés sur divers scénarios d'intégration d'un éjecteur à vapeur dans un procédé de captage d'absorption/désorption. Le solvant de référence était de 20% en masse de monoéthanolamine (MEA). Trois configurations principales ont été étudiées, selon le choix du fluide utilisé pour produire la vapeur secondaire : éjecteur sur condensat, éjecteur sur pauvre ou éjecteur sur riche. La première publication de revue scientifique a porté sur le procédé de désorption et a présenté une méthode de raccourci basée sur les propriétés du mélange CO_2-MEA-H_2O à l'équilibre. Les simulations ont révélé des réductions dans la quantité requise d'énergie de haute qualité, de 10 à 25%. Un simulateur de procédé commercial, Aspen Plus, a été utilisé pour les deux autres publications. Dans la deuxième publication de revue scientifique, le module cinétique *rate-based* a été utilisé, au lieu du module d'équilibre, pour la modélisation de l'absorbeur et du désorbeur, permettant des évaluations énergétiques plus près des valeurs qu'on retrouve dans la littérature courante. Une étude a été réalisée pour comparer un scénario de préchauffage de la vapeur primaire par des rejets thermiques externes avec un scénario d'intégration de la chaleur interne. Cette deuxième publication a montré des économies d'énergie de haute qualité, de 10 à 14%, les scénarios avantageux ayant été «éjecteur sur condensat» et «éjecteur sur pauvre».

Mots-clés: Captage de CO_2, postcombustion, éjecteur, rejets thermiques, MEA, non-condensable

ABSTRACT

The main goal of the doctoral project is to determine to what extent the optimal integration of single-phase ejectors might reduce the large amount of energy required to capture carbon dioxide from electric power generation facilities. More specifically, the objective is to determine if ejectors can be advantageously integrated into a post-combustion absorption/desorption carbon dioxide (CO_2) capture process using monoethanolamine (MEA). The integrated ejectors will use waste heat of 100 °C from the electric power plant. The upgraded waste heat can partially replace valuable turbine steam that would otherwise be taken from the power plant. The second objective of the thesis is to experimentally evaluate the performance of a steam ejector where the ejector secondary fluid is a mixture of steam and a non-condensable gas, in this case CO_2.

Two steam ejector nozzles, of 4.60 mm and 4.23 mm diameter, were evaluated over a range of secondary fluid CO_2 levels, up to 42% by mass. The primary pressure was maintained at 450 kPa with 10 °C superheat and the secondary pressure was 70 kPa. It was found that the critical exit pressure did not change as the mass fraction of CO_2 in the secondary fluid increased. The entrainment ratio, however, increased approximately linearly over the experimental range. An improvement of 23% in the entrainment ratio, as compared with pure steam, was found when the secondary fluid contains 42% CO_2 by mass. This behaviour is in sharp contrast to the experimentally observed behaviour of a pure steam ejector, where an increase in entrainment ratio comes at the expense of a decrease in the ejector exit critical pressure.

Three published papers investigated various scenarios for the integration of a steam injector into an absorption/desorption post-combustion capture process. The reference solvent was 20% weight monoethanolamine (MEA). Three principal configurations were studied, according to the choice for the liquid flow used to produce the ejector secondary steam: ejector on condensate, ejector on lean or ejector on rich. The first journal publication focused on the desorption process and presented a shortcut method based on CO_2-MEA-H_2O equilibrium vapour liquid data. The simulations revealed reductions in the required amount of valuable energy from 10 to 25%. A commercial process simulator, Aspen Plus, was used for two other publications. In the second journal publication, the kinetic rate-based module was employed to model the absorber and desorber, providing energy evaluations closer to values in the open literature. A study was included comparing preheating the primary steam with waste heat or by heat integration. The rate-based simulation found valuable energy savings of 10 to 14%, with the "ejector on condensate" and "ejector on lean" again being the advantageous scenarios.

Keywords: CO_2 capture, post-combustion, ejector, waste heat, MEA, non-condensable

ACKNOWLEDGEMENTS

To begin with, I would like to express my gratitude to my research director, Mikhail Sorin. I very much enjoyed our discussions on all things related to energy efficiency, and his help in seeing the "big picture". His kind, patient and insightful attitude was a continuing source of motivation. Also, thanks for the financial support at various points during the project.

I would like to thank my co-director Zine Aidoun, for his comments and guidance throughout the project and his help with the thesis. I appreciated his steadfast and pleasant demeanor along the long road to experimental results.

My thanks also go to the other jury members for having accepted to review the thesis, and for providing helpful comments and suggestions. I still fondly remember my visit to the Université de Sherbrooke in 2008 to speak with Nicolas Galanis about the possibility of starting a Master's degree. I have benefitted from his teaching and suggestions, right up to the conclusion of the Doctoral program. Thanks to Hachimi Fellouah, who had also kindly accepted to be on the Master's jury, and has again accepted for the PhD jury. I would like to say thanks to Roberto Sunyé for agreeing to help review the thesis and be a member of the jury.

Financial support was very much appreciated by the intervention of Sophie Hosatte of Canmet Energy, principally through the Research Assistant Program of the Government of Canada. I am also grateful that she believed in the experimental project, and facilitated, among other things, my use of computer, a desk, and a friendly work environment.

Very special thanks must be offered to Hristo Sapoundjiev at Canmet Energy, for pragmatic advice, active participation and continual interest throughout the whole experimental phase of the project. Our many discussions and exchanges not only allowed me to complete the experimental work, but were an ongoing source of inspiration in the enjoyable search for innovative applications that combine energy and ejectors. I also wish to acknowledge my many fruitful and amiable exchanges with Stéphane Günther, whose imaginative problem-solving skills were appreciated both on the test bench and with Excel programming.

During the long months of computer simulations, and the inevitable isolation, I was happy to start many a day with my UdeS office colleague Tenon Charly Kone. I was often encouraged by Charly's upbeat disposition and impressive work habits. Thanks also go the Mohamed Khennich and Oumar Samaké, particularly in the earlier part of the project, for discussions and encouragement. To name a few, thanks to fellow students who had a kind word or offered help along the way: Mohamed Hossam Eldakamawy, Ghofrane Sekrani, Mohamed Hafid.

Finally, every thesis and article ends with a list of references. I would be negligent without recognizing the cheerful and helpful contribution of Hélène Bernier, librarian at the Frère-Théode library at the Université de Sherbrooke.

TABLE OF CONTENTS

LIST OF FIGURES

LIST OF TABLES

CHAPTER 1 INTRODUCTION

The warming of the planetary climate and the increasing atmospheric concentration of carbon dioxide (CO_2) is becoming more and more a worldwide concern. The burning of fossil fuels is the largest source of greenhouse gas associated with human activity, mainly due to CO_2 emissions [11]. The capture and long-term storage of CO_2 in geological reservoirs is a viable option to mitigate climate change. This process is now commonly called "Carbon Capture and Storage", or simply CCS. The most efficient method of capturing CO_2 is to target large point source emitters. If large point emitters are defined as sources that are greater than 0.1 M tonnes of CO_2 per year, then there are currently more than 8,000 such global sites [64]. As shown in Fig. 1.1, electric power plants represent over 75% of the total emissions of these large stationary sources [64].

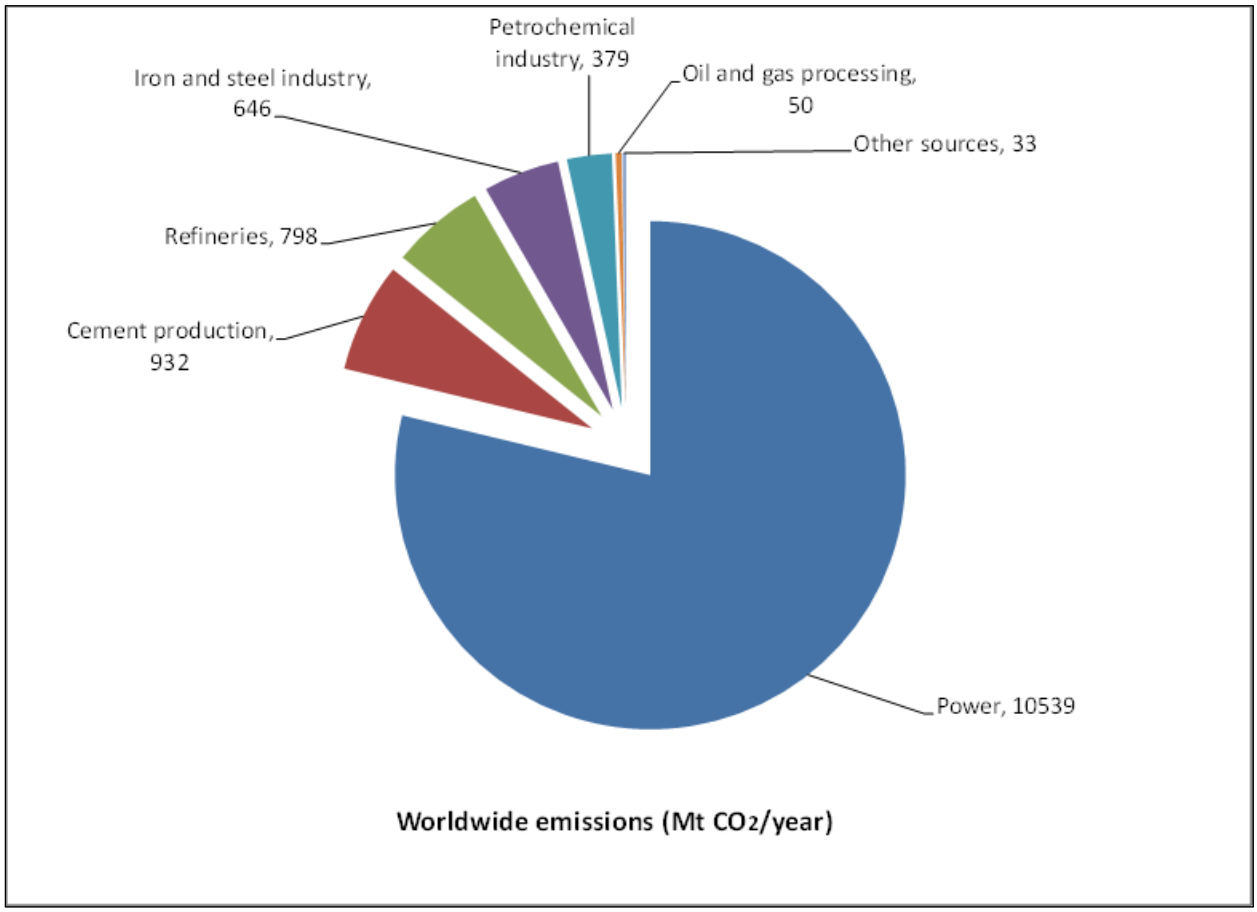

Fig. 1.1 Large point source emitters, over 0.1 M tonnes of CO_2 per year [64]

Energy consumption in general, and fossil fuel combustion in particular, is expected to increase steadily over the next several decades, as indicated in Fig. 1.2. Despite a growing interest in renewable energy sources, and in energy sources that do not emit CO_2, technical and socio-economic challenges are such that the production of electricity from carbon sources remains a worldwide reality. China currently produces 75% of its electricity from coal [111], and many countries have very large coal reserves, possibly lasting for hundreds of years.

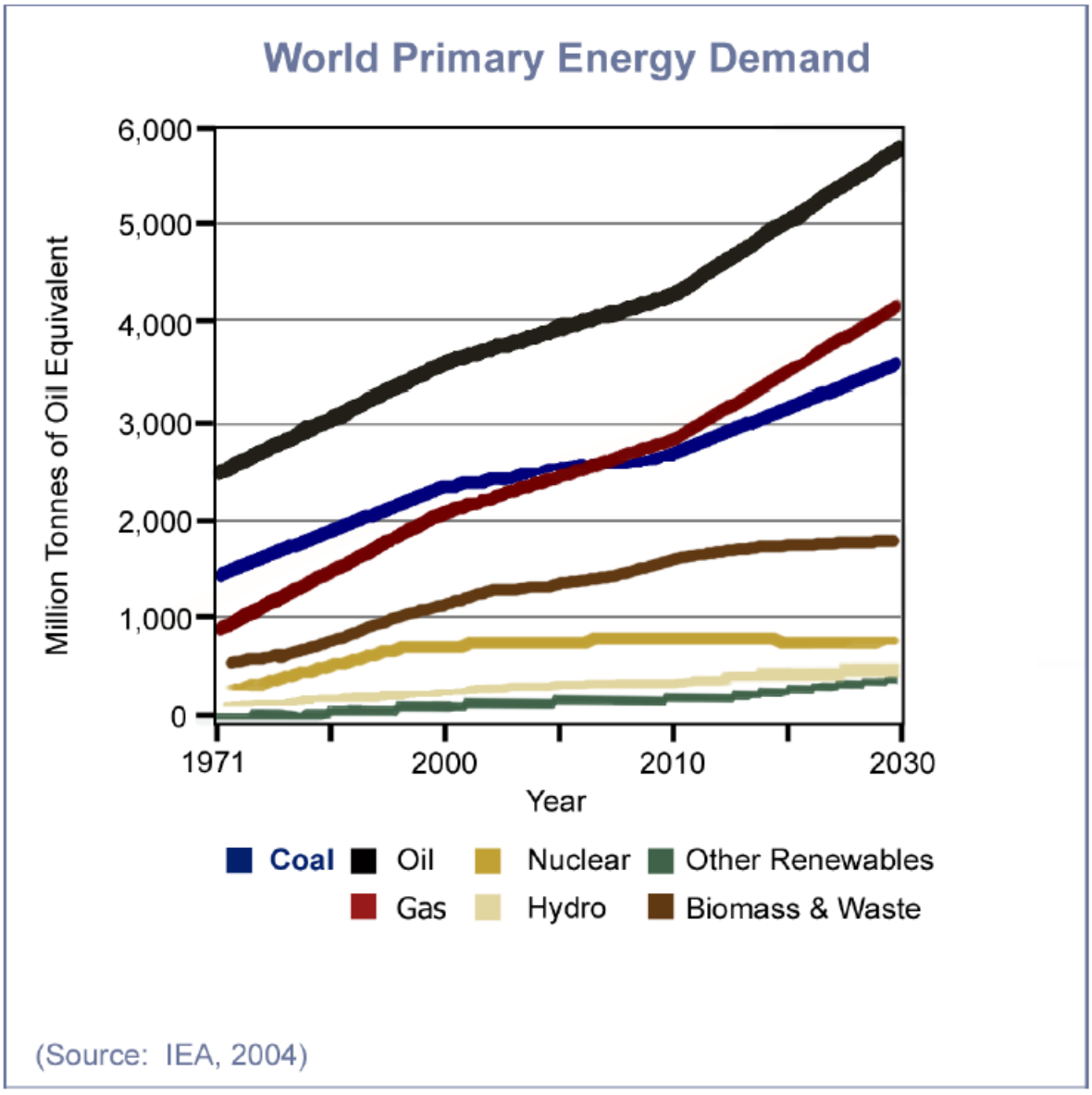

Fig. 1.2 Worldwide energy consumption from primary sources [111]

The technology that is best adapted for the separation of CO_2 from other combustion gases is the process of absorption/desorption [64, 93]. This technology is very energy intensive, mostly due to the energy required to regenerate the solvent. For example, in a coal-fired power plant, a CO_2 capture system could consume from 15 to 30% of the gross power plant output [40]. Absorption/desorption processes suitable for CO_2 capture have elaborate equipment configurations and complex gas and liquid flow plans, including pressure drops, heat and mass transfer operations, and the rejection of heat to the environment. Not in this context, but in other areas, ejectors are recently the subject of much research, especially with the goal of improving energy efficiency and in waste heat upgrading [2, 30, 99, 108].

Despite the simplicity of ejectors and their wide application range, these thermofluid devices are not systematically evaluated when new energy-related challenges arise. The internal behaviour of ejectors involves many complex phenomena: the flow of gas and/or liquid at high speed, shock waves, turbulent and boundary layer effects, phase change, flow choking and finally mass, energy and momentum transfer. Historically, the development of ejector applications is very closely tied to the experimental and theoretical work completed for each specific application. One of the challenges in developing new applications is having access to tools which are general enough in nature to evaluate the potential of a proposed ejector application, knowing that the most accurate modelling tools are those which have been experimentally evaluated for very specific requirements over a narrow range of operation.

In the area of post-combustion CO_2 capture the literature concerning ejector applications is very limited. As will be seen in the section on the state of the art, the literature available on certain ejector applications and on ejector models continues to grow. In the context of the current doctoral project, the target research question is the following: To what extent can the incorporation of an ejector into a post-combustion carbon capture system improve the overall energy efficiency?

1.1 Research project description

The research project includes both computer simulation and experimental methods. The experimental work was completed at CanmetENERGY in Varennes, Quebec. CanmetENERGY is a technology centre of Natural Resources Canada. A custom test bench was built and used to quantify the effect of entrained secondary CO_2 on the performance characteristics of a gas-gas steam ejector. As part of the doctoral project I actively participated in the test bench construction process, including the numerous modifications required to bring the bench to a fully functional level. Both preliminary and advanced simulations were completed on a monoethanolamine (MEA) based post-combustion CO_2 carbon process with the goal of evaluating the optimal integration method of a steam ejector into the capture process.

1.2 General objectives

The general goal of the research project is to evaluate the potential for energy improvements that can be achieved in carbon capture processes through the use of ejectors. An important aspect of the potential energy improvement is the upgrading of waste heat through the action of the ejector. More specifically, this project will evaluate the possible use of ejectors in post-combustion capture of CO_2 using amine based absorption/desorption. Because the method for incorporating the ejector into the capture process is not unique, various process layout scenarios must be evaluated. The influence of the entrained non-condensable gas in the behaviour of the ejector and the capture process will be accounted for.

1.3 Specific objectives

- Experimentally evaluate the behaviour of a specific steam jet ejector that operates in the appropriate temperature and pressure range for post-combustion CO_2 capture.
- Experimentally evaluate and quantify the performance characteristics of a steam activated ejector, where the ejector secondary fluid contains a mixture of CO_2 and H_2O in the ejector secondary fluid.
- Develop a method of evaluating the optimal integration of a gas-gas ejector into a post-combustion CO_2 capture process.
- Complete preliminary equilibrium-based simulation analyses of a post-combustion CO_2 capture process based on absorption/desorption and find the optimal configuration.
- Complete a realistic rate-based simulation analysis of a post-combustion capture process and find the optimal configuration. Commercial process simulators that contain a "rate-based" module account for the very complex chemical kinetics of the CO_2-MEA-H_2O chemistry. These modules are known to give more realistic results, but also to be more likely to suffer from non-convergence problems in the process simulation.
- Evaluate the effect of entrained CO_2 in the ejector secondary fluid both on the overall capture process and on the behaviour of the steam activated gas-gas ejector.

1.4 Originality

The main originality of this thesis lies in the combination of the following elements: the use of a gas-gas ejector; a post-combustion absorption/desorption CO_2 capture process; the upgrading of waste heat external to the capture process. In other words, external waste heat, upgraded through the action of the ejector, is used to partially replace the valuable steam that would otherwise be withdrawn from the turbine steam in an electric power generation facility.

The experimental work in the thesis is the first work done specifically to evaluate the behaviour of steam ejector where the ejector secondary fluid contains a mixture of CO_2 and H_2O.

The simulations completed in this project are the first to analyse the role of the entrained CO_2 on both the local ejector behaviour and the overall capture process behaviour in a post-combustion absorption/desorption CO_2 capture process.

1.5 Thesis plan

Chapter 2 presents the state of the art relating to the project, including the main CO_2 capture processes, chemical absorption simulation challenges, ejector modelling and available information and entrained mixtures other than pure steam or air. Chapter 3 describes the experimental work that was completed on pure steam ejectors and the effect of entrained mixtures of steam and CO_2. Additional experimental information is included which may be helpful more generally to others working in the area of ejector research. Chapters 4 and 5 are the peer reviewed journal publications that were completed in the doctoral project. Both contain abstracts, both in French and English, as well as a section "Avant-Propos", in French, which gives the status of the articles as well as their contribution to the thesis. Chapter 4 relates to the simpler equilibrium-based simulations, concentrating on the desorber, which compared three studied process configurations. Chapter 5 extends the work of Chapter 4, by including the absorber and desorber, as well as applying more realistic rate-based models within a commercial chemical process simulator, Aspen Plus. Finally, Chapter 6 presents thesis conclusions.

CHAPTER 2 THE STATE OF THE ART

2.1 Carbon capture processes

At the beginning of the doctoral project there was no full-scale application of a CO_2 capture system at an electric power generating facility. In 2014, however, the first full scale carbon capture and storage (CCS) process was put on stream at the Boundary Dam power plant in Saskatchewan, Canada. In that case the CCS process was applied to a pulverised coal burning electric plant, where for one of the power production units 90% of the CO_2 is removed from the combustion gases. More generally, however, there are three major paths for carbon capture for power production facilities, as shown in Fig. 2.1: post-combustion, pre-combustion and oxyfuel [64, 77, 94].

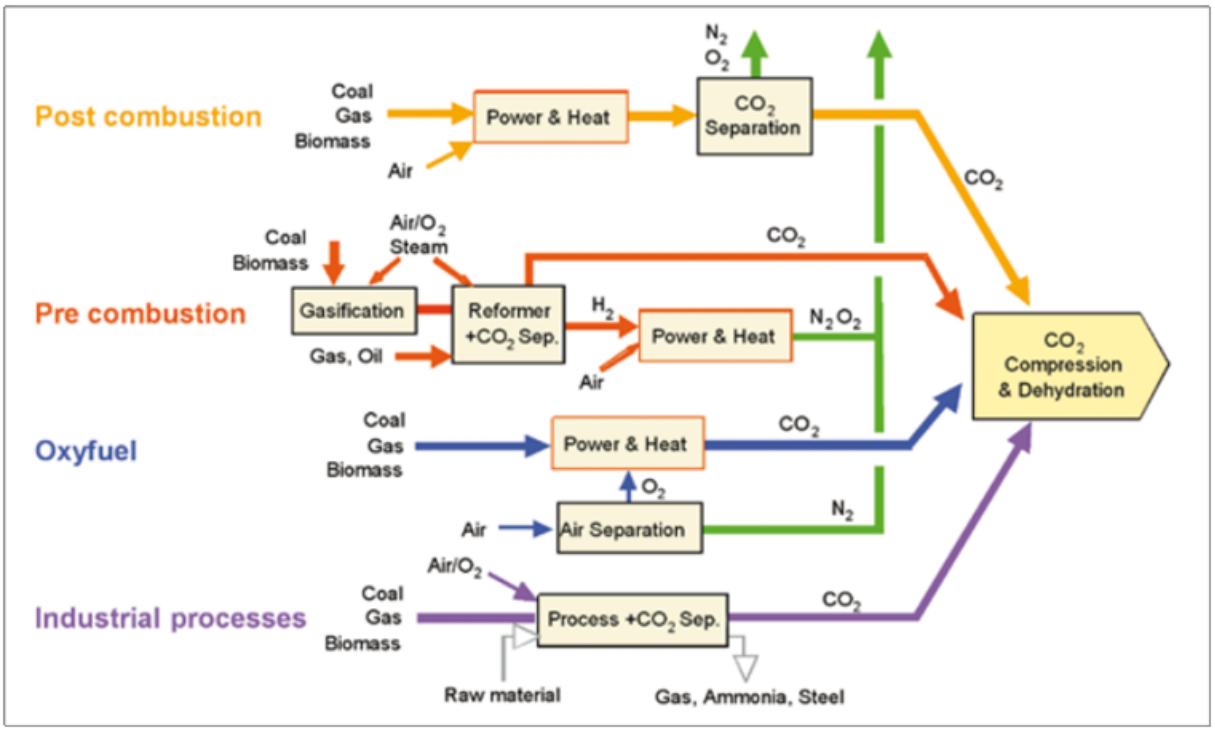

Fig. 2.1 CO_2 capture pathways [64]

In post-combustion, a capture system would be installed downstream of the current power plant. In this kind of an installation, a very large volume of atmospheric pressure gas must be

treated, where the combustion gases contain a relatively low fraction of CO_2. For example, 12 to 15% by volume of CO_2 is typical of coal-fired flue gas. For existing power plants the majority of researchers agree that the most appropriate and mature post-combustion capture option is with chemical absorption based on amine solvents [64, 66]. This technology is already widespread, but must be adapted to the special challenges to handle the very high volumes associated with post-combustion capture.

In the pre-combustion pathway, as shown in Fig. 2.1, the fuel is only partially oxidized in the first gasification step. The intermediate gas mixture is known as synthesis gas, which is mainly a mixture of carbon monoxide (CO) and hydrogen (H_2). Depending on the ratio of H_2 to CO, the synthesis gas can be used as a feedstock for downstream chemical processes, or directed towards a power plant to complete the final combustion process. When power generation is the final goal, the intermediate synthesis gas is further reacted with steam, producing final products of H_2 and CO_2 at high pressure, in the range of 3 to 4 MPa. At this final stage the output gas contains close to 40% by volume CO_2 [77]. This high pressure and CO_2 rich gas mixture lends itself to the less energy intensive process of physical absorption. After the CO_2 is removed by physical absorption, the hydrogen can be burned in a highly efficient combined gas-steam power generation plant.

The oxyfuel capture pathway, shown in Fig. 2.1, begins with the combustion of the carbon fossil fuel with almost pure oxygen, resulting in a combustion gas that is around 80% CO_2 [77] . Although this technology is currently only at demonstration scale, it has the advantage of producing an exhaust gas that can simply be de-watered and sent to long term storage. Because the nitrogen present in atmospheric air does not take part in the combustion process, the equipment size can be significantly reduced and certain efficiency improvements are possible. The disadvantage of the oxyfuel pathway is that oxygen must first be removed from the air, typically by cryogenic means or through the use of membranes. Both air separation techniques require a significant energy input.

The choice of the best technology for the separation of CO_2 from a gas stream, presented in schematic form in Fig. 2.2, is a function of the concentration of CO_2, the pressure and temperature of the gas stream to be treated, and of the equipment and operating costs. The four main separation technologies are absorption (with a liquid sorbent), adsorption (with a solid sorbent), cryogenics or with membranes. Typically the liquid sorbent is simply referred to as the

solvent. Absorption is the most commercially widespread of the separation choices. Absorption technology is further subdivided into chemical and physical absorption. Chemical absorption is based on the fact that CO_2 is an acid gas, as are sulfur dioxide (SO_2), nitrogen mono and dioxide (NO_x) and hydrogen sulfide (H_2S). All of the acid gases have a tendency to partially dissociate in contact with water, increasing the acidity of the resulting aqueous solution. Basic, or alkaline solvents can scrub CO_2 from gas stream even when the CO_2 partial pressure is very low, such as in post-combustion. Because of the chemical reactions involved in the process, high levels of energy are required in the desorption step to reverse the chemical reactions and regenerate the sorbent. In physical absorption, the absorbed gas is not chemically changed, and molecules of the absorbed gas are simply moved from the gas mixture to the liquid mixture. Physical absorption thus requires less energy to regenerate the solvent than in chemical absorption, but high pressures are required for the absorption process, with the solvent typically being regenerated by dropping the pressure in the desorption step.

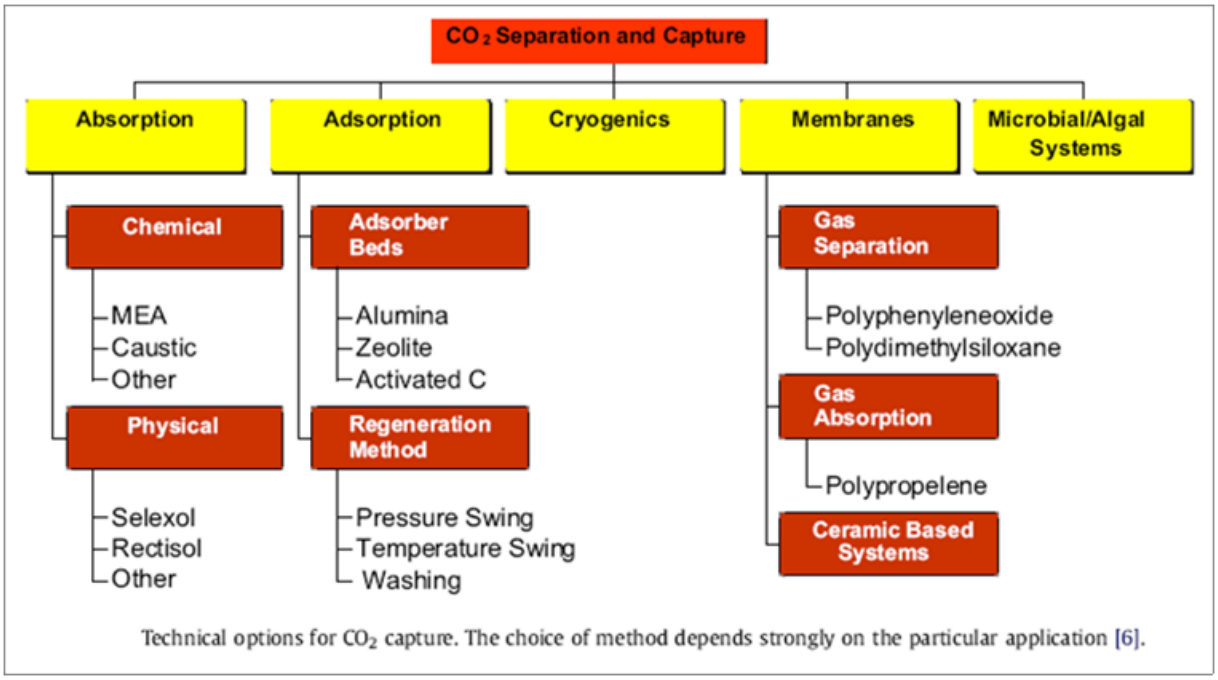

Technical options for CO_2 capture. The choice of method depends strongly on the particular application [6].

Fig. 2.2 CO_2 separation technologies [94]

Adsorption (with a solid sorbent), cryogenics and membrane technologies, shown in Fig. 2.2, are still an area of much research [77, 94], but they are not at the same feasibility level as is absorption in the context of carbon capture. More recently, newer separation processes are being studied which more specifically target CO_2 capture. In chemical looping, for example, a metal oxide is used to transfer the oxygen from the air to the fuel, and thus there is no direct contact

between the air and the fuel. In chemical-looping combustion (CLC), shown in Fig. 2.3, there is an inherent separation of the CO_2, thus no downstream separation process is required [1].

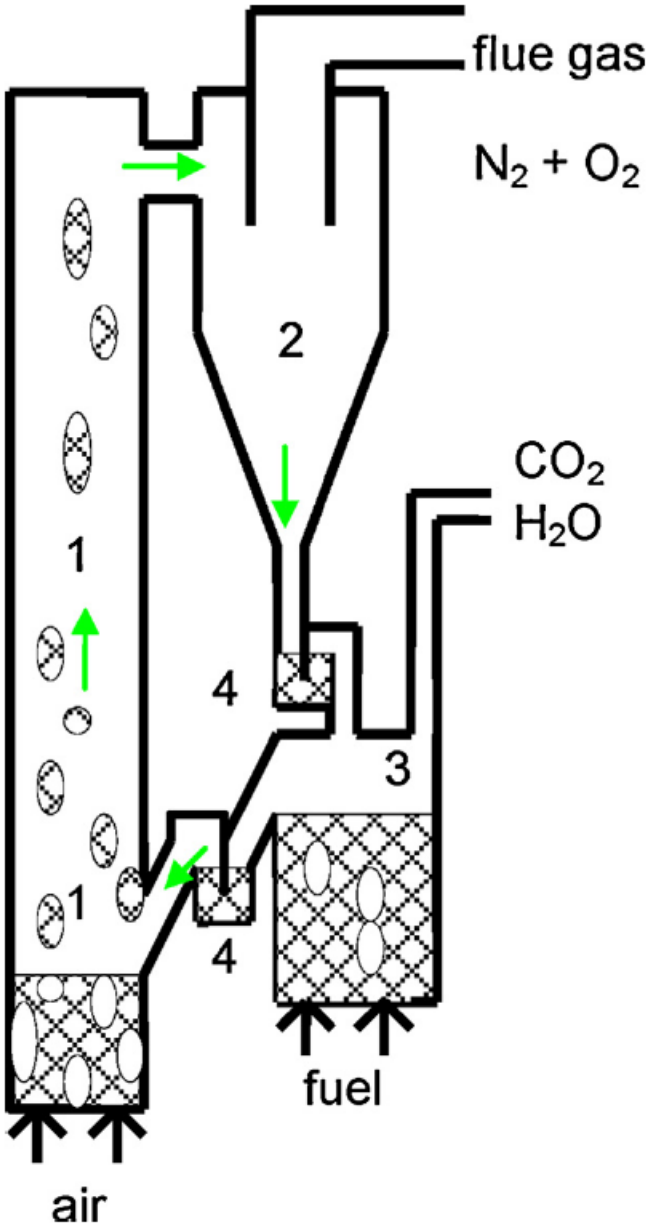

CLC process, exemplified by two inter-connected fluidized reactors. (1) Air reactor and riser, (2) cyclone, (3) fuel reactor, (4) loop seals.

Fig. 2.3 Chemical-looping combustion [1]

Strategies that aim to reduce the cost of CCS include the use of new solvents, mixtures of solvents, and new process configurations. Recent solvent studies include Idem et al.[39], Yokoyama et al.[118] and Ohashi et al.[74]. The amine family of solvents, being the oldest in

area of CO_2 capture, continues to change and advance [53, 54]. Van Wagener and Rochelle [112] evaluated various configurations, including multi-stage expansion, multi-pressure desorption, mechanical recompression and a heated intermediate column. Jassin and Rochelle [40] also evaluated innovative configurations, finding that a multi-pressure column with mechanical recompression was the most interesting option. Also in the context of new process configurations, but where the solvent is potassium carbonate in the Benfield process [45], ejectors have been proposed for steam compression for the purpose of reallocating heat within the process to reduce the energy consumption at the reboiler. In the area of ammonia production using the Benfield process, Lu et al. [59] proposed recompression with an ejector using plant steam to reduce the steam required in the reboiler. It must be noted that in these systems the proposed ejectors are intended to upgrade heat already within the absorption/desorption process in their respective applications. Part of the originality of the current thesis is the use of waste heat, external to the capture process, to reduce the amount of valuable energy that must be consumed within the absorption/desorption process.

Solutions of water and amine solvents have been used in chemical absorption for the capture of CO_2 from natural gas and from hydrogen since the 1930s [45, 93]. Monoethanolamine (MEA) was one of the first amine solvents to be commercially used for this purpose, and is still used in aqueous solutions from 20 to 30% by weight. Pilot plant tests completed in the 1980s showed the successful post-combustion capture of CO_2, where the fuel was either coal or natural gas [93]. The biggest technological challenge to this capture option remains the reduction of the energy required to regenerate the solvent, which is more than 60% of the total energy of the CCS process [48].

A simplified version of the traditional chemical absorption/desorption CO_2 capture process is shown in Fig. 2.4. The process flow layout is very similar to the original image that accompanied the patent of R.R.Bottoms in 1930. The white arrows indicate the transfer of heat and the black arrows show the fluid flow. The CO_2 is transferred from the combustion flue gas that rises in the absorber, to the solvent mixture that descends the absorber. The solvent mixture entering the top of the absorber contains relatively little CO_2 and is thus called the lean solvent. The solvent mixture that exits the bottom of the absorber is highly concentrated in absorbed CO_2, and is thus called the rich solvent. The rich solvent passes from the absorber bottom to the top of the desorber, typically called the stripping column or simply the stripper. In the stripping column

the heat added to the reboiler, at the bottom of the column, produced the steam necessary to desorb the CO_2, which rises in the column. The desorbed CO_2 leaves the top of the column where it is separated from the water in the condenser, compressed and sent to long term storage.

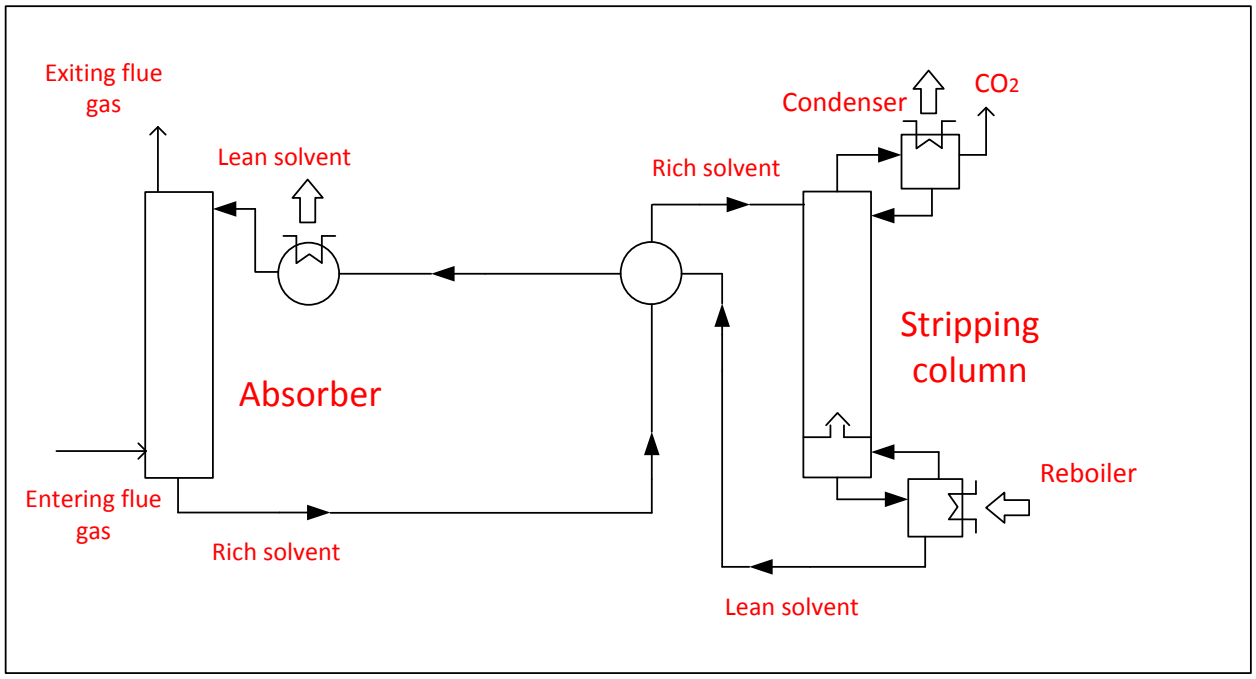

Fig. 2.4 Traditional absorption/desorption CO_2 capture

As will be detailed in Chapters 4 and 5, the thesis will evaluate three key scenarios for integrating a steam ejector, which upgrades external waste heat, into the traditional capture process shown in Fig. 2.4. The various scenarios principally aim to answer two questions. Where should the ejector exit steam be placed in the stripping column? What stream should be used to produce the secondary steam for the ejector? Because of the specific nature of these questions, this information is not available in the literature.

2.2 Process modelling

The history of separation processes relating to liquids and gases traces back to simple batch distillation, and then later to multiple stages of distillation in series, as carried out in a distillation column. Before the advent of modern computers, distillation columns were understood as stacked theoretical trays, where experimentally determined vapour/liquid equilibrium data was used, in combination with mass and energy conservation, to model the behaviour of each tray and then the whole column. Given that equilibrium is not actually achieved for each tray in the column, a correction factor must be applied to model a real distillation column. Even with the commercial development of packed columns, where individual trays are completely replaced with specially shaped packing material to maximize contact between the rising gas phase and the descending liquid phase, the idea of the theoretical tray remains. The construction of the theoretical trays is described in chapter 2 of Kohl and Nielsen [45].

With the arrival of digital computers, it became possible to create much more sophisticated models that take into the account the actual size of each portion of the column, including the packing material and the column diameter, as well as the chemical reaction rates in the difficult case of chemical separation processes. There is now a trend towards programming tools that use this most recent generation of "rate-based" modelling, which model not only the equilibrium thermodynamics, but also the chemical kinetics of each theoretical tray in the column. As will be discussed, there are many subtleties to each of the simulation approaches and more specifically to the modelling of chemical CO_2 capture processes.

Experimental evaluation of the basic reference capture process, such as shown in Fig. 2.4, is prohibitively expensive, and even more so if alternative process configurations are to be evaluated. Process modelling and simulation are thus key tools for CO_2 capture research. L.E. Oi reviewed the challenges of modelling the process, particularly within the absorption and desorption columns, identifying four main programming tasks: reaction kinetics, gas/liquid equilibrium properties, gas and liquid flows, and pressure drop [76]. Large commercial chemical process simulation packages are available, which generally allow the user to choose "equilibrium" based modelling or "rate-based" modelling. For example, Aspen Plus is available with an amines package, appropriate for the CO_2-MEA-H_2O mixture, and can be used in either

equilibrium or rate-based simulations. Rate-based models have been shown to be more accurate than the equilibrium models [49]. Nagy et al. explained why rate-based models, particularly for the complex and highly non-ideal mixture of CO_2-MEA-H_2O in chemical absorption/desorption, generates results that are closer to published experimental data [69].

Software convergence problems are common in chemical process simulations, even for the computationally less sophisticated equilibrium models. One approach to manage the convergence problem is to complete preliminary simulations with an open loop simplification, as discussed by Arachchige et al. [81], and then in a second phase redo the simulation with a closed loop. For this reason, the use of equilibrium models continues to be used, for example in the study by Yokoyama [119], who studied the reboiler duty in a CO_2 captures system where the solvent solution was 20% wt. MEA.

When equilibrium vapour/gas data is available, custom software can be prepared to model specific portions of the capture process. Lucia et al. [60] used this approach to study minimum energy requirements of the stripping column for various loading conditions of the lean stream. Initial guess values, such as those generated by simpler equilibrium models, can significantly reduce simulation time or even allow converge in more sophisticated models [6, 75]. Shortcut methods can provide first guess values for subsequent simulations, allow pre-screening of potential solvents, and a means of evaluating alternative process configurations [60, 73].

Another layer of difficulty is added when the dynamic behaviour of the capture process is studied. This area of research is important to understand the behaviour of the capture process where the power plant attempts to follow demand load, or to account for process fluctuations during start up and shut down. Gáspár and Cormos [33] studied the dynamic behaviour using a custom code built with Matlab and Simulink. Karimi et al. studied the dynamic behaviour of three different configurations of the capture process, using equilibrium models within a commercial process simulator, Unisim Design with the Amine Package.

Mores et al. [67] developed a mathematical model of the traditional capture process and then completed various optimization studies in the General Algebraic Modeling System (GAMS). Their custom model accounts for reaction kinetics, the hydraulics of the chosen packing material and the overall tower pressure drop. The mathematical model was validated by comparing the results with those of the commercial simulator HYSYS.

2.3 Ejector modelling

Henri Griffard invented the steam activated ejector in 1858. This device served as a pump to fill the water tank of steam locomotives [30]. In 1901, Charles Parsons used a steam ejector to remove non-condensable gases from condensers. Maurice Leblanc, in 1910, was the first to incorporate an ejector into a refrigeration cycle, again with steam being the primary driving fluid [18].

In its simplest form an ejector is a tube with two entrances at one end and a single exit at the other. The primary flow, at high pressure, enters the ejector through a relatively small nozzle along the central axis. The secondary flow, at a lower pressure than that of the primary fluid, enters in an annular region surrounding the nozzle. The exiting of the primary fluid from the nozzle creates a low pressure region, inducing the secondary fluid to enter and accelerate towards the central part of the ejector body. By the time the two fluids have reached the ejector exit they have become a single homogenous mixture, at a pressure intermediate between that of the primary and secondary entrance pressures.

Ejector applications are numerous and varied, for example serving to produce vacuum, to compress or partially compress, to mix fluids, or as a fluid expander, to name a few. More recently, ejectors are the subject of much research in the hope of energy efficiency improvements with their incorporation into various processes. In order to categorize these applications, it is often helpful to group them according to the number of phases entering the ejector: single-phase and two-phase.

Fig. 2.5 shows the incorporation of a single-phase ejector into a thermally activated heat pump application, where the refrigeration effect is driven by the thermal energy entering at the generator. This configuration offers many possibilities in the use of solar energy in combination with a single-phase ejector [2, 65]. The configuration also lends itself to the upgrading of waste heat, such as the gas turbine exhaust, as studied in a cycle proposed by Petrenko et al.[84], which produces both power and a refrigeration effect. Absorption refrigeration is also an application where single-phase ejectors offer the possibility of energy efficiency improvement [4, 106]. These absorption refrigeration applications can also include solar energy [5, 36].

Fig. 2.6 shows a less well-known R22 refrigeration cycle, proposed by Bergander et al. [10], that corporates a two-phase ejector, where the driving fluid is a gas and the secondary

fluid is a liquid. In this cycle the compressor completes the first stage of compression, up to 2/3 of the condenser pressure, and the ejector supplies the second stage of compression. An improvement of up to 38% was calculated for the coefficient of performance (COP). The experimental work found an improvement of up to 16% compared with the conventional vapour compression cycle.

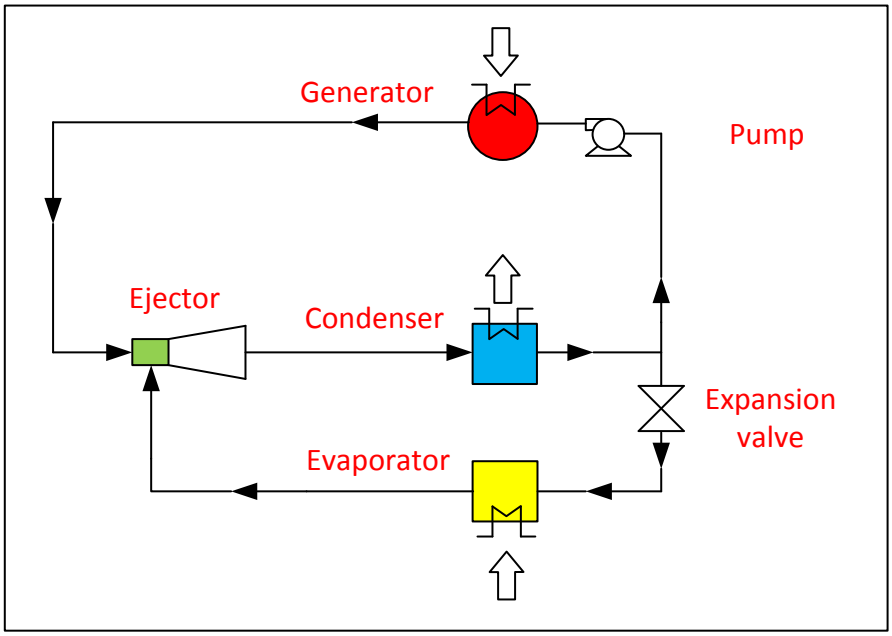

Fig. 2.5 Ejector application: thermally activated heat pump

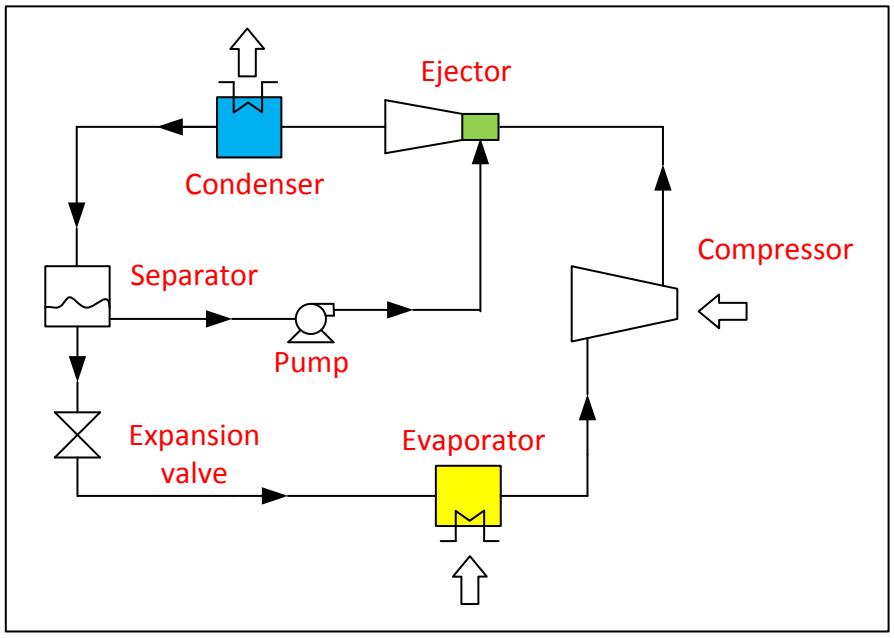

Fig. 2.6 Ejector application: ejector as the second stage of compression

Fig. 2.7 shows a refrigeration cycle using a two-phase ejector, where the ejector replaces the expansion valve in the traditional vapour compression cycle [99, 108]. The use of an ejector as an expansion device in a vapour compression system with R12 was studied by Kornhauser [46]. His theoretical work found an improvement of up to 21% as compared with a system having a thermostatic expansion valve. In an experimental study, using R134a as the working fluid, Reddick et al. [34] showed an improvement in the COP of between 3.9% and 7.6%. More recently, Sag and Ersoy [95] also completed experimental work with R134a, finding an improvement in the COP of 5 to 13% as compared to the traditional vapour compression cycle.

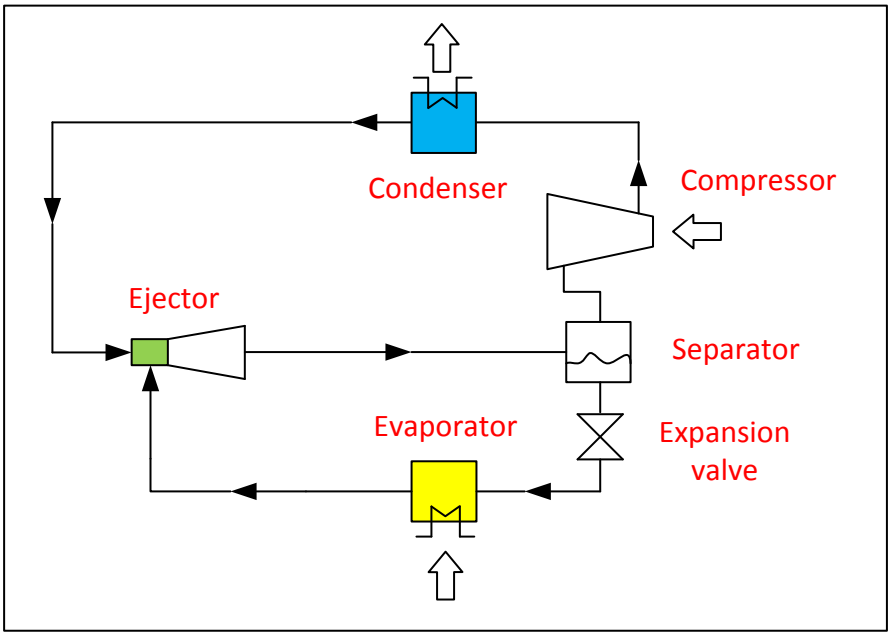

Fig. 2.7 Ejector application: ejector as an expansion device

The study of refrigeration systems where an ejector is used as an expander continues, particularly since the development of this technology by Denso in Japan, with the commercialization of the "cool box" option available on the Toyota Highlander in 2008 in North America. In this application the ejector is part of the air-conditioning system that supplies a cooling effect to a central enclosed console for food and drinks. In 2010 Denso also developed an air-conditioning system for the Toyota Prius, again using an ejector as an expander. Deng et al. [25] showed an improvement of 22% in a theoretical study using CO_2 as the refrigerant in a transcritical cycle. Elbel et al. [29] found an improvement of 8% in the refrigeration capacity and 7% in the COP in their experimental work on a transcritical CO_2 cycle.

Before discussing the modelling of ejectors, it is necessary to discuss the operating modes of an ejector and the associated fluid flow phenomena. For thermodynamic cycles where the ejector exit is connected to a condenser, as in Fig. 2.5, for fixed temperatures in the evaporator and the generator, the mass flow rates and thus their ratio are only a function of the condenser pressure and the ejector geometry. Generally ejectors have a fixed geometry, but adjustable needles have been used to control the primary nozzle area in both single-phase [123] and two-phase ejectors [90]. Assuming a fixed ejector needle position, and thus fixed ejector geometry, there exists a characteristic condenser pressure called the critical pressure, below which the entrainment ratio will remain constant. The entrainment ratio is the ratio of the secondary mass flow to that of the primary. When the exit pressure is at this critical pressure, the ejector is said to operate in "critical" mode. When the condenser pressure is below the critical pressure, the ejector operates in a stable mode, often called "double choked" mode. If the condenser pressure increases beyond the critical pressure the entrainment ratio diminishes, and the ejector is said to operate in "off design" or "single choked" mode. If the condenser pressure, or equivalently the ejector exit pressure, is allowed to further increase, the secondary flow will drop to zero and will actually reverse. The ejector is no longer functioning in a useful way, and this situation is simply referred to as "reverse flow" or ejector malfunction.

Unfortunately, in two-phase ejector applications, as shown in Fig. 2.7, no experimental work has shown the equivalent behaviour associated with the idea of the critical pressure. In single-phase ejectors the prediction of the critical pressure is a means of evaluating a particular ejector design model, and the experimental determination of the critical pressure helps to characterize a particular physical ejector. Most ejectors are designed to operate at or just below the critical pressure, and thus to have a constant stable entrainment ratio.

Fig. 2.8 shows the separation region where the secondary flow detaches from the ejector wall, the mixing region, as well as a shock train region and its associated pressure profile in the lower part of the image. In single-phase ejectors it is known that when the exit pressure increases the shock train moves upstream towards the primary nozzle [9, 102]. Condensation is another phenomenon in the ejector which makes the behaviour of the flows more complex [62]. According to the type of study, experimental or theoretical, it is suggested that the primary fluid be superheated to avoid condensation shocks within the ejector [3, 14, 79, 125].

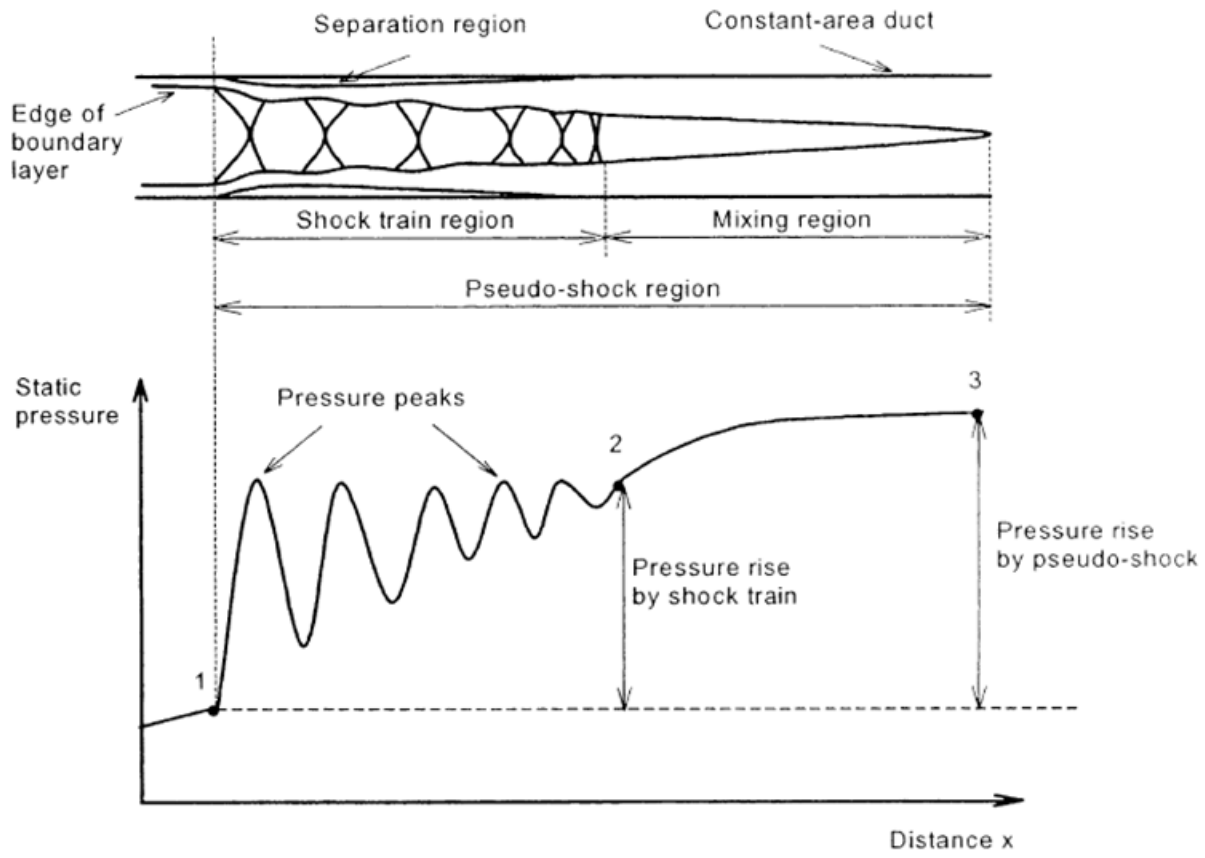

.

Fig. 2.8 Description of the different flow regions [8]

Studies that connect the ejector geometry to its fluid behaviour are of importance for both the design of ejectors and for the validation of more theoretical studies. The use of a movable needle in single-phase applications [55, 113, 114] allows the ejector to be slightly modified so that the cycle can operate at the critical pressure, providing more system control even if the input and output conditions around the ejector change. In two-phase applications, an adjustable needle can offer advantages for system control [29, 50, 57].

Menegay and Kornhauser suggested that the initial poor performance of refrigeration cycles that use a two-phase ejector as an expander was due to the non-equilibrium conditions in the motive nozzle [63]. They proposed allowing a partial expansion of the primary liquid upstream of the nozzle, thus creating many small bubbles which would act as bubble nucleation sites, possibly aiding the primary flow breakup in the mixing section. Taking these ideas into account, Reddick et al. incorporated both an adjustable needle and a fixed throat into their ejector design, finding the best results when the adjustable throat and fixed throat had the same area [90].

Leaving aside the possibility of an adjustable primary throat area, Fig. 2.9 shows the minimum parameters required to characterize ejector geometry. Petrenko et al. [83, 84] suggested that an increase of 25 to 30% is possible in the entrainment ratio when the mixing section, often cylindrical, is constructed with a conical section upstream of the cylindrical portion. Sarkar [97] and also Nehdi et al. [71] completed a theoretical study on the effect of a geometric ratio, that of the area of the cylindrical mixing section to the area of the nozzle exit, on the cycle performance. Several experimental studies have dealt with the effect of various aspects of ejector geometry. Chaiwongsa et al. [15] studied the effect of the primary throat diameter with R134a. Elbel et al. [29] evaluated diffuser included angles of 5°, 10° and 15°, finding the best results for 5° with CO_2. As they indicated, the best angle is a trade-off between a larger angle associated with boundary layer separation induced efficiency reduction and a very small angle associated with increased frictional pressure drop for very long diffusers.

Ejector modelling is still a very diversified and evolving research area. Models are classified into three families: dynamic (often referred to as CFD for computational fluid dynamics), thermodynamic (0D or 1D) and empirical or semi-empirical [35]. The subcategory of single-phase or two-phase is still very useful. It should be noted, however, that there is often phase change within an ejector, at least for a portion of the flow, and that the designation of single-phase of two-phase is generally used to indicate if the ejector input streams are of the same or different phases.

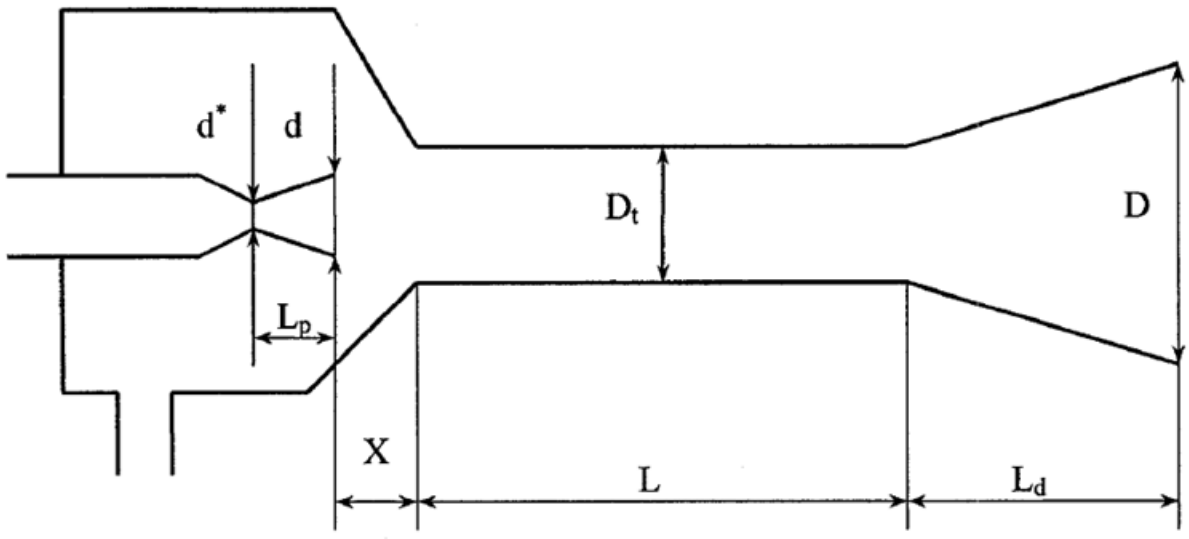

Fig. 2.9 Geometric parameters for a traditional ejector [62]

Recent research on dynamic models is very active and continues to improve our understanding of specific local effects in the ejector [8, 55, 61, 62, 102]. Although these models offer advantages in terms of the precision of the results, they are very complex, need a lot of time to prepare, and they require a suitable choice for both the mesh size and the kind of turbulent model. It has been suggested as recently as 2013 that although CFD can accurately predict ejector performance for critical mode operation, in sub-critical mode these models can generate errors in the 40-50% range in terms of entrainment ratio prediction [16]. A more realistic evaluation of well-built CFD models is that they provide critical mode operation entrainment prediction values within 1-4% of experimental results, depending on the choice of the turbulence model [22]. Most of the thermodynamic single-phase models simulate critical mode operation [14, 23, 27, 38, 79, 83, 103, 106]. Chen et al. [16], to the contrary, accounted for the three modes of operation in their model. In two-phase thermodynamic models, the flow mode is not generally specified.

Although the internal workings of the ejector are not the focus of the thesis, it is hoped that going into a little more detail on ejector models at this point could be helpful to those who are trying to bridge the knowledge gap between ejectors, on the one hand, and CO_2 capture processes on the other. After taking a slightly closer look at thermodynamic ejector models, we will discuss the state of the art on empirical models which are more directly of use in the simulation of capture processes.

The basic equations for the modelling of an ejector begin with the conservation of mass, momentum and energy.

$$\sum \rho_i u_i A_i = \sum \rho_e u_e A_e$$

$$P_i A_i + \sum m_i u_i = P_e A_e + \sum m_e u_e$$

$$\sum m_i \left(h_i + \frac{u_i^2}{2} \right) = \sum m_e \left(h_e + \frac{u_e^2}{2} \right)$$

Although not shown above, the second law of thermodynamics also imposes the condition that the system entropy should remain constant in an ideal process, or should increase in a real process. The additional equations that are required are largely tied to the strategy of representing the shock wave train and all of the other non-isentropic phenomena within the ejector. Many researchers, working in the area of single-phase ejectors, choose to represent the shock wave train

as a normal shock [4, 24, 31, 38, 42, 79, 83, 84, 103, 125]. According to the design choice, the location of this simplifying normal shock wave is generally in the constant diameter portion of the ejector, possibly at the entrance, the exit, or somewhere between the two. In two-phase flow, the normal shock wave approach is not used [29, 46, 47, 58, 97, 98].

The equations describing normal shock waves are easier to formulate when the ideal gas law is assumed, but this is not required. Outside the area including the shock wave, if there is one, the choice of using the assumption of the ideal gas law or real gas properties varies from one author to another. In two phase flow, or when a normal shock wave is included in the model, the assumption of a homogeneous mixture is almost always made. This assumption imposes the same flow velocity for both the gas phase and the liquid phase in the mixture. As a first approximation, the speed of sound is often approximated by the gas phase. Certain homogeneous models calculate the "two-phase" speed of sound, such as Cardemil et al. [14] in a model that is essentially single-phase, or Liu et al. [58]. Samaké et al. [96] used the Wood approximation for the two-phase speed of sound. Several recent studies do not require the calculation of the speed of sound, as the primary and secondary throat areas are defined in terms of the maximum mass flow per unit area [7, 32, 44, 96]. In these studies the calculation and discussion of the speed of sound is merely for comparative purposes, particularly for comparison with the ideal isentropic case, and is not required for the ejector model. The question of what equation is the most appropriate for quantifying the speed of sound in two-phase flow was addressed by Ameur et al. [7], where equations proposed by Wood, Attou, Nakagawa and Ameur were compared. The Wood and Ameur equations gave results closest to REFPROP values, but there is still a need for experimental validation of the two-phase speed of sound. As a conceptual tool in the ejector design, however, there may not in fact be a need for this parameter.

The explicit representation of the friction of the fluid flow along the inner walls of the ejector is not generally done in thermodynamic models. Selvaraju and Mani [103], however, incorporated a friction factor into their model, and later this same approach has been used by certain other authors in order to account for the length of each section of the ejector [21, 28, 41].

Almost all thermodynamic models, as much in the area of single-phase [16, 27, 38, 79] as in two-phase [12, 56, 71, 97], use isentropic coefficients, especially for the primary nozzle, the secondary nozzle, and for the exit diffuser. Coefficients that apply to the transfer of the momentum exchange in the mixing section are also common [14, 27, 58]. Unfortunately these

models are not directly comparable with each otherls, even for models that compare favorably with experimental results, given that each model does not use the same assumptions, secondary relations, geometry or limit conditions.

Rather than applying a constant isentropic coefficient to the acceleration and deceleration processes in the ejector, the concept of applying a fixed polytropic efficiency has been applied for the first time to ejectors by Samake et al. [96], Galanis and Sorin [32], and Khennich et al. [44]. Polytropic efficiency was used in turbine design to characterize the isentropic efficiency of each turbine stage [105]. By applying this concept to ejector design, the overall efficiency is a function of the inlet and outlet pressures, which is more realistic, rather than a fixed efficiency, as occurs when a constant isentropic coefficient is assumed.

The first mathematical model of an ejector began with Keenan and Neumann (1942), and applied to a single-phase air ejector [43]. Keenan et al. [42] introduced two concepts for characterizing the ejector mixing process. In "Constant Pressure" mixing, the primary nozzle exit is upstream of the constant area section of the ejector, as shown in Fig. 2.9. In "Constant Area" mixing, the exit of the primary nozzle is in the same plane as the entrance to the cylindrical portion of the ejector. Munday and Bagster [68] introduced the idea of the fictive throat in their "Constant Area" ejector model, as a means of explaining the observed constant secondary mass flow when the ejector operates below the critical exit pressure. Eames et al. [27] accounted for irreversibility in their model by introducing isentropic efficiencies for the primary nozzle, diffuser and the mixing chamber.

In two-phase ejectors, in 1990 Kornhauser [46] presented a 1D model that used isentropic coefficients. Several researchers continued in the same way, but modified the starting assumptions [12, 29, 57, 71]. Nehdi [71] introduced a simplifying relationship for the mixing section. Bilir et al. [12] supposed that the pressure at the exit of the primary nozzle was equal to the secondary pressure in the same plane, and varied this unknown pressure in order to optimize the studied cycle performance. Liu et al. [58] did not impose the same pressure for the two fluid flows at the exit of the primary nozzle. In all of these two-phase cases, there is very little published information with which proposed models can be validated.

Empirical models, when they are available for the operating range and working fluid of interest, offer an excellent starting point for exploratory ejector application studies. R.B.Power [86] built a graph for single-phase steam ejectors, based on an amalgam of available

commercial steam ejector suppliers' data, which describes the entrainment ratio as a function of the pressures at the ejector entrance and exit ports. This graph, shown in Fig. 2.9, is not strictly a model, but it contains the performance characteristics of actual steam jet ejectors over a very wide range of operating parameters. El-Dessouky et al. [31] published empirical relations for steam ejectors, for ejector operation in critical and sub-critical modes. Other empirical models or semi-empirical models exist, but their application range is very restricted [35].

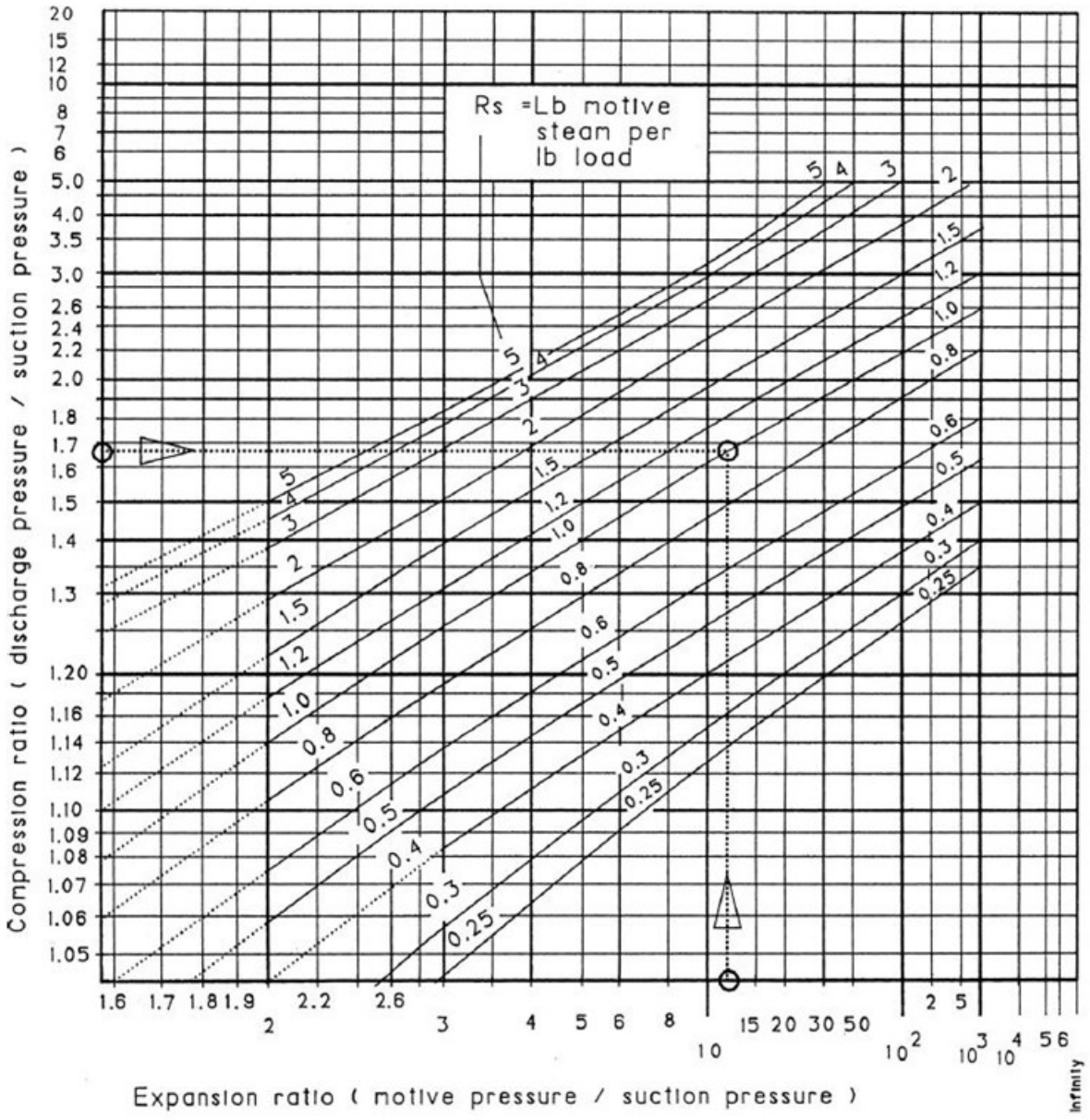

Fig. 2.10 Steam ejector composite behaviour [87]

2.4 Non-condensable gases and steam ejectors

From a very general perspective, there is interest in further understanding the performance of steam ejectors when the secondary fluid contains a mixture of steam and a non-condensable gas. In the case of steam power cycles, the overall cycle efficiency is a function of the pressure difference between the boiler and the condenser. The temperatures associated with these two pressure extremes define the Carnot thermal efficiency. Removing non-condensable gases from the condenser allows the minimum pressure to be slightly lower, thus increasing the overall efficiency of the Rankine power cycle. In that application and any application involving heat transfer where steam is the working fluid, the heat transfer coefficient is increased when non-condensable gases are removed. In the case of geothermal steam, currently an underutilized resource, it is important to know how to account for non-condensable gases both for ejector design purposes and operational reasons.

In the 1930s ejectors were already widely used in power plants for the exhausting of air from condensers and for the purpose of priming pumps [116]. Steam and air were the principal working fluids. Steam refrigeration systems had already been commercialized, but it was believed that refrigeration applications could be made more efficient and applied more widely if better information was available on the performance of ejectors using other working fluids, both condensable and non-condensable. Work and Haedrich completed an experimental study that included working fluids having molecular weights of 18 to 154 kg/kmol [116]. The experimental work was completed using two commercially available ejectors having different design compression ratios. The primary throat sizes were 0.063 inches (1.60 mm) and 0.104 inches (2.64 mm).

In 1946 the Heat Exchange Institute in the USA sponsored a research program to evaluate the behaviour of steam ejectors where the secondary fluid was not air [37]. Holton completed a study where the secondary fluid molecular weight ranged from 2 to 137 kg/kmol [37]. Steam was used as the primary fluid for all tests. Both single stage and two-stage commercial ejectors were included in the study. For the secondary fluid, 13 pure gases and 12 gas mixtures were evaluated. Fig. 2.11 shows the "entrainment ratio" on the vertical axis with the secondary fluid molecular weight on the horizontal axis. Here "entrainment ratio", which was also referred to as the "air

equivalent ratio" in the article, indicates the correction factor that should be applied to the expected secondary mass flow of a steam ejector that pumps air as the secondary fluid.

DeFrate and Hoerl [24] published a general ejector design graph, shown in Fig. 2.12, which has the advantage of showing ejector design characteristics over a wide range of parameter values for the ejector working fluid. The graph suggests that ejector geometry can be specified by knowing the ratio of two of the three port pressures, and by knowing the entrainment ratio. Although this work was not experimental, and was one of the first published results applying digital computers to ejector design, the text in the article suggests how to adapt the graphical results when the working fluids have dissimilar molecular weights.

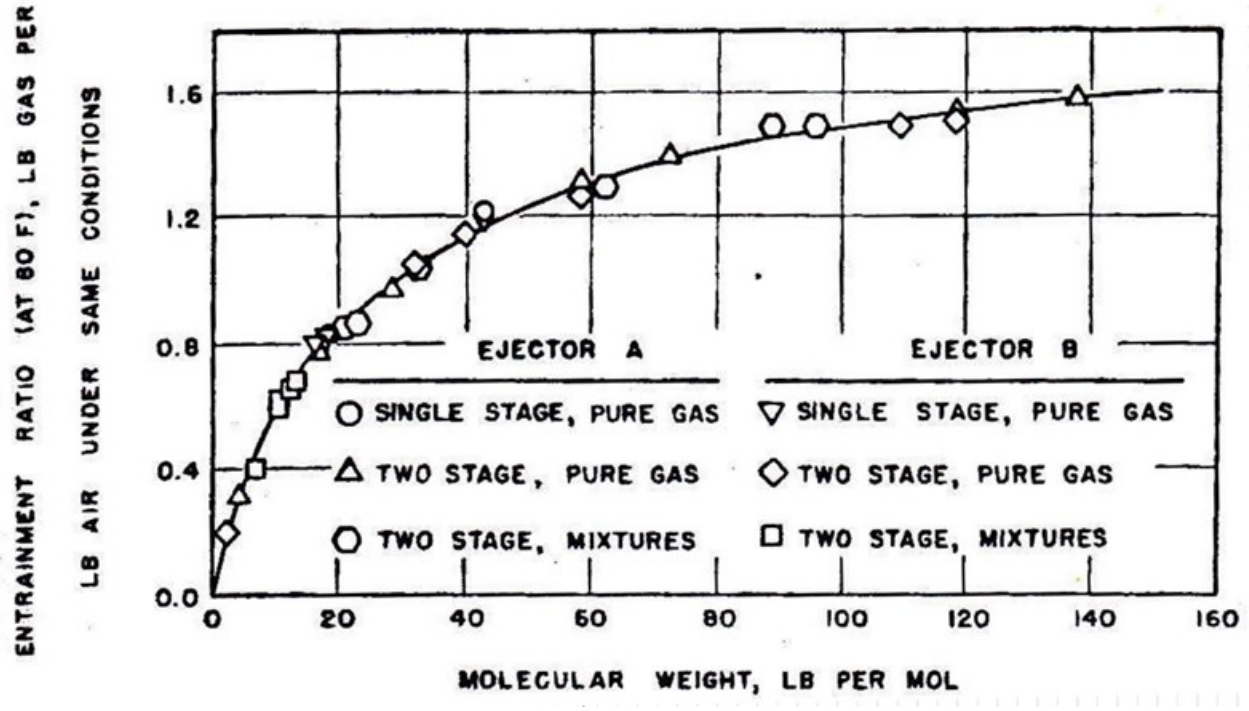

Fig. 2.11 Secondary flow correction factor compared with air [37]

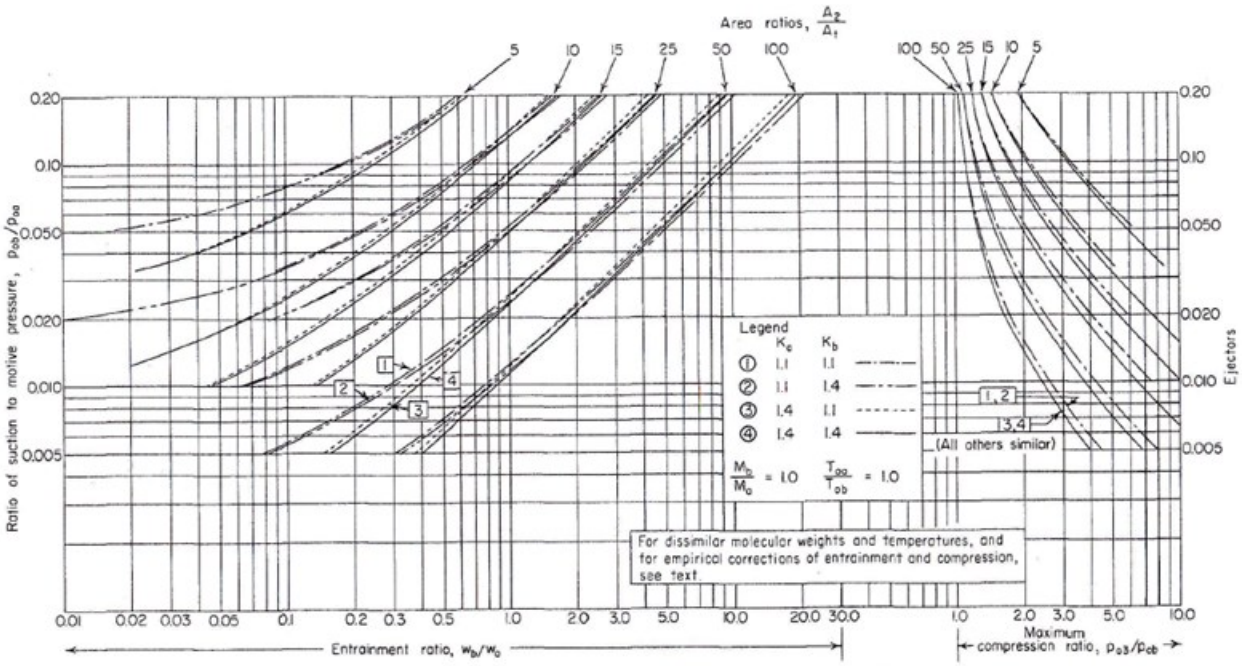

Fig. 6-72. Optimum design curves for single-stage ejectors. [*DeFrate and Hoerl, Chem. Eng. Progr.*, **55**, *Symp. Ser.* 21, 46 (1959).]

Fig. 2.12 Optimal ejector design curve [24]

CHAPTER 3 EXPERIMENTAL EVALUATION OF THE EFFECT OF ENTRAINED CO_2 ON A STEAM EJECTOR

3.1 Introduction

This chapter will describe the experimental portion of the doctoral project that was completed at CanmetENERGY, in Varennes, Quebec, Canada. The Varennes Research centre, belonging to Natural Resources Canada, is a research and technology facility specializing in the advancement of clean energy. The purpose of the experimental program, from the point of view of the current thesis, was to study the impact of entrained CO_2 on the performance of a steam ejector. It was also hoped that the experience gained on the experimental evaluation of combinations of steam and non-condensable gases would provide a solid foundation for future related work.

The test facilities made available to the project included technical support services and a custom test bench designed and constructed at CanmetENERGY, Varennes, Quebec, Canada. The test bench was part of the "Advanced Post-Combustion CO_2 Capture Technology" project, and is generally referred to as the APCCO2 test bench within the facility. The test bench has two main design objectives. First, to provide experimental validation to the characteristics of a steam activated ejector, where the secondary fluid is a mixture of steam and a non-condensable gas, in particular CO_2. Second, the test bench is to provide a simple yet versatile capability of simulating a desorption process, possibly with water and monoethanolamine (MEA) as the solvent solution. Other solvent solutions are also possible. In the work completed in the current doctoral project, the test bench was operated with pure steam as the motive fluid and with various combinations of steam and CO_2 as the ejector secondary fluid.

As a note to the reader, the presentation of the methods and results sections will not be strictly separate and independent from each other. This approach will allow some of the preliminary learning and general behaviour of the test bench to be incorporated into the methods section. The results section, thus lightened, will concentrate on the various parameters that affect the performance of the steam ejector.

3.2 Methods

This section is divided into four sections. First, the test bench will be described, followed by a description of the instrumentation and associated uncertainty. Next, the geometry of the ejectors and nozzles will be presented. Finally, the method used to create a typical performance curve will be discussed. Detailing the experimental procedure for the creation of a performance curve will necessarily involve describing the operation of the test bench, as well as discussing the principal parameters and measurements that will be referred to in the results section.

3.2.1 The experimental test bench

Fig. 3.1 presents a simplified schematic of the APCCO2 test bench. The figure does not

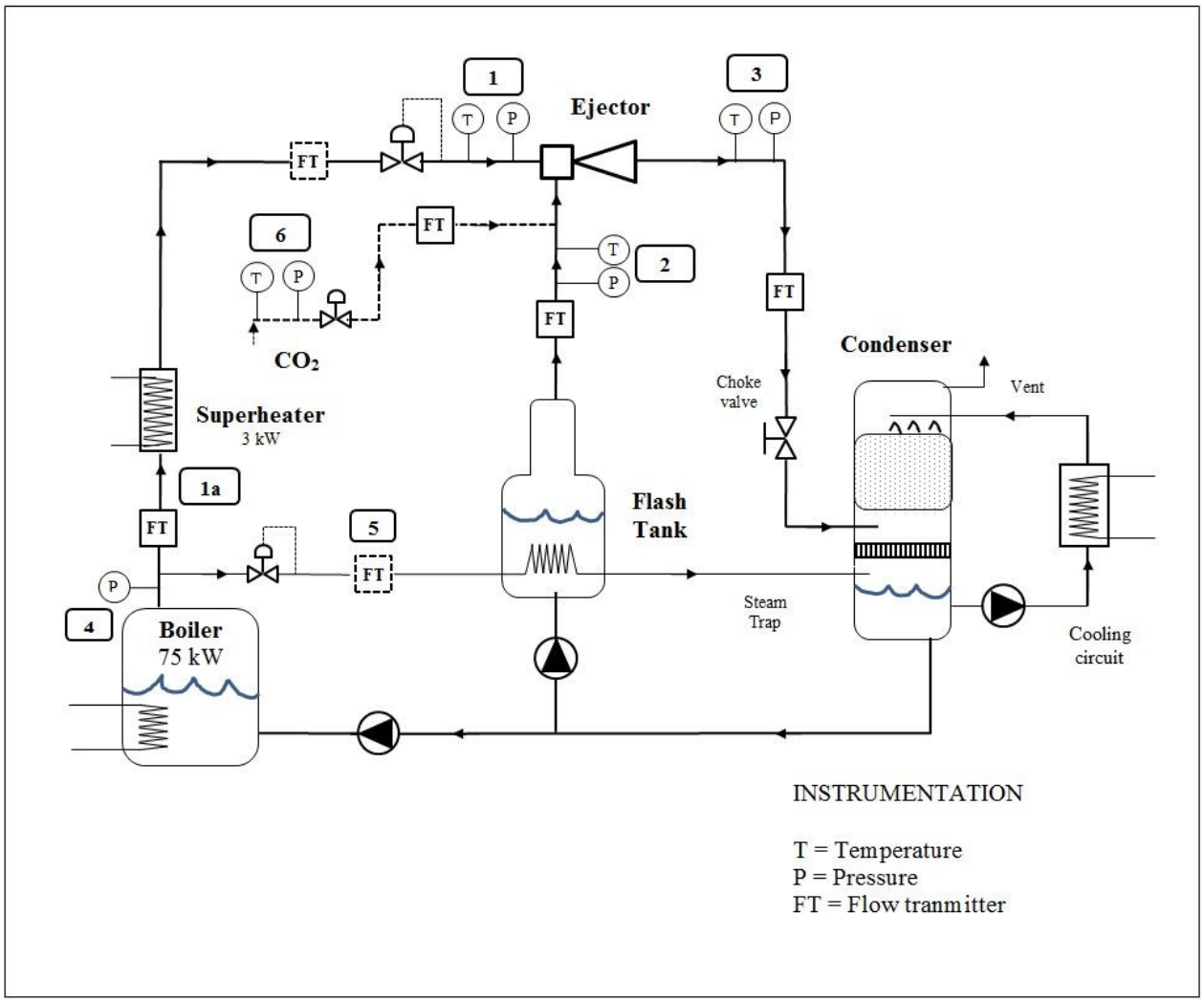

Fig. 3.1 Simplified APCCO2 process plan

show the safety valves, filling lines, drain lines and numerous control valves, check valves, manual shutoff valves, steam traps, strainers, and probe fittings that make up the test bench. Instead, the schematic concentrates on the operational elements that are directly referred to in the thesis. The same approach will be taken for the instrumentation, where the key measurement probes are noted in Fig. 3.1, and will be detailed in the instrumentation section.

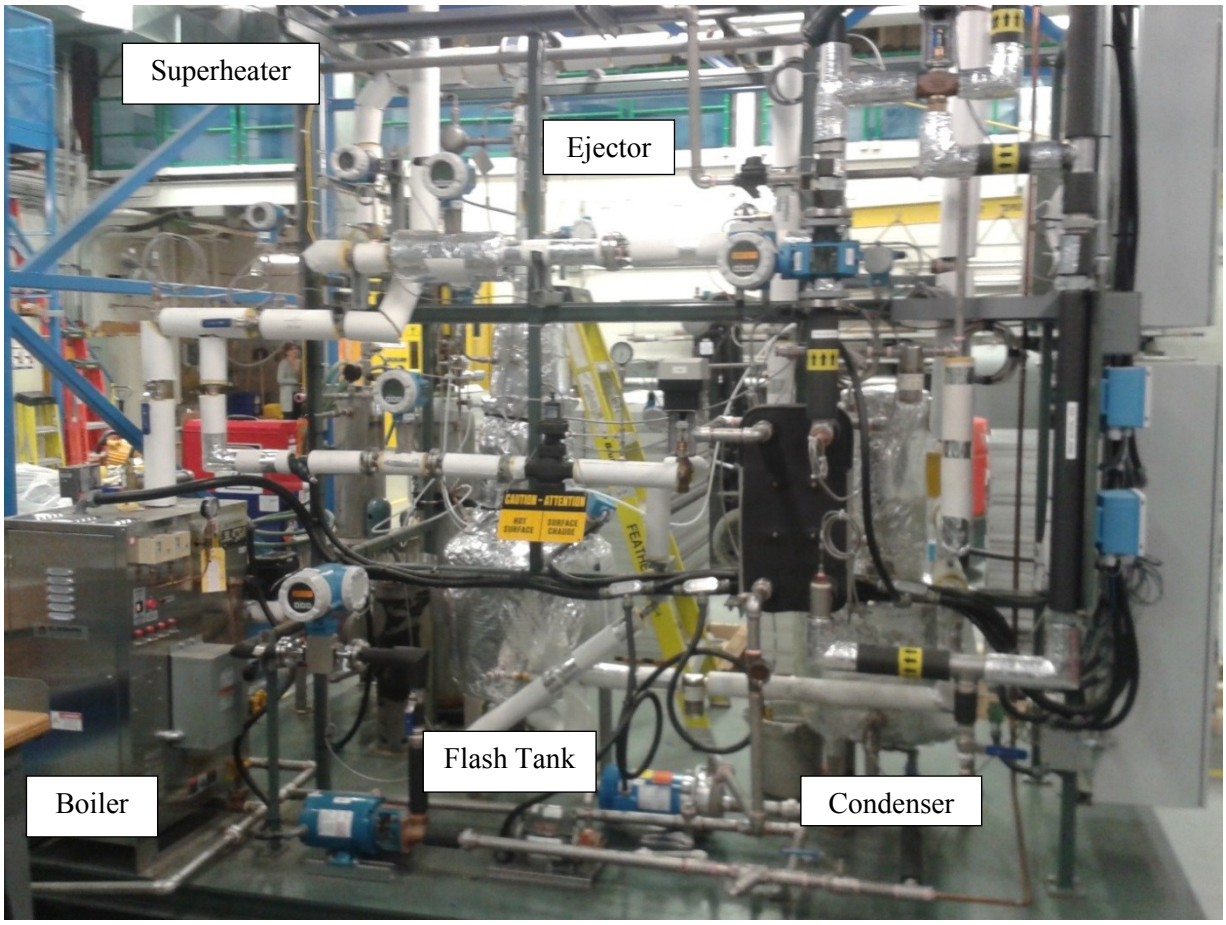

Fig. 3.2 Test bench, view facing the boiler

As shown in Fig. 3.2, the test bench is comprised of five major components: a boiler, superheater, ejector, flash tank and condenser. A 75 kW electric boiler, with a maximum pressure of 600 kPa, is the principal source of energy input to the test bench. The boiler has four electric elements which cycle on and off as part of the output pressure control system. The steam leaving the boiler is split into two branches. The main branch passes through a 3 kW superheater and continues until the ejector primary port. The secondary branch leaves the boiler and is directed toward the flash tank. This secondary branch of steam does not make contact with the fluid in the

flash tank, but rather is confined to a separate steam coil. The condensate leaving the steam coil passes through a steam trap where it is directed to the bottom portion of the condenser.

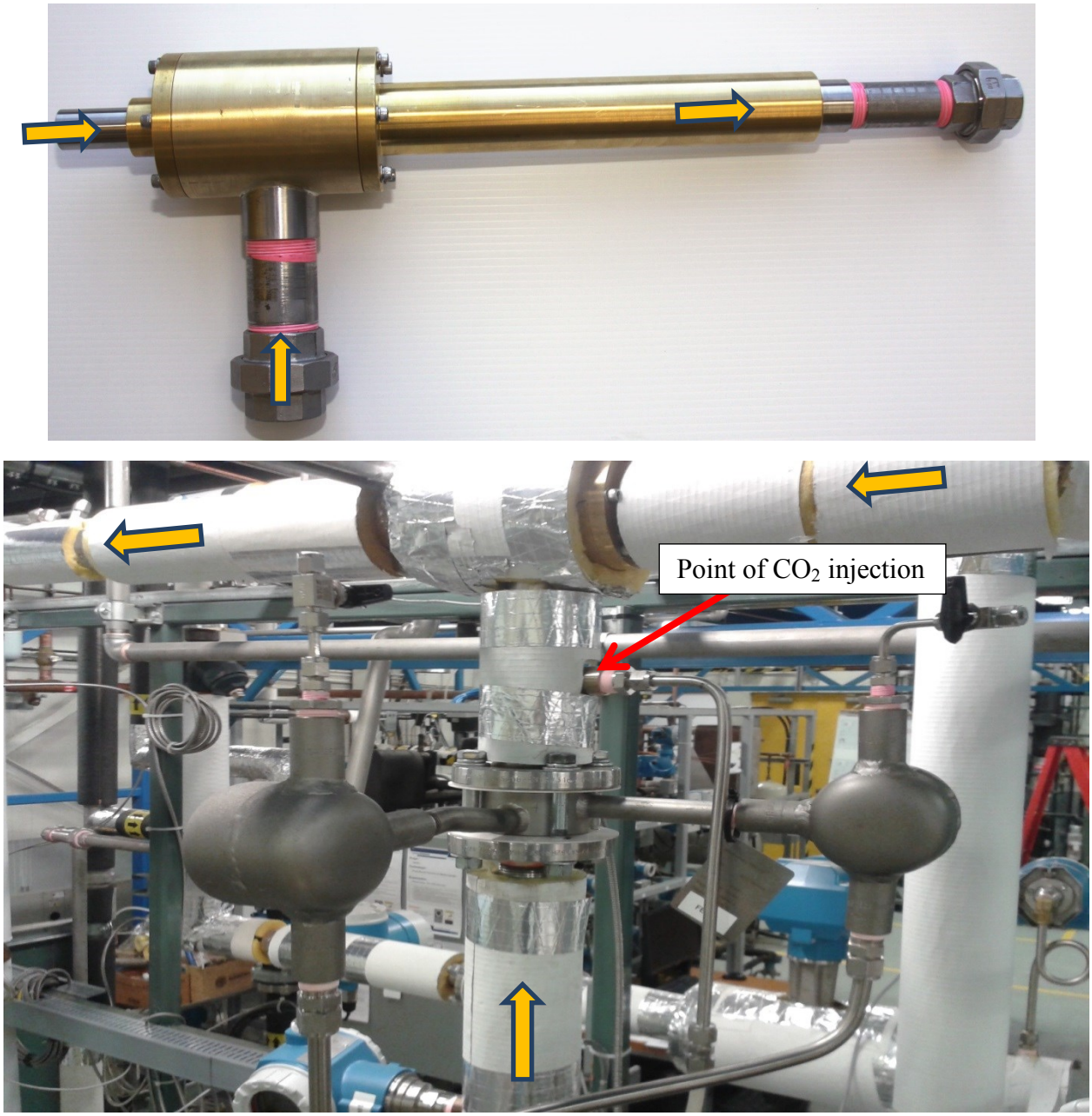

Fig. 3.3 Ejector no. 1 in top image; Installed ejector in bottom image.

The ejector is shown both at the top of Fig. 3.1 and Fig. 3.3. The ejector has three ports, two entering and one exiting, with the flow direction indicated in Fig. 3.3. The primary port receives steam that has passed from the boiler, through the superheater, and finally through a manually adjustable regulator immediately upstream of the ejector. The secondary port receives steam, or possibly a mixture of steam and CO_2, arriving from the flash tank. The exit of the ejector is connected to a direct contact atmospheric condenser. The manual valve between the ejector exit and the condenser, labelled in Fig. 3.1 "choke valve", plays an important role in the creation of performance, or "choking" curves. As is shown in Fig. 3.2 and Fig. 3.3, all of the potentially hot surfaces of the test bench are insulated to minimize heat exchange with the surroundings.

The condenser serves not only to condense all of the steam arriving from the ejector exit, but also to vent any CO_2 to the atmosphere. Fig. 3.4 shows another view of the test bench, here with the condenser at the left side of the image. The unit is of the direct contact type, where rising steam from the ejector is brought into direct contact with descending water, all within a ceramic wafer matrix. A separate cooling circuit, shown in Fig. 3.1, draws water from the base of the condenser, cools it as it passes through a heat exchanger, and returns it through spray nozzles to the top of the condenser. The heat removed from the heat exchanger is in turn passed to the ambient environment by way of another external cooling circuit, not shown in Fig. 3.1. As mentioned previously, the bottom of the condenser also receives the liquid condensate from the steam coil used to indirectly heat the flash tank. Connected to the bottom of the condenser is another line which both periodically returns water to the boiler, and maintains the liquid level in the flash tank. The condenser is also equipped with an automatic filling circuit, not shown in Fig. 3.1, where makeup water is periodically required to maintain the level in the base of the condenser. In the absence of injected CO_2 into the test bench, there is generally little flow through the condenser atmospheric vent piping. Venting will, however, exceptionally occur whenever the condenser temperature overshoots the target temperature of 90 °C and the water boils, or to handle the release of CO_2 during certain experiments.

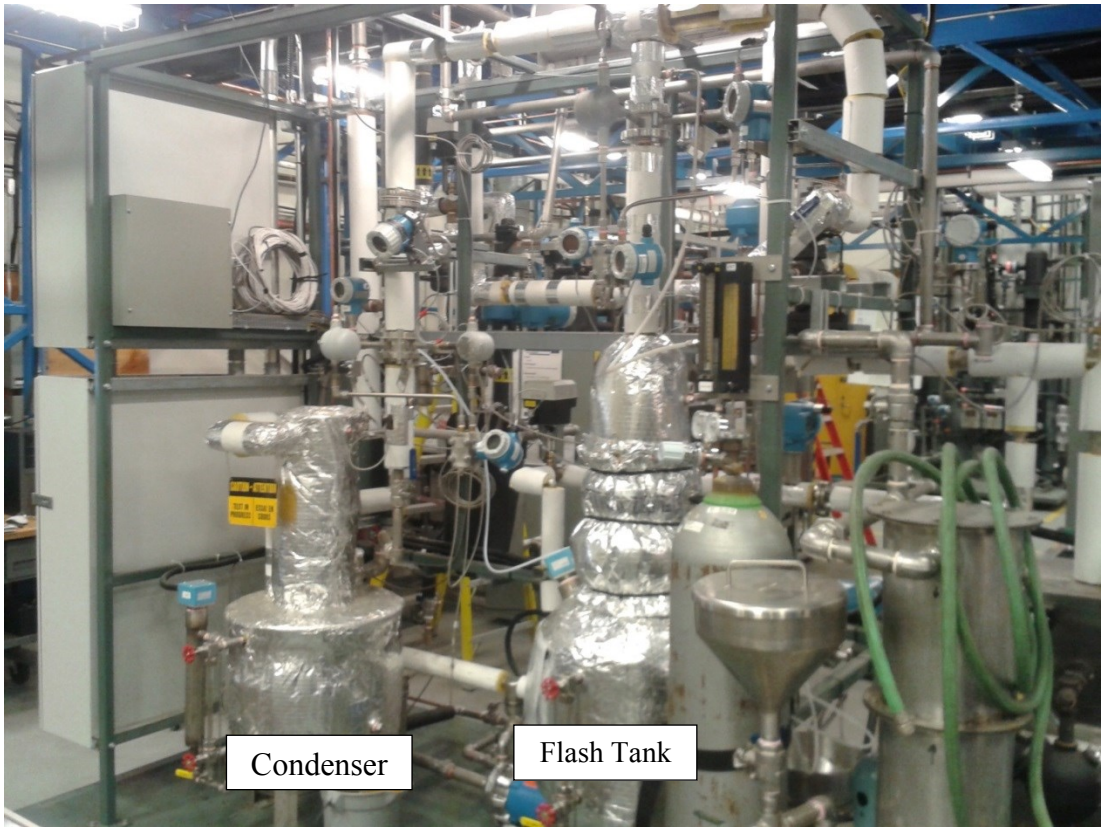

Fig. 3.4 Test bench, view facing the flash tank

In general, flash tanks are used to separate liquids from gases, either as a result of pressure drop or heating, or both. In the APCCO2 test bench, the purpose of the flash tank is to provide saturated steam or a mixture of steam and CO_2 to the ejector secondary port. This 160 litre vessel is controlled by pressure rather than temperature. The steam entering the heating coil is only that amount required to maintain the target pressure. The flash tank was designed to safely operate at the desired target pressure, covering a possible pressure range from below atmospheric up to the same maximum pressure as that of the boiler. The flash tank, condenser and boiler are each equipped with a sight glass for liquid level indication.

The CO_2 injection system consists of a pressurized CO_2 cylinder, adjustable regulator, a preheat circuit, a pressure and temperature probe, a rotameter calibrated for CO_2, and an injection point upstream of the ejector secondary port. In industry CO_2 metering systems typically use a heated tank regulator as a means of countering the effect of the rapid cooling of the CO_2 as it leaves the high pressure tank. For experimental purposes, the APCCO2 bench is equipped with a

small custom heat exchanger which preheats the CO_2 slightly in a separate loop passing through the liquid portion of the flash tank. The CO_2 then passes through a rotameter before being injected upstream of the ejector secondary port.

A graphical user interface, shown in Fig. 3.5. , allows the test bench operator to know the current state of each component, in particular the temperature, pressure and mass flow. The interface also provides warning and automatic shut off features to protect both the operator and test bench equipment. Troubleshooting is possible using the interface, as individual temperatures or pressures can be plotted as a function of time. Access to the data acquisition system is possible through a special report building interface page. Typically, the report that is completed at the end of a series of experiments is exported and analyzed offline with Microsoft Excel.

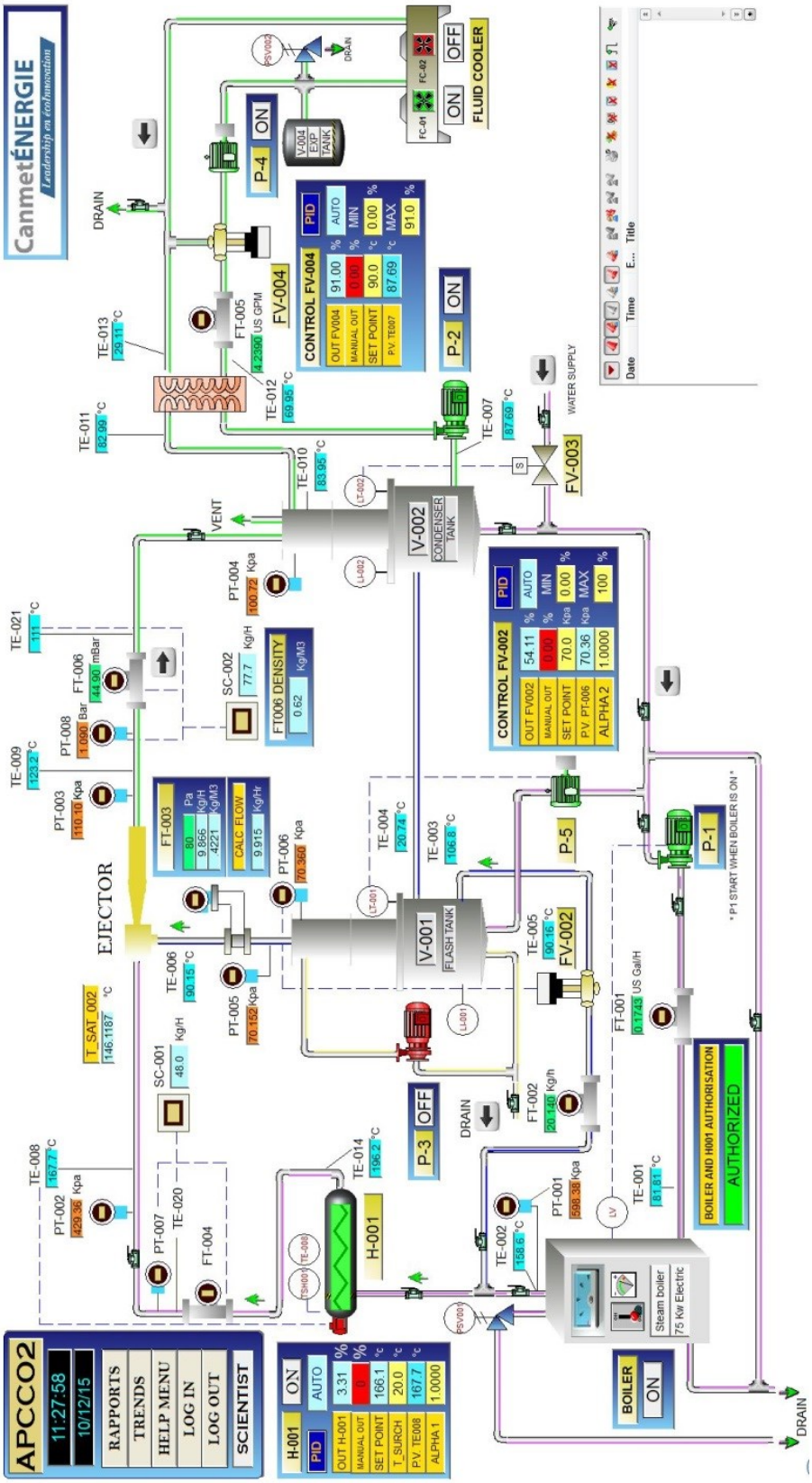

Fig. 3.5 The graphical user interface of the APCCO2 test bench

3.2.2 Instrumentation and measurement uncertainty

The APCCO2 test bench is well equipped with temperature and pressure probes. Fig. 3.1 only shows the probes that are referred to within this thesis. Table 3.1 indicates where these selected probes are located in Fig. 3.1, as well the property that they measure, the probe label, and additional comments. The flow meters are identified as either being of the vortex or orifice type. These same probes will again be referred to in the results section. The flow meters indicated with dashed lines in Fig. 3.1 refer to the earlier location of the meters in the test bench. The final location of each flow meter is indicated with images drawn in solid lines in Fig. 3.1. The reason for the movement of some flowmeters during the project is that they are very sensitive to both a lower and a higher flow range. As there was an evolution in the ejector geometry used over the life of the project, and an associated change in the mass flow rates, the flow meters were adapted or relocated accordingly.

Table 3.1 Selected probe identification guide

Location no.	Location description	Property	Probe	Comment
1	Primary	temperature	TE008	
1	Primary	Pressure	PT002	
1	Primary	mass flow	GF001	vortex type, ejector no. 1, no. 2
1a	Primary	mass flow	FT002	vortex type, ejector no. 3
2	secondary	temperature	TE006	
2	secondary	Pressure	PT006	
2	secondary	mass flow	FT003	
3	Exit	temperature	TE009	
3	Exit	Pressure	PT003	
3	Exit	mass flow	GF002	orifice type
3	Exit	mass flow	FT006	orifice type, pressure drop used for offline
4	Boiler	Pressure	PT001	
5	steam coil	mass flow	FT002	ejector no. 1, no. 2
6	CO_2 injection	temperature	TE004	
6	CO_2 injection	Pressure	PT004	
6	CO_2 injection	mass flow	Rota_2	volumetric flow, must be converted to mass flow

Table 3.2 provides more specific information about the probes referred to in Fig. 3.1. When ordering flow meters, in this case from Endress+Hauser, it is important to specify the intended lower and upper flow range. In the case of orifice flow meters, this flow information will be used by the manufacturer to determine the orifice hole diameter that is most appropriate. The "uncertainty" values shown in Table 3.2 are fairly conservative estimates of the reading error. Depending on the absolute values of the mass flow, it is possible for the flow meters to produce readings closer to the true value.

Table 3.2 Manufacturers' information and uncertainty for selected probes

Ref. no.	Probe	Manufacturer/Description	Uncertainty
1	TE008	1/10 DIN RTD, bayonet style, Dia. = 0.188 in., L = 7.5 in	+/- 0.1 °C
1	PT002	Endress+Hauser, PMP71-UBC2P11RAAAA, 0-10 bar (150 psia)	+/- 0.5%
1	GF001	Endress+Hauser, Prowirl 73F25, DN25, 1", #73F25-SK4AA5NAB4AW	+/- 2%
1a	FT002	E+H, Prowirl 73F15, DN15, 1/2", #73F15-SK4AA5NAB4AW	+/- 2%
2	TE006	1/10 DIN RTD, bayonet style, Dia. = 0.188 in., L = 7.5 in	+/- 0.1 °C
2	PT006	Endress+Hauser, PMP71-UBC2H11RAAAA, 0-1 bar (15 psia)	+/- 0.5%
2	FT003	Endress & Hauser, Deltatop DO62C (DP/O corner tap / single bore)	+/- 1.5%
3	TE009	1/10 DIN RTD, bayonet style, Dia. = 0.188 in., L = 7.5 in	+/- 0.1 °C
3	PT003	Endress+Hauser, PMP71-UBC2M11RAAAA, 0-4 bar (60 psia)	+/- 0.5%
3	GF002	Endress & Hauser, Deltatop DO62C (DP/O corner tap / single bore)	+/- 1.5%
3	FT006	note: This is the same physical meter as GF002. Here delta P is used.	+/- 1.5%
4	PT001	Endress+Hauser, PMP71-UBC2P11RAAAA, 0-10 bar (150 psia)	+/- 0.5%
5	FT002	E+H, Prowirl 73F15, DN15, 1/2", #73F15-SK4AA5NAB4AW	+/- 2%
6	TE004	1/10 DIN RTD, bayonet style, Dia. = 0.188 in., L = 7.5 in	+/- 0.1 °C
6	PT004	Endress+Hauser, PMP71-UBC2M11RAAAA, 0-4 bar (60 psia)	+/- 0.5%
6	Rota_2	Cole-Parmer, T-32605-71, 0 – 110 sL/min CO_2	+/- 5% Full scale.

3.2.3 Ejector and nozzle geometry

Table 3.3 lists the design input values that were the starting point for each of the three ejectors used during the experimental program. Each ejector was designed using a 1D detailed computational model which is able to do both design and simulation [79]. The model had to be adapted for the purpose of modelling steam, as the model was originally developed for working fluids more common in refrigeration applications. For design purposes it was assumed that the primary and secondary fluids were at saturation conditions. The mass flow units in Table 3.3 are shown in kg/h, as these units will be used throughout the thesis. The notes immediately following the table indicate the original values and units in the ejector design. The ejector exit pressures noted in the table were not strictly design input, but were noted as a theoretical output for information purposes.

Table 3.3 Ejector design input data

Ejector	T1 °C	P1 kPa	m1 kg/h	T2 °C	P2 kPa	m2 kg/h	P_exit kPa	Notes
1	133.5	300	55.2	90	70.2	22.1	145.5	1
2	147.9	450	72.0	90	70.2	28.8	~150	2
3	147.9	450	28.8	90	70.2	14.4	156	3

Notes:

1. The design value of the secondary mass flow, m2, was originally based on a target of 14 kW of thermal power in the flash tank, where the latent heat of vaporization at 90 °C of 2283 kJ/kg implies a secondary mass flow of 0.00613 kg/s or 22.1 kg/h.
2. The original input values for the primary and secondary mass flow rates were as follows: m1 = 0.020 kg/s, m2 = 0.008 kg/s.
3. The original input was m1 = 0.008 kg/s, m2 = 0.004 kg/s.

During the course of the experimental program there was a progressive evolution in the design of the ejector body and the primary nozzle. Fig. 3.6 defines the most important dimensional elements, including important lengths, diameters and the associated half-angles.

Table 3.4 presents the ejector body dimensions for the three ejectors tested, while Table 3.5 lists the primary nozzle dimensions. Each ejector was designed with a matching primary nozzle. Specifically, ejector no. 1 is matched with nozzle v1, ejector no. 2 with nozzle v2.1, and ejector no. 3 with nozzle v3.1.B. In the case of ejector no. 2, there were in total three nozzles evaluated: v2.1, v2.2, and v2.3. For ejector no. 3 there were two nozzles evaluated: v3.1.B and v3.2.B. Fig. 3.7 shows all of the nozzles evaluated during the test program, showing their relative proportions. In the results section the reasons for the evolution in ejector geometry will be discussed. The evolving design geometry generally occurred in response to trying to match the ejector operational characteristics to those of the experimental test bench, while at the same time aiming to produce the desired ejector performance curves in the parameter range of interest.

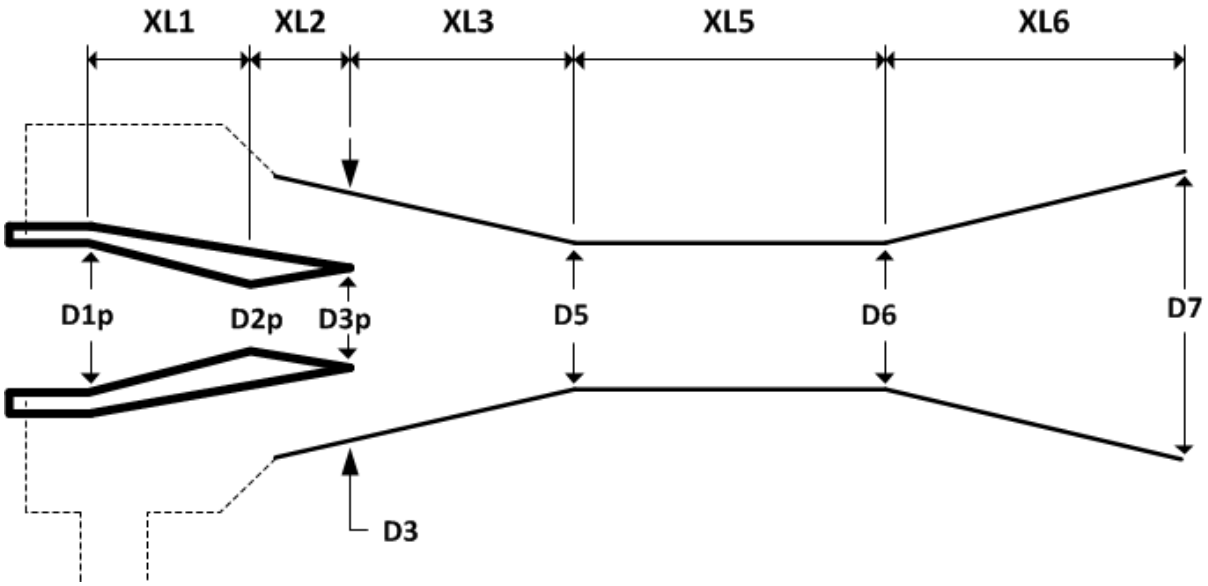

Fig. 3.6 Ejector geometry

Table 3.4 Ejector body dimensions

Ejector Body	Convergent Mixing	Constant Area	Diffuser
1	D3 = 28.30 mm D5 = 18.00 mm XL3 = 44.14 mm Angle = 6.7°	D5 = 18.00 mm D6 = 18.00 mm XL5 = 90.00 mm	D6 = 18.00 mm D7 = 25.30 mm XL6 = 110.00 mm Angle = 1.9°
2	D3 = 14.50 mm D5 = 14.00 mm XL3 = 10.00 mm Angle = 1.5°	D5 = 14.00 mm D6 = 14.00 mm XL5 = 95.00 mm	D6 = 14.00 mm D7 = 25.41 mm XL6 = 80.00 mm Angle = 4.08°
3	D3 = 12.30 mm D5 = 9.05 mm XL3 = 20.00 mm Angle = 4.0°	D5 = 9.50 mm D6 = 9.50 mm XL5 = 58.00 mm	D6 = 9.50 mm D7 = 28.97 mm XL6 = 139.24 mm Angle = 4.0°

Table 3.5 Primary nozzle dimensions

Nozzle	Primary Convergent	Primary Divergent	Nozzle Exterior
v1	D1p = 22.22 mm D2p = 8.00 mm XL1 = 31.80 mm Angle = 12.6°	D2p = 8.00 mm D3p = 14.00 mm XL2 = 57.20 mm Angle = 3.0°	D3p_ext = 14.00 mm Angle 4.9°
v2.1	D1p = 22.22 mm D2p = 6.60 mm XL1 = 34.66 mm Angle = 12.7°	D2p = 6.60 mm D3p = 9.00 mm XL2 = 20.0 mm Angle = 3.43°	D3p_ext = 9.20 mm Angle 12.1°
v2.2	D1p = 22.22 mm D2p = 4.90 mm XL1 = 38.44 mm Angle = 12.68°	D2p = 4.90 mm D3p = 9.00 mm XL2 = 34.17 mm Angle = 3.43°	D3p_ext = 9.20 mm Angle 8.8°
v2.3	D1p = 22.22 mm D2p = 4.90 mm XL1 = 38.44 mm Angle = 12.68°	D2p = 4.90 mm D3p = 9.00 mm XL2 = 34.17 mm Angle = 3.43°	D3p_ext = 9.20 mm Angle 2.0°
v3.1.B	D1p = 22.22 mm D2p = 4.60 mm XL1 = 67.54 mm Angle = 7.43°	D2p = 4.60 mm D3p = 6.17 mm XL2 = 15.01 mm Angle = 3.0°	D3p_ext = 6.68 mm Angle 4.0°
v3.2.B	D1p = 22.22 mm D2p = 4.24 mm XL1 = 64.21 mm Angle = 7.97°	D2p = 4.24 mm D3p = 6.17 mm XL2 = 18.34 mm Angle = 3.0°	D3p_ext = 6.68 mm Angle 4.0°

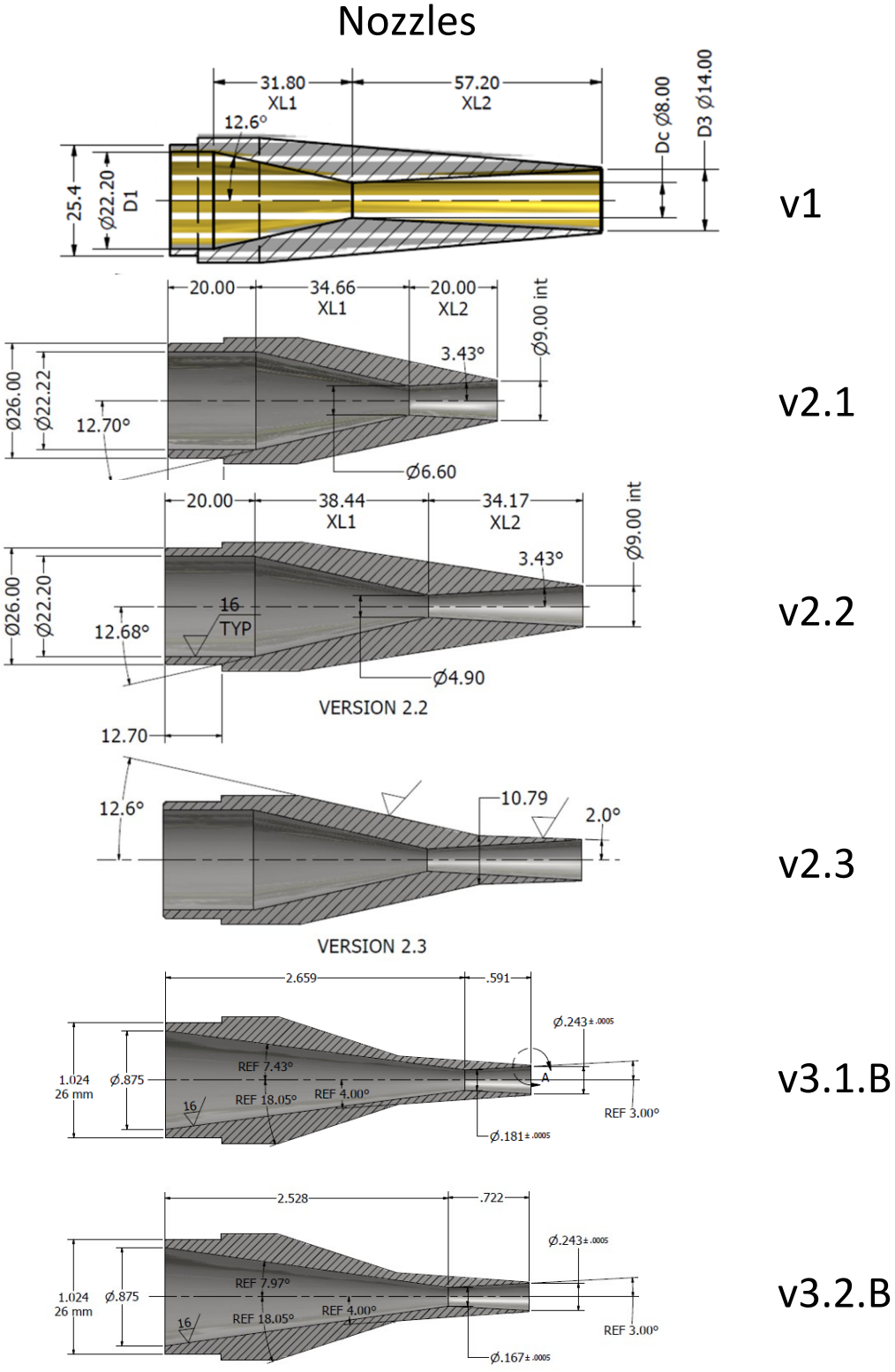

Fig. 3.7 Nozzle geometry evolution

3.2.4 Preparation of a typical ejector performance curve

The principal method that will be used in this experimental project is the creation of a performance curve, which could also be called a "choking curve". A performance curve is a chart showing the entrainment ratio, m2/m1, on the vertical axis and the ejector exit pressure, or alternatively the compression ratio P_exit/P_sec, shown on the horizontal axis. This method will begin by explaining the general operation of the test bench, followed by describing how the collected information is converted into the desired performance curve. The figures that are presented here were taken from the early part of the experimental program, before the choices concerning the target amount of superheat, ejector input conditions and ejector geometry were finalized. Although the method described here is typical of the data to be discussed in the results section, these figures also contain some specific details that will be referred to again later. In the method described here, only pure steam is used for the primary and secondary fluids.

The first step in preparing a performance curve is to verify that the appropriate ejector body and nozzle are installed in the test bench. The primary nozzle is positioned such that the desired value of XL3 is obtained. This parameter, which characterizes the nozzle position, is shown in Fig. 3.6. Table 3.4 lists the nominal design value XL3 for each of the three ejectors under the heading "Convergent Mixing". In the case of the current method description, the ejector number 2 is chosen, with nozzle v2.3 installed such that the nozzle is positioned with XL3 = 23 mm. Once it is verified that the ejector and nozzle are in position, the next step is to turn on the boiler. The pump which is part of the circuit designed to remove heat from the condenser is then turned on. It is verified that the manual valve at the ejector exit is in the fully open position. After having reached operating pressure, the main boiler valve is opened.

While boiler steam begins circulating through the test bench, the target operating parameters are set. These include the primary regulator pressure, the amount of superheat in the primary steam, the secondary pressure in the flash tank and the condenser target temperature. Given that the condenser downstream of the ejector operates at atmospheric pressure, the chosen temperature of the condenser basically determines the temperature of the water returning to the boiler. Experience has found that a temperature of 90 °C gives the most stable boiler pressure. To minimize the risk of damaging the primary steam superheater, the element is not turned on until

the primary mass flow stabilizes. With all of the key parameters set at their target values, the test bench is left in operation until steady state conditions are achieved.

Once the test bench is at steady state conditions, the time is noted. In the case of the November 24, 2015 test, the test bench was at steady state conditions at 16h00. Once the current state has been maintained for ten minutes, the manual valve at the ejector exit is closed slightly, with the goal of increasing the exit pressure by a small but noticeable amount. The time and nominal exit pressure are noted. The exit pressure is thus increased incrementally in timed intervals of at least ten minutes until the final target pressure is reached. The final pressure is chosen to be just before the ejector cut-off pressure, the pressure at which some of the primary steam will start entering the secondary port of the ejector. In general, it is possible to conduct several performance tests in series, as long as sufficient time is left between each trial setup for the test bench to reach steady state conditions. In the current case of the November 24, 2015 test, only one set of conditions is being evaluated. After completing the test, the ejector exit valve is completely opened and the superheater is shut off. The boiler is then shut off, followed by closing the boiler exit valve, and shutting off the pump circuit that removes heat from the condenser. A file is then saved with the data acquisition system, from which the analysis of the results will be completed at a later time using Excel to organize the raw data. In the following text the standard family of curves of temperature, pressure, and mass flow will be described, and how the associated information will be used to produce the performance curve.

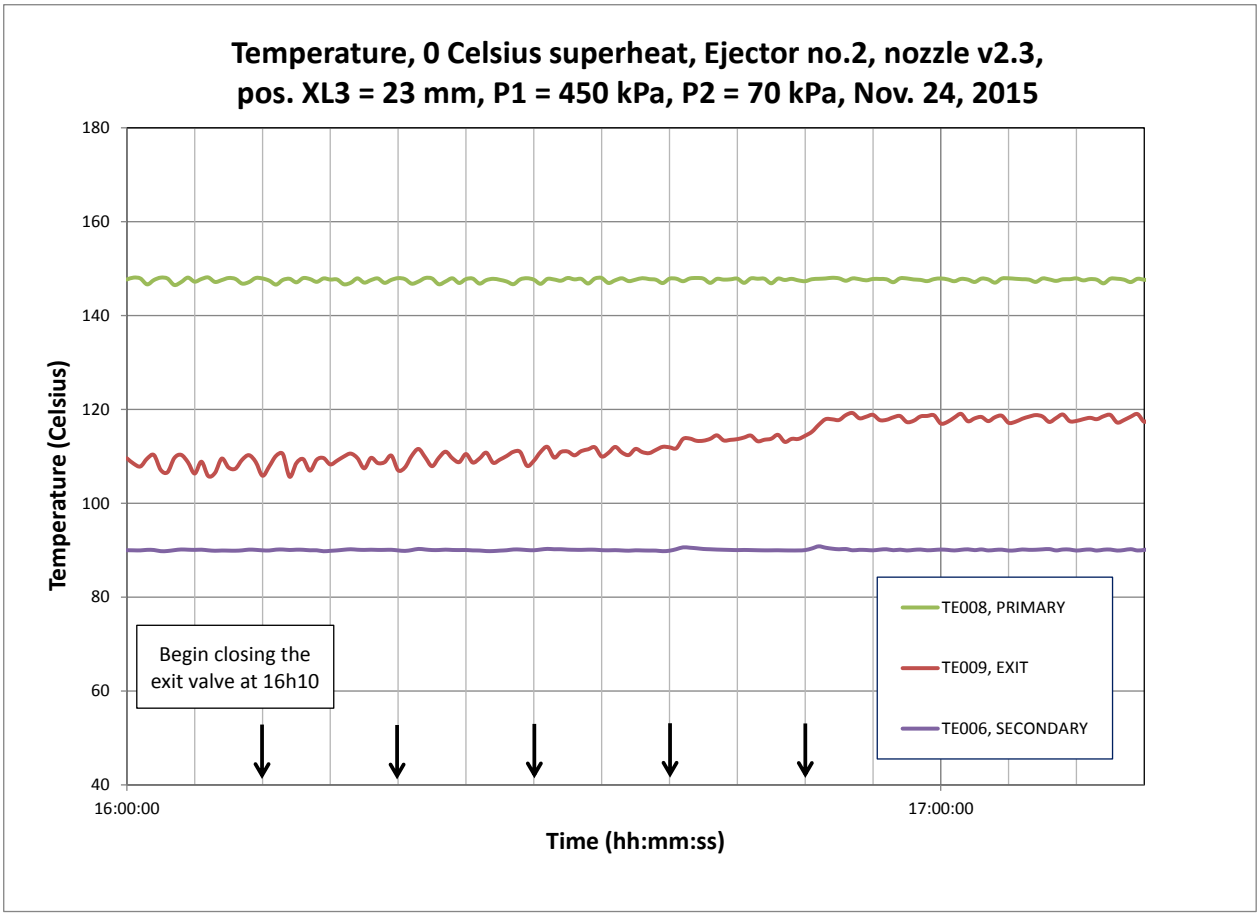

Fig. 3.8 Ejector temperatures, November 24, 2015

Fig. 3.8 shows the temperature progression throughout the test. Each of the arrows in the figure indicates that the ejector exit valve was slightly closed at that time. The uppermost curve shows the primary temperature, labelled "TE008, PRIMARY" in the chart legend. The temperature of the steam leaving the ejector, labelled "TE009, EXIT" is seen to rise progressively, which will be seen to be associated with the increasing amount of hotter primary steam as the secondary mass flow decreases.

Fig. 3.9 shows the pressure progression throughout the experiment. The top curve shows the pressure variations very close to the boiler, labelled "PT001, BOILER". The variations are the effect of the cycling on and off of the four electric heating elements in the boiler, combined with the effect of the cycles of the automatic refilling of the boiler by the boiler pump. The water pumped into the boiler comes from the condenser, and thus this introduction of slightly cooler water, typically at 90 °C, causes further pressure variations in the boiler pressure. In Fig. 3.9, the

second curve from the top, "PT002, PRIMARY", is the pressure after the primary pressure regulator, and is essentially the pressure of the primary steam at the ejector entrance. It can be noticed in the third curve from the top of the chart, "PT003, EXIT", that the pressure begins to rise in steps corresponding to the changing exit valve position as the performance test progresses. In the case of the November 24, 2015 test, the following ejector exit pressures averages and corresponding times were noted: 112 kPa at 16h10, 113 kPa at 16h20, 115 kPa at 16h30, 120 kPa at 16h40 and finally 125 kPa at 16h50. Fig. 3.10 presents a closer look at the ejector exit curve pressure for "PT003, EXIT", changing the vertical pressure scale to more clearly see the trend.

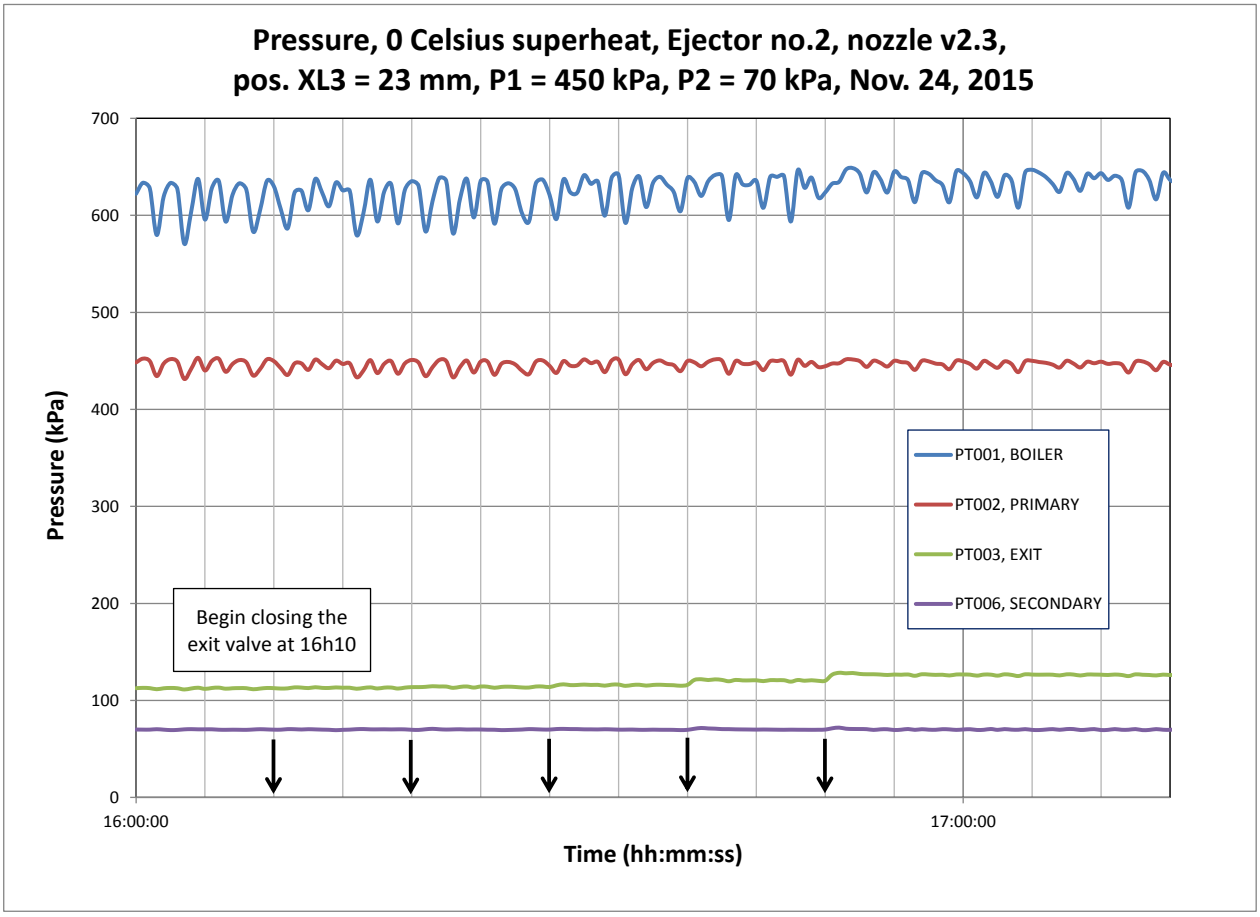

Fig. 3.9 Ejector pressures, November 24, 2015

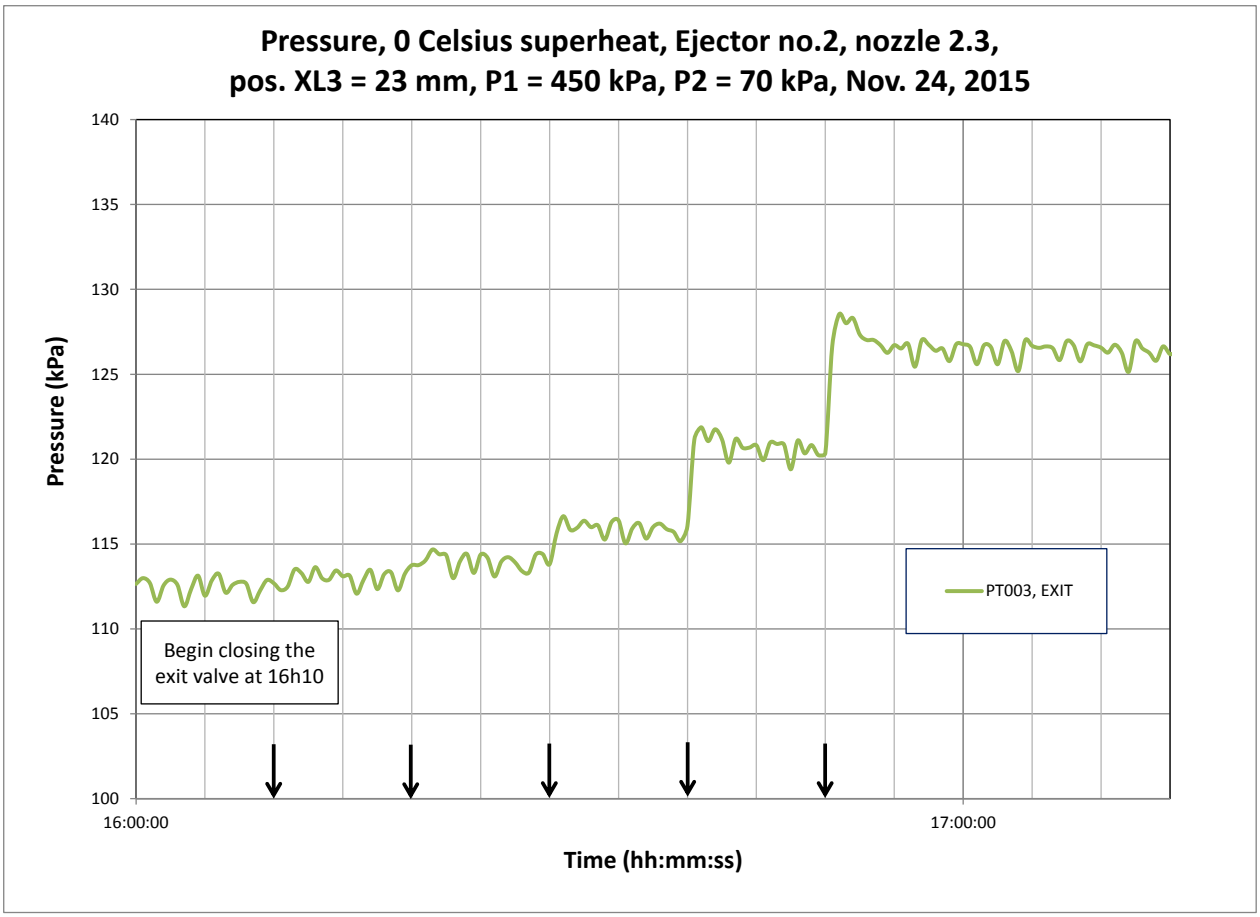

Fig. 3.10 Ejector exit pressure, November 24, 2015

Fig. 3.11 shows the mass flow recorded during the experiment, as well as a few additional flow parameters created to help judge the quality of the overall mass balance. Three curves show respectively the primary, secondary and exit mass flows: "GF001, PRIMARY", "FT003, SEC", and "GF002, EXIT". It is worth noting here that it is always good experimental practice to retain the information concerning the theoretical parameter that is desired, and some identification of the measurement device that was used to measure the parameter. Although this may appear to add extra unnecessary information, which is not always of theoretical interest, it is essential in building confidence in the experimental results and troubleshooting specific instrumentation errors or detecting measurement drift.

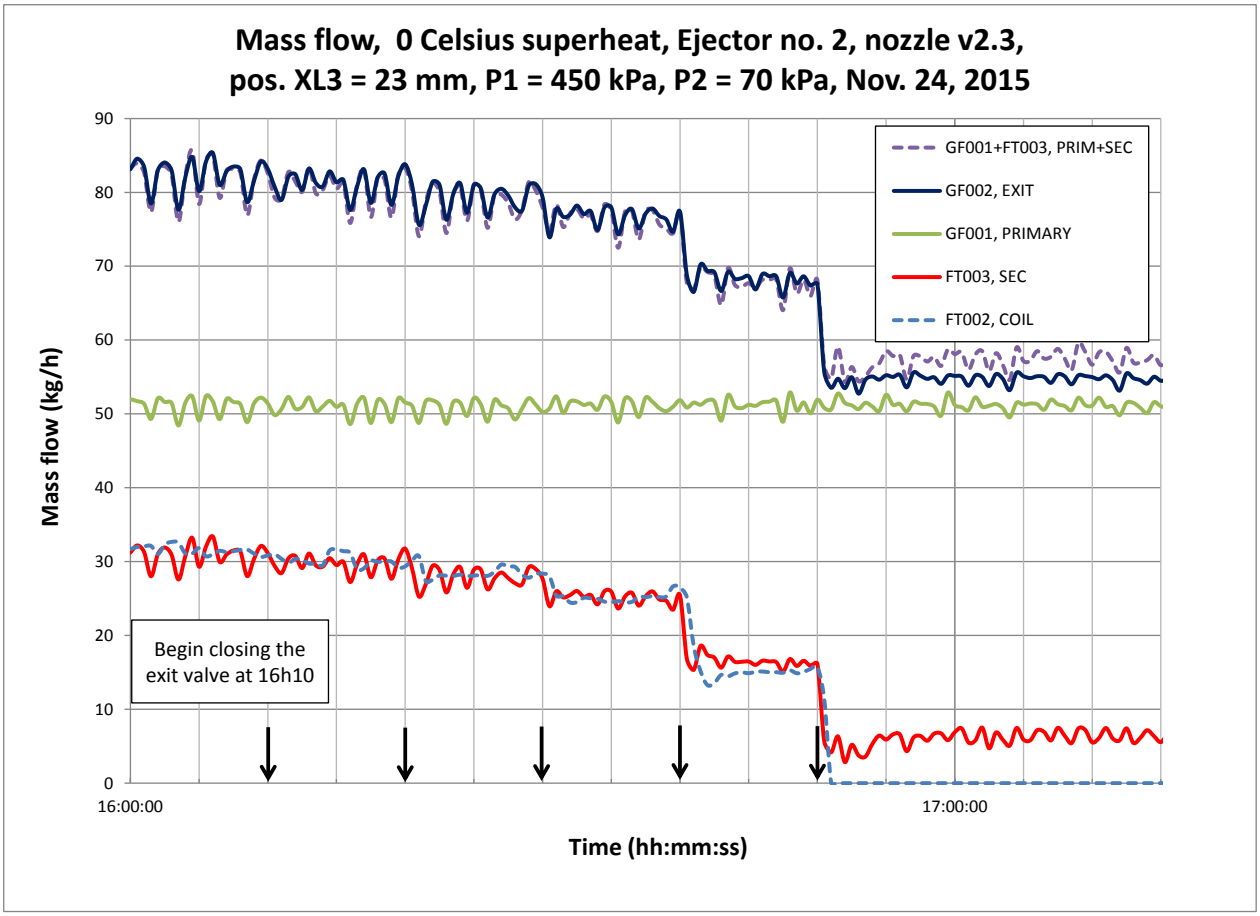

Fig. 3.11 Mass flows, November 24, 2015

Additional useful information is also shown in Fig. 3.11, beyond the three main mass flows. The curve "FT002, COIL" is seen to follow very closely the flow rate of the secondary steam, "FT003, SEC". It turns out that the mass flow rate of steam used to heat the flash tank, "FT002, COIL", for flow rates above approximately 8 to 10 kg/hr, gives an excellent verification of the orifice flow meter "FT003", used to measure the secondary steam flow. There are three main reasons for the very close agreement between the steam coil mass flow rate and the ejector secondary mass flow rate. First, at this point in the experimental project the flash tank was very well insulated, and condensing steam in the coil is directly responsible for the evaporation of the water in the flash tank. Second, although the pressure of the steam in the steam coil is at a slightly higher pressure that the operating pressure of the flash tank, the latent heat of evaporation is almost constant within this pressure range. Third, for most of the experiment both flow meters are operating within their respective appropriate ranges.

In the uppermost portion of the Fig. 3.11 are two almost overlapping curves. "GF002, EXIT" is the mass flow as measured at the ejector exit. The curve identified "GF001+FT003, PRIM+SEC" is prepared within Excel as a visual indication of the quality of the overall ejector mass flow balance. It is simply the mathematical sum of the measured primary flow "GF001, PRIMARY" and the secondary flow "FT003, SEC". In the case of the November 24, 2015 experiment, the overall mass balance is excellent for the purposes of preparing a performance curve.

Table 3.6 Selected raw data, November 24, 2015

	Primary mass flow	Exit mass flow	Secondary mass flow	Deduced Secondary mass flow	Entrainmnent ratio based on SEC*	Entrainmnent ratio based on SEC	Exit pressure	Secondary pressure
	GF001 (kg/h)	GF002 (kg/h)	SEC FT003_MASS (kg/h)	SEC* GF002-GF001 (kg/h)	SEC*/GF001	SEC/GF001	PT003 (kPa)	PT006 (kPa)
average (-->)	51.1	82.5	30.9	31.4	0.61	0.60	112.5	70.0
std. dev.(-->)	1.3	2.1	1.6	1.1	0.02	0.02	0.5	0.3
TIMESTAMP								
16:02:00	52.1	83.0	31.0	30.9	0.59	0.60	112.6	69.9
16:02:30	51.6	84.0	31.9	32.4	0.63	0.62	112.9	69.5
16:03:00	51.5	83.0	30.9	31.5	0.61	0.60	112.6	69.7
16:03:30	48.4	77.6	27.6	29.2	0.60	0.57	111.3	70.2
16:04:00	51.5	82.1	30.8	30.5	0.59	0.60	112.3	70.4
16:04:30	52.4	84.8	33.2	32.4	0.62	0.63	113.1	70.2
16:05:00	49.1	80.2	29.3	31.0	0.63	0.60	112.0	70.3
16:05:30	52.4	84.1	32.0	31.7	0.61	0.61	112.9	70.3
16:06:00	51.7	85.3	33.4	33.7	0.65	0.65	113.2	69.9
16:06:30	49.3	81.0	30.0	31.7	0.64	0.61	112.1	69.8
16:07:00	52.0	82.9	31.0	30.8	0.59	0.60	112.6	69.9
16:07:30	51.6	83.5	31.5	31.9	0.62	0.61	112.8	69.8
16:08:00	51.3	83.1	31.4	31.8	0.62	0.61	112.7	69.7
16:08:30	48.9	78.7	28.0	29.8	0.61	0.57	111.6	70.1
16:09:00	51.4	81.6	30.4	30.1	0.59	0.59	112.3	70.4
16:09:30	52.2	84.2	32.1	32.0	0.61	0.62	112.9	70.2
16:10:00	51.4	83.2	31.2	31.8	0.62	0.61	112.7	69.9

Table 3.6 lists some of the details, for the condition of the ejector exit valve fully open, of the data file associated with the November 24, 2015 experiment. The seventeen values, indicated under the TIMESTAMP column on the left side of the table, are each associated with 37 values

captured by the data acquisition system every 30 seconds. Between each ten minute time block from the experiment for a fixed exit valve position, horizontal lines in the data file which indicate that the test bench is not at steady state are removed from the data set. Table 3.6 shows the stable process starting from 16:02:00, which is the first value under the leftmost TIMESTAMP column. The average and the standard deviation are calculated for all of the data columns. The first three data columns show the primary mass flow, exit mass flow and secondary mass flow respectively. The column identified as "SEC*" is deduced from the difference between the exit and primary mass flow values, here GF002-GF001. In the current case the values of SEC and SEC* are almost identical. In general, whenever there is some doubt concerning the accuracy of the secondary flow meter, especially at low mass flow levels, the SEC* parameter can be used. The next two columns show two estimates of the entrainment ratio, one based on SEC* and the other on SEC. The two right most columns in Table 3.6 show respectively the ejector exit pressure and secondary pressure.

Table 3.7 Data for performance curve, November 24, 2015

Primary mass flow	Exit mass flow	Secondary mass flow	Deduced Secondary mass flow	Entrainmnent ratio based on SEC*	Entrainmnent ratio based on SEC	Exit pressure	Secondary pressure
GF001 (kg/h)	GF002 (kg/h)	SEC FT003_MASS (kg/h)	SEC* GF002-GF001 (kg/h)	SEC*/GF001	SEC/GF001	PT003 (kPa)	PT006 (kPa)
51.1	82.5	30.9	31.4	0.61	0.60	112.5	70.0
50.9	81.3	29.8	30.4	0.60	0.58	113.1	70.1
50.8	79.5	28.0	28.7	0.56	0.55	113.9	70.0
51.2	76.7	25.1	25.5	0.50	0.49	115.9	70.0
51.2	68.2	16.4	17.0	0.33	0.32	120.6	70.1
51.2	54.8	5.9	3.6	0.07	0.11	126.6	70.1

In the same manner as shown above, the averages are calculated for each of the fixed positions of the ejector exit valve. Table 3.7 summarizes the average values that will be used in the plotting of the performance curve. In this instance the parameter SEC* will be used to represent the secondary mass flow and to calculate the entrainment ratio. A minimum of 15

individual sampled values will be used in all cases to calculate the average. Reading down the second column from the right in Table 3.7, labelled "Exit pressure, PT003", it can be seen that the ejector exit pressure increased gradually in steps from 112.5 kPa to 126 kPa.

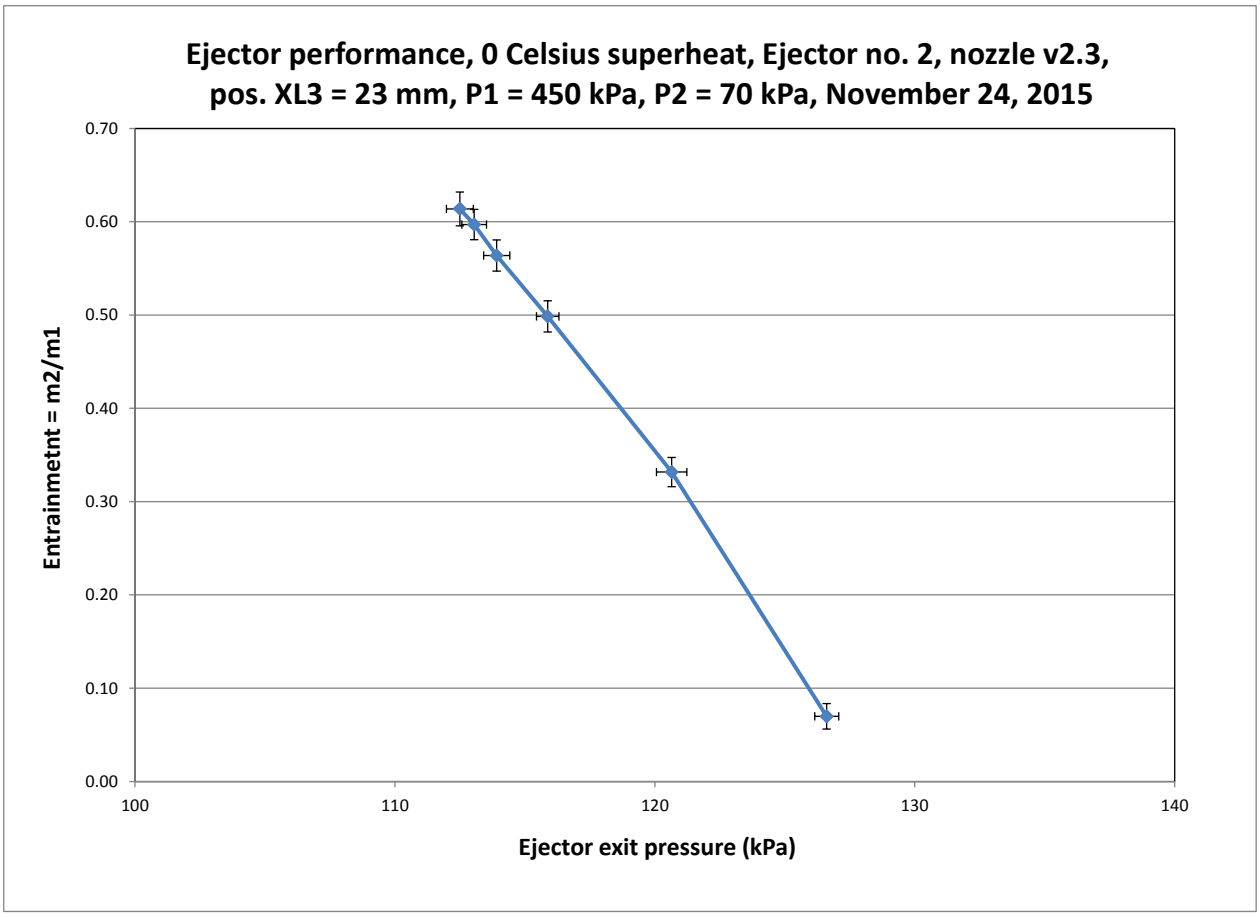

Fig. 3.12 Performance curve, November 24, 2015

Fig. 3.12 shows the result of plotting the average entrainment ratio values in Table 3.7 versus the average exit pressure readings. As can be noticed by the general form of the performance curve, during the early part of the project the ejector was operating in the single choked mode, and thus the expected horizontal portion of the curve is not present. Fig. 3.13 shows a performance curve from the later portion of the experimental program, showing the traditional form of an ejector operating in double choked mode. In fact, Fig. 3.13 shows the

reference performance curve, operating at the final reference conditions, with which all other performance curves will be compared in the results section.

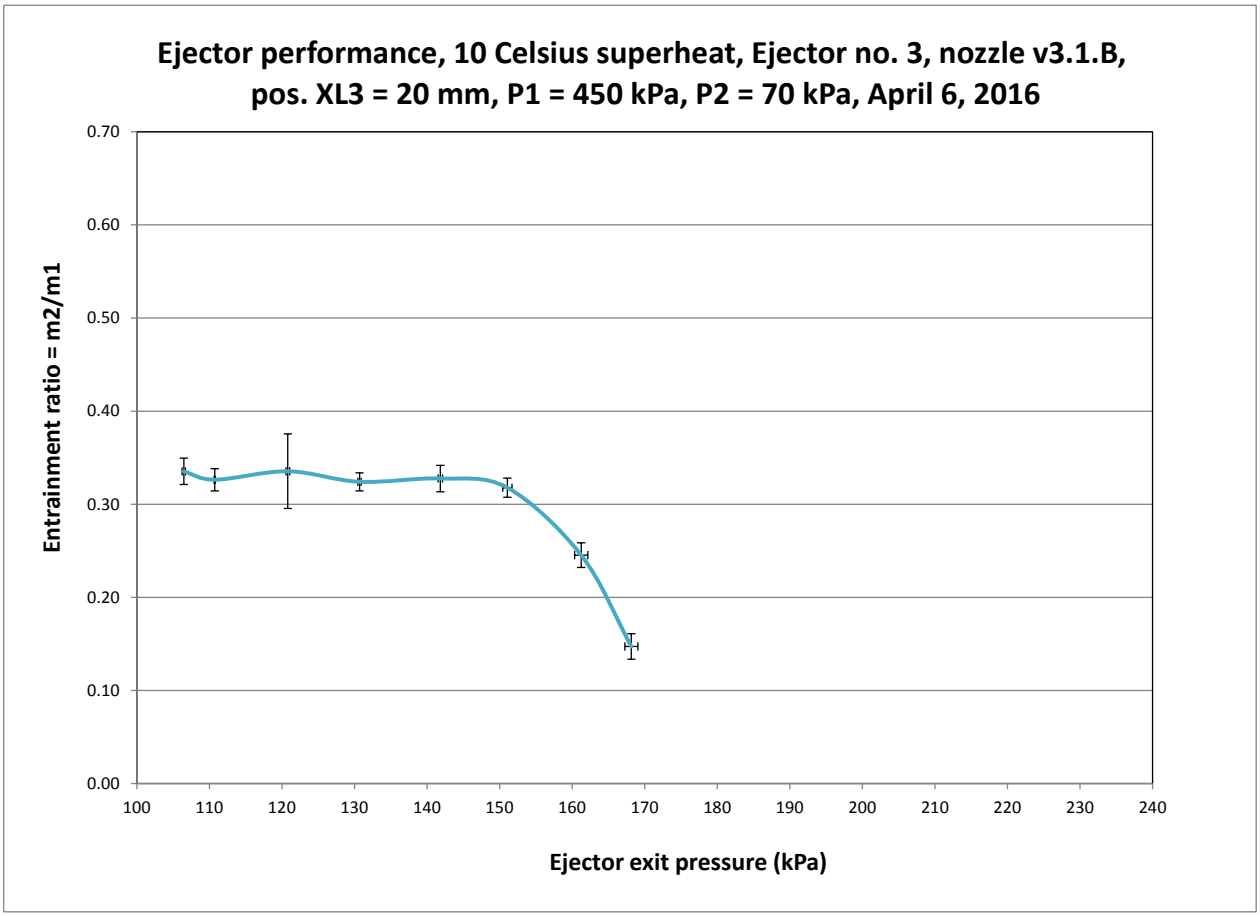

Fig. 3.13 Performance curve, April 6, 2016

3.3 Results

Although the results section comprises several smaller studies, it can best be understood as being made up of three overlapping themes. To begin with, in the first portion, all of the lessons related to the characterization of pure steam ejectors are presented. The focus here was on identifying a stable parameter range of operation, and to explore some of the potentially important aspects of steam ejectors: amount of primary superheat, primary and secondary input port conditions, ejector and nozzle geometry, and primary nozzle position. Armed with a good overall characterization of the test bench and two primary nozzles, the second portion of the results section evaluates the impact of varying levels of CO_2 in the steam ejector secondary fluid on the ejector performance. The goal was not to repeat all of the pure steam studies with CO_2, but rather to target a key subset of the reference pure steam tests for comparison purposes. In particular, the final comparisons were done, with and without CO_2, on two specific nozzles, for a primary pressure of 450 kPa with 10 °C superheat, with a secondary pressure of 70 kPa, at a fixed nozzle position of XL3 = 20 mm. In the third and final portion of the results section, the impact of the CO_2 will be compared with previous studies, and the groundwork will be laid for the use of the experimental information in the context of ejector enhanced carbon capture processes.

It is worth noting that all of the results before the section 3.3.12 were completed with pure steam in the primary and secondary ejector ports. Section 3.3.12 is entitled "Effect of CO_2 on performance", and is followed by other sections dealing with the presence of CO_2 in the secondary flow. All of the presented sub sections, or mini-studies, will consider the effect of a particular parameter on ejector performance. In the results section "ejector performance" is always a synonym for ejector entrainment ratio, m2/m1. For the purpose of hopefully providing useful information for other experimenters, lessons learned along the way will be shared with the reader.

3.3.1 Effect of primary fluid superheat

In the early experimental work an emphasis was placed on having sufficient superheat, with an initial target of 20 °C. Due to the wide range of variation in the primary mass flow, including test bench start up and shut down, the electric superheater burned out on several

occasions. As a result, a larger more robust superheater was installed, complete with more conservative protective circuits designed to deactivate the unit if the electric heating element surface temperature was too high, or if the mass flow rate was too low. As the ejector design evolved there was a progression toward smaller primary mass flow rates, with the result that the risk of the superheater automatically shutting off during an experiment increased. The overall effect of this experience was thus to favour the lowest level of superheat that would be sufficient for stable test bench operation. As will be discussed shortly, that value was eventually fixed at 10 °C.

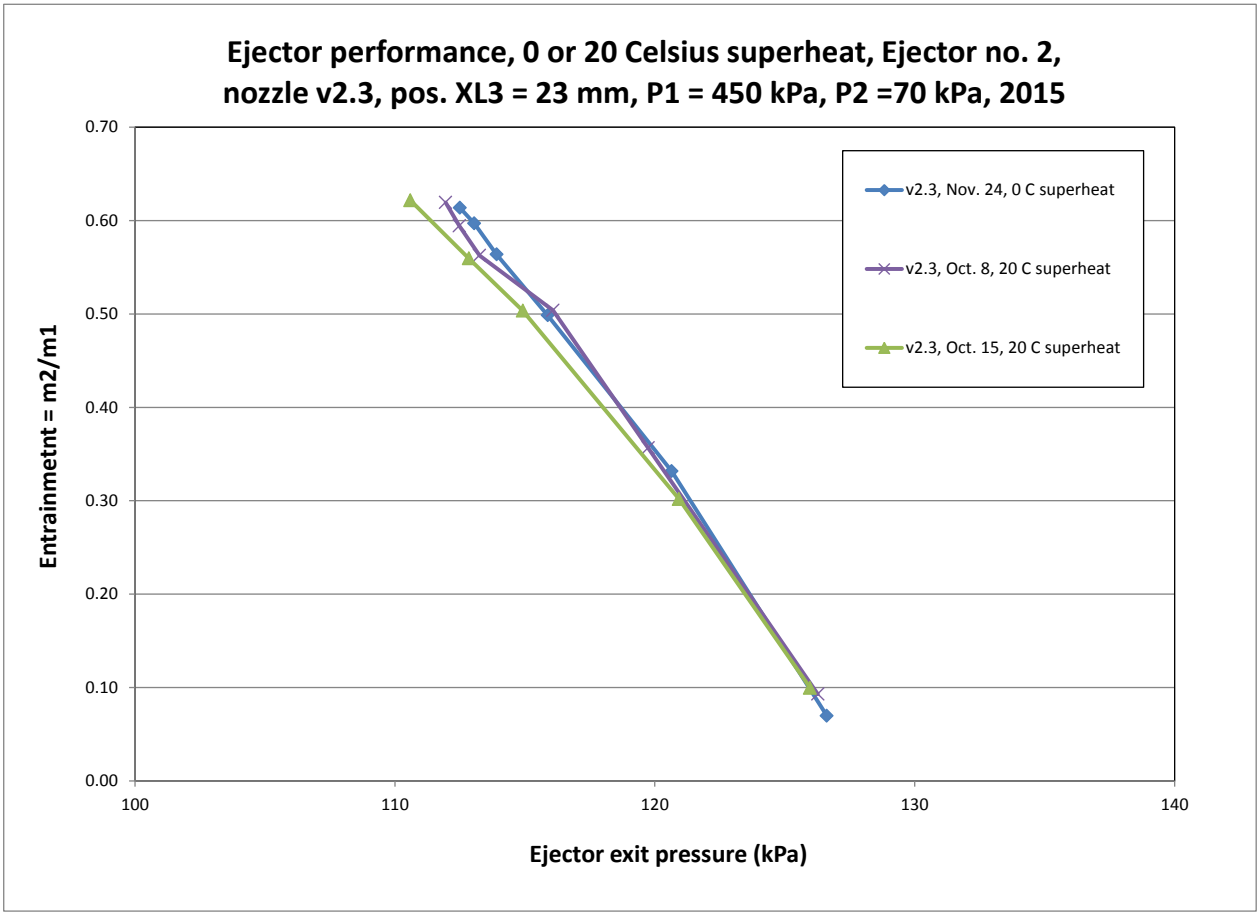

Fig. 3.14 Two levels of superheat: 0 and 20 °C, ejector no.2

Fig. 3.14 compares some early performance curves, with superheat levels of 0 and 20 °C. It was observed that in this case there was no noticeable effect on the steam jet ejector performance. As was discussed in the methods section 3.2.4., the November 24, 2015 test results, with 0 °C superheat, were based on an excellent mass balance, as was shown in Fig. 3.11. A later

comparative study on superheat, Fig. 3.15, uses the final reference parameter choices: Ejector no. 3, nozzle v3.1.B at position XL3 = 20 mm, P1 = 450 kPa and P2 = 70 kPa. At face value, it would appear from the graph as if 0 °C superheat had a very significant detrimental effect on the ejector performance in this case. As will be explained, that conclusion would be wrong.

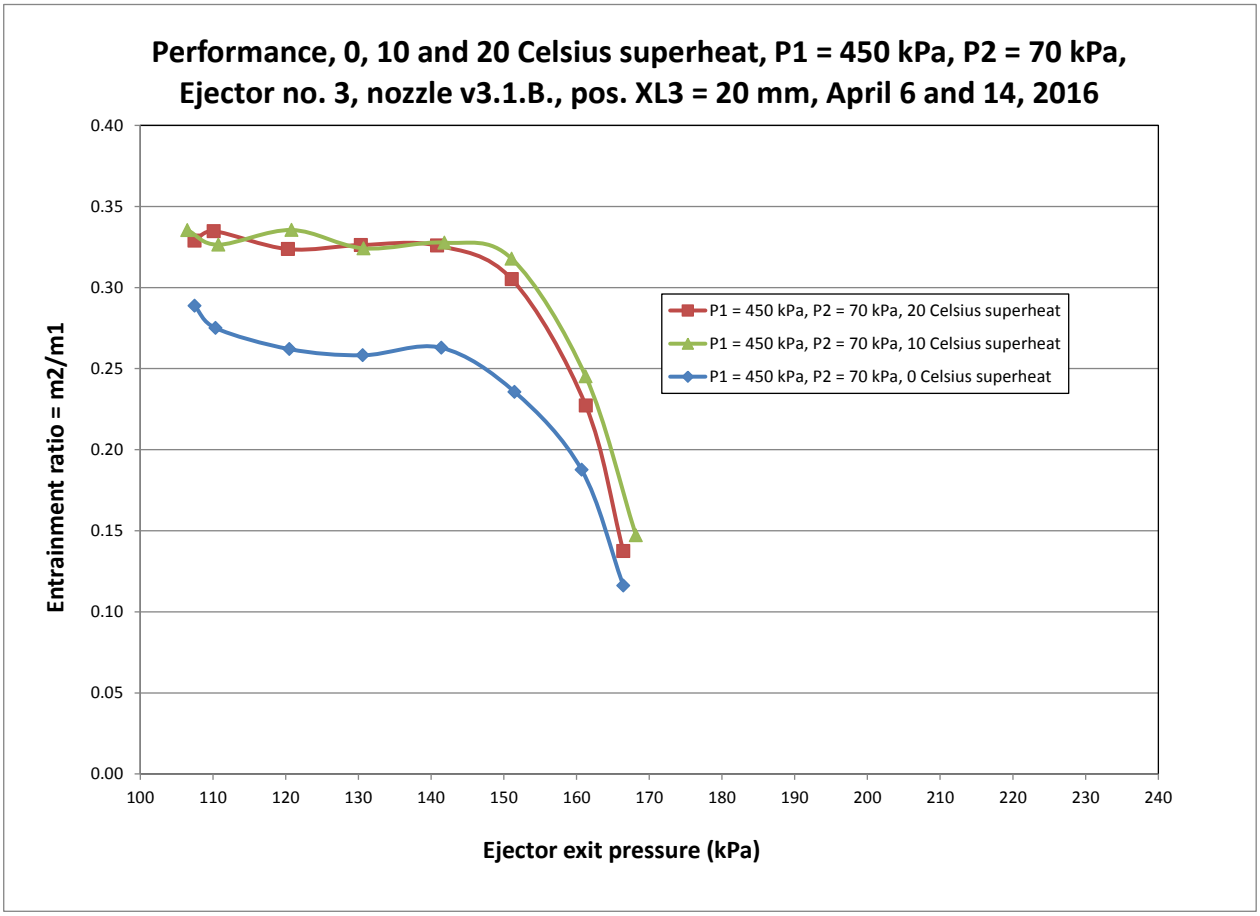

Fig. 3.15 Three levels of superheat: 0, 10 and 20 °C, ejector no.3

After further analysis of the information leading to the creation of Fig. 3.15, the appropriate conclusion is that 0 °C is not a prudent choice for the test bench with this ejector and set of operating parameters. Fig. 3.16 shows the mass flow rate of the test of April 14, 2016, applicable to the superheat levels of 0 °C and 20 °C. As can be seen in the right half of the Fig. 3.16, the mass flow balance for the 20 °C superheat case is very good. In particular, the primary mass flow rate FT002 is quite stable. On the left hand side of Fig. 3.16, it is noticeable that the primary mass flow rate FT002 fluctuates significantly, and that the average mass flow rate is greater than the level on the right hand side of the same figure. In comparing Fig. 3.11 with Fig.

3.16, the primary mass flow can be seen to decrease from approximately 50 kg/h with ejector no.2 to 40 kg/h with ejector no. 3. It is quite possible that both the primary flow regulator and the primary flow meter could be affected by wet steam. The mechanical dynamic response of the primary regulator could very possibly change as the mass flow level decreases.

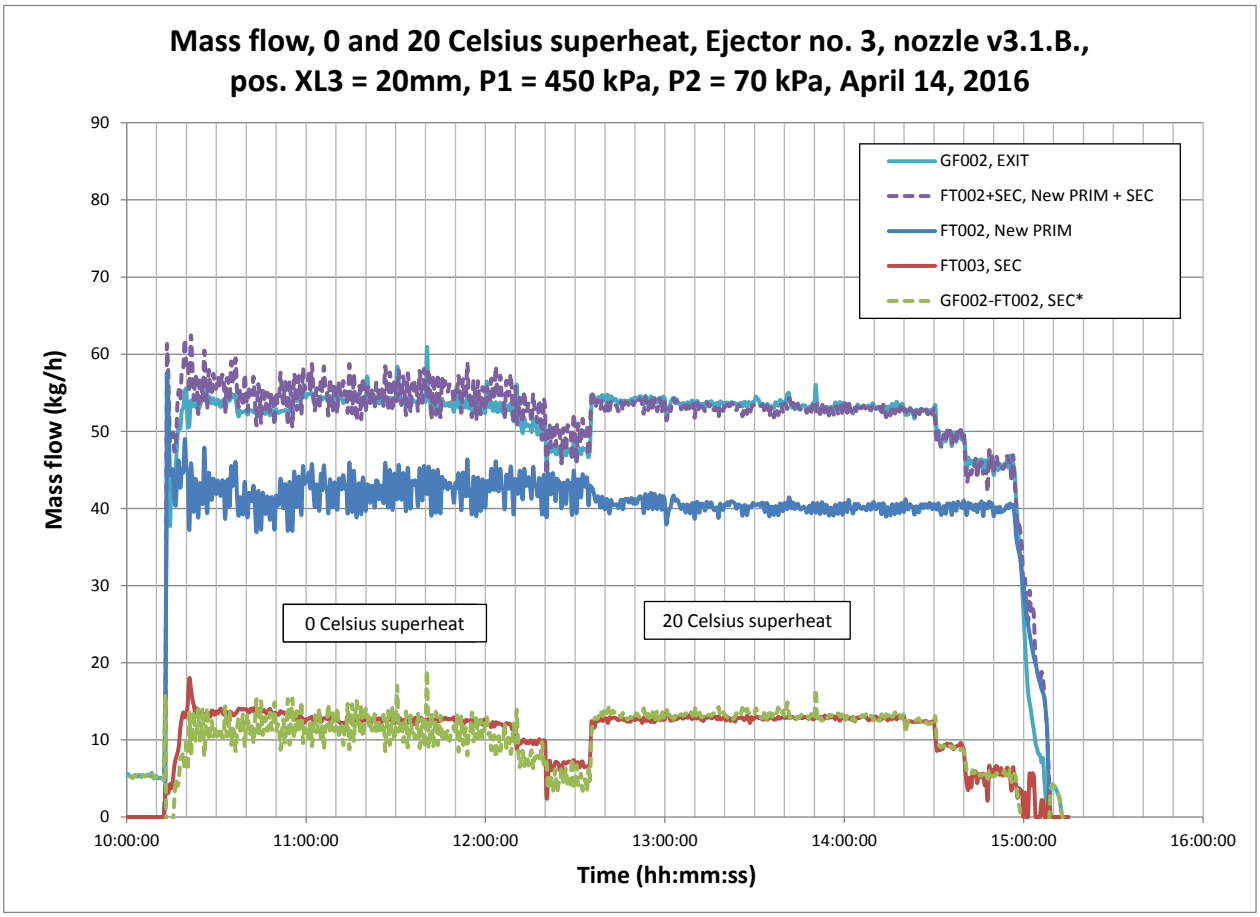

Fig. 3.16 Mass flows, April 14, 2016

A possible explanation of the behaviour in Fig. 3.16 and the resulting performance curve in Fig. 3.15, is that the wet saturated steam passing through the primary regulator did in fact cause many small fluctuations in the mass flow rate through the regulator, as the regulator continuously attempted to maintain the target pressure. The primary flow meter used during the tests of April 14, 2016 was a vortex style flow meter. This meter uses the von Karman effect, where vortices are alternatively formed and shed from the buff body inserted in the fluid steam within the flow meter. The flow velocity is proportional to the frequency of the vortices created by the flow in contact with the bluff body. The fluctuations in the mass flow rate likely caused a

high false reading of the primary mass flow rate. A further visual clue to this proposed explanation is that the FT002+SEC curve in Fig. 3.16, the sum of the primary and secondary measured flow rates, is apparently higher that the curve of the exit mass flow rate, GF002. On the right hand side of the same figure, the FT002+SEC curve almost overlies the GF002 curve. Recall that for the right hand side of Fig. 3.16 the steam has 20 °C superheat.

The conclusion of the previous results and discussion is that for the operating configuration of interest for the test bench, a level of superheat greater than 0 °C and less than 20 °C would be preferable. Given that no noticeable difference in ejector performance was noticeable in Fig. 3.14, or in Fig. 3.15 for the 10 °C or 20 °C curves, it was decided to use 10 °C superheat as the default parameter choice for all of the final tests. Given the risk of delay and possible damage operating the ejector with superheat at levels above 20 °C, it was decided not to investigate this question further within the scope of the thesis project. Chunnanond and Aphornratana also found that the amount of superheat had little effect on the primary mass flow, but suggested that some superheat could prevent damage to the ejector which might otherwise be caused by the wet motive steam [19].

3.3.2 Effect of the primary nozzle position and the nozzle shape

As was mentioned in the introduction and the discussion on superheat, in the early phase of the experimental project it was not possible to produce a performance curve with the ejector operating in double choked mode. In parallel with this fact was the open question of wanting to know to what extent the position of the primary nozzle might impact the ejector performance. The main motivation for the evolution of the various nozzle and ejector geometries, shown in Table 3.4 and Table 3.5, was to move towards configurations that would produce the desired double choked performance curve, operate over a parameter range of interest, be compatible with the test bench capabilities, and that would operate within the accurate range of the flow meters. The fact that the test bench was designed with an atmospheric condenser also imposed pressure constraints on the range of ejector exit pressures that could be expected. Along the way important practical lessons were learned about the importance of the exterior geometry of the primary nozzle.

Fig. 3.17 presents a schematic image of the conical mixing section for ejectors no. 2 and no. 3. In both the upper portion of the image, for ejector no. 2 with nozzle v2.1, and the lower portion of the image, for ejector no. 3 with nozzle v3.1.B, the images are accurately proportioned. In both cases the exit end of the primary nozzle is shown using a dashed line, with the nozzle located at the nominal design position. Both images show the dimension XL3, which is the distance in millimeters between the exit tip of the nozzle and the entrance to the cylindrical portion of the ejector body. Both ejector 2 and ejector 3 were designed with a preliminary value for XL3. As indicated in Fig. 3.17 below, the nominal design positon for ejector 2 was 10 mm, noted as 2A, while for ejector 3 it was 20 mm, noted as 3B. The values of XL3 noted in Fig. 3.17 indicate the nozzle positions that were evaluated. In this project the parameter XL3, measured in mm, will be used to indicate the nozzle position in all charts.

Nominal nozzle positions for ejectors 2 and 3

Ejector 2

Position	Distance (mm)
2A	10
2B	13
2C	15
2D	23

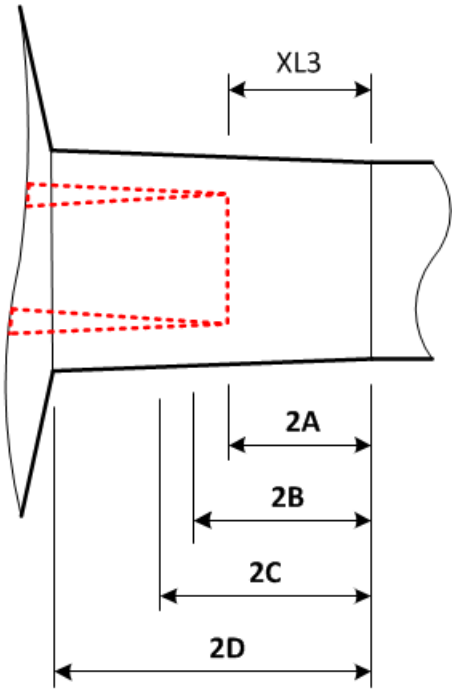

Ejector 3

Position	Distance (mm)
3A	10
3B	20
3C	30

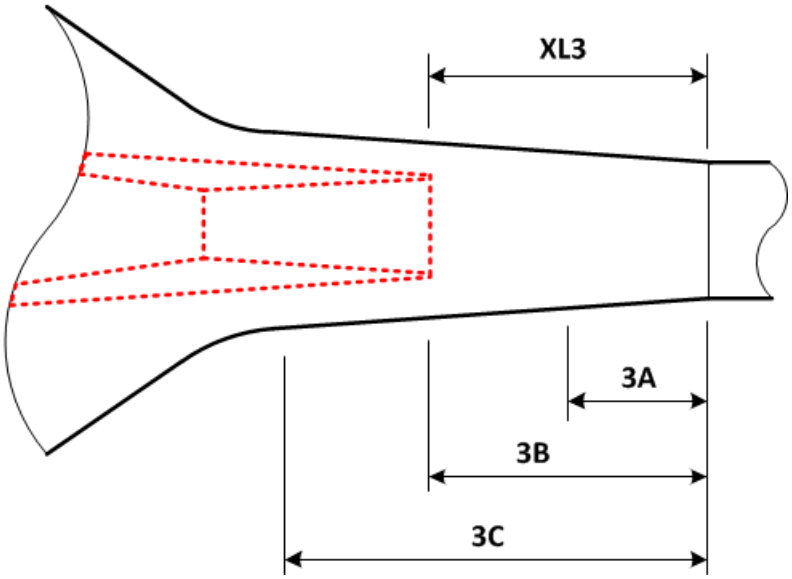

Fig. 3.17 Schematic of nozzle position and shape

Fig. 3.18 compares three performance curves for ejector no. 2, with the nozzle positon as a parameter: XL3 = 13, 15, and 23 mm. It was observed that the performance increased as XL3 increased, with the highest performance corresponding to the alignment of the nozzle tip with the

start of the conical mixing portion of the ejector body, as can be seen in the upper portion of Fig. 3.17. Given that the nominal design position was for 10 mm for ejector no.2, this result was unexpected. Fig. 3.19 presents a larger view of the combination of nozzle v2.1 and ejector no. 2. The explanation of the observed increasing performance curves in Fig. 3.18 is related to the geometry of the exterior surface of the nozzle, in particular the half-angle of the outer surface of the nozzle, and its relationship to the half-angle of the conical mixing portion of the ejector body. In this particular case the nozzle exterior half-angle was 12.1°, while the ejector conical mixing portion angle was 1.5°. Thus, in order to guaranty that secondary fluid can accelerate smoothly up to the mixing chamber fictive throat, it is important to satisfy the condition that the nozzle exterior half-angle must be less than or equal to the half-angle of the conical mixing portion of the ejector body. Fig. 3.20 shows the related geometry of ejector no. 3 and nozzle v3.1.B. In this later case the nozzle exterior half-angle was 4°, having the same half-angle as the ejector conical mixing portion.

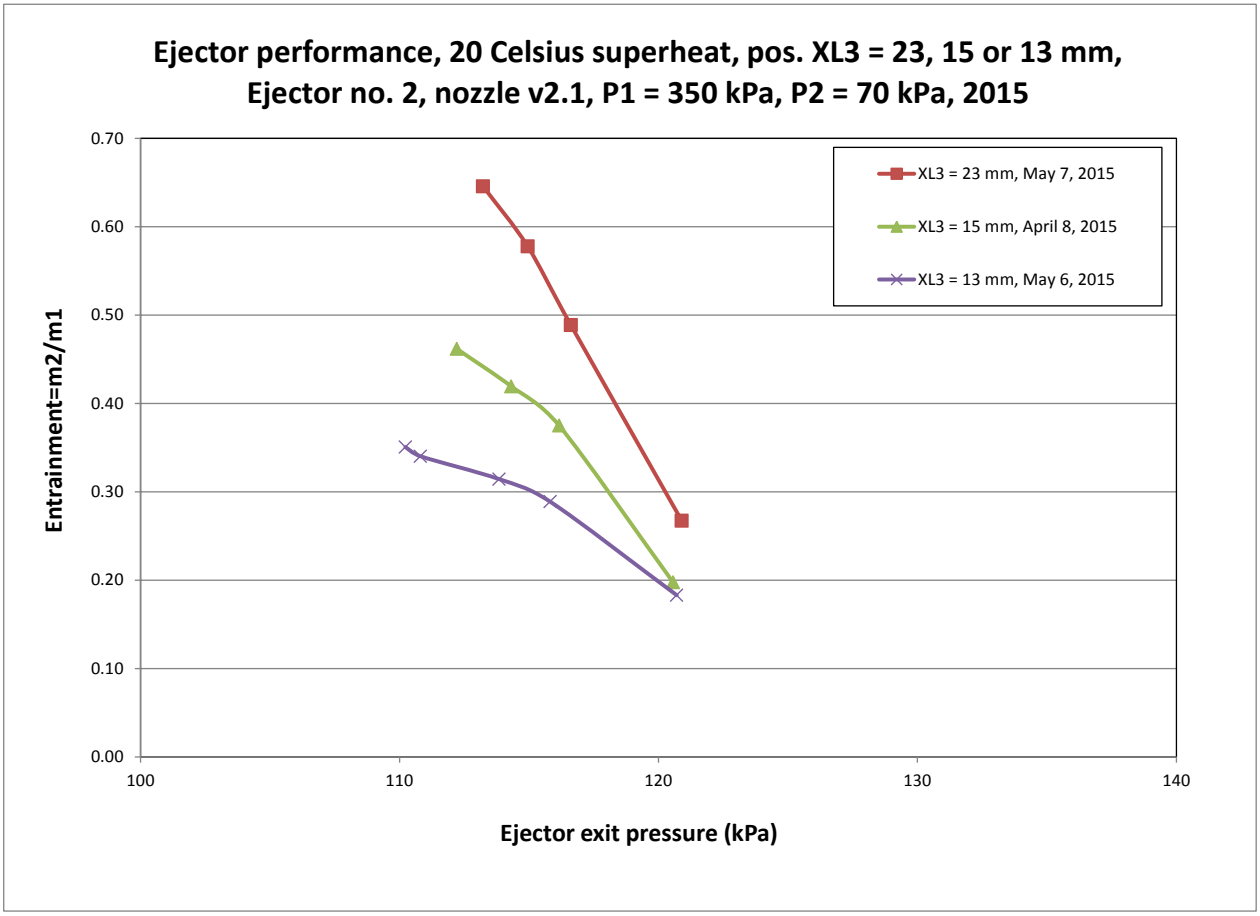

Fig. 3.18 Three nozzle positions: XL3 = 13, 15 and 23 mm, ejector no.2

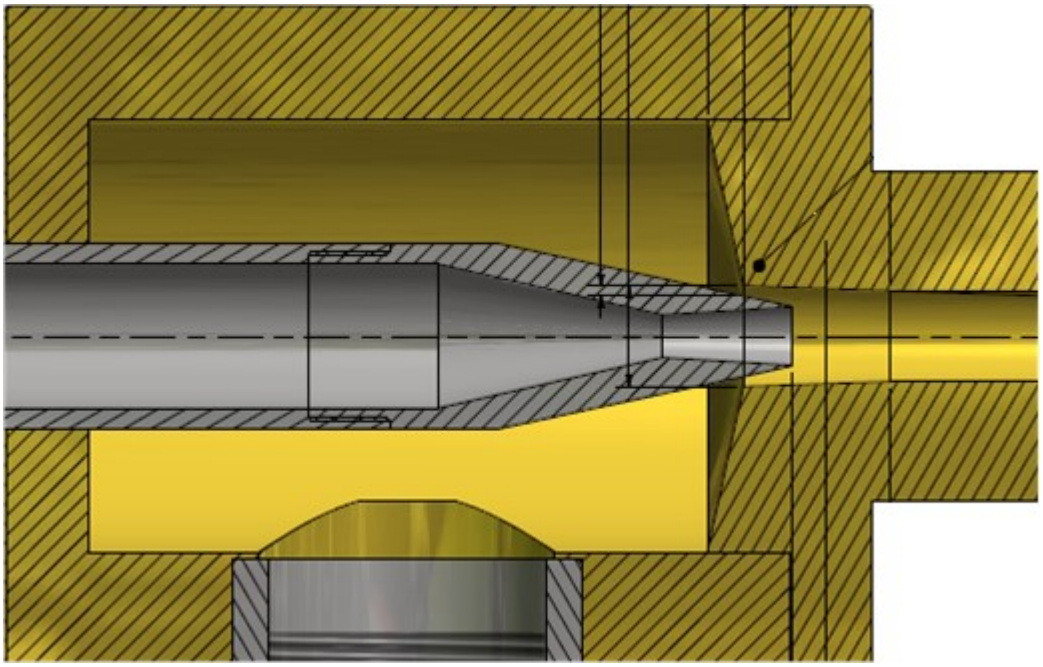

Fig. 3.19 Ejector no.2, nozzle v2.1

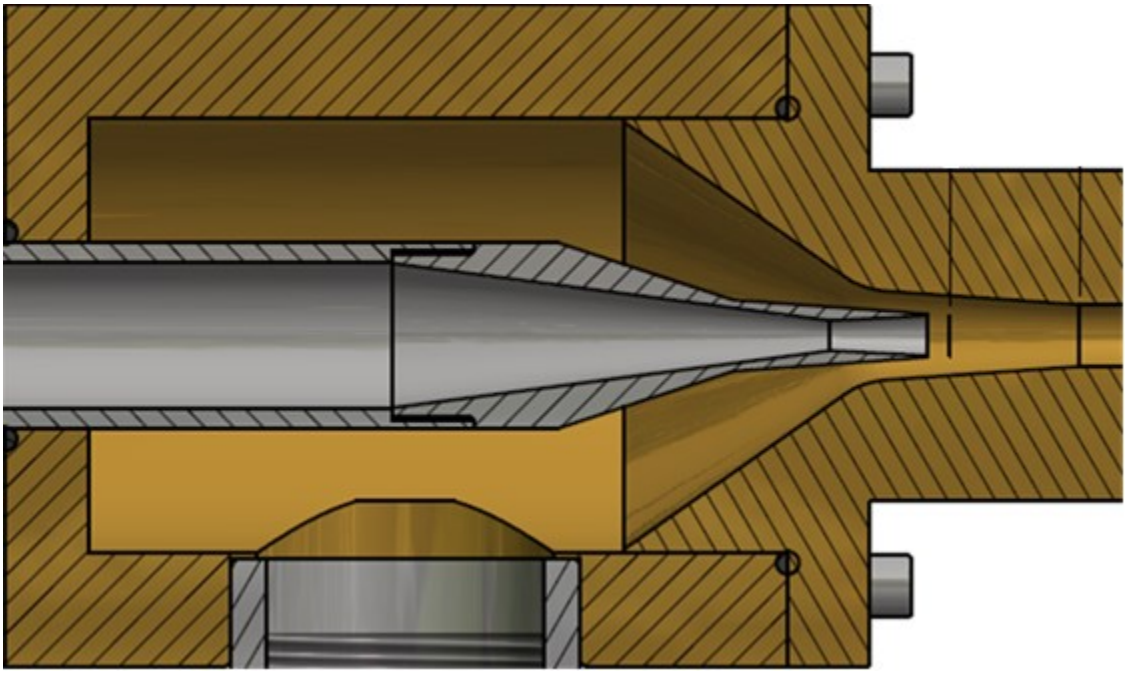

Fig. 3.20 Ejector no. 3, nozzle v3.1.B

Fig. 3.21 shows a comparison of the effect of the nozzle position on performance, for ejector no. 3 and nozzle v3.1.B. In this case, the evaluated nozzle positions were XL3 = 10, 20 and 30 mm. The three nozzle positions evaluated are those shown in the lower portion of Fig. 3.17, with XL = 20 mm being the nominal design position. The ejector was operated at the final reference parameter values. The primary pressure was set to 450 kPa with 10 °C superheat, with the secondary pressure at 70 kPa. The top two curves, for the nozzle positions of XL3 = 30 mm and 20 mm, have identical ejector performance curves. When the nozzle was positioned at XL3 = 10 mm, there is a noticeable rounding off of the curve at the approach of the critical pressure, as well as a decrease in the critical pressure. It appears that the critical pressure is only 130 kPa for the XL3 = 10 mm, while it is closer to 150 kPa for the 20 mm and 30 mm curves.

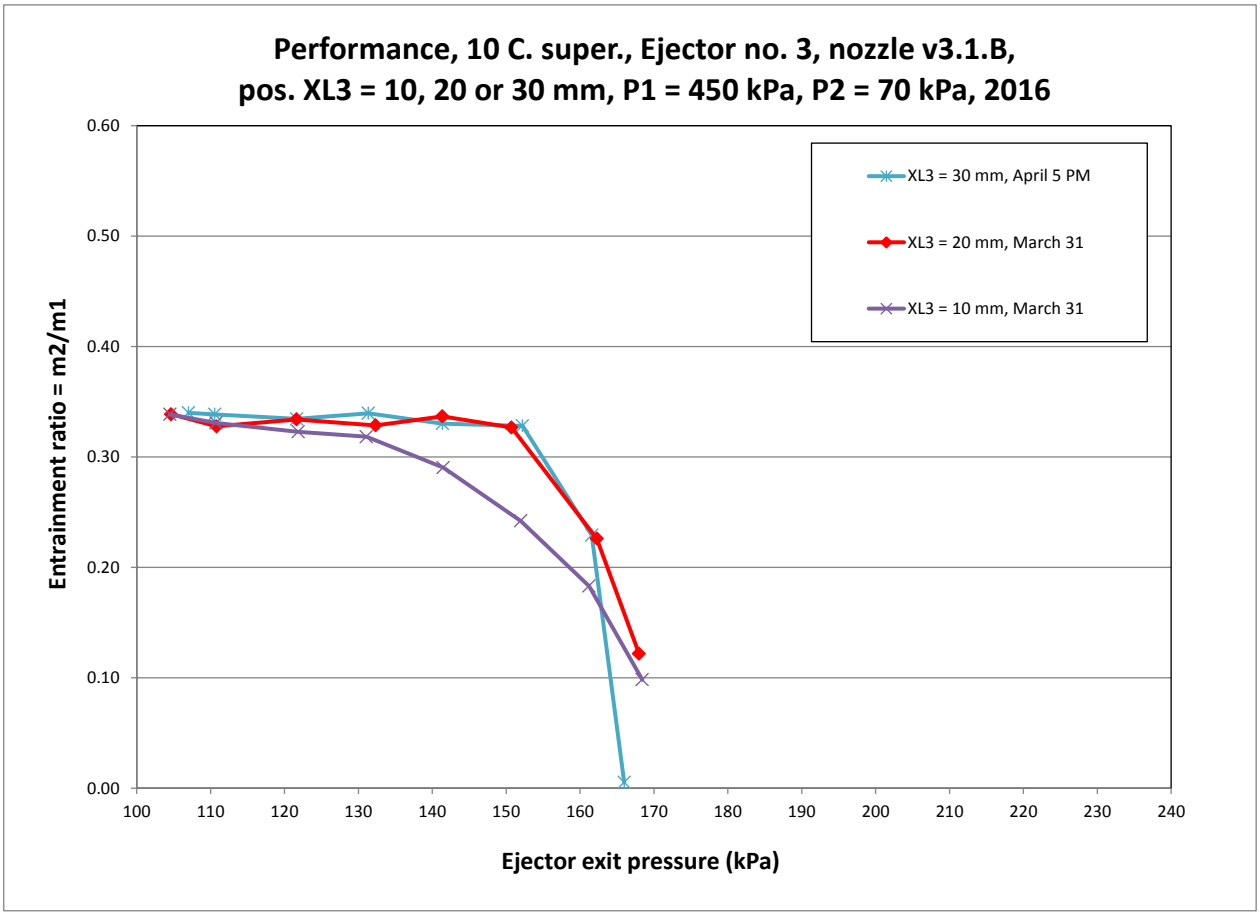

Fig. 3.21 Three nozzle positions, nozzle v3.1.B

Fig. 3.22 is another comparison of the three nozzle positions of XL3 = 10, 20 and 30 mm, although in this case for the nozzle v3.2.B. Recall that Table 3.5 and Fig. 3.7 show the differences between nozzles v3.1.B and v3.2.B, with the principal difference being that nozzle v3.2.B has a slightly smaller throat diameter. The exterior surfaces of both nozzles share the same geometry. The three performance curves shown in Fig. 3.22for nozzle v3.2.B show the same trend as for the v3.1.B nozzle, although in this case the comparison is not as sharp. The critical pressure for the XL3 = 10 mm corresponds to 130 kPa, while both the XL3 = 20 and 30 mm curves correspond to a critical pressure of roughly 140 kPa. It would appear in retrospect that the main guiding principle to follow is that the nozzle positon XL3 should respect a particular minimum distance. A distance that is slightly greater than the minimum value does not appear to be detrimental to ejector performance. A distance slightly shorter than the minimum results in a decrease in the value of the critical pressure, which is associated with the rounding off of the performance curve in the transition from double choked mode to single choked mode.

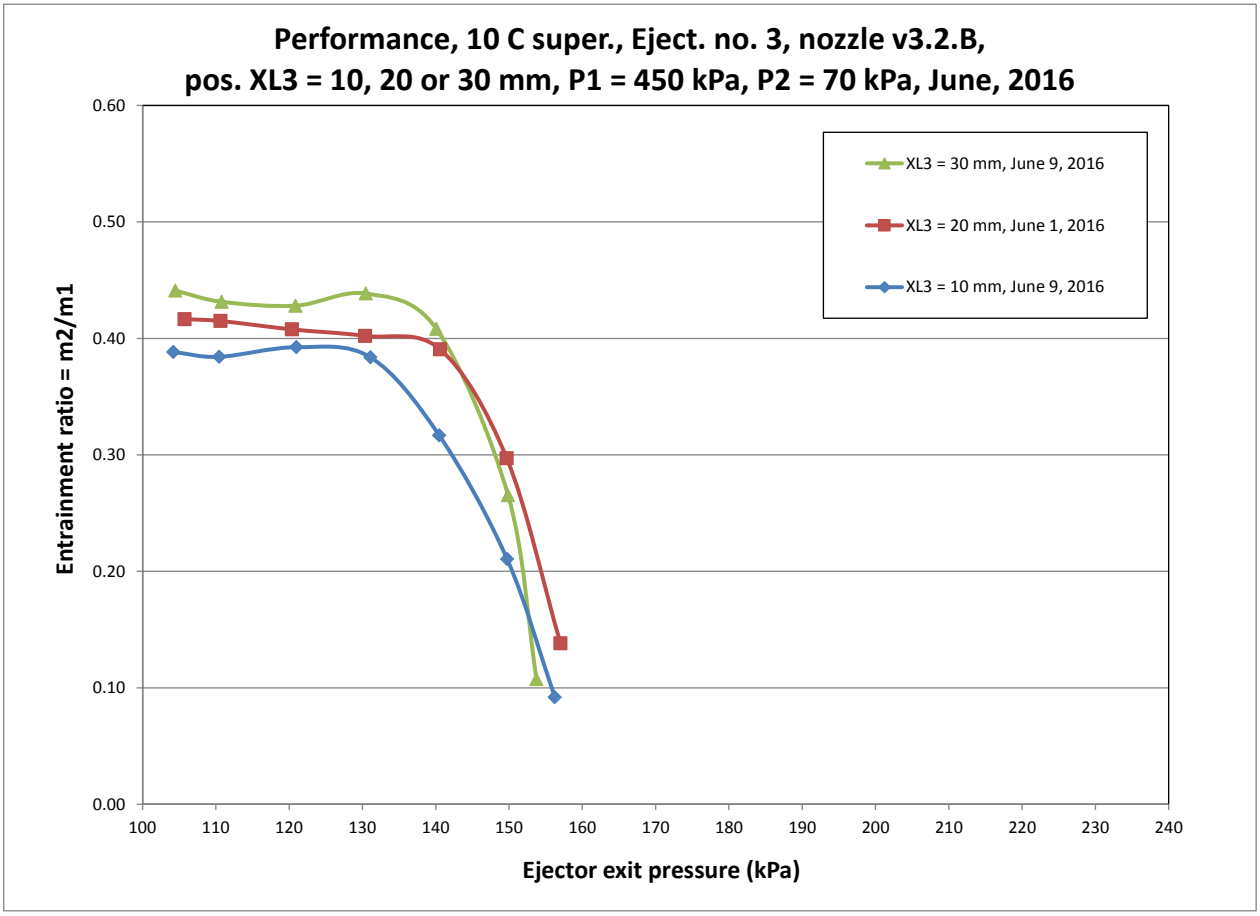

Fig. 3.22 Three nozzle positions, nozzle v3.2.B

For the purposes of this doctoral project it was decided to fix the nozzle positon at XL3 = 20 mm for the final portion of the experimental program. It should be noted here that in the actual test bench the repositioning of the nozzle was not a rapid risk-free procedure. Each time the nozzle was repositioned required removing the nozzle, making appropriate measurements, inspecting and if required replacing the O-ring, and finally retightening the nozzle into the ejector. The experimental risks associated with this procedure include the possibility of creating a leak, slightly moving the nozzle during the final tightening, and not being able to readily verify the nozzle tip positon from the outside of the ejector. Any future experimental work on the impact of nozzle positon would benefit from an improved nozzle positioning mechanism and procedure.

3.3.3 Reference steam conditions for ejector no. 3 and nozzle v3.1.B

Having completed preliminary evaluations of the effect of primary steam superheat and the nozzle position, and arrived at a good combination of ejector geometry and test bench capabilities, an experimental test program was prepared for pure steam. Table 3.8 shows the combination of primary pressure and secondary pressure conditions for which nine performance curves were completed. The reference program was based on ejector no. 3 with nozzle v3.1.B. The level of superheat was set to 10 °C, with a nozzle position of XL3 = 20 mm. The condenser set point temperature was fixed at 90 °C for all tests. The goal was to have a reasonably wide range of reference values with which other tests could be compared. As will be discussed later, a subset of the values in Table 3.8 will be compared with different nozzle geometry for pure steam.

Table 3.8 Experimental program for ejector no. 3, nozzle v3.1.B

		Secondary Pressure (kPa)		
		50	70	90
Primary Pressure (kPa)	550	x	x	x
	450	x	x	x
	350	x	x	x

3.3.4 Performance of nozzle v3.1.B, various primary pressures, secondary pressure of 70 kPa

Fig. 3.23 shows three performance curves, with three different levels of primary pressure, and a fixed secondary pressure of 70 kPa. The primary pressure levels were 350, 450 and 550 kPa. All three of the curves show the traditional form of an ejector performance curve, with a horizontal plateau corresponding to double choked mode, following by the decreasing entrainment in the single choked mode region. It can be seen that for each increasing level of primary pressure there is an associated decrease in the entrainment ratio and an increase in the critical pressure.

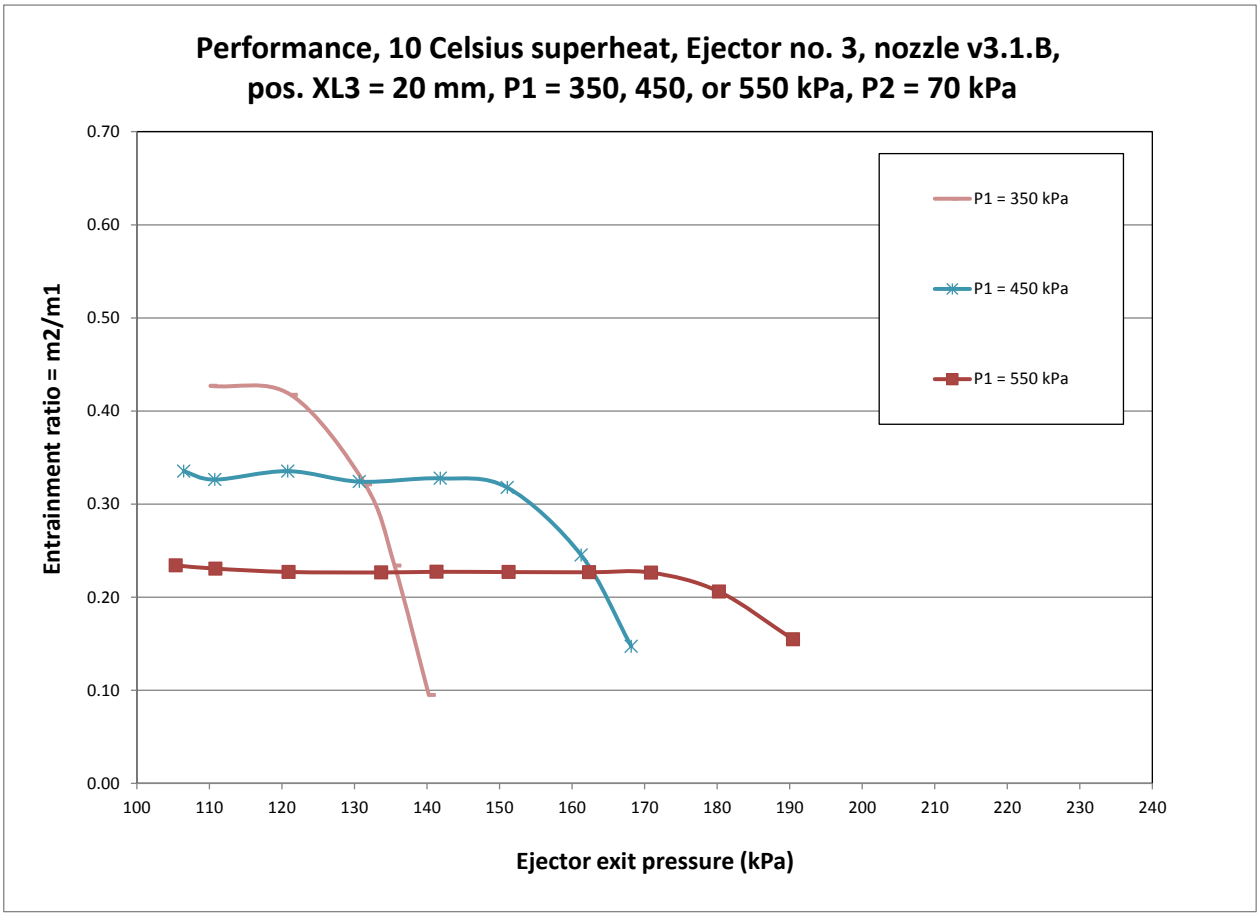

Fig. 3.23 P1 = 350, 450 or 550 kPa, P2 = 70 kPa, nozzle v3.1.B

3.3.5 Performance of nozzle v3.1.B, various secondary pressures, primary pressure of 450 kPa

In Fig. 3.24 are presented three performance curves, in this case with the primary pressure fixed at 450 kP and with three different levels of secondary fluid pressure. The secondary fluid pressure, which in the test bench configuration refers to the flash tank pressure, was set at 50, 70 and 90 kPa. It is clear that as the secondary pressure increases so does the entrainment ratio. There is also the suggestion of an increase in critical pressure with increasing secondary pressure, but this effect is not uniform. Increasing the secondary pressure from 50 to 70 kPa appears to increase the critical pressure from the value of 140 kP at P2 = 50 kP to the value of 150 kPa at P2 = 70 kPa. There appears to be no change in the critical pressure as the secondary pressure is increased from 70 kP to 90 kPa.

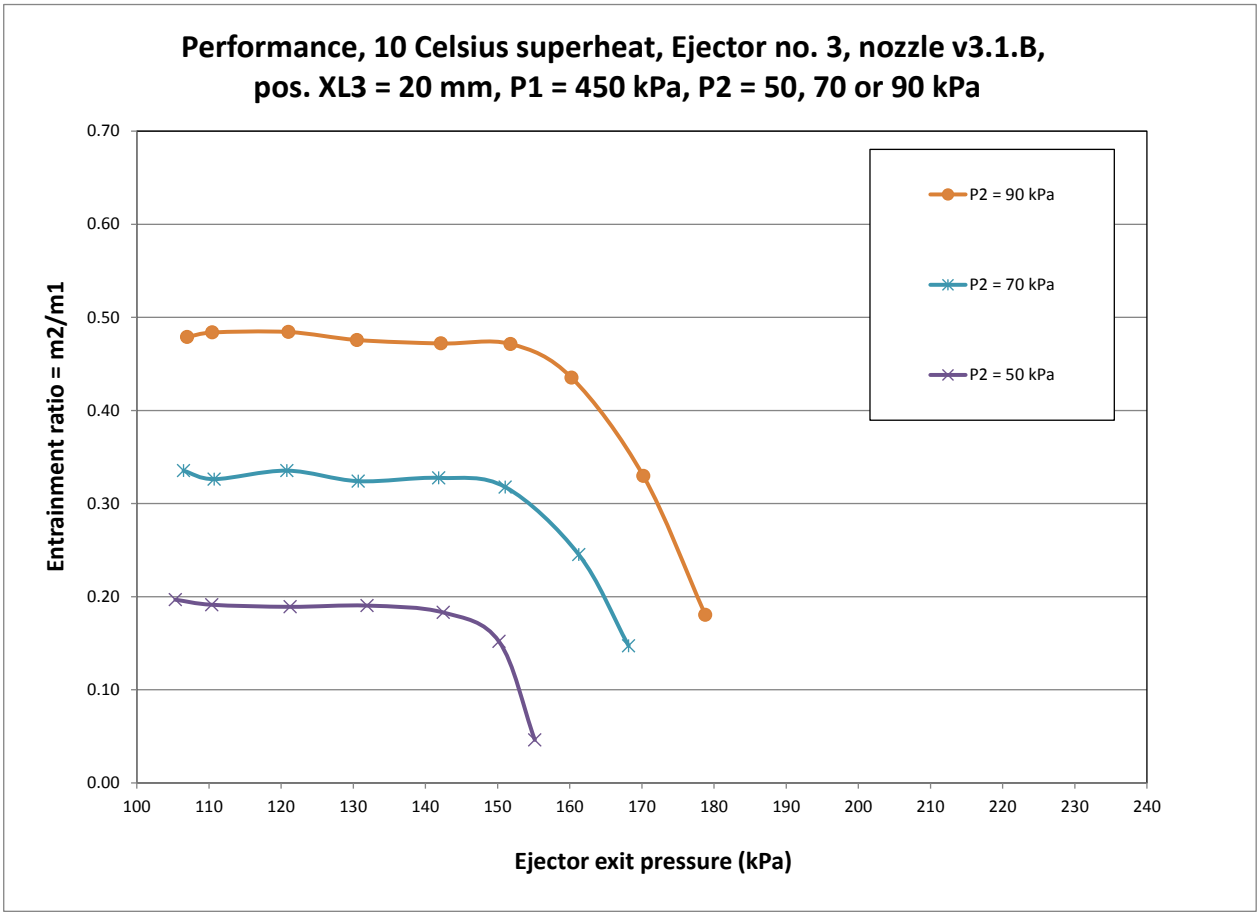

Fig. 3.24 P1 = 450 kPa, P2 = 50, 70 or 90 kPa, nozzle v3.1.B

3.3.6 Performance of nozzle v3.1.B, various primary and secondary pressures

Fig. 3.25 groups together all of the performance curves that were produced based on the experimental plan shown in Table 3.8. The same information is shown in Fig. 3.26, but in this case the critical pressure points have been grouped together forming two families of curves: curves of constant primary pressure and curves of constant secondary pressure. Plotting the entrainment ratio with the ejector exit pressure on the abscissa is most useful when considering an actual potential application, in which case the downstream process will place important constraints on the minimum pressure that must be provided at the ejector exit.

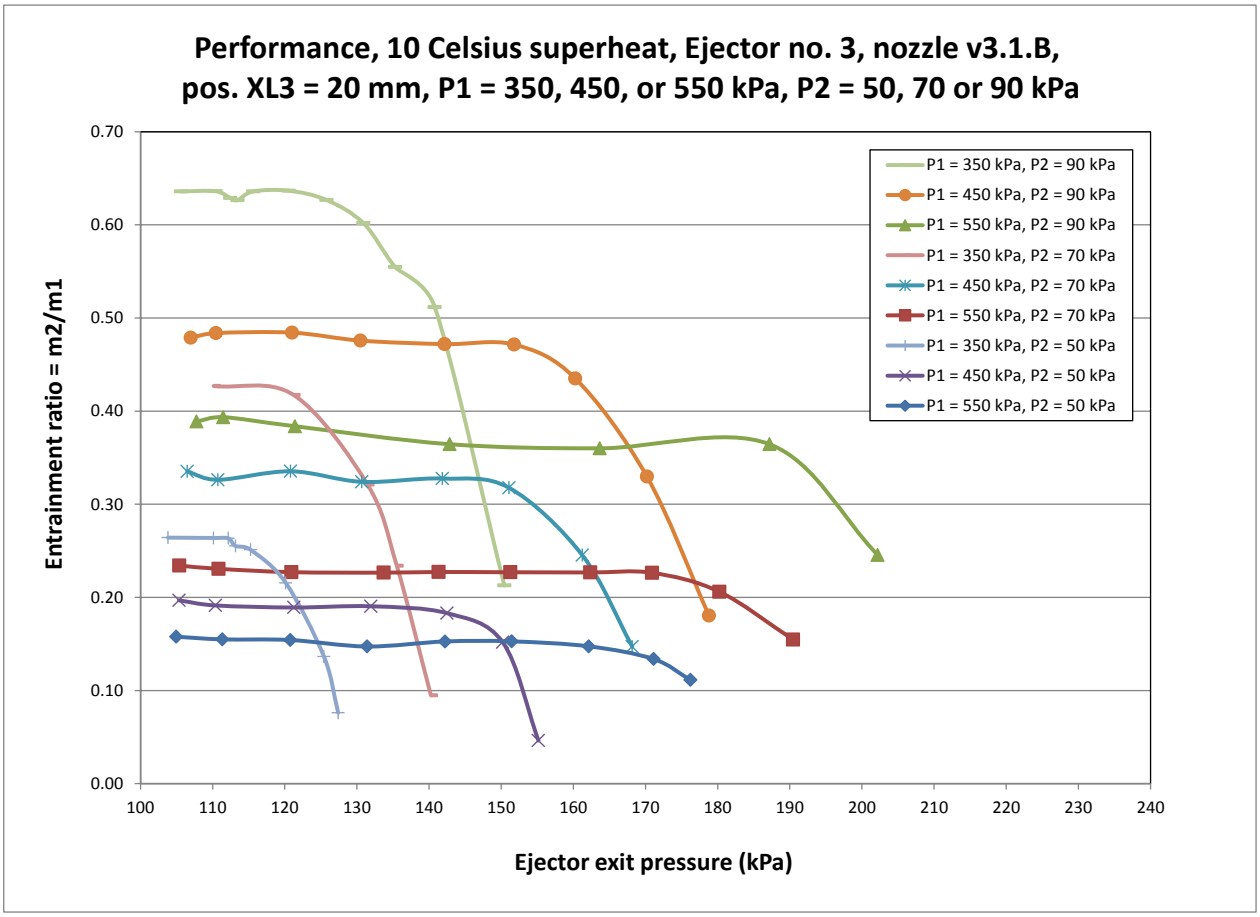

Fig. 3.25 Various primary and secondary pressures, nozzle v3.1.B

From a more theoretical point of view, as often seen in the open literature, there is interest in plotting the compression ratio along the abscissa. Fig. 3.27 presents the family of 9 performance curves with the compression ratio on the horizontal axis. Although all of the curves lie within a certain band, they do not form a smooth master curve. Attempts to join matching critical pressure points for primary or secondary curves of the same pressure resulted in some crossover of the final curves.

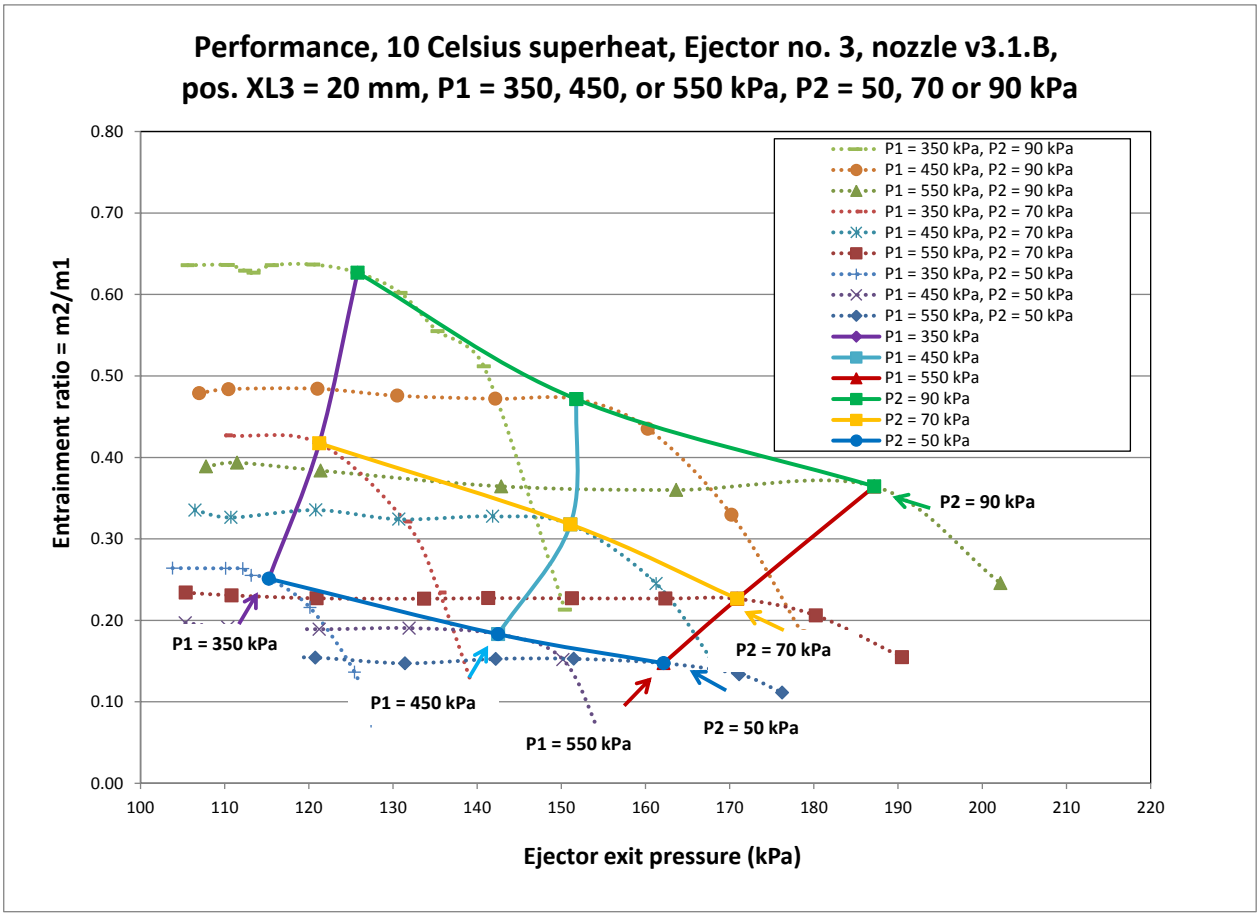

Fig. 3.26 Critical pressures, various primary and secondary pressures, nozzle v3.1.B

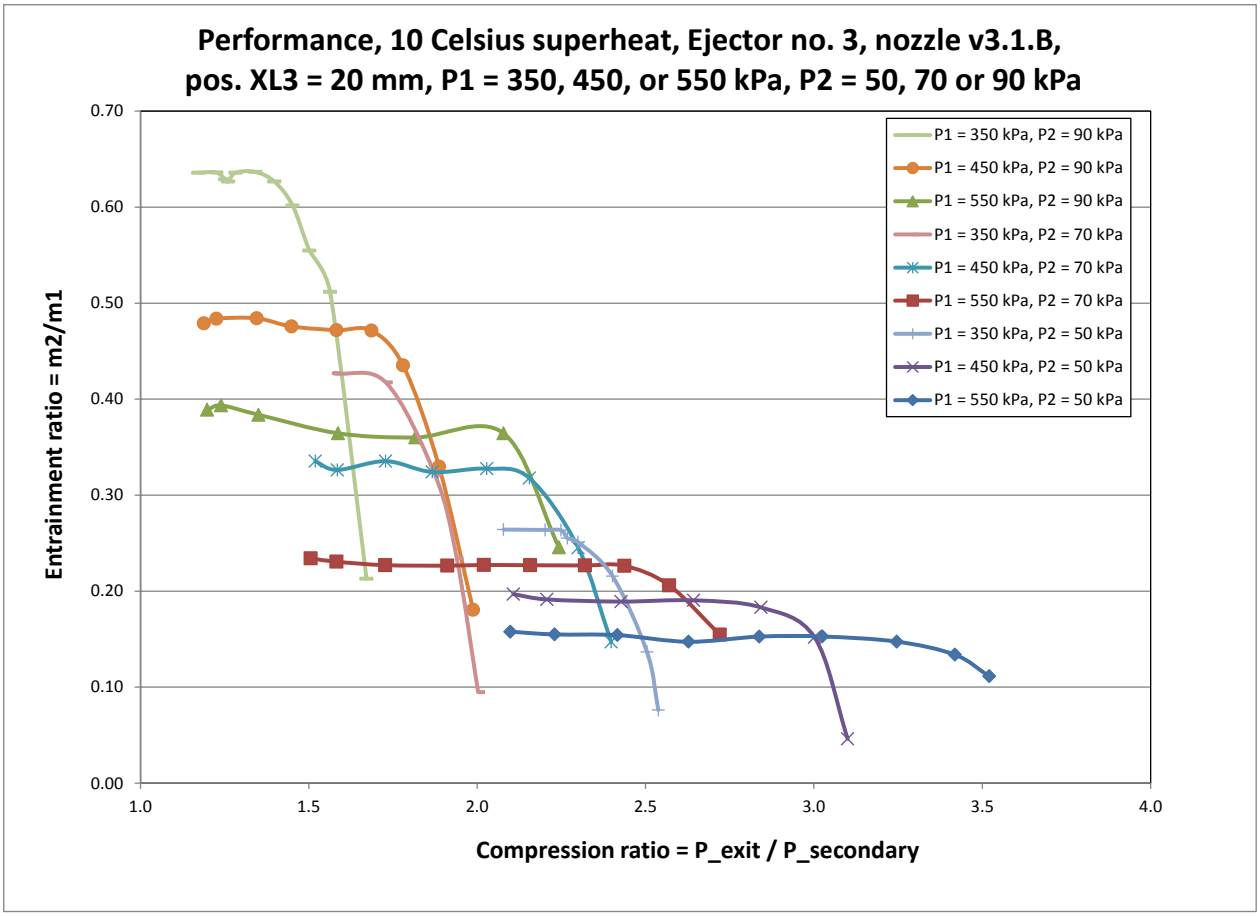

Fig. 3.27 Performance curves, various primary and secondary pressures, nozzle v3.1.B

3.3.7 Performance, nozzles v3.1.B and v3.2.B, pure steam, various input pressures

The original idea of designing and fabricating more than a single nozzle was twofold. First, the primary goal was to maximize the chance that the combination of the nozzle geometry and the ejector geometry would permit the creation of double choked performance curves that were within the operating range of the existing test bench. Second, having more than a single nozzle would provide further insight into the impact of the relationship between the nozzle geometry, in particular the primary throat diameter, and the ejector geometry, specifically the ejector body diameter.

For the purpose of brevity, the experimental results based on the smaller throat diameter nozzle v3.2.B (4.24 mm) will not be described independently of the previous results. Instead,

these results will be directly presented against the backdrop of the results of the larger throat diameter of nozzle v3.1.B (4.60 mm). As was the general approach previously, the emphasis is on the effect of the change in nozzle throat diameter on ejector performance, rather that the absolute characteristics of a particular ejector nozzle. Table 3.9 shows the experimental grid that was planned for evaluating the nozzle v3.2.B using pure steam for both the primary and secondary fluids. The five associated performance curves were, as was the previous case, created with 10 °C superheat, with a nozzle position of XL3 = 20 mm, and with the condenser temperature set to 90 °C.

Table 3.9 Experimental program for ejector no. 3, nozzle v3.2.B

		Secondary Pressure (kPa)		
		50	70	90
Primary Pressure (kPa)	550		x	
	450	x	x	x
	350		x	

Fig. 3.28 presents a global view of the combined performance curves for both nozzles. For each of the 14 performance curves the critical pressure condition is emphasized with a lozenge, or diamond, shape marker. The figure includes variations in nozzle choice (v3.1.B or v3.2.B), primary pressure (P1 = 350, 450 or 550 kPa) and secondary pressure (P2 = 50, 70, or 90 kPa). As a first characterization of the performance curves, there is a strong connection between the measured critical pressure compression ratio and the entrainment ratio. It is clear, however, that the compression ratio alone is not sufficient to understand the whole family of performance curves.

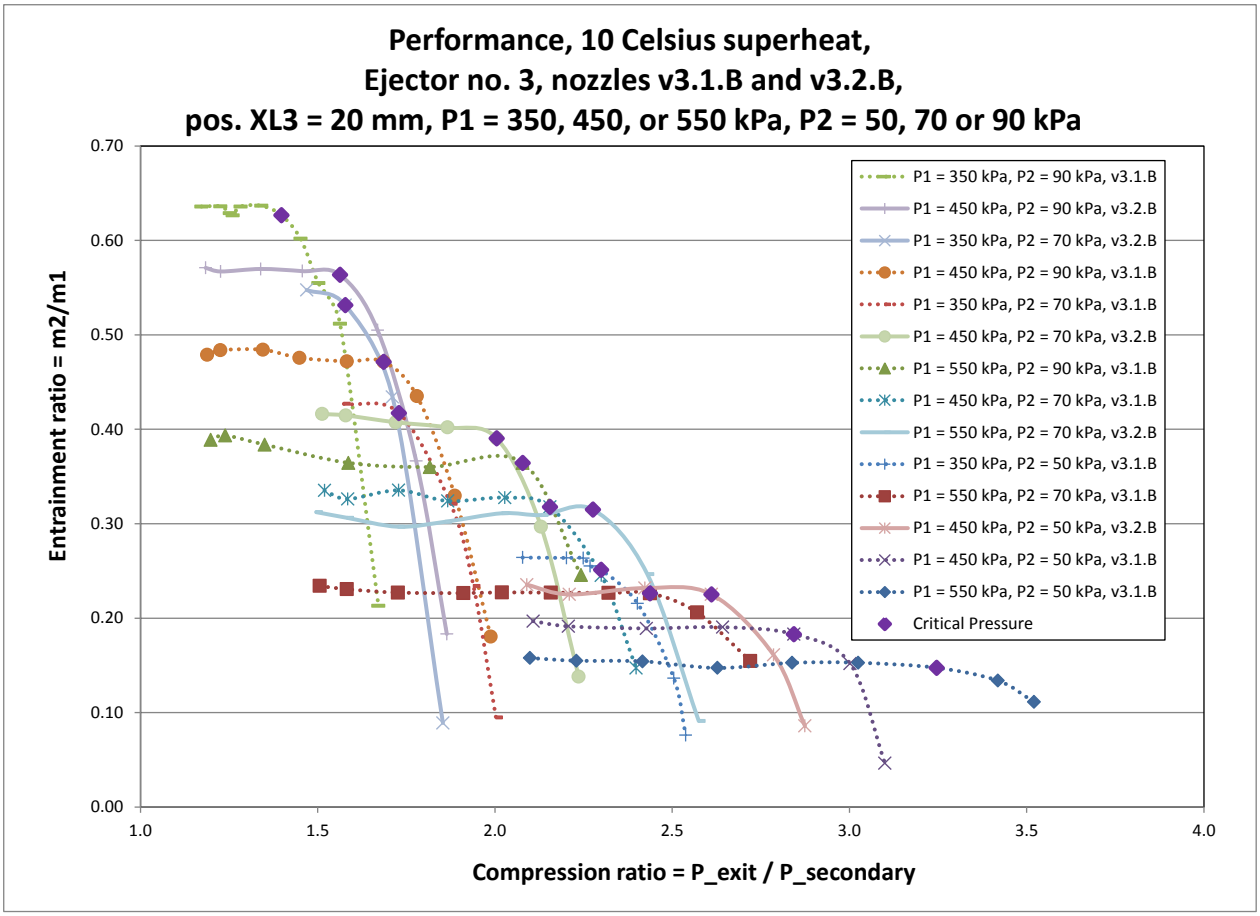

Fig. 3.28 Performance curves with critical pressures, nozzles v3.1.B and v3.2.B

3.3.8 Performance, nozzles v3.1.B and v3.2.B, various primary pressures, secondary pressure of 70 kPa

Fig. 3.29 compares the performance of both nozzles, where the secondary pressure is held constant at 70 kPa, and the primary pressure is varied (350, 450 or 550 kPa). Two additional curves are indicated in the chart legend, "v3.2.B, Critical, P2 = 70 kPa" and "v3.1.B, Critical, P2 = 70 kPa", which link together the critical pressure conditions for the respective nozzles. As can be seen in Fig. 3.29, for the same ejector input pressures, the nozzle with the smaller throat diameter, v3.2.B, will supply a larger entrainment ratio. The increased entrainment ratio, however, comes at the expense of a lower critical pressure at the ejector exit. Fig. 3.30 compares the situation where we consider starting from a given experimental condition, for example a primary pressure of 450 kPa and nozzle diameter of 4.23 mm (v3.2.B), as indicated

by the point "A", and we wish to evaluate either increasing the nozzle diameter, in the direction of the point "B", or increasing the primary pressure, in the direction of the point "C". In this case, moving in the direction of point "B" implies increasing the nozzle diameter to 4.60 mm (v3.1.B). Moving from point "A" to point "B" implies increasing the primary pressure to 550 kPa. Both options increase the primary mass flow. It is worth noting that the slope of the proposed change on the entrainment versus exit pressure chart will not be the same in both cases. The more advantageous choice is very much tied to the specific process constraints, such as the strict requirement to maintain a minimum ejector exit pressure, or the economic impact of increasing the primary pressure, which is generally more expensive, versus increasing the entrainment ratio, which is a major cost benefit. Table 3.10 summarizes the general results of this discussion, leaving aside the comparison of nozzle throat diameter change versus primary pressure change.

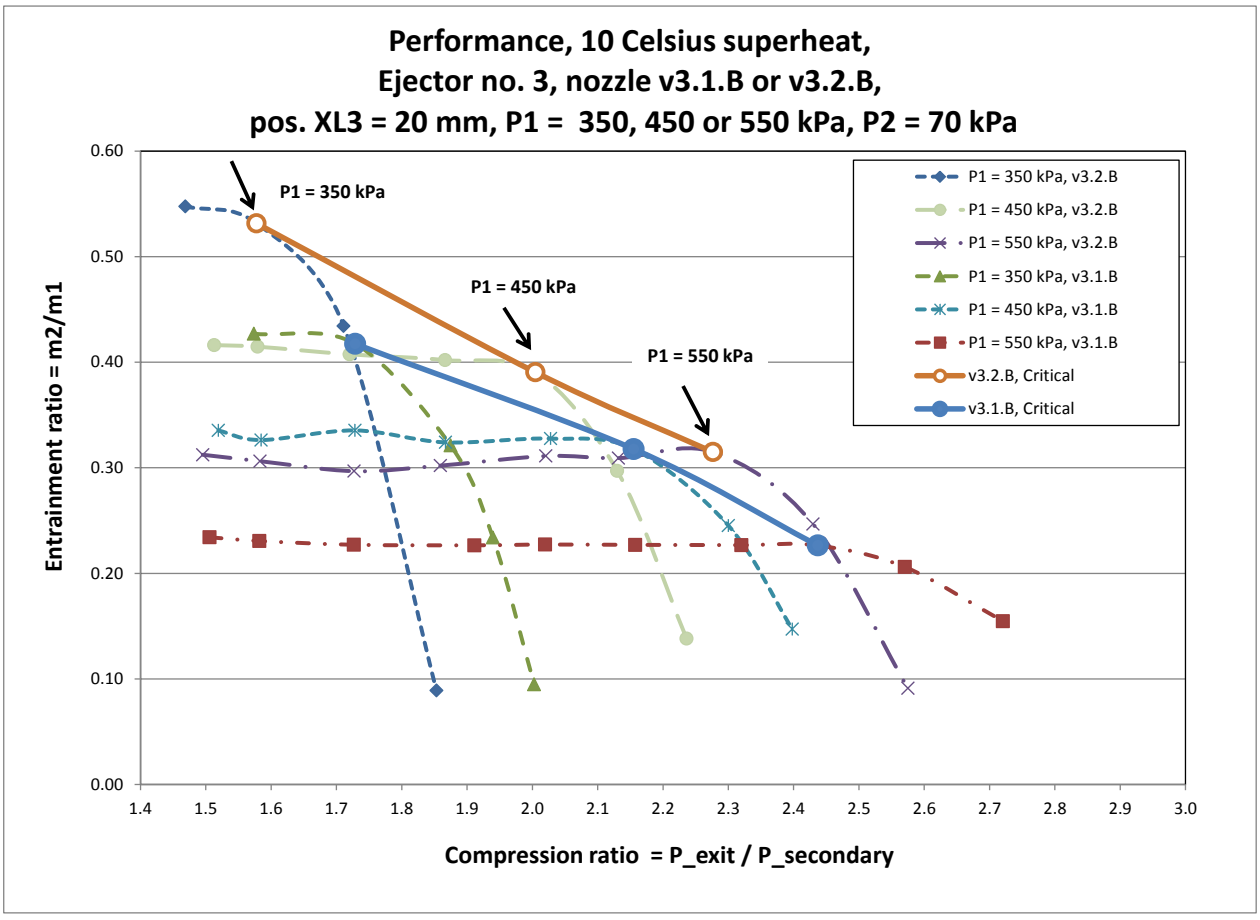

Fig. 3.29 Various primary pressures, P2 = 70 kPa, nozzles v3.1.B and v3.2.B

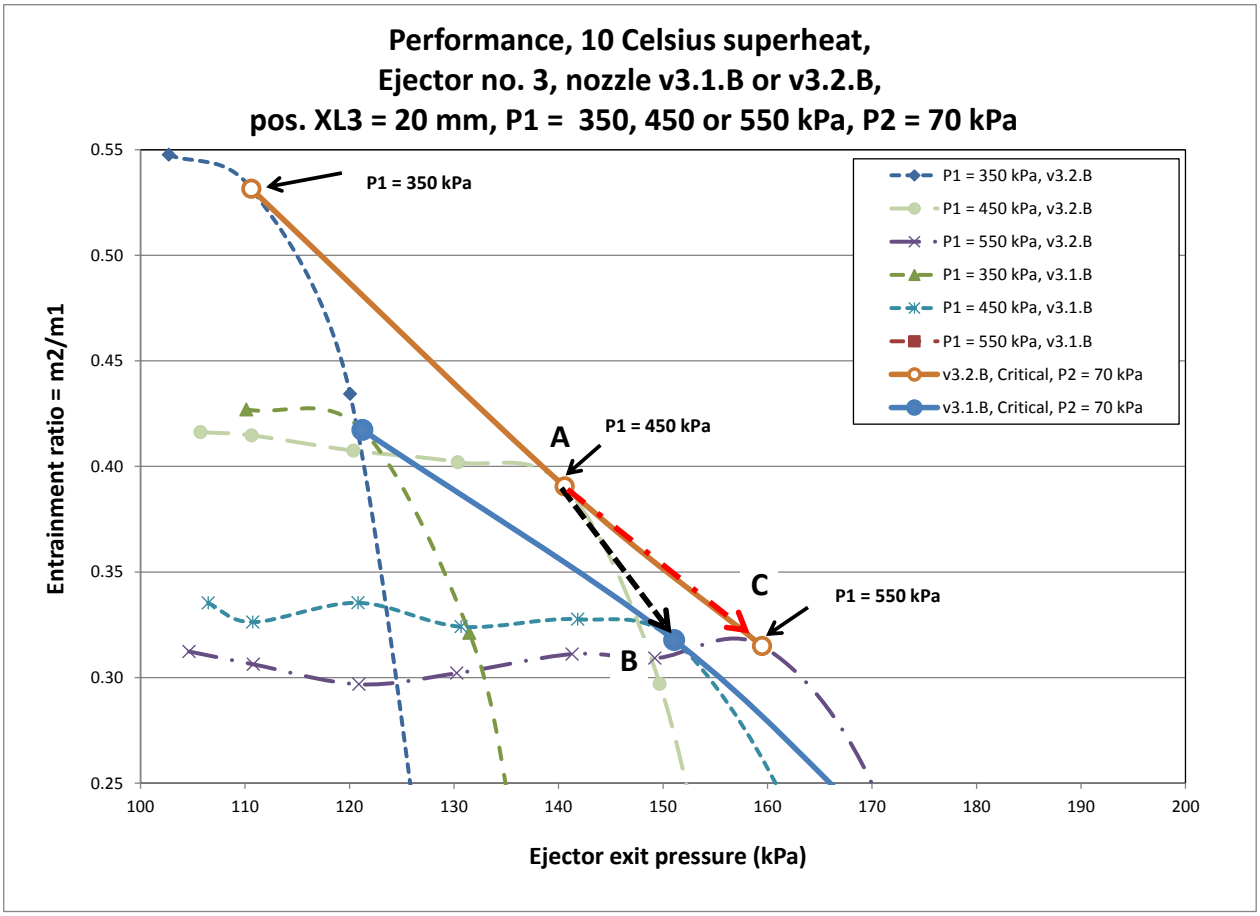

Fig. 3.30 Various primary pressures, P2 = 70 kPa, nozzles v3.1.B and v3.2.B, analysis

Table 3.10 Comparison of nozzles v3.1.B and v3.2.B, for constant secondary pressure P2

Input Conditions		Output result	
Change	Keep Constant	Critical Pressure	Entrainment ratio
increase nozzle diameter	primary pressure secondary pressure	increases	decreases
increase primary pressure	nozzle diameter secondary pressure	increases	decreases

3.3.9 Performance, nozzles v3.1.B and v3.2.B, various secondary pressures, primary pressure of 450 kPa

Fig. 3.31 compares the performance of both nozzles, where the primary pressure is maintained at 450 kPa while the secondary pressure is varied (50, 70 or 90 kPa). Again, two additional curves are indicated in the chart legend, "v3.2.B, Critical, P1 = 450 kPa" and "v3.1.B, Critical, P1 = 450 kPa", which link together the critical pressure conditions for each of the nozzles. Increasing the secondary pressure has the same general effect for both nozzles, that of increasing the entrainment ratio. For both nozzles, increasing the secondary pressure from 50 to 70 kPa resulted in an increased critical pressure. Increasing the secondary pressure from 70 to 90 kPa, however, resulted in no change in the critical pressure.

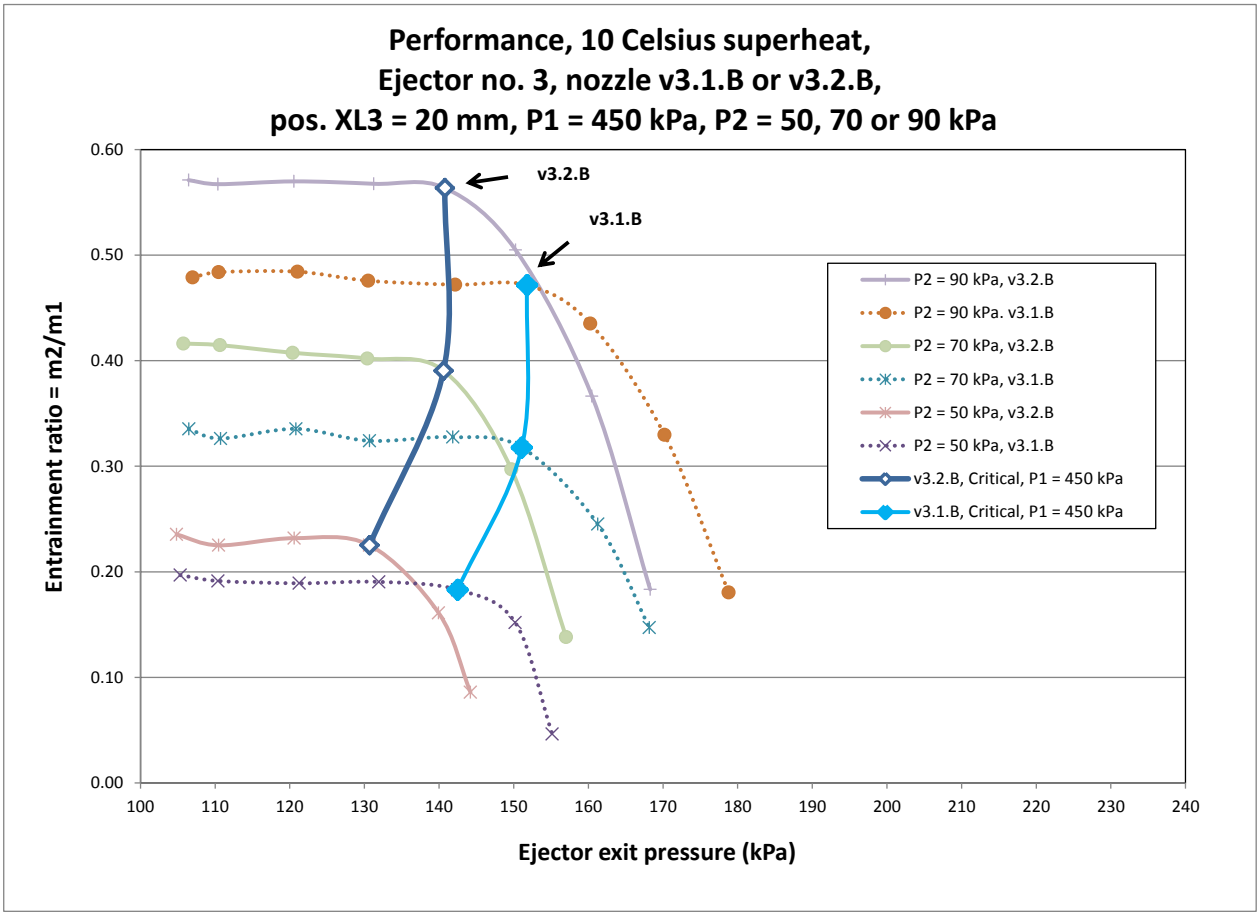

Fig. 3.31 P1 = 450 kPa, various secondary pressures, nozzles v3.1.B and v3.2.B

Fig. 3.32 compares the situation where we start from a given experimental condition, for example a secondary pressure of 70 kPa and nozzle diameter of 4.23 mm (v3.2.B), as indicated by the point "A", and we wish to consider either increasing the nozzle diameter to 4.60 mm (v3.1.B), in the direction of the point "B", or increasing the secondary pressure to 90 kPa, in the direction of the point "C". Increasing the primary nozzle diameter results in a decrease in entrainment ratio and an increase in critical pressure as we move from point "A" to point "B". For the example shown in Fig. 3.32, increasing the secondary pressure, thus moving from point "A" to point "C", increases the entrainment ratio, with no effect on the critical pressure. Table 3.11 summarizes what was observed in this discussion.

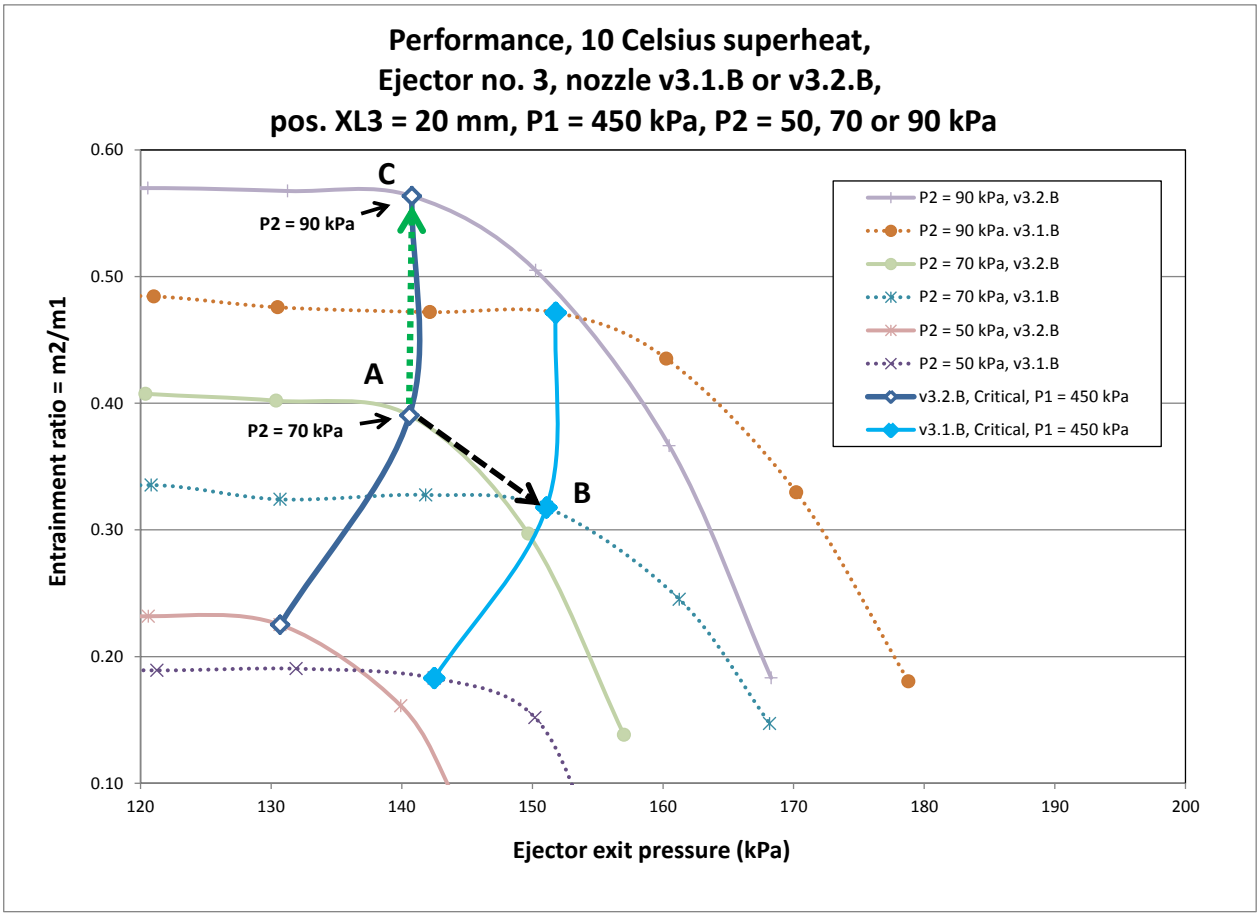

Fig. 3.32 P1 = 450 kPa, various secondary pressures, nozzles v3.1.B and v3.2.B, analysis

Table 3.11 Comparison of nozzles v3.1.B and v3.2.B, for constant primary pressure P1

Input Conditions		Output result	
Change	Keep Constant	Critical Pressure	Entrainment ratio
increase nozzle diameter	primary pressure secondary pressure	increases	decreases
increase secondary pressure	primary pressure nozzle diameter	same or increases	increases

3.3.10 Effect of the diameter ratio $(D5/D2p)^2$ on the compression ratio

The observed impact of ejector and nozzle geometry on performance for the nozzles v3.1.B and v3.2.B can be extended slightly by including other available experimental information. Table 3.12 compares three separate geometry configurations for similar, but not identical, input pressures. The table shows the measured "as manufactured" nozzle throat diameters D2p, as opposed to the design values. It can be seen that as the geometry ratio $(D5/D2)^2$ increases, there is a corresponding increase in entrainment ratio and a decrease in both the critical pressure and the compression ratio.

Table 3.12 Diameter ratio $(D5/D2p)^2$ and compression ratio (Cr)

Ejector	Nozzle	D2p (mm)	D5 (mm)	Primary Pressure (kPa)	Secondary Pressure (kPa)	Critical Pressure (kPa)	Entrain.	Cr	$(D5/D2p)^2$
2	v2.3	5.17	14.00	450	60	111.1	0.56	1.85	8.16
3	v3.2.B	4.23	9.50	450	70	140.6	0.39	2.00	5.04
3	v3.1.B	4.59	9.50	450	70	151.1	0.32	2.16	4.28

For comparison purposes, it is interesting to note the area ratio of the constant diameter portion of the ejector mixing chamber to that of the primary nozzle, or the ratio $(D5/D2p)^2$ using our nomenclature, can be found to have a wide range of values in the literature. Using R11 as the working fluid, Nadhi et al. evaluated seven values, from 4 to 13.44, and found 9.87 to be optimal

[70]. Eames et al. worked on a small-scale steam jet refrigerator test bench with a $(D5/D2p)^2$ value of 81, $(18\text{ mm}/2\text{ mm})^2$ [27]. Zhang et al. investigated the behaviour of a steam ejector where the throat of the primary nozzle could be adjusted by moving a spindle or needle [123]. They showed that the entrainment ratio changed from roughly 0.6 to 0.45 to 0.1 as the $(D5/D2p)^2$ value changed respectively from 4.99 to 4.58 to 4.45. The values in Table 3.12 thus are in general agreement with the experimental findings of Zhang et al. [123].

3.3.11 Summary of observed effects for pure steam

Table 3.13 presents a summary of the effects discussed in the previous sections for pure steam. Generally the trends shown in the table are in agreement with other published experimental results [19, 27, 123]. One surprise is the fact that the critical pressure did not increase in all cases when the secondary pressure was increased, as shown in the third row from the top in Table 3.13. Although this observation could be a combination of experimental error and coincidence, the observation did apply to performance tests for two nozzles evaluated on different days. Referring to Fig. 3.26, it can be seen that the critical pressure did in fact increase for the cases where the primary pressure was fixed at 350 kPa or 550 kPa for nozzle v3.1B. The increase in critical pressure was also observed for the v3.2.B nozzle for the primary pressure fixed at 350 kPa or 550 kPa. Further experimental work would be required to clarify this point.

Table 3.13 Summary of experimental results for pure steam

Input Conditions		Output result	
Change	Keep Constant	Critical Pressure	Entrainment ratio
increase nozzle diameter	primary pressure secondary pressure	increases	decreases
increase primary pressure	nozzle diameter secondary pressure	increases	decreases
increase secondary pressure	primary pressure nozzle diameter	same or increases	increases
increase $(D5/D2)^2$	primary pressure secondary pressure	decreases	increases

3.3.12 Effect of CO_2 on performance

In the current thesis, the main subject of interest is the use of steam ejectors to minimize the energy penalty of post-combustion carbon capture processes. Very preliminary work in the thesis suggested that amount of CO_2 that might be present in the secondary steam, for the scenarios of interest, would be in the range of trace CO_2 up to around 10% by mass. The first tests were conducted with CO_2 injected at a known volumetric flow rate into the flash tank, at levels below 10% mass fraction CO_2. It was found that at this low level of CO_2, given the uncertainty in the measurement of the mass flow, it was not possible to make meaningful conclusions about the effect of the CO_2. In that early phase, the CO_2 and secondary steam passed through the same flow meter, adding another level of uncertainty to the calibration and calculation of the secondary mass flow rate. It was decided that significantly higher levels of CO_2 should be evaluated in order to work in a range more appropriate to the test bench capabilities. Other countermeasures put in place to favour successful experimentation included moving the injection point of the CO_2 downstream of the secondary steam flow meter, yet upstream of the ejector secondary port. The piping was also changed to allow higher levels of CO_2 flowrate, and numerous modifications were made, including enhancing the insulation around the orifice flow meters at the ejector secondary port. It was decided that the target parameter values for the CO_2 studies would be 10 °C superheat for the ejector primary, a primary steam pressure of 450 kPa, and a secondary pressure of 70 kPa. The ejector nozzle exit would be positioned 20 mm upstream of the constant area section of the ejector body (XL3 = 20 mm). Two nozzle diameters would be evaluated, that of 4.24 mm for nozzle v3.2.1 and 4.60 mm for nozzle v3.1.B.

This portion of the experimental chapter will be presented as follows. First, comparative performance curves will be discussed separately, with varying levels of CO_2, for each of the nozzles. The idea of the "Entrainment ratio correction factor" will be explained, and the results for both nozzles will be discussed together. Next, the results will be compared to those of W.C. Holton. With the Holton results as an ongoing reference point, the effect of the role of the critical pressure will be discussed. Finally, this section on the effect of CO_2 on performance will be given its larger context, where in the prologue the results will be tied to the upcoming thesis section dealing with post-combustion ejector enhanced carbon capture.

3.3.13 Nozzle v3.1.B performance curves, for varying CO_2 levels

On June 28, 29 and 30 of 2016, experiments were completed with the nozzle v3.1.B using controlled amounts of CO_2 in the secondary fluid. Fig. 3.33 shows the whole range of performance curves that were produced, with CO_2 levels of 0, 20, 40 or 60 L/min. After comparing the quality of the mass balances for the tests, the June 28 mass balance was found to be the least accurate, where the secondary flow was probably exaggerated. The most accurate data was collected during the June 30 tests. A comparison of the June 29 AM mass balance with that of the June 30 mass balance found that when there was 0 L/min CO_2, the secondary mass flow rate of pure steam was close to 14 kg/h on the 29th and to 13 kg/h on the 30th. It is not possible to say which value is closer to the true value, but the June 30 results have the advantage of consistently having the same secondary mass flow for the whole day of testing when the CO_2 flow was returned to 0 L/min.

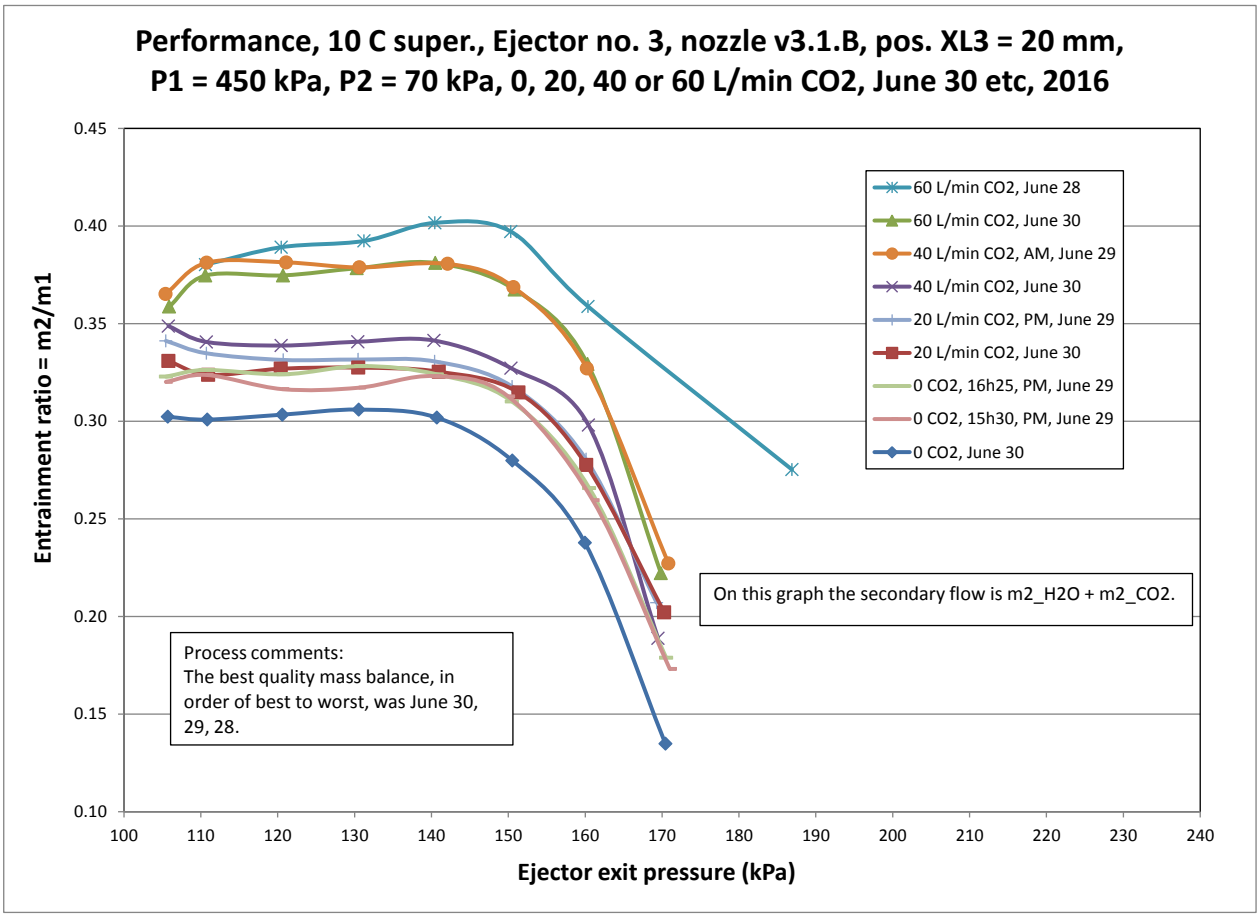

Fig. 3.33 Available performance curves with CO_2, nozzle v3.1.B

Fig. 3.34 shows the mass flow rate results relating to the June 30 tests. During the experimental work with CO_2 there are certain details relating to the use of the flow meters which were different than the experimental work with pure steam. When CO_2 is contained in the secondary flow, the exit flow meter results GF002 are no longer valid, as they are calibrated for pure steam. While CO_2 is injected, the secondary orifice flow meter FT003 measures only the pure steam leaving the flash tank. In Fig. 3.34 "m2_H2O" refers to the secondary mass flow of pure steam (kg/h), while "m2_CO2" refers to the secondary mass flow of pure CO_2 (kg/h). Thus, the mass flow of CO_2 through the rotameter and injected into the ejector secondary is shown in Fig. 3.34 as "Rota_2, m2_CO2". The combined secondary flow is shown in the legend as "FT003+Rota_2, m2_H2O + m2_CO2". The primary flow is identified as "FT002, New PRIM". The best estimate of the exit flow is "FT002+SEC+m2_CO2, New PRIM+m2_H2O+m2_CO2".

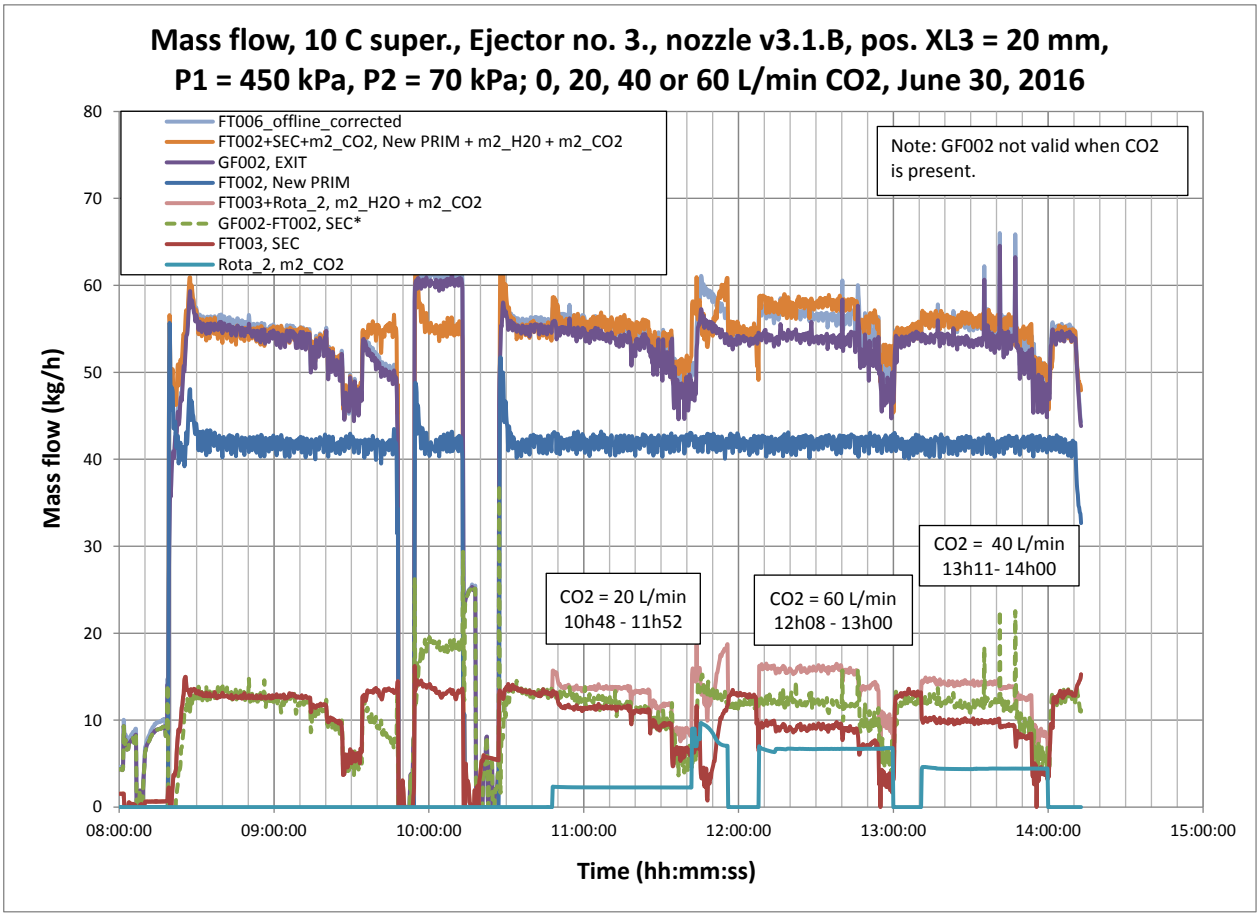

Fig. 3.34 Mass flows, various CO_2 levels, nozzle v3.1.B, June 30, 2016

Fig. 3.35 presents the performance curves having the highest quality mass balance of the available experimental results for the nozzle v3.1.B. It is immediately noticed that the general shape of the performance curves, with increasing CO_2 flow rate, does not generally change. It would appear from this figure that the critical pressure marking the transition between single choked mode and double choked mode is not a function of the amount of entrained CO_2 over the parameter range of the tests. This family of performance curves will be used as the basis of subsequent analysis and comparison with the nozzle v3.2.B results.

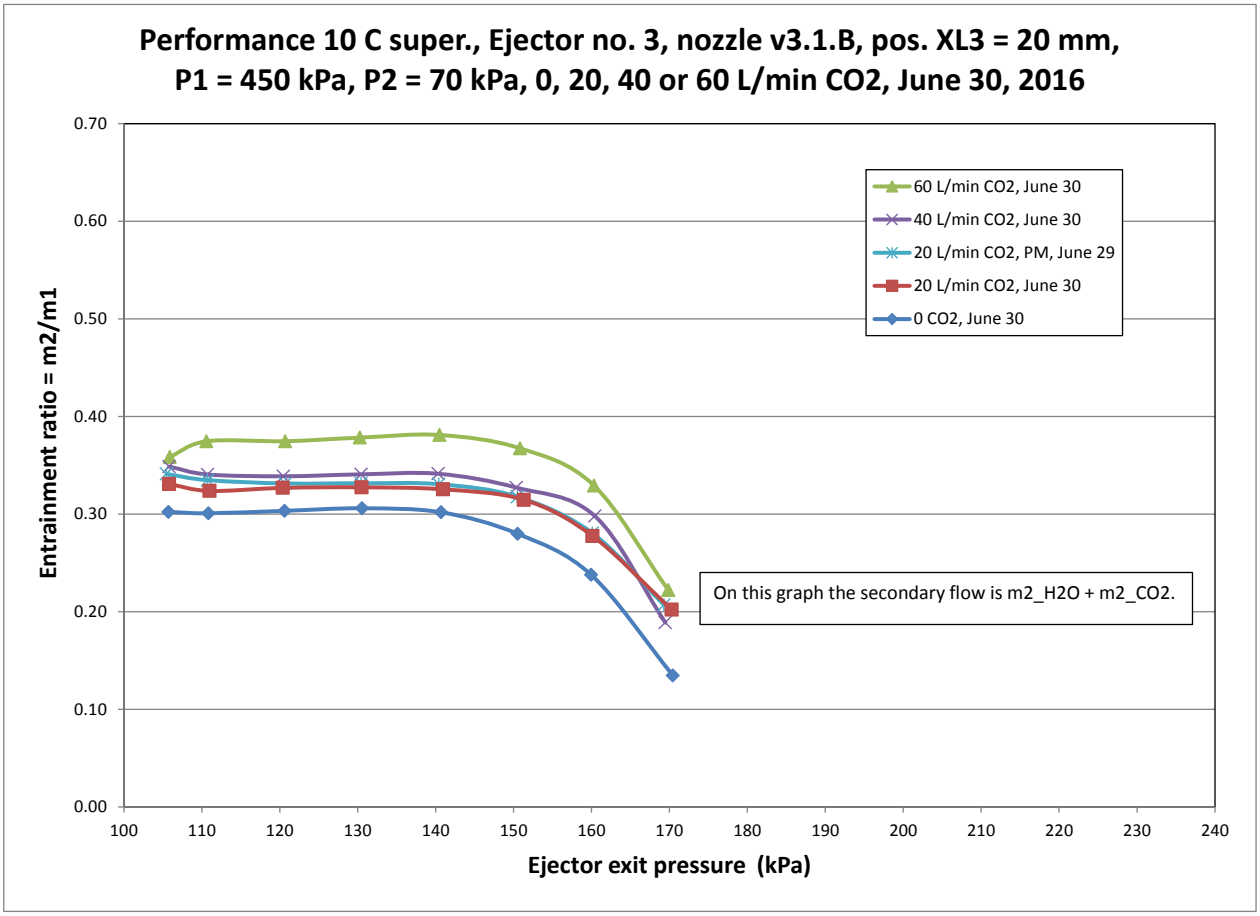

Fig. 3.35 Reference performance curves for various levels of CO_2, nozzle v3.1.B

Table 3.14 is intended to give a better idea of the mass flow of CO_2 that corresponds respectively to the volume flow rates of 0, 20, 40, and 60 L/min. For example, as noted in the third column from the left, under the heading "m2_CO2", the volumetric flow rate of 40 L/min

on rotameter 2 (Rota_2) corresponds to a mass flow rate of 4.4 kg/h of CO_2, which is 31% of the mass of the secondary flow in this case. The conversion of the volumetric flow rate into mass flow rate takes into account the calibration curve for the rotameter, as well as the recorded pressure and temperature of the CO_2 leaving the rotameter. The right most column in Table 3.14 here introduces the "Entrainment ratio correction factor". This is the change in the entrainment ratio using CO_2 that was observed as compared to the entrainment ratio where pure steam is used at the same input conditions. For example, for 20 L/min of injected CO_2, it was found that the entrainment ratio was 0.33, as opposed to 0.31 for pure steam, thus giving an entrainment ratio correction factor of 1.07.

Table 3.14 CO_2 mass flow rates with P_exit = 130 kPa, nozzle v3.1.B

CO_2 (L/min)	m2_H2O SEC (kg/h)	m2_CO2 Rota_2 (kg/h)	m2 (kg/h)	m1 (kg/h)	CO_2 mass fraction	m2/m1	Correction factor
0	12.8	0.0	12.8	41.7	0.00	0.31	1.00
20	11.5	2.3	13.7	41.9	0.17	0.33	1.07
40	9.9	4.4	14.3	41.9	0.31	0.34	1.11
60	9.2	6.7	15.9	42.1	0.42	0.38	1.24

3.3.14 Nozzle v3.2.B performance curves, for varying CO_2 levels

Experiments were completed with CO_2 for the nozzle v3.2.B on June 1st, 7, 8, 21 and 30. The June 7 and 8 results had very good mass balances. The June 8 results are shown in Fig. 3.36. The key observations are as follows:

1. No downward drift for the secondary (FT003) or exit (GF002) flow meter.
2. A very good mass balance with steam only, before and after CO_2 injection.
   ie. GF002 = FT002 + FT003, or EXIT = PRIM + SEC
3. The corrected gas flow rate at the ejector exit (FT006_offline_corrected) agreed well with the sum of the primary, secondary ("m2_H2O") and injected CO_2 ("m2_CO2") mass flow rates.

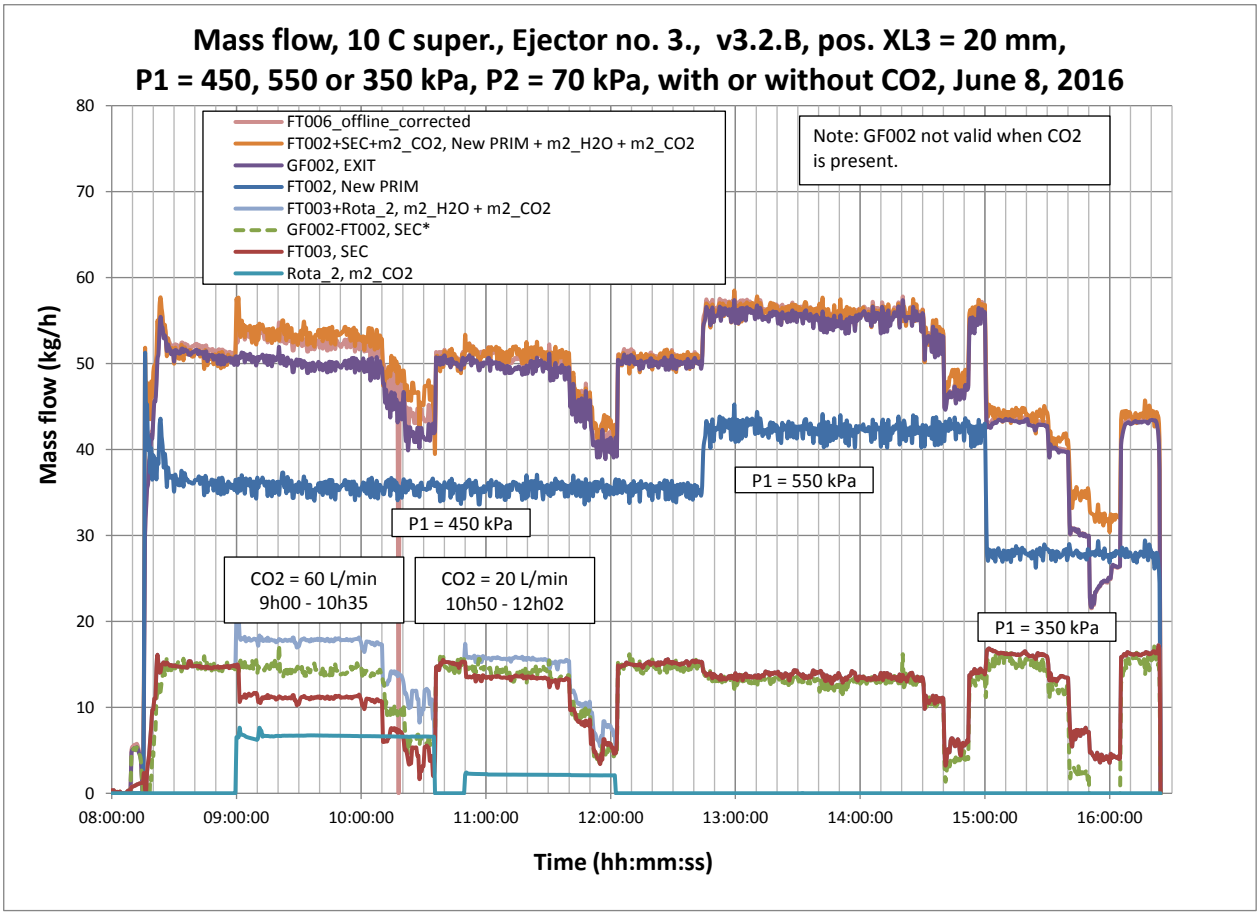

Fig. 3.36 Mass flows, various CO_2 levels, nozzle v3.2.B, June 8, 2016

Several of the available performance curves for nozzle v3.2.B are shown in Fig. 3.37. As can be seen, there is some overlap between the performance curves for the 60 and 80 L/min CO_2. There were in fact CO_2 flow control problems associated with the 80 L/min tests, so this curve will be eliminated from further consideration. In the upcoming analysis of the curves, given the importance of the pure steam reference curve, with 0 L/min CO_2, it was decided to average the three available reference curves for pure steam. Thus, a composite curve was produced by averaging the results from the June 1st test, and from two tests completed on June 21. Fig. 3.38 shows the resulting composite reference performance curve. The family of performance curves shown in Fig. 3.38 will be used as the basis for subsequent analysis and comparison. As was also observed with the nozzle v3.1.B results, the performance curves for the nozzle v3.2.B maintain the same general shape and the same critical pressure as the flow rate of CO_2 is increased from 0 to 60 L/min.

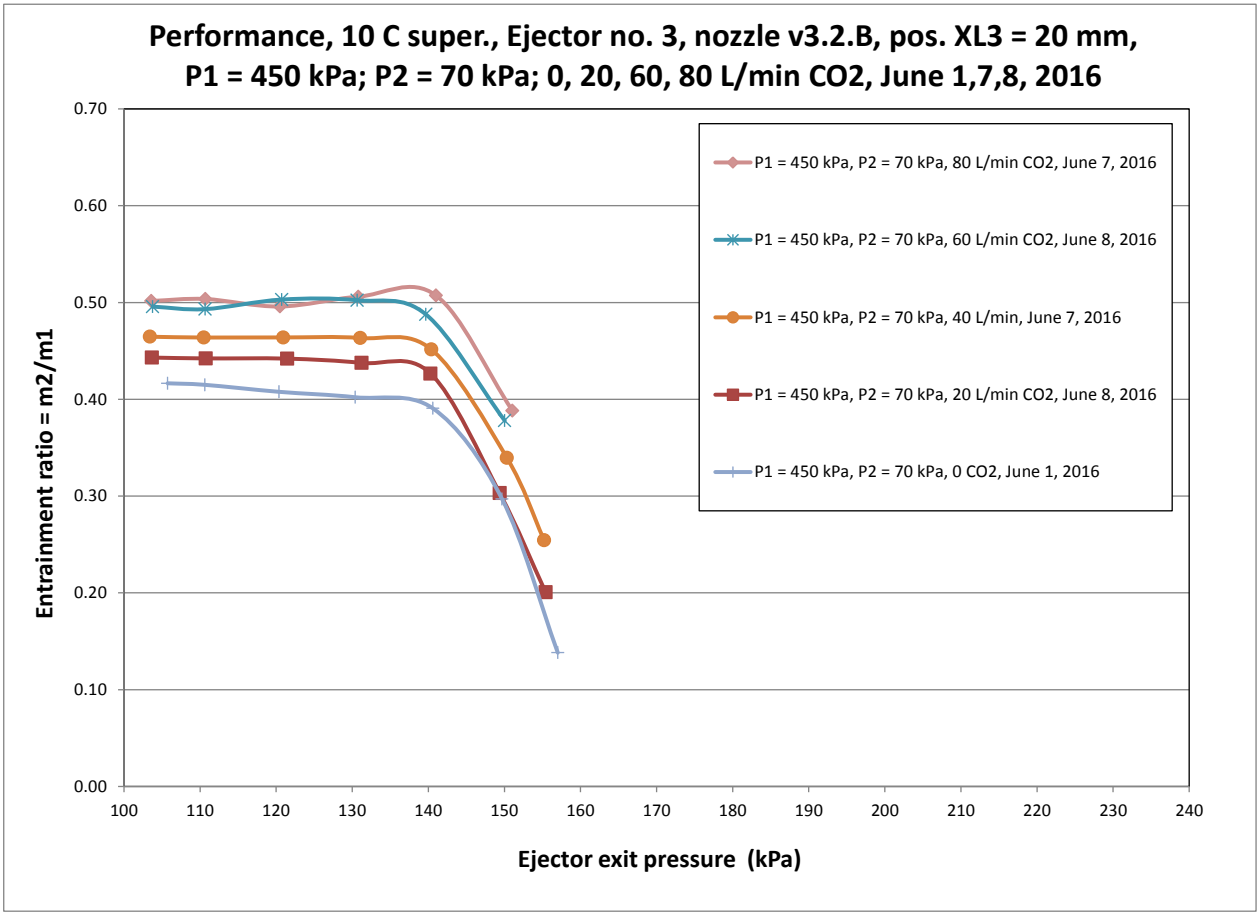

Fig. 3.37 Available performance curves with CO_2, nozzle v3.2.B

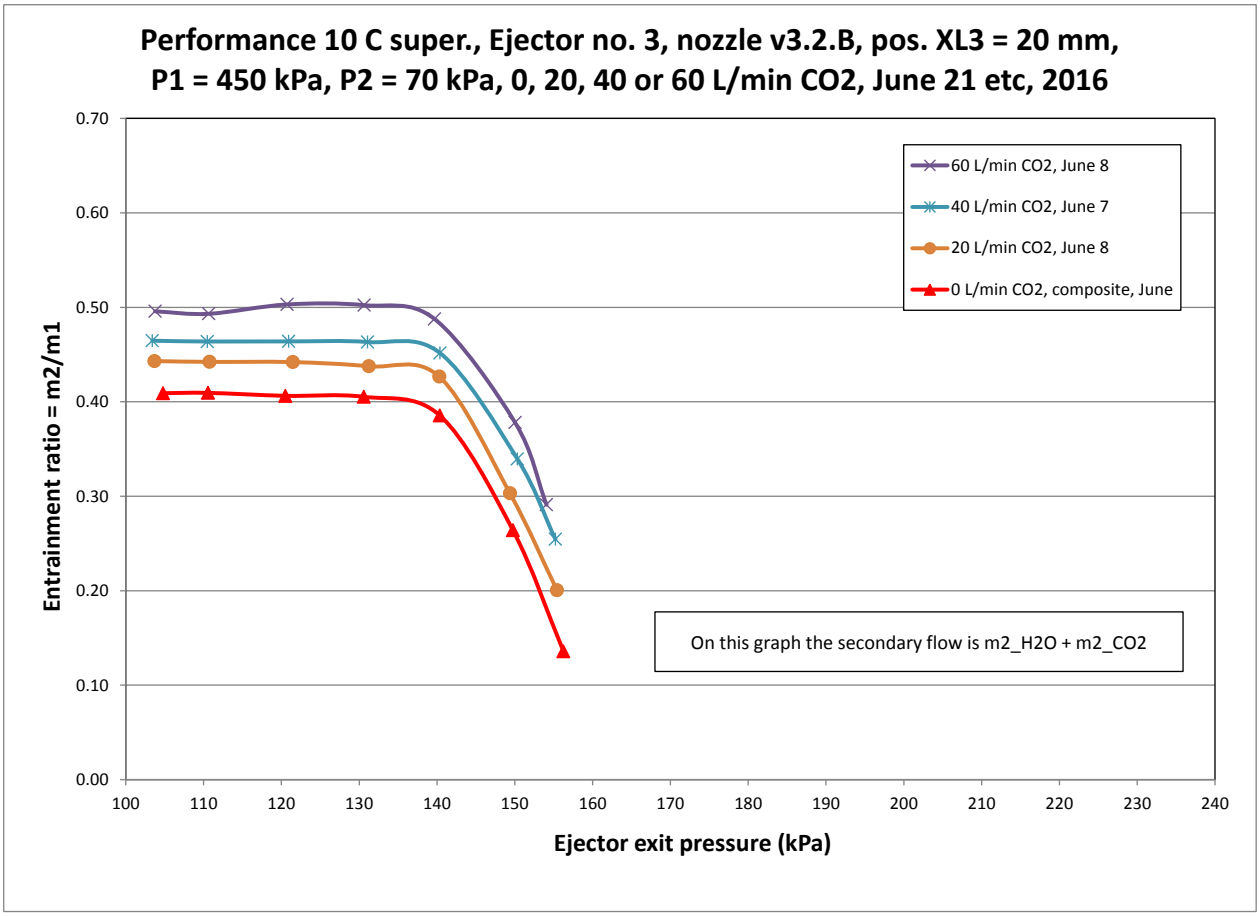

Fig. 3.38 Reference performance curves for various levels of CO_2, nozzle v3.2.B

Table 3.15 presents the flow rate information corresponding to an ejector exit pressure of 130 kPa, for each of the reference performance curves for nozzle v3.2.B. Again, considering the performance curve for 40 L/min of CO_2, the mass flow rate of CO_2 is 4.4 kg/h and corresponds to 27% of the mass of the secondary fluid. The "Entrainment ratio correction factor" is 1.14. Specifically, this is the ratio of the entrainment ratio at 40 L/min CO_2 of 0.46, to that of pure steam entrainment ratio of 0.41. It is interesting to note that the largest value of the entrainment ratio correction factor is 1.24 for 60 L/min, which is numerically equivalent to the nozzle v3.1.B value shown in Table 3.14.

Table 3.15 CO_2 mass flow rates with P_exit = 130 kPa, nozzle v3.2.B

CO_2 (L/min)	m2_H2O SEC (kg/h)	m2_CO2 Rota_2 (kg/h)	m2 (kg/h)	m1 (kg/h)	CO_2 mass fraction	m2/m1	Correction Factor
0	14.4	0.0	14.4	35.5	0.00	0.41	1.00
20	13.4	2.2	15.6	35.6	0.14	0.44	1.08
40	12.1	4.4	16.5	35.6	0.27	0.46	1.14
60	11.2	6.7	17.9	35.6	0.37	0.50	1.24

3.3.15 Entrainment ratio correction factor, both nozzles, preliminary results

In order to begin comparing the effect of the nozzle diameter on the entrainment ratio correction factor, a conservative approach would be to consider an ejector exit pressure for which both nozzles were operating in their stable mode, with or without the presence of CO_2. In other words, an exit pressure must be selected that is below the critical pressure. For this purpose, a pressure of 130 kPa is chosen, which can be visually verified by referring to Fig. 3.35 and Fig. 3.38. The respective entrainment ratio correction factors are compared in Fig. 3.39, with the volume flow rate of CO_2 shown in L/min on the abscissa. The slight dip in the v3.1.B correction factor at 40 L/min is likely caused by experimental error associated with the manual control of the CO_2 rotameter.

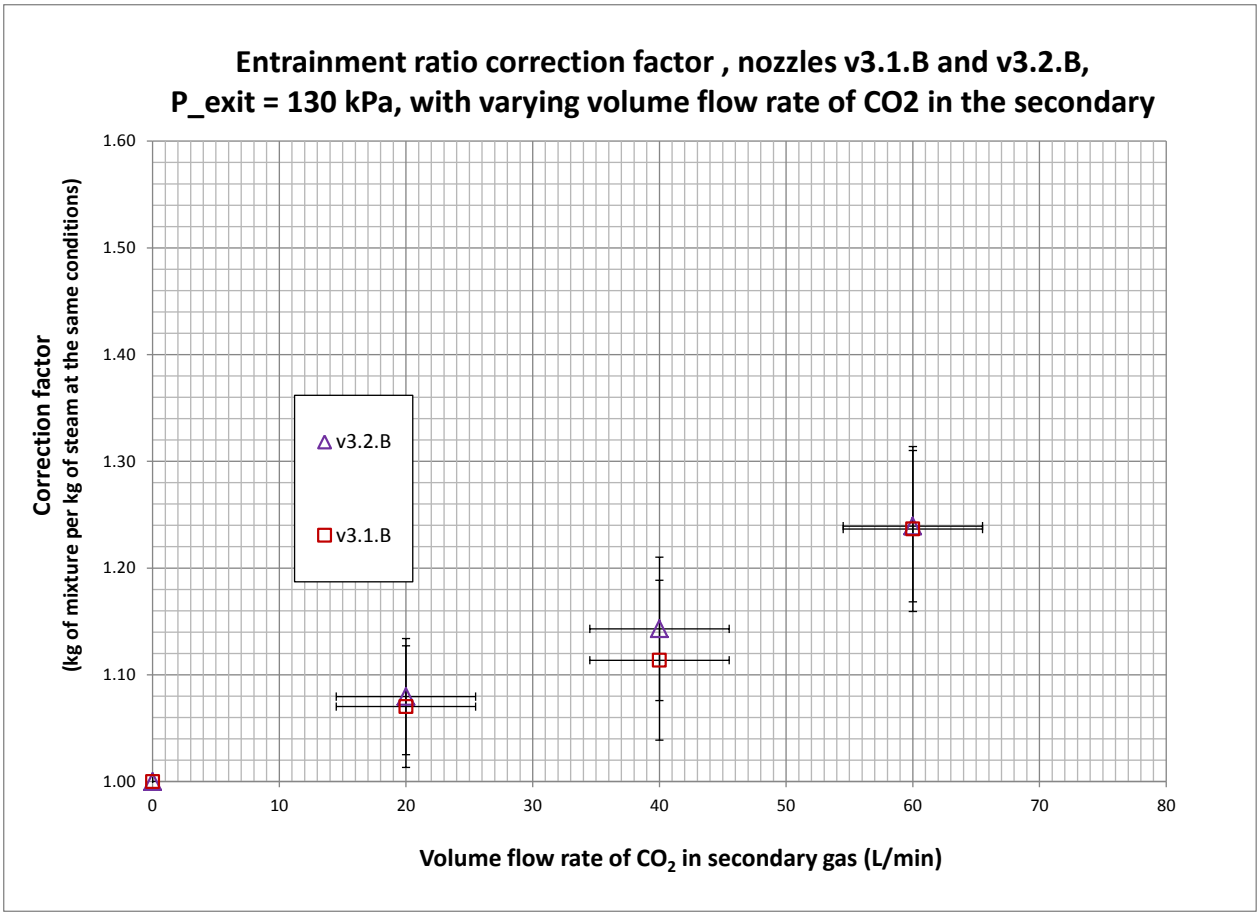

Fig. 3.39 Correction factor for varying CO_2 volume flow rates

In Fig. 3.40, the amount of CO_2 injected into the ejector is quantified in terms of the mass fraction of CO_2 in the ejector secondary fluid. The chart suggests that for the same mass fraction of CO_2 in the secondary, the smaller diameter nozzle v3.2.B had a more significant increase in the entrainment ratio correction factor. This may be related to the fact that both the entrainment ratio and the pure steam secondary flow rates were greater for the smaller diameter nozzle v3.2.B. For example, for 0 L/min of CO_2, the nozzle v3.2.B entrainment ratio and secondary steam flow rates ("m2_H2O) were 0.41 and 14.4 kg/h in Table 3.15, whereas the corresponding values for the larger throat diameter nozzle v.3.1.B were respectively 0.31 and 12.8 kg/h in Table 3.14.

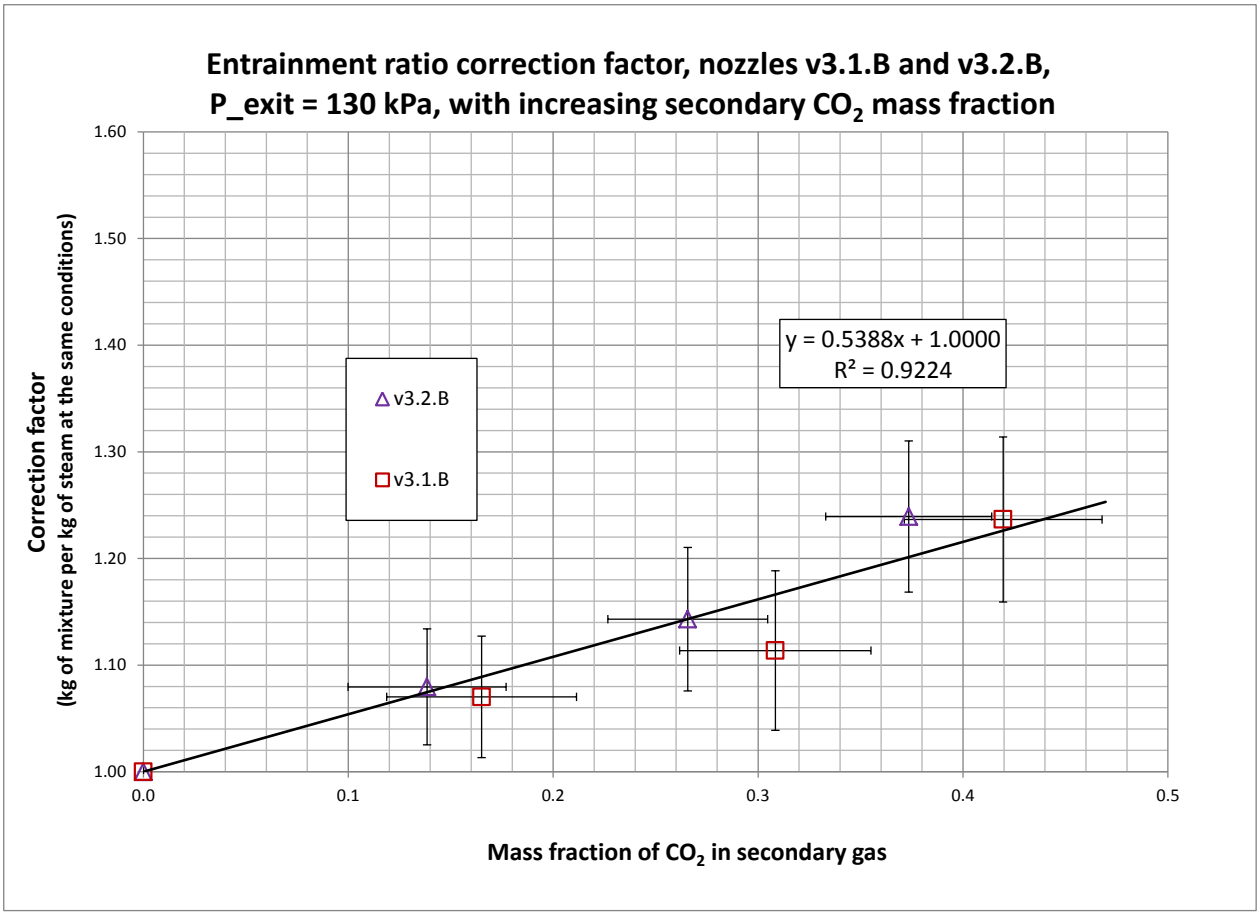

Fig. 3.40 Correction factor for varying CO_2 mass flow rates

3.3.16 Comparison with the empirical results of W.C. Holton

The concept of the "Entrainment ratio correction factor", discussed in the previous sections, is very similar to the idea used by W.C. Holton in his 1951 article [37]. In his experimental study, steam was used as the primary fluid and air was considered the reference fluid drawn into the ejector secondary port. The study determined the change in ejector performance as a function of the molecular weight of the ejector secondary fluid, evaluating 13 pure gases and 12 mixtures. A graph was published which shows the expected correction factor that should be applied to the ejector entrainment, or "air equivalent" in Holton's terminology, as a

function of the molecular weight of the secondary fluid. Fig. 3.41 recreates Horton's curve, identified in the chart legend as "Air as secondary reference fluid, Horton, 1951".

For the purposes of the current thesis study, an analogous "steam equivalent" curve was created based on Holton's publication. Mixtures of H_2O and CO_2 will span the molecular weight range of 18.02 to 44.01 kg/kmol, as shown in Table 3.16. By considering a range of mass fraction values of CO_2, from 0 to 1, and calculating the corresponding molecular weight, Horton's published curve was used to determine the values in the "Air Equivalent" column of Table 3.16. Each value in the "Steam Equivalent" column is normalized for steam, where the matching value in the Air Equivalent column is divided by 0.81. The resulting values are plotted in Fig. 3.41, identified in the legend as "Steam as secondary reference fluid, Holton, 1951". This reference curve will serve as validation of our experimental work in the upcoming discussion.

Table 3.16 Preparation of the "Entrainment ratio correction factor" for "Steam Equivalent"

Mass fraction CO_2	Molecular Weight (kg/kmol)	Air Equivalent (kg/kg)	Steam Equivalent (kg/kg)
0.00	18.02	0.81	1.00
0.10	19.15	0.84	1.03
0.20	20.43	0.86	1.06
0.30	21.90	0.89	1.09
0.40	23.59	0.91	1.12
0.50	25.57	0.95	1.16
0.60	27.91	0.98	1.20
0.70	30.72	1.02	1.25
0.80	34.16	1.07	1.31
0.90	38.46	1.13	1.38
1.00	44.01	1.19	1.46

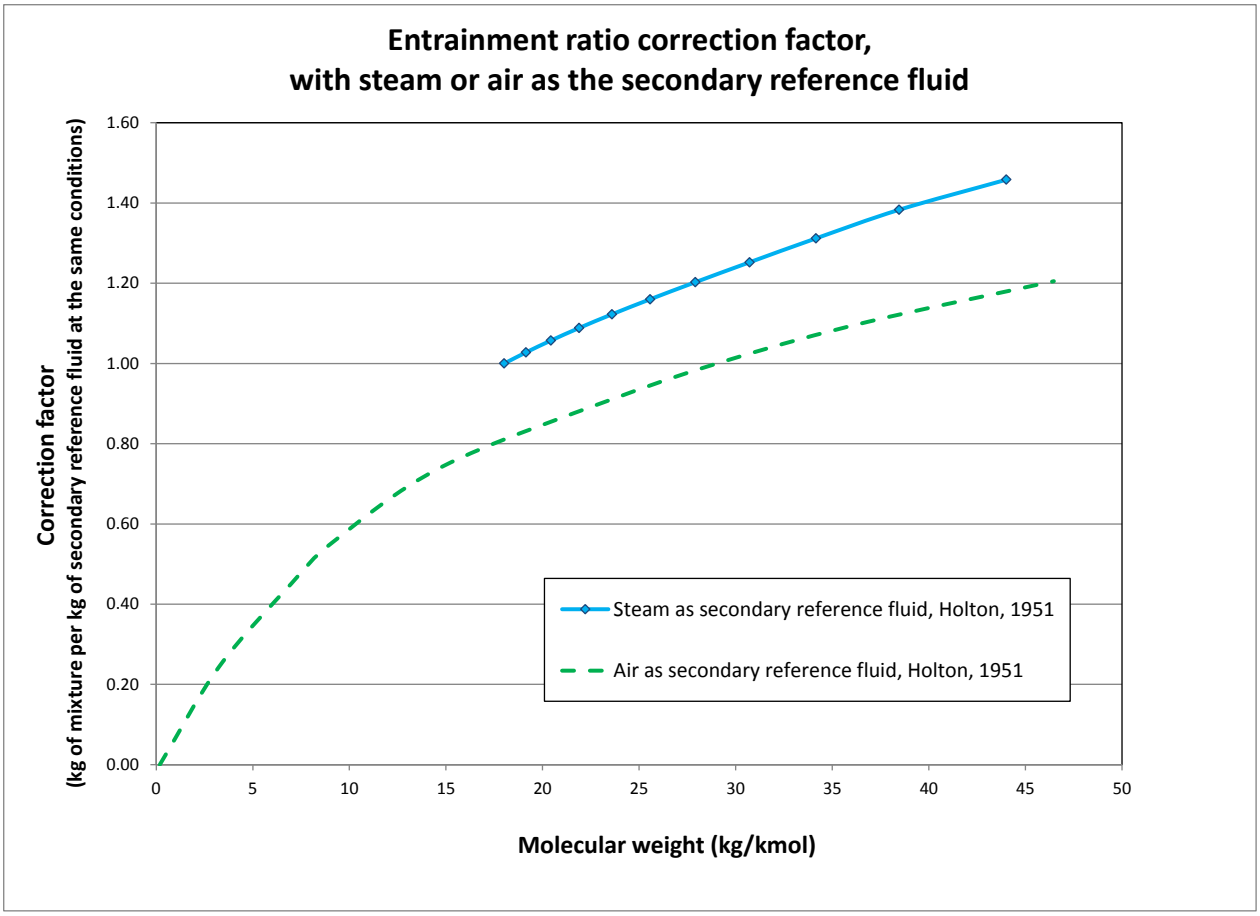

Fig. 3.41 Holton reference correction factor as a function of molecular weight

3.3.17 Effect of ejector exit pressure on the entrainment correction factor

The effect of a certain amount of CO_2 in the entrained secondary steam on the overall ejector entrainment ratio is not necessarily linear as the ejector exit pressure changes. Fig. 3.42 presents the entrainment ratio correction factor for the nozzle v3.1.B, with ejector exit pressures taken as a parameter. By referring to Fig. 3.35, it can be seen that an exit pressure of 130 kPa is conservatively below the critical pressure, 140 kPa is approximately equivalent to the critical pressure, and 150 kPa is definitely higher than the critical pressure for the v3.1.B nozzle. The chart in Fig. 3.42 also shows the Holton reference curve, discussed in the previous section. The correction factors are closest to the Holton curve when ejector exit pressure is at or below the critical pressure. For the curve corresponding to an ejector exit pressure of 150 kPa, where the

ejector was operated above the critical pressure, the entrainment ratio factor is furthest from the Holton reference curve.

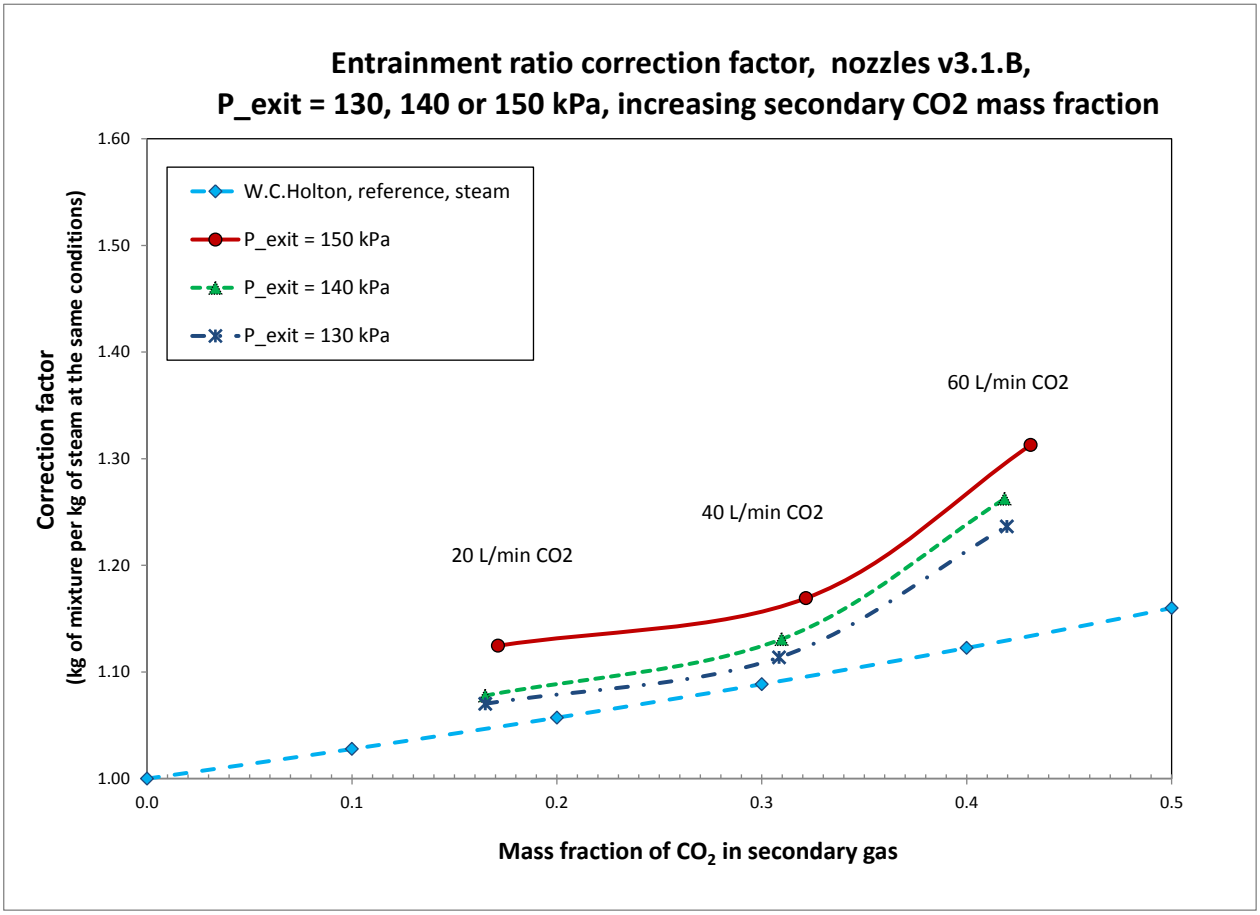

Fig. 3.42 Correction factor, various exit pressures, nozzle v3.1.B

The entrainment ratio correction factor, which will now simply be referred to as the correction factor, is compared for both the v3.1.B and v3.2.B nozzles in Fig. 3.43. The trends observed with the v3.1.B nozzle are repeated in the chart. For the v3.2.B nozzle, the correction factors corresponding to an ejector exit pressure of 150 kPa are significantly far from the Horton reference curve, and increasingly so as the mass fraction in the secondary gas increases. Referring again to the performance curves for nozzle v3.2.B shown in Fig. 3.38, in this case an exit pressure of 150 kPa is clearly well above the critical pressure. Taking into account the preceding comments, in the following section the exit pressure of 130 kPa will be chosen as the reference pressure for characterizing the effect of CO_2 on the performance of steam ejectors. In

the Holton article there was no discussion of role of critical pressure, but it can be reasonably assumed that the ejectors were operated in the stable or double choked mode.

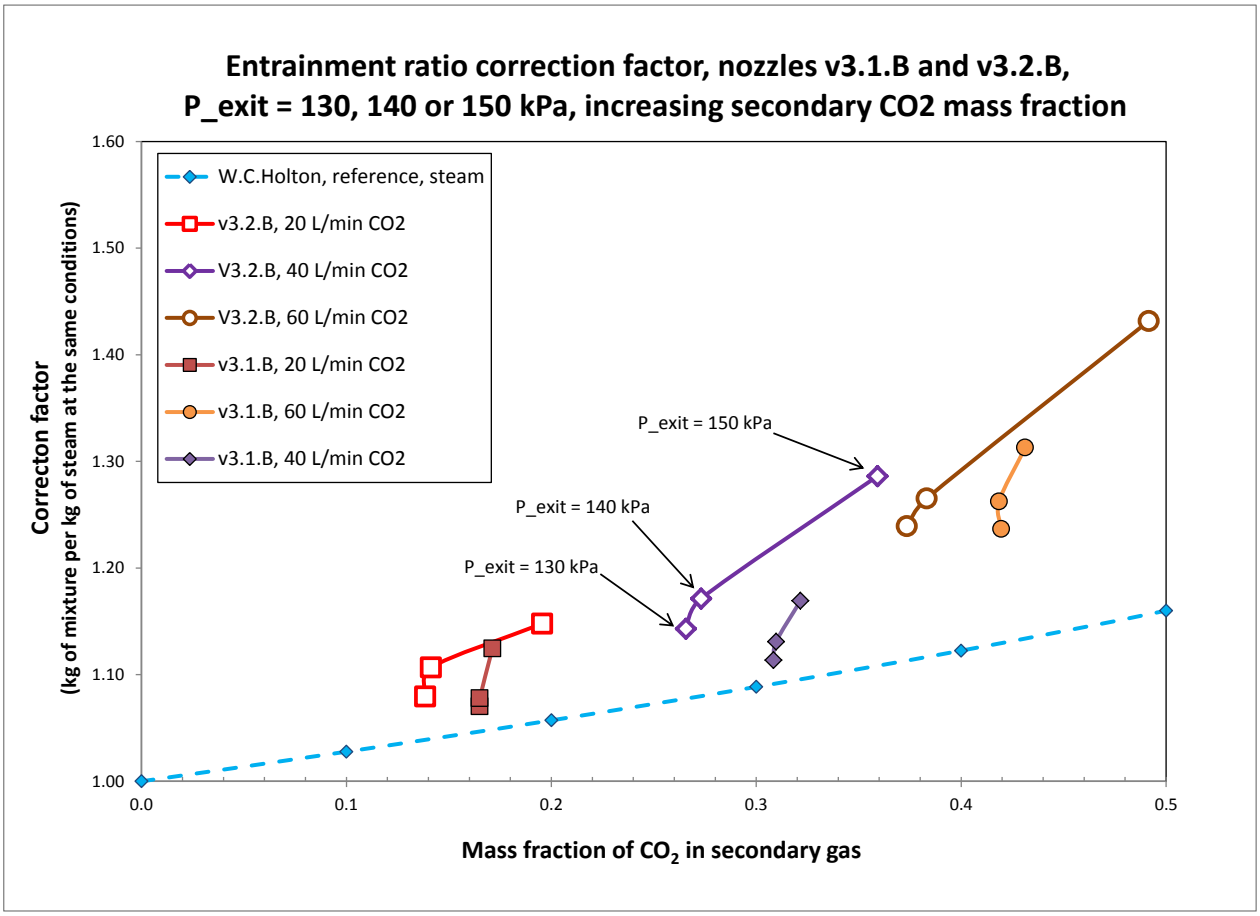

Fig. 3.43 Correction factor, various exit pressures, nozzles v3.1.B and v3.2.B

3.3.18 Effect of CO_2 on steam ejector performance

The global experimental findings for nozzles v3.2.B and v3.1.B can now be compared with the empirical results of W.C. Holton, as is shown in Fig. 3.44. The results of a linear regression, using the combined data from both nozzles, are shown directly on the chart. Given the limited amount of data, a higher order polynomial regression would be unwarranted. The experimental results are similar to those of Holton, but indicate that a larger correction factor should be expected than indicated by Holton.

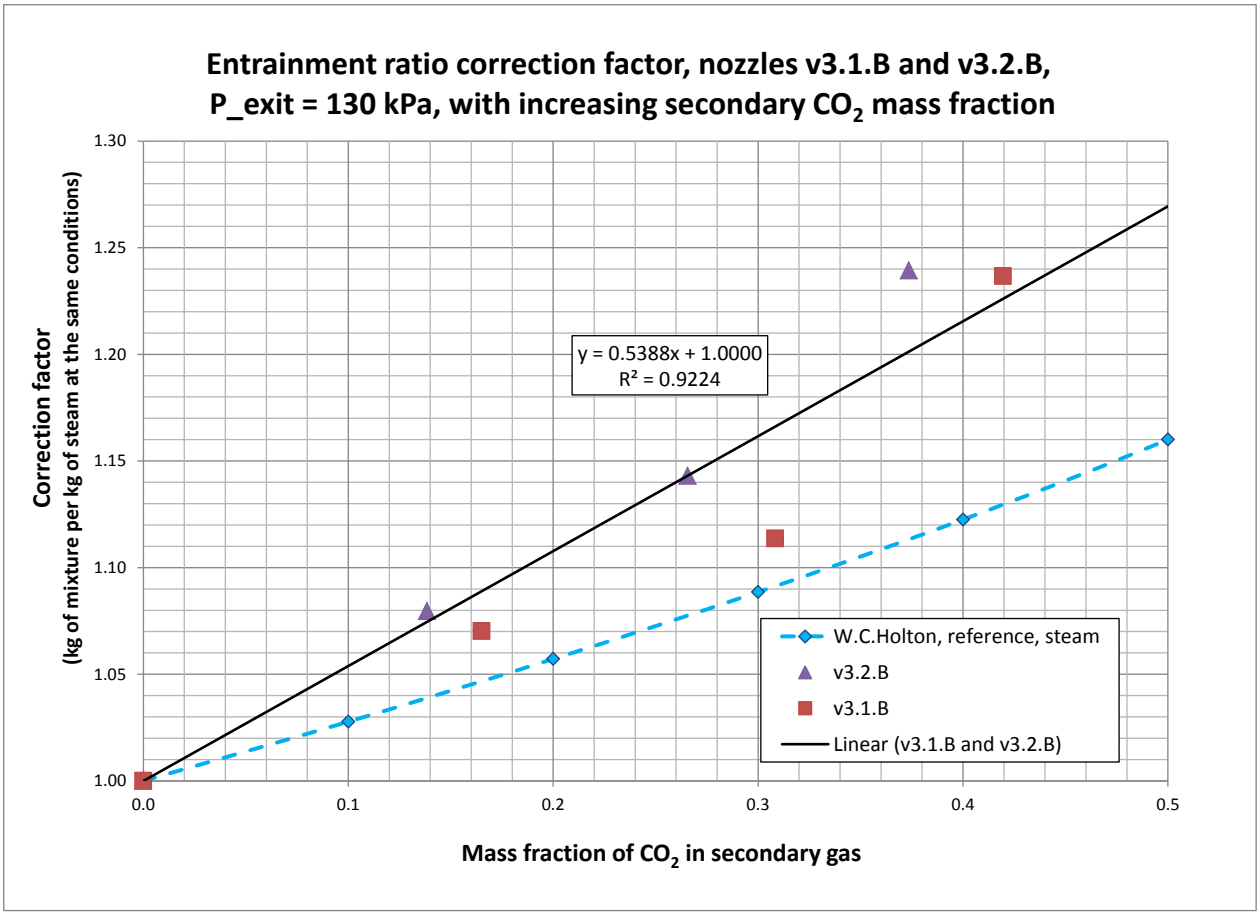

Fig. 3.44 Experimental results versus Holton reference, nozzles v3.1.B and v3.2.B

In Fig. 3.45 the linear regression curve of the combined experimental results is extrapolated to cover the possible range of CO_2 mass fraction values, from 0 to 1. In this chart we also show results from three published works. The lowest curve in Fig. 3.45 is from the experimental work of Work and Haedrich, completed in 1939 [116]. The curve above the Holton reference curve is derived from a molecular weight correction factor proposed by DeFrate and Hoerl in their 1D thermodynamic article of 1959 [24]. Their correction factor is simply the square root of the ratio of the actual secondary fluid molecular weight mixture to that of pure steam. It is interesting to observe that there is an increasing trend in the historic estimates of the correction factor, increasing in the following order: Work and Haedrich, Holton, DeFrate and Hoerl, the current experimental thesis results. There is reasonably good agreement between the APCCO2 test bench results and the work done by W.C. Holton, however our experiments indicate that correction factor for CO_2 is slightly higher than the values predicted by Holton. Considering both

the curve based on the work of W.C. Holton, and the results of the current thesis experimental work, Fig. 3.45 indicates that an improvement of approximately 50% would be expected in the performance of a steam ejector where the secondary fluid is pure CO_2 gas.

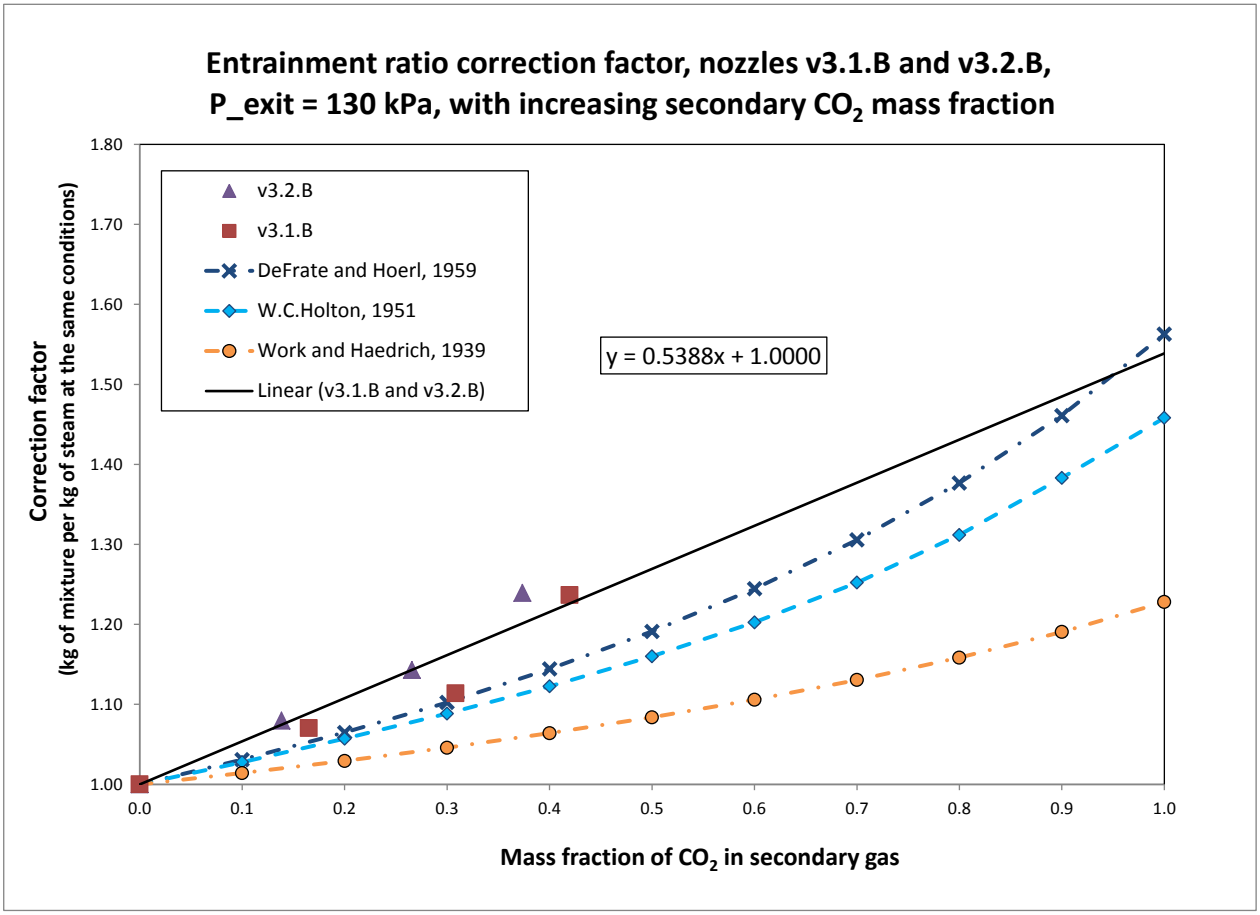

Fig. 3.45 Extrapolated experimental results compared with published data

Using the linear regression shown in Fig. 3.44 we can summarize the test bench results, for the experimental parameter range that was evaluated, by stating that an improvement of 23% was found in the performance of a steam ejector when the secondary steam contains a 42% CO_2 by mass. It is important to note that this increase in entrainment ratio does not come at the expense of the critical pressure. This is in sharp contrast to the usual trade-off in steam ejectors, or ejectors more generally, where an improvement in the entrainment rate comes at the expense of a decrease in the critical pressure that the ejector can provide. This conclusion could be helpful in degassing applications or in encouraging new applications where steam activated ejectors use secondary mixtures containing non-condensable gases.

3.3.19 Prologue to post-combustion ejector enhanced carbon capture

At this point it would be helpful to ask the reader to step back from the presentation of the experimental results, and allow the introduction of some notions that will only be described in full detail later in the thesis. This break with the sequential presentation of the thesis will prepare the groundwork for the upcoming discussion on carbon capture processes, and will make the connection with the experimental results. Basically, the test bench work led to a simple linear model of the expected change in the performance of a steam ejector as a function of the mass fraction of CO_2 in the secondary fluid. How can this information be beneficial in the larger context of post-combustion CO_2 capture? Assuming that it can be shown that a steam ejector can be advantageously used in a carbon capture process, what changes will occur when we account for the modified ejector entrainment characteristics when the secondary steam contains some CO_2?

As will be discussed later, it will be shown that a steam injector can in fact reduce the amount of valuable energy required to regenerate the solvent in post-combustion carbon capture. The choice of the appropriate position for placing the ejector in the capture process is very important, and can make the difference between a significant net benefit or, to the contrary, an additional energy drain on the capture process. Suffice it to say at this point that three principal scenarios, or cases, were studied, here identified as "Ejector on condensate", "Ejector on lean" and "Ejector on rich".

Table 3.17 provides estimates of the mass fraction of CO_2 that are contained in the secondary fluid entering the steam ejector for each of the three principal study cases. The two central columns of the table are headed respectively "Equilibrium model" and "Rate-based model". The information in the column headed "Equilibrium model" was used first as a guide to the experimental plan designed to quantify the effect of the entrained CO_2 on the steam jet performance. These results were based on the relatively simpler and computationally more stable process simulation results, assuming more ideal equilibrium thermo-physical properties of the solvent used in the post-combustion capture process [89]. In Table 3.17 the column entitled "Rate-based model" provides the similar information as in the "Equilibrium model", but in this column the estimates are expected to be much more realistic. These results are drawn from one of the journal articles that contribute a chapter to the thesis [92]. The column to the extreme right in

Table 3.17 applies the linear equation of Fig. 3.44, $y = 0.5388\,x + 1.0000$, to estimate the entrainment ratio correction factor for each simulation scenario. Extra digits are shown in Table 3.17 to show the trend for the various cases. For both the "Ejector on condensate" and "Ejector on lean" cases, the estimated increase in the entrainment ratio of a steam ejector is less than 0.5% and is thus insignificant.

In the case of the "Ejector on rich" simulation, however, the entrainment ratio would be expected to increase by approximately 7% as compared to a pure steam ejector. As will be shown in chapters 3 and 4, it turns out that the "Ejector on rich" case has no net benefit, and in fact would be expected to increase the valuable energy cost of the studied post-combustion carbon process. In the "Ejector on rich" simulation the increased performance due to the presence of entrained CO_2 in the secondary fluid will unfortunately exacerbate an already unpalatable scenario.

Table 3.17 Simulation cases and the mass fraction of entrained CO_2

Simulation case	Equilibrium model, Mass % CO_2 in secondary	Rate-based model, Mass % CO_2 in secondary	Correction factor based on the rate-based model
Ejector on condensate	0.32	0.13	1.0007
Ejector on lean	1.04	0.73	1.0039
Ejector on rich	7.531	13.56	1.0731

It can be stated at this point that the empirical steam model used in the publications that contribute to this thesis have been experimentally verified from the point of view of the possible impact of the effect of entrained CO_2 on the assumed steam ejector performance model. It should also be noted that for other potential applications, not including post-combustion carbon capture, that the improvement in the performance of a steam ejector as the portion of entrained non-condensable gas increases has been quantified and verified experimentally. A key experimental finding is, contrary to the experience with pure steam jet ejectors, that when ejector performance is increased due to the presence of CO_2 in the secondary fluid, the improvement does not come at the expense of a reduction in critical pressure.

3.4 Conclusions

An experimental test bench was designed and built at CanmetENERGY which allowed the characterization of the performance of a steam ejector where the secondary fluid contains a non-condensable gas. In the context of post-combustion carbon capture, the experimental program chose carbon dioxide as the non-condensable gas for the study. The main components of the test bench are a 75 kW electric boiler, a 3 kW electric superheater, a gas-gas ejector, a flash tank, a condenser, and a system for injecting a stable known mass flow of CO_2 into the secondary fluid of the ejector.

In order to provide a reference point for comparison purposes, performance curves were prepared for pure steam with ejector primary pressures of 350, 450 and 550 kPa and ejector secondary pressures of 50, 70 and 90 kPa. Despite the finding that superheat had little effect on the primary mass flow, the superheat was maintained at 10 °C to assure stable flow meter behaviour and to minimize the risk of ejector damage. The effect of the distance between the nozzle exit tip and the start of the cylindrical portion of the ejector, XL3, was evaluated. Two primary nozzle diameters, of 4.60 mm and 4.23 mm, were evaluated and the ratio of the ejector cylindrical area to the primary nozzle area was discussed.

Both nozzles were evaluated over a range of CO_2 levels, up to approximately 40% by mass of the ejector secondary fluid. The primary pressure was maintained at 450 kPa with 10 °C superheat and the secondary pressure was 70 kPa. It was found that the critical exit pressure did not change as the mass fraction of CO_2 in the secondary fluid increased. The entrainment ratio, however, increased approximately linearly over the experimental range. For example, an improvement of 23% in the entrainment ratio, as compared with pure steam, was found when the secondary fluid contains 42% CO_2 by mass. This behaviour is in sharp contrast to the expected and experimentally observed behaviour of a pure steam ejector, where an increase in the entrainment ratio comes at the expense of a decrease in the ejector exit critical pressure. The experimentally observed increase in entrainment ratio, as compared with pure steam, was found to be slightly higher than previous published results. This work is the first known evaluation of the change in steam ejector behaviour, with an entrained non-condensable gas, where the effect is studied at exit pressures above and below the critical pressure.

CHAPTER 4 ENERGY SAVINGS IN CO_2 (CARBON DIOXIDE) CAPTURE USING EJECTORS FOR WASTE HEAT UPGRADING

4.1 Avant-propos

Auteurs et affiliations :

- Christopher Reddick, Doctorant, Département de génie mécanique, Université de Sherbrooke, 2500 boul. de l'Université, Sherbrooke, Québec J1K2R1
- Mikhail Sorin, Professeur, Département de génie mécanique, Université de Sherbrooke
- Fernand Rheault, PhD, anciennement de CanmetÉNERGIE, Ressources naturelles Canada, 1615 boul. Lionel-Boulet, case postale 4800, Varennes, Québec

Publication : Energy 65 (2014) 200-208

Référence : [91]

Contribution à la thèse :

Cet article contribue à la thèse de deux façons. D'abord, il présente une méthode raccourcie qui modélise un désorbeur, l'équipement le plus énergivore dans un procédé de captage de gaz carbonique. Deuxièmement, l'article montre le potentiel d'amélioration énergétique où un éjecteur revalorise des rejets thermiques au profit de la réduction de la consommation d'énergie de haute qualité.

Résumé français :

La plus grande barrière technique au déploiement à pleine échelle de la technologie d'absorption pour le captage de gaz carbonique en postcombustion est la grande consommation d'énergie nécessaire pour la régénération du solvant. Cet article présente une nouvelle application des éjecteurs pour la revalorisation de rejets thermiques, externe au procédé de captage, en vue de réduire la consommation de vapeur de turbine à coût élevé qui doit être fournie à la régénération du solvant. Une méthode raccourcie est proposée afin de modéliser et d'optimiser un procédé de captage de CO_2 en postcombustion d'une centrale thermique au charbon. Le procédé de captage est modifié par l'utilisation des éjecteurs qui servent à revaloriser des rejets thermiques. Bien que la méthode raccourcie s'applique à tout solvant, la monoéthanolamine (MEA) est le solvant de référence pour cette étude. L'étude évalue l'influence de la position du point d'injection de la vapeur dans la colonne de désorption, la pression du désorbeur, et la source de vapeur secondaire pour l'éjecteur. En appliquant la méthode raccourcie proposée, nous montrons que l'intégration optimale de l'éjecteur permet une réduction de 10 à 25% de consommation de l'énergie de haute qualité. Les meilleurs résultats se produisent lorsque la vapeur est injectée au point le plus bas dans le désorbeur, remplaçant en partie la vapeur à turbine provenant de la centrale thermique par la vapeur produite à partir de rejets thermiques.

4.2 Abstract

The biggest technical barrier to full scale deployment of absorption technology for post-combustion carbon capture in electric power plants is the high energy consumption for solvent regeneration. This paper presents a new application of ejectors to upgrade external waste heat for the purpose of reducing the amount of valuable turbine steam that is required to supply the solvent regeneration process. A shortcut method is proposed to model and optimize a coal fired post-combustion CO_2 capture process enhanced with ejector driven waste heat upgrading. Although the method can be used for any solvent, monoethanolamine (MEA) is the reference solvent for this study. The study evaluates the influence of the position of the point of steam injection into the stripper tower, the CO_2 loading of the solvent entering the reboiler from the stripper, the stripper pressure, and the source of the secondary ejector steam. By using the proposed method it is found that the optimal ejector integration allows a 10 to 25% reduction in the amount of valuable steam. The best results occur when the injected steam is sent to the bottom of the stripper tower, partially replacing the valuable steam from the power plant with waste heat derived steam.

Keywords: CO_2 capture; post-combustion; ejector; waste heat; MEA

4.3 Introduction

The warming of the global climate and the associated rising concentration of atmospheric carbon dioxide (CO_2) is a growing planetary concern. The combustion of fossil fuels is responsible for the majority of human produced emissions of greenhouse gases, principally due to CO_2 [11]. CO_2 capture and storage (CCS), the process of the separation of CO_2 from industrial and energy related sources and its subsequent long-term storage, is a viable option to mitigate climate change. Targeting large stationary sources of CO_2 is the most efficient way to introduce CCS on a large scale. Considering only worldwide stationary sources of at least 0.1 $MtCO_2$/yr, there are nearly 8000 such sites, where electric power generation plants represent over 75% of the total 13,466 $MtCO_2$/yr [64]. Flue gases from such power plants typically contain less than 15% CO_2 by volume.

The three main CO_2 capture technologies applicable to the combustion of fossil fuels include post-combustion, pre-combustion and oxy-fuel techniques [77]. Of these, only post-combustion technology lends itself to the retrofitting of existing fossil fuel based power plants. There is agreement among many researchers that the most appropriate and historically mature technology for the removal of CO_2 from post-combustion flue gases is by chemical absorption using amine solutions [64, 66, 93].

Amine solutions have been used to remove CO_2 from natural gas and hydrogen since the 1930s [45, 93]. Monoethanolamine (MEA) was one of the first amines used on a commercial basis as a sorbent solution, and is still widely used as an aqueous solution from 20 to 30 wt%, and is considered the reference solvent for comparison purposes. As a method of post-combustion CO_2 capture, small scale plant trials were successfully completed in the 1980s on both gas-fired and coal-fired plants [93]. To date no full scale implementation of flue gas scrubbing has been installed due to high cost and the lack of legislative necessity. The research community, however, has been very active both in experimental development and in the modelling of CO_2 capture systems. The main challenge in reducing the overall cost, and in particular the operating cost, is to reduce the energy required to regenerate the solvent in the desorption column, or stripper, which consumes over 60% of the total energy required for CCS [48]. This energy must be taken from the expensive steam which is used to create electricity in the power plant. The

energy consumption in the desorber reboiler is approximately 15 to 30% of the net power production of a coal-fired power plant [40].

Strategies to reduce the cost of CCS include the use of new solvents or solvent mixtures, novel system configurations for the process equipment, and efforts to find the optimal combination of the two. Recent studies on solvents, for example, include Idem et al. [39] , Yokoyama et al. [118] and Ohashi et al. [74]. Van Wagener and Rochelle [112] evaluated configurations which included multi-stage flash, multi-pressure columns, mechanical vapour recompression and an interheated column, finding the most significant improvement with the interheated column. Jassim and Rochelle [40] evaluated mechanical vapour recompression, multi-pressure and simple strippers, finding that the multi-pressure with mechanical vapour recompression was an attractive option. Also in the context of novel configurations, but where hot potassium carbonate is used as the absorbent in the Benfield process [45], ejectors have been proposed for the use of vapour recompression for the purpose of reallocating internal energy within the system, thus reducing the energy consumption in the reboiler. More recently, in the context of the CO_2 capture from synthetic ammonia using the Benfield process, Lu et al. [59] proposed the use of thermal vapour recompression using an ejector to reduce energy consumption of the solvent reboiler. Other efforts to reduce the reboiler consumption include redirecting heat from the flue gases [118, 120]. Flue gas temperatures vary from 100 °C to 150 °C depending on the point at which the flue gases are measured, such as upstream of the flue gas desulphurization unit (FGD) [120].

Because of the prohibitive cost of experimental evaluation of possible alternatives, modelling and simulation are key tools for CO_2 capture research. L.E. Oi presented an overview of the modelling challenges, which are divided into four tasks: absorption and reaction kinetics, gas/liquid equilibrium, gas and liquid flows, and pressure drop [75]. Different types of models are used to simulate the reactive absorption process, where rate-based models are shown to be more accurate than equilibrium-based ones [49]. Convergence problems with these models are well known, and often an initial guess value is required to significantly reduce simulation time or to allow convergence [6, 75]. Shortcut methods [60, 73] can provide an important development tool for both the pre-screening of potential solvents, as a means of evaluating potential process configurations, and as a way of providing first guess values for subsequent more sophisticated software tools.

In this paper the authors investigate the concept of combining ejector technology with the use of waste heat, external to the absorption/desorption process, as a means of reducing the quantity of valuable energy which must be used to regenerate the solvent. The aim is to replace a portion of the valuable steam from the electric power plant with low cost waste heat, thus reducing the operating cost of CO_2 capture in post-combustion processes. In particular, thermal vapour compression is used to upgrade external waste heat, thus reducing the more expensive steam that must be taken from the electric generating station. A shortcut method is developed to model the stripper in MATLAB and to show the potential of the concept in post-combustion CO_2 capture using MEA.

4.4 Process concept

A simplified version of the traditional process flow diagram for chemical absorption/desorption of CO_2, very similar to the original diagram accompanying the 1930 patent by R.R.Bottoms, is shown in Fig. 4.1. CO_2 is transferred from the rising flue gases passing through the absorber to the descending lean solvent. The enriched absorbent solvent leaves the bottom of the absorber and passes to the top of the stripping column. In the stripper, thermal energy from the reboiler creates the steam required to desorb the CO_2 from the solvent, allowing the CO_2 to be collected from the top of the stripper, compressed and sent to long-term storage. The hot lean solvent leaves the bottom of the stripper and returns to the absorber to close the cycle. The heat exchanger between the two columns allows the hot lean stream coming from the stripper to preheat the cooler rich solvent leaving the absorber, thus lowering the heat duty of the reboiler.

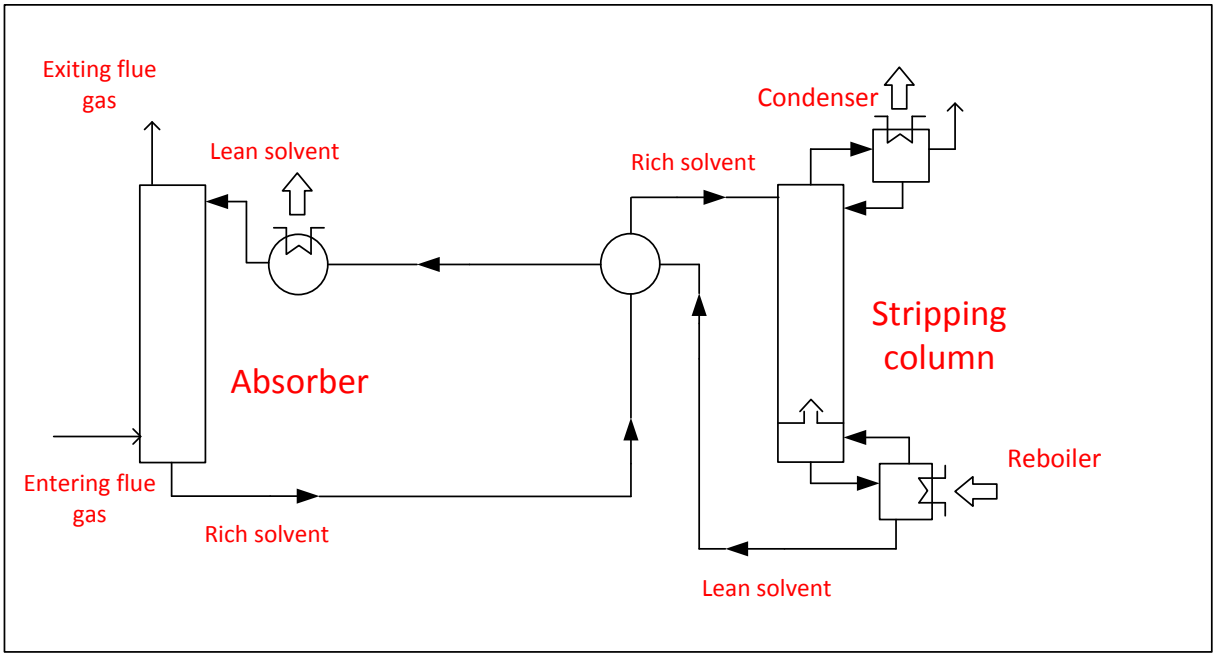

Fig. 4.1 Traditional CO_2 capture process using absorption/desorption

Fig. 4.2 shows the arrangement of a typical ejector heat pump system. Thermal energy applied to the generator causes heat from the lower temperature at the evaporator to be moved to the higher temperature at the condenser. The ejector primary fluid, at a relatively high pressure, enters the ejector by way of the primary nozzle along the central axis of the ejector. The secondary fluid, at a pressure lower than the primary fluid, enters the annular chamber around the primary nozzle. Within the entrance portion of the ejector, the high speed exit of the primary fluid from the nozzle creates a low pressure, inducing the secondary fluid to enter the ejector and to accelerate towards the central portion of the ejector. The two fluids mix in the central portion of the ejector and once mixed, slow down in the final diverging section, creating a higher pressure at the ejector outlet than at the secondary entrance. The two most important characteristics of an ejector are the entrainment ratio ω, the ratio of the mass flow rate of the secondary fluid to that of the primary fluid, and the compression ratio Cr, defined as the ratio of the ejector outlet static pressure to the static pressure at the secondary entrance.

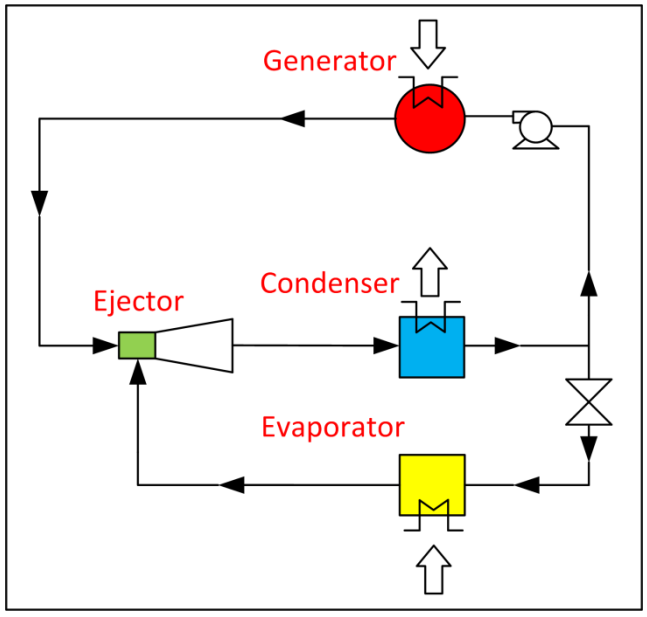

Fig. 4.2 A thermally driven heat pump

Fig. 4.3 shows the proposed generic ejector/stripper arrangement. A flash tank, heated with waste heat and used to create the secondary steam to the ejector, here plays the role of the evaporator. The motive steam entering the primary nozzle of the ejector originates from the stripper reflux condensate, first preheated with waste heat in the primary steam preheater, and further vaporized using plant steam in the primary steam generator. Finally, the condenser in Fig. 4.3 serves the same purpose as the condenser in Fig. 4.2. The thermal energy entering the primary steam generator causes heat from the lower temperature at the flash tank to be fed at a higher temperature through the stripper to the condenser. In this study three liquid sources are considered for feeding the flash tank; the condensate, the lean and the rich solvent.

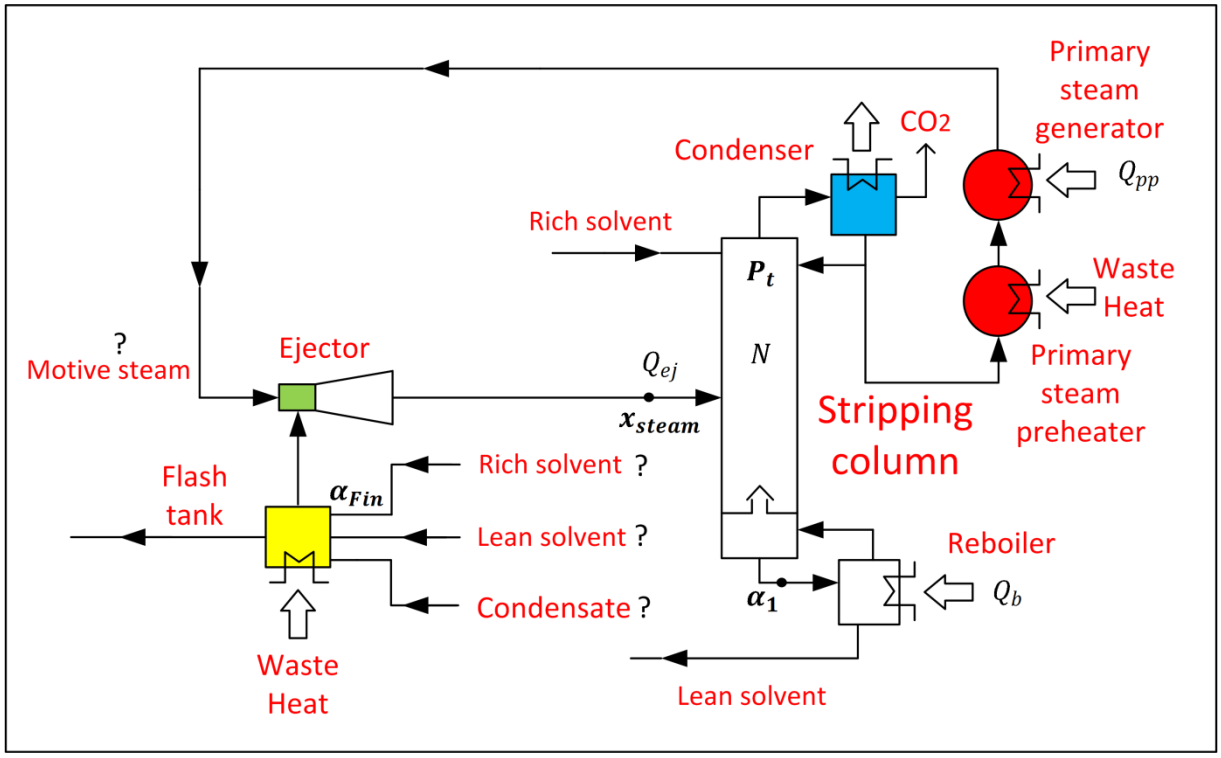

Fig. 4.3 An example of heat pumping of waste heat in a CO_2 capture system

4.4.1 Problem statement

The main objective of the optimization problem is to minimize the sum of the heat duty of the primary steam generator and the reboiler, subject to the fixed solvent solution flow rate, rich and lean solvent CO_2 loadings and the number of theoretical trays in the stripping tower. The shortcut method required to solve such a problem must be able to model the variable position of the point of injection into the desorber, as well as the variable proportion of steam to carbon dioxide entering the tower at that point. Unlike the shortcut method of Notz et al. [73], which is mainly intended for comparing solvents of little known thermo-physical characteristics, here the reference solvent equilibrium properties are known and the model accounts for both variable desorber temperature and gas flow rate. Four optimization variables are chosen and are presented in Fig. 4.3: the stripper tower pressure, P_t; the CO_2 loading of the solvent entering the reboiler, α_1; the position of the live steam entering the tower, x_{steam}; and the CO_2 loading at the flash tank entrance, α_{Fin}.

4.5 Model description and assumptions

To calculate the heat duty of the primary steam generator and the reboiler, models will be presented for the reboiler, ejector and flash tank, and for the stripper tower. These models will then be used to construct the equilibrium and operating curves [45], calculating the total amount of valuable heat duty, Q_{val}, for various values of the four optimization variables: P_t, α_1, x_{steam} and α_{Fin}. Available experimental vapour liquid equilibrium (VLE) data [104] includes the equilibrium partial pressure of CO_2 as a function of temperature and CO_2 loading, as shown in equation (4.1), as well as the heat of absorption as a function of a given absolute change in CO_2 loading values, as shown in equation (4.2).

$$P_{CO2} = f(\alpha, T) \tag{4.1}$$

$$H = f(\alpha_{low}, \alpha_{high}) \tag{4.2}$$

4.5.1 Absorber

For the purpose of the shortcut model it is assumed that the volumetric flow rate of the rich and lean solvent solution, L, stays constant and may be calculated with equation (4.3) using the mass balance of the absorption process [104].

$$n_{CO2} = L * M * \Delta\alpha \tag{4.3}$$

4.5.2 Stripping tower assumptions

- heat losses from the tower are negligible
- the tower operates at a constant pressure
- the vapour pressure of the solvent is negligible compared to that of CO_2 or H_2O
- the CO_2 or H_2O are ideal gases and form an ideal mixture
- the solvent flow rate L is constant throughout the tower
- the temperature of the solvent descending from any slice, $T_{L,i}$, is at the same temperature as that of a boiling mixture having the same CO_2 loading
- the reboiler is at equilibrium conditions
- the rich stream entering the stripper is at boiling temperature

4.5.3 Ejector and flash tank assumptions

- the condensate destined for ejector primary motive steam generation is partially preheated with waste heat
- the primary motive fluid for the ejector is saturated steam
- the flash tank is preheated with waste heat and is at constant pressure, P_F
- the temperature of the CO_2 at the ejector exit, T_{ej}, corresponds to the H_2O saturation temperature at the tower pressure, P_t.

4.5.4 The reboiler model

The model of the stripping tower reboiler, shown in Fig. 4.4, is based on the simplified energy balance defined by equation (4.4) [104]. The main assumptions for equation (4.4) are that the solvent volumetric flow rate L is constant, and that the sensible heats of the CO_2 and H_2O vapour are negligible. Considering each term in equation (4.4), the reboiler provides the energy necessary to heat the solvent entering the reboiler, to cause the desorption of CO_2 that takes place in the reboiler, and to volatize the water that will accompany the CO_2 into the gas phase. Equation (4.5) is the mass balance of CO_2 for the reboiler. Equation (4.6) allows calculating the amount of vapour in ideal gas phase as a function of the ratio of partial pressures, while equation (4.7) expresses the stripper tower pressure with Dalton's Law. The equilibrium data for H_2O are given by Raoult's law in equation (4.8), and equations (4.9) and (4.10). The equilibrium data for

CO_2 are given in equations (4.1) and (4.2). Finally, equation (4.11) defines the molar gas fraction of CO_2 leaving the reboiler, necessary for building the operating curve.

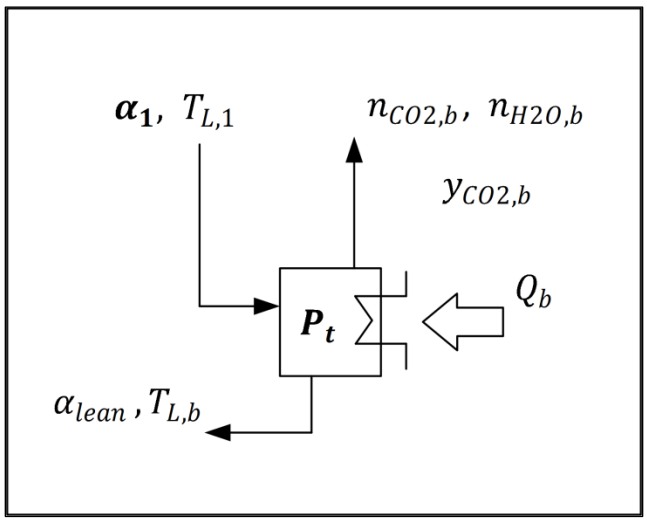

Fig. 4.4 The reboiler model

$$Q_b = L * C_P * \left(T_{L,b} - T_{L,1}\right) + n_{CO2,b} * H + n_{H2O,b} * r_{fg} \tag{4.4}$$

$$n_{CO2,b} = L * M * (\alpha_1 - \alpha_{lean}) \tag{4.5}$$

$$n_{H2O,b} = n_{CO2,b} * P_{H2O} / P_{CO2} \tag{4.6}$$

$$P = P_{H2O} + P_{CO2} \tag{4.7}$$

$$P_{H2O} = X * P_{H2O,sat} \tag{4.8}$$

$$P_{H2O,sat} = 0.0003487 * T^3 - 0.050657 * T^2 + 3.3088 * T - 71.687 \quad (4.9)$$

$$r_{fg} = -5 * 10^{-2} * T^2 - 36.9 * T + 44881 \quad (4.10)$$

$$y_{CO2,b} = \frac{n_{CO2,b}}{n_{CO2,b} + n_{H2O,b}} \quad (4.11)$$

The reboiler model is thus described by 11 equations, (4.1), (4.2) and (4.4) to (4.11), where (4.1) is used twice, once for $T_{L,b}$ and once for $T_{L,1}$. There are 13 unknowns, including two independent optimization variables, P_t and α_1, shown in Fig. 4.3. The constants for the model are α_{lean}, L, X, C_P, and M. For a given tower pressure P_t, the remaining optimization variable α_1 is used to determine all of the reboiler unknowns: $T_{L,b}$, $T_{L,1}$, H, Q_b, r_{fg}, $n_{CO2,b}$, $n_{H2O,b}$, P_{H2O}, P_{CO2}, $P_{H2O,sat}$ and $y_{CO2,b}$.

4.5.5 The ejector and flash tank model

Quantifying the unknown variables around the flash tank and the ejector, shown in Fig. 4.5, requires considering both units at the same time. Making use of published steam ejector design-point performance data [86], equation (4.12) presents the entrainment ratio ω as of function of the compression ratio Cr, where Cr = P_t / P_F , based on the design-point data. Equation (4.12) is valid for the system specifications to be discussed in section 4.5.8. Expression (4.13) defines the traditional ejector entrainment ratio. Given that equation (4.12) and definition (4.13) use a mass basis, the following ejector and flash tank equations are also presented on a mass basis.

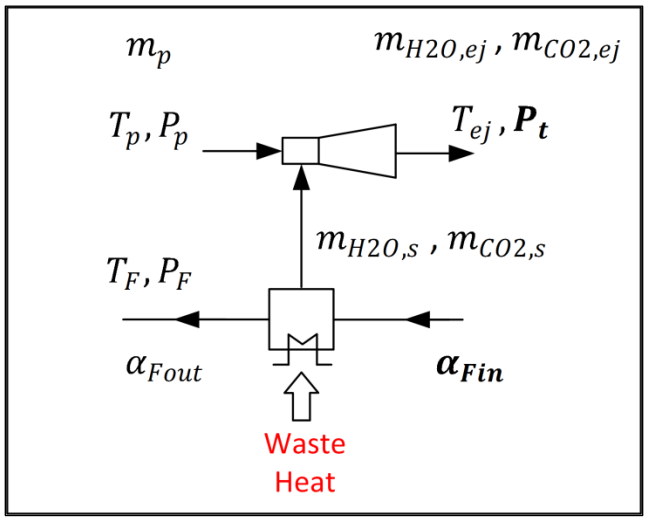

Fig. 4.5 The ejector and flash tank model

$$\omega = 0.5221 * (P_t/P_F)^2 - 2.655 * (P_t/P_F) + 3.53 \tag{4.12}$$

$$\omega = (m_{H2O,s} + m_{CO2,s})/ m_p \tag{4.13}$$

Equation (4.14) presents the energy balance for the ejector. Equations (4.15) and (4.16) show the mass balances for the ejector, while equation (4.17) gives the CO_2 mass balance for the flash tank. Equation (4.18) allows calculating the H_2O vapour mass flow rate in the flash tank gas phase as a function of partial pressures. The flash tank pressure is defined by equation (4.7), assuming the constant pressure that will be given in the system specifications, section 4.5.8. The H_2O equilibrium data are given by Raoult's law in equation (4.8), and by equation (4.9). The CO_2 equilibrium data are described by equations (4.1), (4.19) and (4.20). For convenience, equation (4.21) is introduced, defining the parameter Q_{ej}, representing the absolute H_2O enthalpy flow exiting the ejector.

The ejector and the flash tank are therefore described by 15 equations, (4.1), (4.7) to (4.9), and (4.12) to (4.21), where (4.20) is used twice, once for $h_{CO2,s}$ and once for $h_{CO2,ej}$. The specific H_2O saturation vapour enthalpies h_p and h_s are considered known and are calculated at

the respective pressures P_p and P_F. There are 18 unknowns, including the two optimization variables, P_t and α_{Fin}, and the parameter Q_{ej}, shown in Fig. 4.3. Thus by fixing P_t, α_{Fin} and Q_{ej}, all of the remaining unknowns are determined: $\omega, m_p, m_{H2O,s}$, $m_{H2O,ej}$, $m_{CO2,s}$, $m_{CO2,ej}$, $h_{ej}, h_{CO2,s}$, $h_{CO2,ej}$, $\alpha_{Fout}, P_{H2O}, P_{CO2}, P_{H2O,sat}$, T_{ej}, T_F.

$$m_p * h_p + m_{H2O,s} * h_s + m_{CO2,s} * h_{CO2,s} = m_{H2O,ej} * h_{ej} + m_{CO2,ej} * h_{CO2,ej} \quad (4.14)$$

$$m_p + m_{H2O,s} = m_{H2O,ej} \quad (4.15)$$

$$m_{CO2,s} = m_{CO2,ej} \quad (4.16)$$

$$m_{CO2,ej} = L * M * (\alpha_{Fin} - \alpha_{Fout}) * M_{w,CO2} \quad (4.17)$$

$$m_{H2O,s} = m_{CO2,s} * (M_{w,H2O}/M_{w,CO2}) * (P_{H2O}/P_{CO2}) \quad (4.18)$$

$$T_{ej} = -0.0007 * P_t^2 + 0.4029 * P_t + 66.0026 \quad (4.19)$$

$$h_{CO2} = 0.0004 * T^2 + 0.8299 * T + 191.58 \quad (4.20)$$

$$Q_{ej} = m_{H2O,ej} * h_{ej} \quad (4.21)$$

4.5.6 The stripping tower model

To model the stripper tower it is first divided into a number of slices, N_{slices} , which are used to divide the required desorption task, $\alpha_{rich} - \alpha_1$, into a finite number of steps. The adopted naming convention associates the index "i" with the stream leaving the slice, as shown in Fig. 4.6, with the first slice being above the reboiler. Allowing for the possibility of live steam from the ejector, the position of injection is identified as x_{steam}. The parameter x_{steam} has units of kmol CO_2/kmol solvent because it is associated with the position along the height of the stripper tower and with the CO_2 liquid loading at that point, α_i.

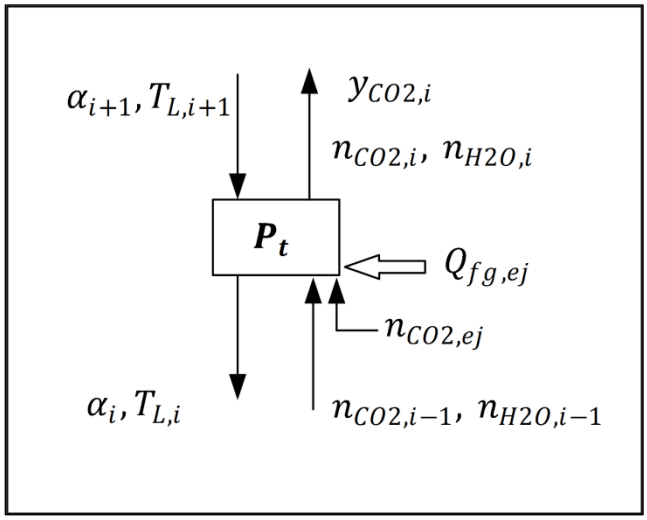

Fig. 4.6 Model of ith stripper slice, with possible steam injection

4.5.6.1 Model of the ith stripping slice

If there is no injection into the tower, or if the steam is not injected into the current slice, then the latent enthalpy of the live steam, $Q_{fg,ej}$, and the CO_2 molar flow rate from the ejector, $n_{CO2,ej}$, are zero. In the case of steam injection, then for the ith slice where $\alpha_i = x_{steam}$, $Q_{fg,ej}$ and $n_{CO2,ej}$ are non-zero.

The model for the ith stripper slice, shown in Fig. 4.6, is based on the same assumptions used in the reboiler model. Equation (4.22) presents the simplified energy balance, where the enthalpy flow rising from the slice below is essentially the latent heat of water vaporization. Equation (4.23) defines the contributed latent enthalpy flow from the ejected steam to the energy balance, $Q_{fg,ej}$. Equation (4.24) is the CO_2 mass balance for the ith slice. Equation (4.7) uses Dalton's law to express the stripper pressure. Equations (4.8), (4.9), (4.10) and (4.25) give the H_2O equilibrium data while equations (4.1) and (4.2) give the CO_2 equilibrium data. Finally, equation (4.26) defines the molar gas fraction of CO_2 leaving the ith slice, necessary for building the operating curve.

$$Q_{fg,ej} + \left(n_{H2O,i-1} - n_{H2O,i}\right) * \ r_{fg} = L * C_p * \left(T_{L,i} - T_{L,i+1}\right) + L * M * (\alpha_{i+1} - \alpha_i) * H \quad (4.22)$$

$$Q_{fg,ej} = \ m_{H2O,ej} * \left(h_{ej} - h_{f,i}\right) \ if \ x_{steam} = \ \alpha_i, else \ Q_{fg,ej} = \ 0 \quad (4.23)$$

$$n_{CO2,i} = L * M * (\alpha_{i+1} - \alpha_i) + \ n_{CO2,i-1} + \ n_{CO2,ej} \quad (4.24)$$

$$h_f = \ -0.0024 * P^2 + \ 1.5827 * P + 2.83.43 \quad (4.25)$$

$$y_{CO2,i} = \frac{n_{CO2,i}}{n_{CO2,i} + n_{H2O,i}} \quad (4.26)$$

When there is no live steam injection in the ith slice, the slice is described by 10 equations, being equations (4.1), (4.2), (4.7) to (4.10), (4.22), and (4.24) to (4.26). There are 12 unknowns, with the only optimization variable being P_t. The known parameters are $n_{H2O,i-1}$, $n_{CO2,i-1}$, $T_{L,i}$ and α_i. For a given tower pressure P_t, fixing α_{i+1} determines all of remaining unknowns: $n_{H2O,i}$, $n_{CO2,i}$, r_{fg}, $T_{L,i+1}$, H, h_f, P_{H2O}, P_{CO2}, $P_{H2O,sat}$ and $y_{CO2,i}$.

When x_{steam}=α_i, the ith stripper model slice is described by 14 equations, the first eleven being equations (4.1), (4.2), (4.7) to (4.10), and (4.22) to (4.26). The ejector model can be considered to provide 3 functions, returning values of $m_{H2O,ej}$, h_{ej} and $n_{CO2,ej}$ for input values of P_t, α_{Fin} and Q_{ej}. There are 19 unknowns, including the optimization variables P_t, x_{steam} and α_{Fin}. The known parameters are $n_{H2O,i-1}$, $n_{CO2,i-1}$, $T_{L,i}$ and α_i. For chosen values of P_t, x_{steam} and α_{Fin}, further fixing Q_{ej} and α_{i+1} determines all of remaining unknowns: $Q_{fg,ej}$, $m_{H2O,ej}$, h_{ej}, $n_{CO2,ej}$, $n_{H2O,i}$, $n_{CO2,i}$, r_{fg}, $T_{L,i+1}$, H, h_f, P_{H2O}, P_{CO2}, $P_{H2O,sat}$ and $y_{CO2,i}$.

4.5.6.2 The equilibrium and operating curves

The construction of the equilibrium and operating curves for the stripper tower is required to quantify the number of theoretical trays, N. The theoretical trays are created in a manner similar to that discussed in chapter 2 of Kohl and Nielsen [45]. The equilibrium curve is obtained for a fixed tower pressure P_t using a MATLAB spline, where for selected values of the CO_2 loading covering the range of experimental data, the temperature is iteratively varied such that the equations (4.1), (4.7), (4.8) and (4.9) are satisfied.

The first step in the construction of the operating curve is to use the reboiler model, fixing the tower pressure P_t and the CO_2 loading of the liquid entering the reboiler from the first tray, α_1. This fixes the first point on the operating curve and determines the reboiler duty Q_b. Continuing the construction of the operating curve requires dividing the desorption task, from α_1 to α_{rich}, into a fixed number of slices, N_{slices}. Making use of the MATLAB's built-in spline functions, two separate spline curves of the operating curve are constructed, corresponding to the integer portion of N_{slices} from α_1 to x_{steam}, and from $x_{steam}$to α_{rich}. Fig. 4.7 presents the results of the shortcut method application for the stripping column with steam injection, showing

the form of the equilibrium and operating curves. The theoretical trays are graphically presented. This approach imposes the numerical limitation that $x_{steam} > \alpha_1 > \alpha_{lean}$ (in practice, a difference of 0.0001 is adequate) in order to avoid a zero length spline. Using this method, all of the α_{i+1} values are thus known once x_{steam} is chosen. If no steam injection is used, the $\Delta\alpha$ steps will be of equal size. Thus, continuing with the same chosen value of P_t as was used for the reboiler, and choosing values for x_{steam}, α_{Fin} and Q_{ej}, it is possible to calculate the molar CO_2 gas fraction, $y_{CO2,b}$ and $y_{CO2,i}$ in equations (4.11) and (4.26), for each liquid CO_2 loading α_i while ascending the stripper tower.

To count the theoretical trays, starting at α_1 on the graph of the equilibrium and operating curves, a vertical line cuts the equilibrium curve at $y_{CO2,1}$. From this point a horizontal line cuts the operating curve at α_2. In a sequential and graphical way each of the trays further up the stripping tower are calculated, up to the limit of the available CO_2 loading data. The topmost tray is in general a portion of a theoretical tray, taking into account the value of α_{rich}. For this reason the operating curve is extended slightly beyond α_{rich}. In general the number of trays calculated will not give the target number of trays N. When no steam injection is used, and thus $Q_{ej} = 0$, for a fixed P_t value, the value of α_1 must be iterated until the target N trays are constructed. When steam injection is used, for fixed values of P_t, x_{steam} and α_{Fin}, the value of Q_{ej} is iterated until the target N trays are constructed.

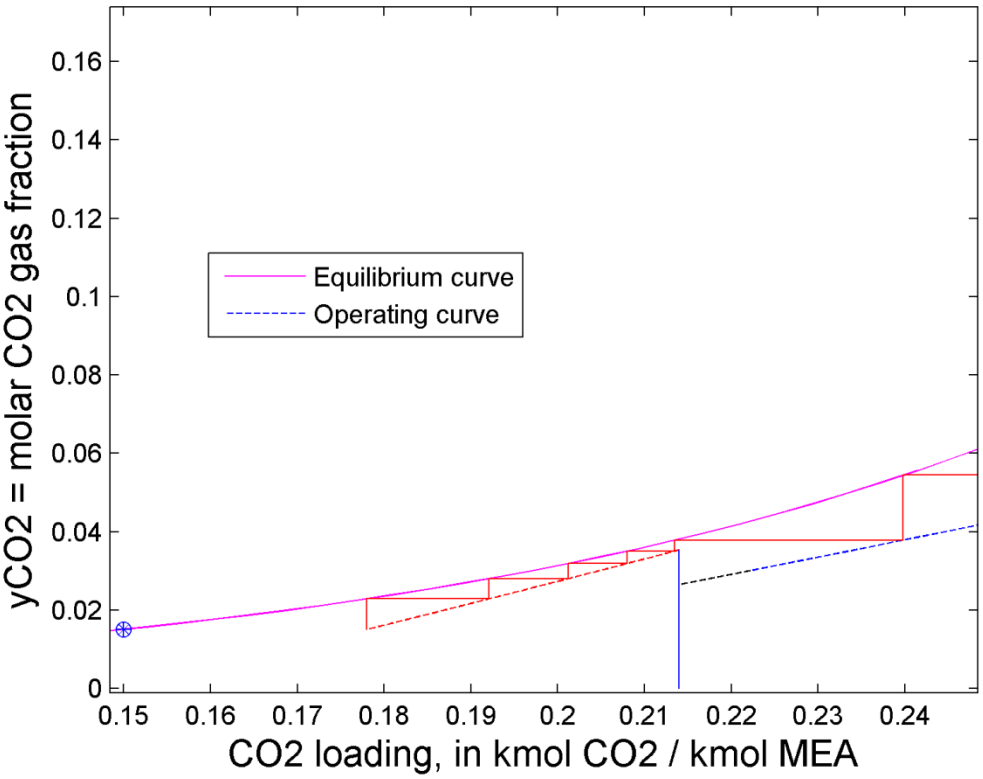

Fig. 4.7 Typical shortcut method equilibrium and operating curves showing steam injection

4.5.7 The valuable heat duty, Q_{val}

Equation (4.27) quantifies the valuable thermal power necessary to regenerate the solvent solution in the stripping tower, Q_{val}, as the sum of the reboiler duty, Q_b, and the valuable heat necessary to prepare the primary motive steam to the ejector, Q_{pp}, both shown in Fig. 4.3. Equation (4.28) defines Q_{pp}, where the ejector primary vapour specific enthalpy, $h_{g,p}$, is calculated at the primary pressure, P_p, and the specific liquid enthalpy leaving the preheater, $h_{f,pp}$, is calculated at the exit temperature from the primary steam preheater, shown in Fig. 4.3.

$$Q_{val} = Q_b + Q_{pp} \tag{4.27}$$

$$Q_{pp} = m_p * (h_{g,p} - h_{f,pp}) \quad (4.28)$$

4.5.8 System specifications

The assumed solvent is a 20% wt. MEA aqueous solution [104], with a molarity of 3.3 kmol/m^3. For the application of Raoult's law of equation (4.8) it is now assumed that the solvent molar fraction of H_2O is constant, where X=0.93. Table 4.1 presents the assumed values for the waste heat and stripper tower data.

Table 4.1 Waste heat and stripper tower data

waste heat temperature	100 °C
flash tank nominal temperature, heated using waste heat	90 °C
ejector primary preheat temperature, heated using waste heat	90 °C
number of theoretical trays (N)	8
number of stripper slices (N_{slices})	40
ejector primary saturated steam pressure (P_p)	300 kPa
flash tank pressure (P_F)	70 kPa
stripper tower pressure (P_t)	125 < P_t < 155 kPa

The flue gas specifications for this study are based on a 400 MW pulverized coal fired power plant [20] and are presented in Table 4.2. The assumed lean CO_2 loading of 0.15 kmol CO_2/kmol MEA and rich CO_2 loading of 0.45 kmol CO_2/kmol MEA fall within the typical range in industry (page 119 Kohl) [45].

Table 4.2 Absorber data

flue gas composition, mole percent	
CO_2	12.12%
H_2O	14.14%
N_2	70.70%
O_2	3.03%
absorber inlet temperature	55 °C
absorber inlet pressure	1 atm
flue gas inlet molar flow rate	69429.5 kmol/h
assumed CO_2 capture percentage	85%
solvent solution molarity (M)	3.3 kmol/m^3
lean solvent solution loading (α_{lean})	0.15 kmol CO2/kmol MEA
rich solvent solution loading (α_{rich})	0.45 kmol CO2/kmol MEA
solvent solution inlet temperature	40 °C
solvent solution outlet temperature	57 °C
solvent solution flow rate (L)	7225 m^3/h
solvent solution heat capacity (C_p)	4187 kJ/°C*m^3

The range of possible values for the four optimization variables, P_t, α_1, x_{steam} and α_{Fin}, are partly a function of available data and partly defined by process heuristics. For simulation purposes the stripper tower pressure P_t can be chosen from 125 to 155 kPa. This range is possible because both VLE data for 20% wt. MEA [104] and ejector design-point data are available [86], as discussed in section 4.5.5. The three considered liquid sources that feed the flash tank are the reflux condensate with $\alpha_{Fin} = 0$, the lean solvent from the stripper with $\alpha_{Fin} = 0.15$, and lastly the rich solvent to the stripper with $\alpha_{Fin} = 0.45$. For the condensate feed with $\alpha_{Fin} = 0$ there is no flash tank desorption. The amount of desorption occurring in the flash tank is that determined by the equilibrium CO_2 loading of the liquid leaving the flash tank, α_{Fout}.

In the largest sense, α_1 can be chosen between α_{lean} and α_{rich}. In a similar manner, x_{steam} can be chosen between α_1 and α_{rich}. Given that the optimization problem is to minimize the valuable heat duty to regenerate the solvent, it is necessary to take into account the well-known heuristic concerning the point of closest approach between the equilibrium and operating curves, the pinch point [51, 104]. Specifically, the injection of energy in to the stripper tower by way of live steam above the pinch point wastefully transfers energy from the tower to the

condenser at the top of the tower. Thus the upper limit for both x_{steam} and α_1 is expected to be below the pinch point for the case of 8 theoretical trays without steam injection and equals 0.21 kmol CO_2/kmol MEA as will be illustrated in the next section.

4.6 Simulation results

4.6.1 Model validation without steam injection and the pinch point definition

For the case without steam injection, 8 trays and a stripper tower pressure of 154 kPa, the reboiler duty is 1859 GJ/h. This corresponds to 5.9 GJ/tCO_2 and is similar to a value of 5.8 GJ/tCO_2 in Lucia et al. [60] which also uses 20 wt% MEA. A literature value of the specific reboiler duty of 30 wt% MEA is 4.0 GJ/tCO_2 [76], while pilot-plant data [73] is in the range of 4 to 5 GJ/tCO_2. It should be recalled that the described shortcut method is not intended as a process design tool. It is used in this study to compare and optimize various scenarios of integrating an ejector into the absorption/desorption process for CCS. No convergence problems were experienced. The pinch point of the stripping column corresponds to 0.21 kmol CO_2/kmol MEA.

4.6.2 Influence of the position of the point of steam injection, x_{steam}, $\alpha_{Fin} = 0$

Recalling that when there is no live steam injection in a stripper of fixed pressure P_t, then the CO_2 loading entering the reboiler, α_1, determines the reboiler duty Q_b for the fixed number of trays N. The optimization variables α_{Fin} and x_{steam} play no role. When steam injection is simulated, although α_1 determines Q_b, the total amount of valuable heat duty Q_{val} depends on the chosen value of x_{steam} and α_{Fin}. Considering a stripper tower of 8 trays at 140 kPa, with no flash tank desorption with $\alpha_{Fin} = 0$, Fig. 4.8 presents a study of the influence of x_{steam} on the amount of valuable energy, with the CO_2 liquid loading leaving the first tray, α_1 ,as a parameter. For a fixed α_1 value, Q_{val} decreases when x_{steam} decreases. This means that the optimal position of injection is under the first tray for any chosen α_1. The physical explanation of this result is the following. Given there is no trace of CO_2 in the live steam for the case $\alpha_{Fin} = 0$, the lowest point of the stripping column is the optimal point of injection, minimizing the exergy losses due to mixing of the live steam and vapour from the reboiler [51]. Thus, in subsequent simulations x_{steam} is set essentially equal to α_1.

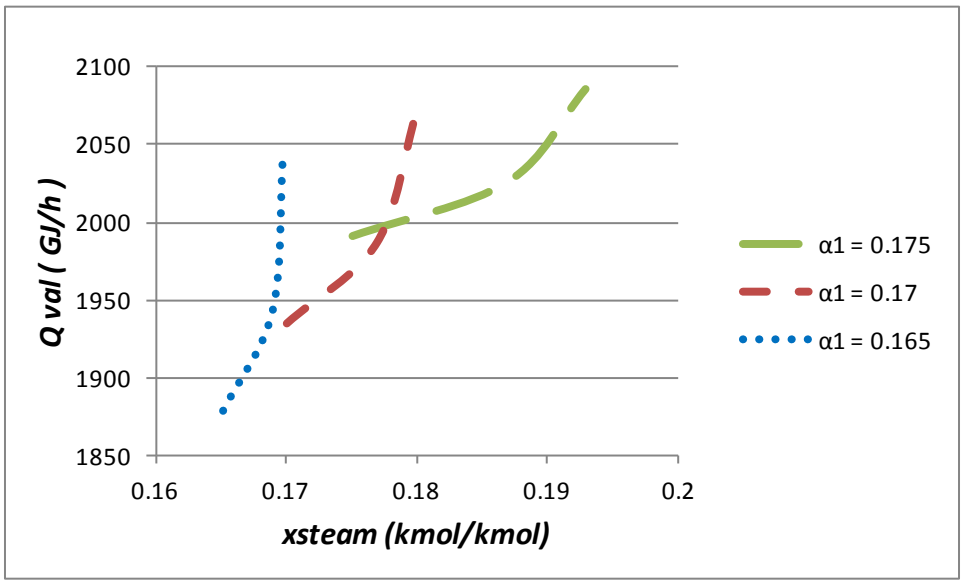

Fig. 4.8 Valuable energy as a function of x_{steam} , P_t = 140 kPa, no flash tank desorption

4.6.3 Influence of the CO_2 loading entering the reboiler from the first tray, α_1, $\alpha_{Fin} = 0$

Applying the simplification of $x_{steam} = \alpha_1$, as explained in the previous section, Fig. 4.9 shows how Q_{val} varies with α_1. For a fixed number of trays (*N*=8), tower pressure (P_t = 140 kPa) and without flash tank desorption ($\alpha_{Fin} = 0$), Q_{val} increases linearly with α_1. The minimized value of Q_{val} corresponds to $\alpha_1 = \alpha_{lean}$. Physically this would correspond to the removal of the reboiler. Thus energy which was previously provided by the reboiler would be replaced by a combination of energy from the ejector primary steam and upgraded energy from waste heat. The conclusion of the results presented in this and the previous section is that the amount of valuable energy is minimized by setting $\alpha_1 = \alpha_{lean} = 0.15$, and $x_{steam} = \alpha_{lean}$. Given that the complete replacement of the reboiler may not be advantageous, either for a retrofit situation or for process flexibility, it would be helpful to consider also a mid-range value of α_1. For *N*=8, this "mid" value of α_1 equals 0.165, being the average of $\alpha_1 = 0.182$ and $\alpha_{lean} = 0.150$. The value $\alpha_1 \approx 0.182$ refers to the situation where no steam injection is used, in which case $Q_{val} = Q_b$.

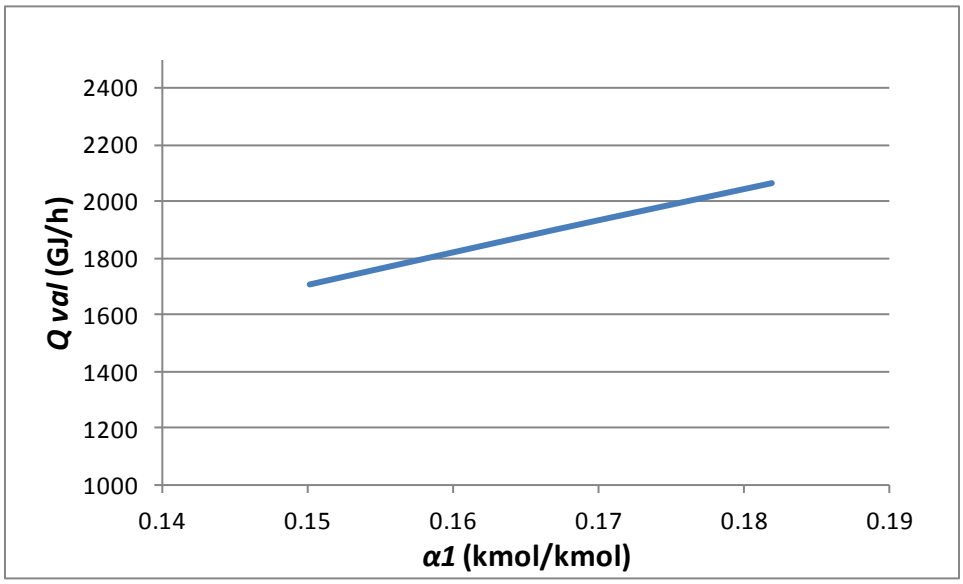

Fig. 4.9 Valuable energy as a function of α_1, P_t = 140 kPa, no flash tank desorption

4.6.4 Influence of P_t and α_1 without CO_2 desorption in the flash tank, $\alpha_{Fin} = 0$

Fig. 4.10 shows Q_{val} as a function of P_t, with α_1 as the parameter. Three values of α_1 are considered: $\alpha_1 = 0.150$ (no reboiler, the maximum amount of steam injection), 0.165 (a mid-range value, as explained in the previous section) and 0.182 (no steam injection). The last value is a baseline reference. When there is no steam injection, the actual α_1 values corresponding to stripper tower pressures of 126, 140 and 154 kPa are respectively 0.18111, 0.18196 and 0.18315 kmol/kmol. With no steam injection, Q_{val} decreases as the tower pressure increases. This effect is diminished, however, when the maximum amount of steam is injected. The reason is that the ejector entrainment ratio ω decreasing with rising stripper pressure P_t, requiring a greater amount of the more valuable primary steam Q_{pp} for a fixed amount of injected steam. The lowest amount of valuable heat duty shown in Fig. 4.10 occurs where the stripper pressure is 154 kPa using maximum steam injection, with $Q_{val} = 1655$ GJ/h.

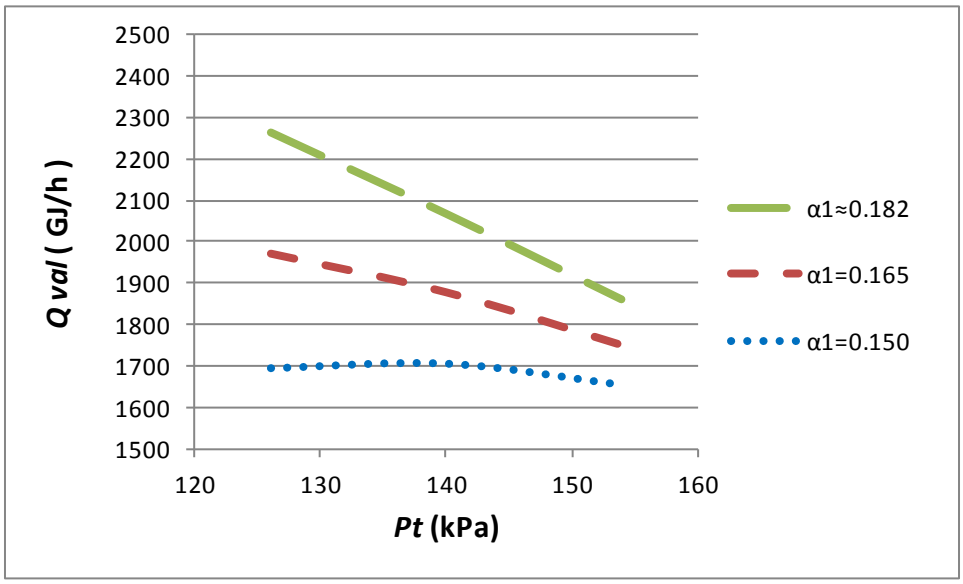

Fig. 4.10 Valuable energy as a function of P_t, with α_1 as a parameter, α_{Fin}=0

4.6.5 Influence of P_t and α_1, with flash tank desorption for $\alpha_{Fin} = 0.15$

In this scenario the lean solvent feeds the flash tank and $\alpha_{Fin} = 0.15$. Fig. 4.11 presents Q_{val} as a function of P_t, with α_1 as a parameter. For the maximum amount of steam injection and with stripper pressures of 126, 140 and 154 kPa, the respective amounts of valuable heat duties Q_{val} are, 1802, 1783 and 1701 GJ/h. These results are of a similar order of magnitude as the $\alpha_{Fin} = 0$ case. In both cases the amount of valuable steam Q_{val} is significantly less than the case where no steam injection is used. It should be noted that similar to the case of $\alpha_{Fin} = 0$, the optimal values of the optimization variables are the following: the position of the live steam entering the tower, $\alpha_1 = \alpha_{lean} = 0.15$ kmol/kmol and $x_{steam} = \alpha_{lean}$ for the case where the reboiler is removed; $x_{steam} = 0.165$ kmol/kmol for the case where the reboiler is present; the optimal value of the stripper tower pressure, P_t, is the maximum allowable value of 155 kPa.

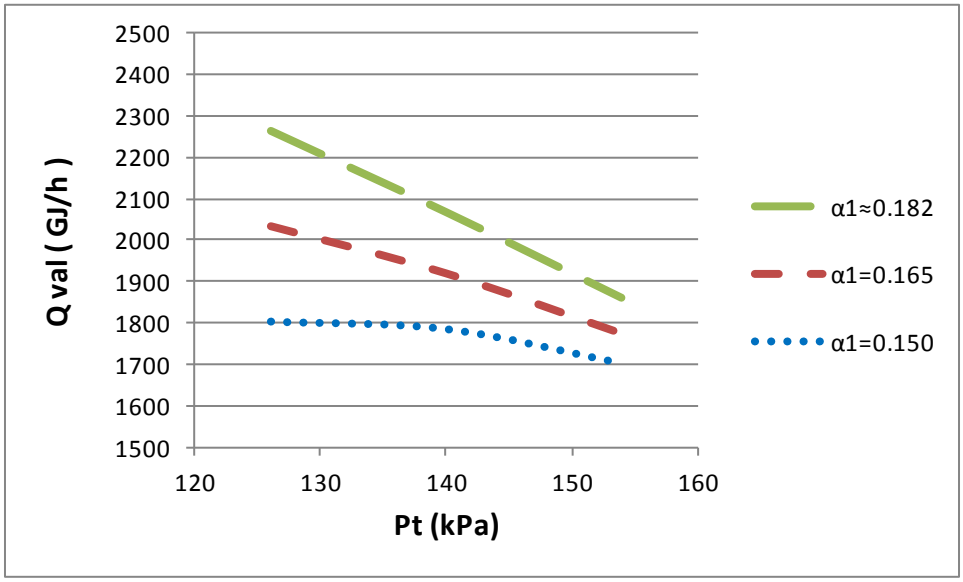

Fig. 4.11 Valuable energy as a function of α_1, with P_t as a parameter, α_{Fin}=0.15

4.6.6 Influence of P_t and α_1 with CO_2 desorption, $\alpha_{Fin} = 0.45$

In this case there is a very large amount of CO_2 released in the flash tank. Fig. 4.12 presents Q_{val} as a function P_t with $\alpha_1$as a parameter. All of the cases of steam injection have much higher values of Q_{val} than the case without steam injection. Thus, there is no interest in using the rich solvent stream as the feed stream to the flash tank and then sending the flash steam through the ejector into the stripping tower.

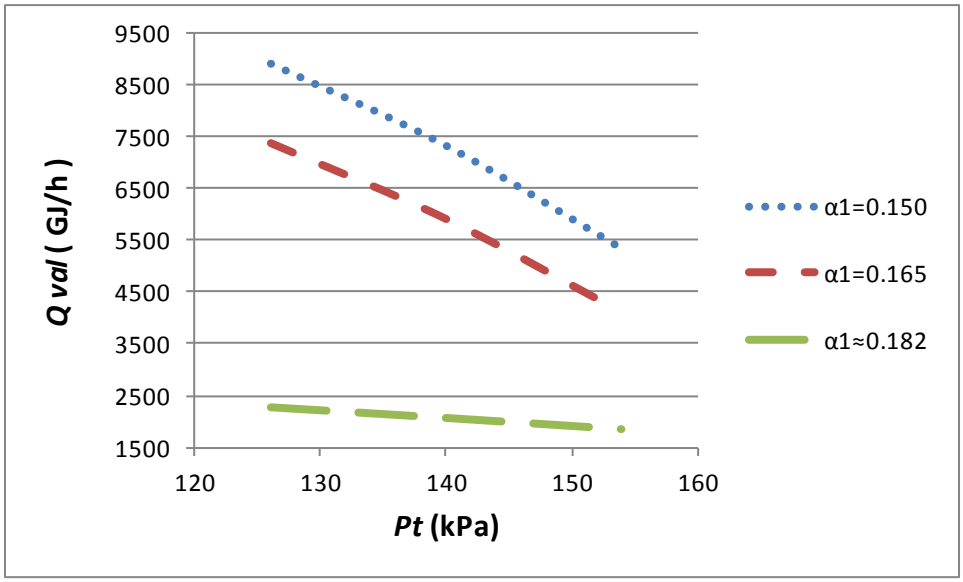

Fig. 4.12 Valuable energy as a function of α_1, with P_t as a parameter, α_{Fin}=0.45

4.6.7 Potential energy savings

An overall graphical summary for the 8 tray stripper tower simulations is shown in Fig. 4.13, based on the energy amounts of Fig. 4.10 and Fig. 4.11. The reduction in the consumption of valuable heat Q_{val} varies from 10 to 25%. On a percentage basis, the highest valuable energy savings occur in decreasing order for tower pressures of 126, 140 and 154 kPa. On an absolute basis, as shown in Fig. 4.10, the lowest values of Q_{val} occur at the highest tower pressure. In all cases showing a reduction in the amount of valuable energy, the best results are obtained when the maximum amount of steam is injected at the base of the tower, effectively replacing the

reboiler duty. Feeding the flash tank with the condensate or the lean solvent are both possible options and offer a significant reduction in the valuable heat duty with respect to the baseline case, without steam injection. Using the rich stream to supply the feed tank and then to inject the resulting steam and CO_2 into the tower is not a viable option and is therefore not presented in Fig. 4.13.

Raynal et al. [88] find in their MEA based CCS economic study of a 630 MWe coal fired plant that the reboiler duty is 82% of the operating cost, where the operating cost is 72% of the total capture cost. Thus the reboiler duty represents 59% of the total CO_2 capture cost. Assuming an average mitigation cost of 50 US$/t$CO_2$ avoided [64], the potential economic benefit of the reduction in the valuable heat, from 10 to 25%, saves from 3 to 7 US$/t$CO_2$ avoided. Associated with the reduction in valuable energy is a corresponding reduction in the environmental impact due to the lower coal consumption, a function of the reference plant thermal efficiency and coal quality.

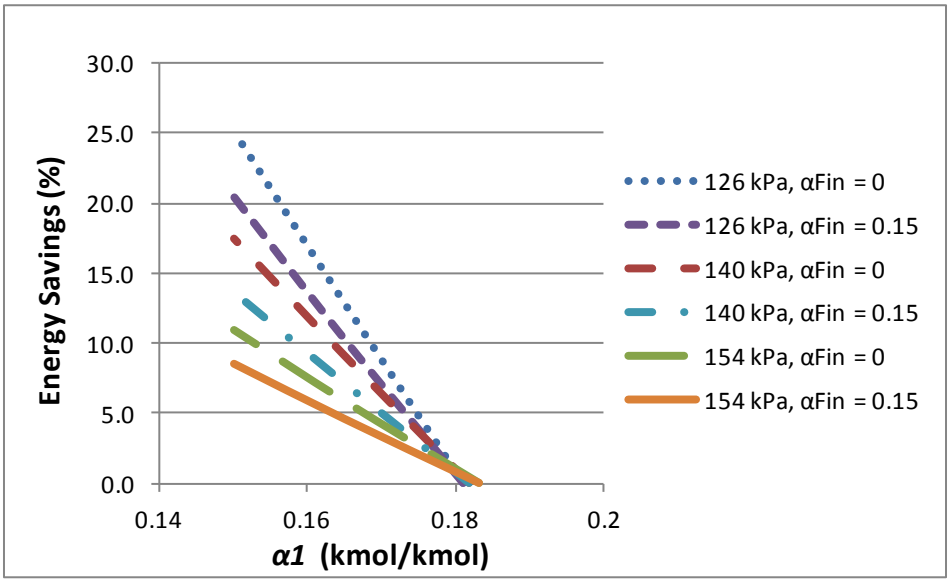

Fig. 4.13 Energy Savings with and without flash tank desorption, N=8

4.7 Conclusions

A shortcut method has been developed for modelling and optimizing a post-combustion CO_2 capture solvent regeneration process enhanced with ejector driven waste heat upgrading. The specific solvent chosen for the study is 20 wt% MEA.

The completed simulations of a tower of 8 trays reveal reductions in the required amount of valuable energy ranging from 10 to 25%. These reductions have been found for the cases when the flash tank is fed with the condensate or the lean solvent streams, corresponding respectively to CO_2 loadings of 0 and 0.15 kmol CO_2/kmol MEA.

The optimal position of the live steam injection has been determined to be the base of the stripper tower. Two scenarios have been analyzed: complete and partial replacement of the stripping column reboiler by live steam injection. The injected steam is produced from a mixture of two sources, one being valuable primary steam, and the other being secondary steam drawn in from a flash tank. The available 100 °C waste heat is used in the flash tank. It has been demonstrated that feeding the flash tank with the rich stream (CO_2 loadings of 0.45 kmol CO_2/kmol MEA) is not a viable option.

The validation of the presented results will be completed in part 2 of the paper using commercial chemical process simulation software. At that time the heat integration for the overall absorption and desorption CO_2 capture system will also be considered. Further, the ejector and the kinetics of the CO_2 desorption in the flash tank will be experimentally studied as a means of better modelling and understanding the overall ejector enhanced CCS process.

4.8 Acknowledgments

The authors would like to thank CanmetENERGY (Natural Resources Canada) for the financial support. They would also like to offer their gratitude to Dr. S. Hosatte, Dr. Z. Aidoun and Dr. H. Sapoundjiev for their help and advice.

4.9 Nomenclature

Table 4.3 Chapter 4 nomenclature

C_p	heat capacity, (kJ/°C*m^3)	*Greek*	
Cr	ejector compression ratio	α	CO_2 loading (kmol CO_2/ kmol MEA)
h	enthalpy of H_2O (kJ/kg)	Δ	difference (e.g. $\Delta\alpha$)
h_{CO2}	enthalpy of CO_2 (kJ/kg)	ω	ejector entrainment ratio
H	heat of desorption (kJ/kmol)		
L	solvent solution flow rate (m^3/h)	*Subscript s*	
M	solvent molarity (kmol/m^3)	*b*	Reboiler
m_p	mass flow rate, ejector primary (kg/h)	*ej*	ejector exit
m_s	mass flow rate, ejector secondary (kg/h)	*f*	saturated liquid
M_w	molecular weight (kg/kmol)	*F*	flash tank
n	molar gas flow rate (kmol/h)	*Fin*	flash tank entrance
N	number of theoretical stripper trays	*Fout*	flash tank exit
N_{slices}	number of stripper slices	*g*	saturated vapour
P	pressure or partial pressure (kPa)	*i*	ith tray or slice
Q	heat or enthalpy flow (kJ/h)	*lean*	solvent leaving reboiler
Q_{fg}	latent enthalpy flow of injected steam (kJ/h)	*L*	solvent solution
Q_{val}	solvent regeneration valuable heat (kJ/h)	*p*	ejector primary
r_{fg}	Molar latent heat of H_2O vaporization (kJ/kmol)	*pp*	primary steam preheater exit
T	temperature (°C)	*rich*	solvent entering stripper
x_{steam}	position of the steam injection (kmol CO_2/ kmol MEA)	*s*	ejector secondary
X	solvent molar fraction of H_2O	*sat*	saturation
y	molar gas fraction	*t*	stripper tower

CHAPTER 5 CARBON CAPTURE SIMULATION USING EJECTORS FOR WASTE HEAT UPGRADING

5.1 Avant-propos

Auteurs et affiliations :

- Christopher Reddick, Doctorant, Département de génie mécanique, Université de Sherbrooke, 2500 boul. de l'Université, Sherbrooke, Québec J1K2R1
- Mikhail Sorin, Professeur, Département de génie mécanique, Université de Sherbrooke
- Hristo Sapoundjiev, PhD, CanmetÉNERGIE, Ressources naturelles Canada, 1615 boul. Lionel-Boulet, case postale 4800, Varennes, Québec
- Zine Aidoun, PhD, CanmetÉNERGIE, Ressources naturelles Canada

Publication : Energy 100 (2016) 251-208

Référence : [92]

Contribution à la thèse:

Cet article contribue à la thèse en validant, par un simulateur commercial, les avantages de la combinaison des trois éléments suivants : le placement stratégique d'un éjecteur ; le procédé énergivore de captage de gaz carbonique en post combustion ; la revalorisation de rejets thermiques.

Dans cet article, contrairement au premier, les procédés d'absorption et de désorption sont modélisés. Dans ce deuxième article de la thèse, certaines idées évaluées dans le premier sont approfondies. En particulier, le cas «éjecteur sur riche» est redéfini, où ici le CO_2 qui sort de l'éjecteur n'est pas envoyé au désorbeur, dans le but de récolter des meilleurs résultats qu'au premier article. Une étude qui compare le préchauffage de fluide primaire soit par des rejets thermiques, soit par l'intégration de chaleur fait partie du deuxième article.

Résumé français :

La réduction de la consommation d'énergie de haute qualité reste le plus grand défi technique au déploiement à pleine échelle du captage de gaz carbonique en postcombustion. Le simulateur commercial Aspen Plus, un logiciel de modélisation de procédé, est appliqué afin de valider la nouvelle application des éjecteurs pour la revalorisation de rejets thermiques dans le captage de gaz carbonique par absorption et désorption. Dans cette application, des éjecteurs augmentent la qualité des rejets thermiques, externe au procédé, afin de réduire la quantité de vapeur de turbine à coût élevé nécessaire pour la régénération du solvant. La consommation énergétique du schéma de base se situe dans la plage de valeurs publiées. Le solvant de référence est une solution aqueuse de 20% par masse de monoéthanolamine (MEA). Trois stratégies de méthode de production de vapeur secondaire à l'éjecteur sont évaluées. La production de la vapeur secondaire à l'éjecteur à partir du condensat du désorbeur ou à partir du solvant pauvre sont des options prometteuses, présentant respectivement des réductions de 10 et 14% dans la consommation de la vapeur de haute valeur. Dans les deux cas, la limite maximale de réduction est imposée par la quantité finie de condensat disponible pour la création de la vapeur secondaire à l'éjecteur. L'utilisation du flux de solvant riche de l'absorbeur, pour la production de la vapeur secondaire à l'éjecteur, ne réduit pas la consommation d'énergie de haute qualité dans le procédé de captage. Le choix de préchauffer l'écoulement primaire à l'éjecteur, soit par des rejets thermiques, soit pas de l'intégration thermique, est aussi discuté.

5.2 Abstract

Reducing the valuable energy consumption of solvent regeneration remains the biggest technical challenge to full-scale deployment of post-combustion carbon capture. Aspen Plus modeling is applied to validate the new application of ejectors to upgrade external waste heat in the conventional absorption and desorption process for carbon capture. In this application, ejectors upgrade external waste heat with the goal of reducing the quantity of valuable turbine steam required to regenerate the solvent. The energy consumption of the base case capture process in this study is within the range of published data. The reference solvent is 20% wt. MEA (monoethanolamine). Three strategies for producing the ejector secondary steam are evaluated. Producing the ejector secondary steam from either the stripping column condensate or from the lean solvent are viable options, showing respectively valuable energy savings of 10 and 14%. In both cases the potential valuable energy reductions are limited by the finite amount of condensate available to create the ejector primary steam. Using the rich solvent stream to produce the ejector secondary stream does not reduce the valuable energy consumption. The choice of preheating the ejector primary fluid by means of waste heat or by heat integration is also discussed.

Keywords: CO_2 capture; post-combustion; ejector; waste heat; MEA; Aspen Plus

5.3 Introduction

The burning of fossil fuels is the main source of greenhouse gases associated with human activity, principally due to the release of CO_2 (carbon dioxide) into the atmosphere [11]. CCS (CO_2 capture and storage) is a promising option to diminish climate change resulting from greenhouse gas emissions. CCS, the process of removing CO_2 from industrial sources and sending it to long-term storage, can most effectively be applied by targeting large scale stationary emission sites. Thermal electric power plants make up more than 75% of the worldwide sites that emit more than 0.1 $MtCO_2$/yr [64]. There are currently more than 8,000 such power plants, which are potential targets for CCS. Although pre-combustion, post-combustion and oxy-combustion are technology paths for carbon capture, post-combustion will be the first applied to retrofitting existing electricity production facilities [77].

The most industrially mature technology for the separation of CO_2 from other gases is the process of absorption and desorption with amine solvents. The absorption of CO_2 and other acid gases, such as hydrogen sulfide, has been used on a large scale since the 1930s in the production of commercial grade natural gas and hydrogen [45, 93]. The usual reference amine is monoethanolamine (MEA), which is often used in the 20% to 30% weight range. Chemical absorption with amine solvents is appropriate for gas streams that contain CO_2 concentrations of 12 to 15% by volume, which are typical of coal-fired flue gases. Absorption/desorption technology adapted for flue gas carbon capture was evaluated on a pilot plant basis in the 1980s [93]. The first full scale CCS process was put on stream in 2014, at the Boundary Dam power plant in Saskatchewan, Canada, using a proprietary amine based solvent. The biggest technical challenge to the absorption/desorption process remains the large amount of energy required to regenerate the solvent, which can consume close to the equivalent of up to 30% of the power plant output [93].

Several recent studies have evaluated alternative solvents, such as Idem et al. [39] or Ohashi et al. [74]. Alternative process configurations have also been studied, including for example multistage flash [112], multi-pressure or interheated stripping columns [40, 112], or a matrix configuration [80] having the rich stream split between two stripping towers at different pressures. In the Benfield process, where hot potassium carbonate is the absorbent, ejectors have been proposed for the purpose of reallocating energy within the capture process [45]. In the

process of separating CO_2 from synthetic ammonia using the Benfield process, Lu et al. proposed ejectors for flashing the lean stream [59]. More recently, ejectors were proposed by Zhang et al. [121] for thermal vapour compression in two improved capture systems.

Another path to reducing the reboiler energy consumption includes redirecting flue gas heat to the carbon capture process [118, 120]. The flue gas temperature upstream of the absorber can vary from 100 to 150 ^{o}C, depending on at what point in the desulphurization process it is taken [120]. Recently, Reddick et al. [89, 91] have shown that the incorporation of a steam ejector, combined with the upgrading of external waste heat, is a promising method of reducing the amount of valuable heat required to regenerate the solvent. Their first study presented a shortcut method using a MATLAB (matrix laboratory) computer program and was based on CO_2-MEA-H_2O physical-chemical properties to model only the desorption process and evaluate the proposed ejector method [91]. In a second study the chemical process simulator Aspen Plus was applied, using equilibrium models, to compare three strategies of ejector incorporation into the absorption/desorption process assuming a stripping column pressure of 140 kPa [89]. The second study used heat integration for the preheating step to prepare the ejector primary steam. It was found that creating the ejector secondary flow from either the stripping column condensate or from the lean stream were promising options, while using the rich stream offered no reduction in valuable steam consumption. Both studies showed the advantages of the ejector application, but did not reproduce well the typical specific energy consumption for the base case, expected to be in the range of 4-5 GJ/tCO_2 [82].

In the current study the authors propose applying Aspen Plus rate-based modeling to evaluate three ejector integration strategies into the carbon capture process, varying the stripping column pressure over the range of 140 kPa +/- 10%. Nagy et al. explain why rate-based models, in contrast with equilibrium based models, give results that are much closer to published experimental results, particularly in the context of the highly non-ideal CO_2-MEA-H_2O reactive absorption/desorption process [69]. Further, in contrast with a previous study [89], a new method of producing the ejector secondary steam from the rich stream will be evaluated in an attempt to prevent the desorbed rich stream CO_2 from entering the stripping tower. Finally, a discussion comparing preheating the ejector primary fluid using heat integration versus waste heat upgrading will be presented within the context of the proposed simulations. The aim of the three

simulation target strategies remains the replacement of a portion of the valuable solvent regeneration heat duty with upgraded low cost waste heat.

5.4 Methods

The methods section is divided into five subsections. Section 5.4.1 will begin by reviewing the conventional base case carbon capture process. Section 5.4.2 explains the basics of an ejector, and how it will be modeled. In section 5.4.3 the notion of valuable energy will be discussed. Section 5.4.4 presents the three ways that the ejector will be incorporated into the capture process in this study. Finally, section 5.4.5 describes how the rate-based Aspen Plus base model was completed, hopefully providing sufficient detail to be of help to other newcomers to carbon capture using Aspen Plus.

5.4.1 Base case CO_2 capture process

A simplified version of the conventional base case absorption/desorption CO_2 capture process is shown in Fig. 5.1. The flue gas to be purified, having already passed through a desulphurization unit, rises in the absorber and contacts the descending solvent solution. The purified flue gas leaves the top of the absorber while the solvent solution, now rich in absorbed CO_2, leaves the bottom. The relatively cool rich solvent stream is preheated in the cross heat exchanger before entering the top of the stripping column. In the stripping column, the rising steam produced in the reboiler provides the required energy to desorb the CO_2. The hot mixture of steam and CO_2 leaving the top of the column is condensed to 40 ^oC, where the CO_2 is separated, compressed, and sent to long term storage. The condensate, at least partially, is returned to the column. The hot stream leaving the bottom of the stripping column, now with a much lower concentration of CO_2 and called the "lean solvent", passes through the cross heat exchanger and is further cooled to 40 ^oC at the top of the absorber. The lean solvent enters the absorber and the process begins again.

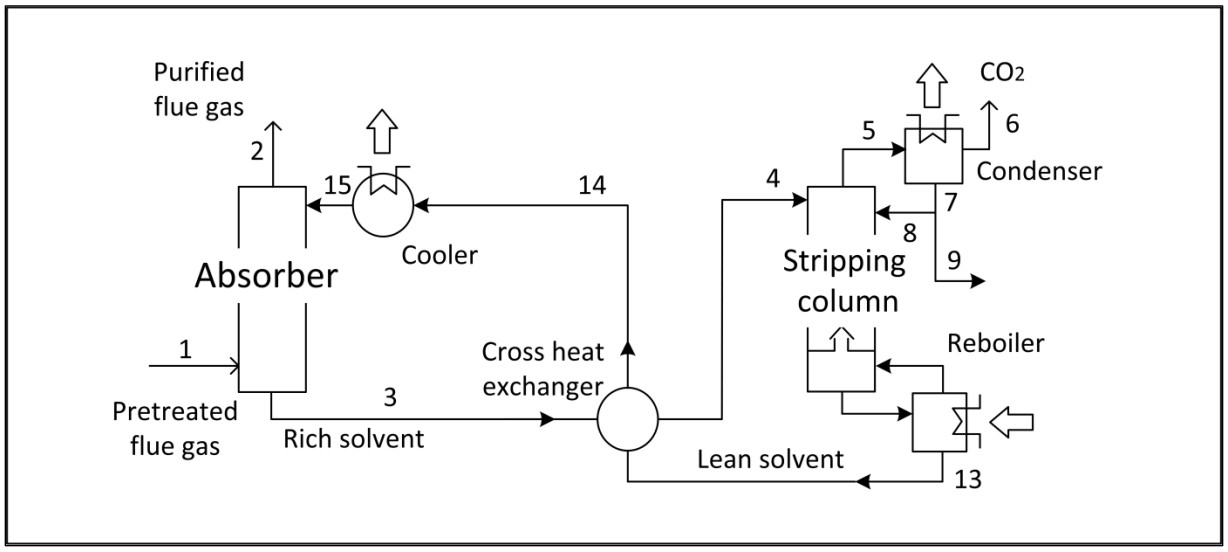

Fig. 5.1 Base case CO_2 capture process using absorption/desorption

5.4.2 Ejector concept

The basic ejector components, shown in the upper portion of Fig. 5.2, were described in previous publications [89, 91]. In brief, the primary fluid refers to the higher pressure steam that enters the ejector nozzle, and that induces the lower pressure secondary fluid to enter the ejector. The secondary fluid is steam with possibly some CO_2. The thoroughly mixed fluids exit the ejector at an intermediate pressure, that of the stripping column. The inset image in Fig. 5.2 introduces the ejector and flash tank symbols that will be discussed in section 5.4.4.

Fig. 5.3 shows the assumed ejector empirical model that will be input into the Aspen Plus simulations. It is the same as that used and described in Reddick et al. [91]. The entrainment ratio, ω, is the ratio of the mass flow rate of the secondary flow, m_{sec}, to that of the primary mass flow rate, m_{prim}. The compression ratio, Cr, is the ratio of the ejector exit pressure, P_{exit}, to that of the secondary entrance pressure, P_{sec}. The primary fluid is assumed to be saturated steam at 300 kPa. For the secondary fluid conditions, we begin with the assumption of having available waste heat at 100 ^{o}C. Supposing a temperature difference of 10 ^{o}C in the heat transfer equipment, and supposing that the secondary fluid is principally saturated steam, the corresponding secondary pressure, P_{exit}, is assumed to be at 70 kPa.

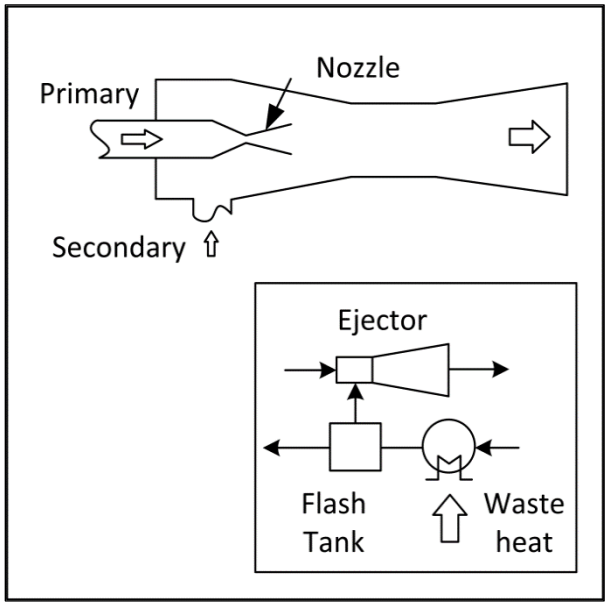

Fig. 5.2 Basic ejector components

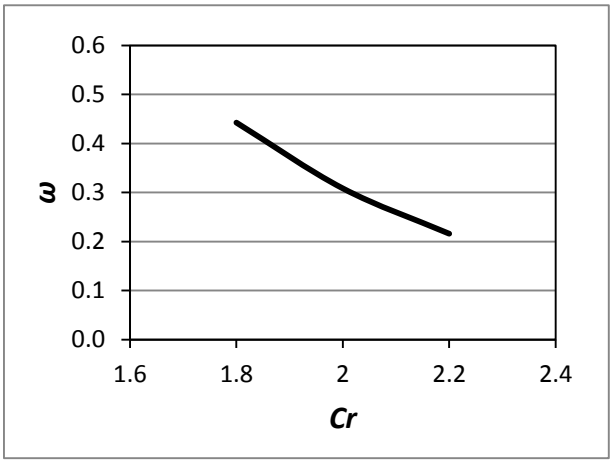

Fig. 5.3 Entrainment (ω) versus compression ratio (Cr) for the ejector model

5.4.3 Problem statement

The goal of the simulations is to minimize the valuable heat duty, Q_{VAL}, that must be extracted from the power plant steam cycle to drive the absorption/desorption process. As shown in equation (5.1), this includes the reboiler duty, Q_{RB}, and the heat duty required to volatize the

ejector primary fluid in the primary steam generator, Q_{SGEN}. The energy consumption for pumping solvent is assumed negligible.

$$Q_{VAL} = Q_{RB} + Q_{SGEN} \tag{5.1}$$

The secondary steam to the ejector will be volatized in a flash tank supplied with waste heat, Q_{FT}. A preheater will provide duty, Q_{PP}, which will allow making use of the available 100 ^{o}C waste heat to raise the primary fluid temperature to 90 ^{o}C. Because the heat Q_{FT} and Q_{PP} are derived from waste heat, they will not be part of the calculation of the valuable heat duty Q_{VAL} necessary for solvent regeneration. A discussion comparing the use of waste heat and heat integration for preheating the primary fluid will be presented in section 5.5.2.

5.4.4 Strategies for ejector integration

Three strategies of incorporating ejector heat upgrading into the conventional carbon capture process will be evaluated, shown in Table 5.1. In all three cases the primary steam to the ejector will be produced by volatizing part of the stripping column condensate, essentially pure water. The secondary steam that will be used by the ejector will be made from three possible liquid sources. These three strategies will be referred to respectively as "ejector on condensate", "ejector on lean" and "ejector on rich". In an effort to harmonize the numbering of the streams in this article, stream numbers 1 to 15 refer to the same location in the process flow layouts in Fig. 5.1, Fig. 5.4, Fig. 5.5, Fig. 5.6 and Fig. 5.7. Alphanumeric stream labels refer to particularities of each of the three strategies, to be discussed shortly. The reflux is the portion of the stripping column condensate that is returned to the top of the stripping column. The reflux ratio in this study refers to the mass flow rate returning to the column (Stream 8), divided by the mass flow of condensate (Stream 7).

Table 5.1 Ejector integration strategies

Case name	Figure	Primary fluid source	Secondary fluid source
"ejector on condensate"	4	condensate	condensate
"ejector on lean"	5	condensate	lean solvent leaving stripper
"ejector on rich"	6	condensate	rich solvent leaving absorber

In the ejector on condensate case of Fig. 5.4, the condensate (Stream 7) separates into three parts: the first (Stream 8) is the reflux, the second (Stream 9) goes through the preheater and the primary steam generator to produce the high pressure ejector primary steam (Stream 11), and the third follows the path (Streams 7a, 7b, 7c) to the ejector secondary, being volatized in a flash tank with waste heat between 7b and 7c.

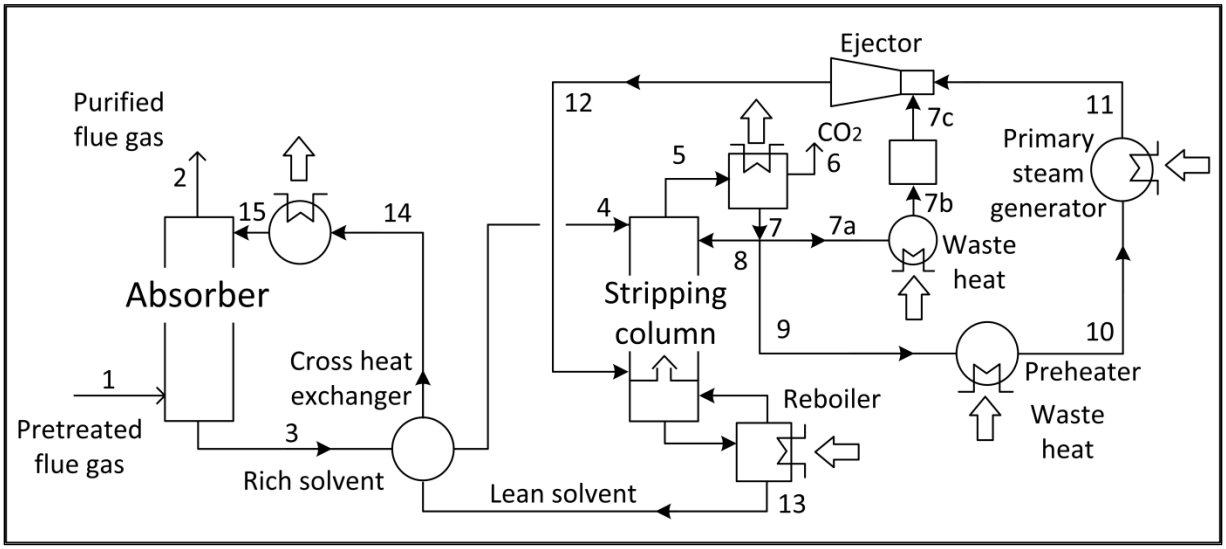

Fig. 5.4 Ejector on condensate case

The ejector on lean case is presented in Fig. 5.5. Here the condensate (Stream 7) separates into two parts: the reflux (Stream 8) and the second part (Stream 9) that goes to the primary steam generator. The lean solvent (Stream 13) exiting the stripping column is split into two parts after the cross heat exchanger: one part (Stream 14a) feeds the flash tank to produce the ejector secondary steam (Stream 14c), the other part (Stream 14e) joins 14d and continues through 14f to the absorber (Stream 15). Based on the results or Reddick et al. [89], a 20% mass fraction of the lean solvent stream (Stream 14) will be split off (Stream 14a) and used to produce the ejector secondary steam.

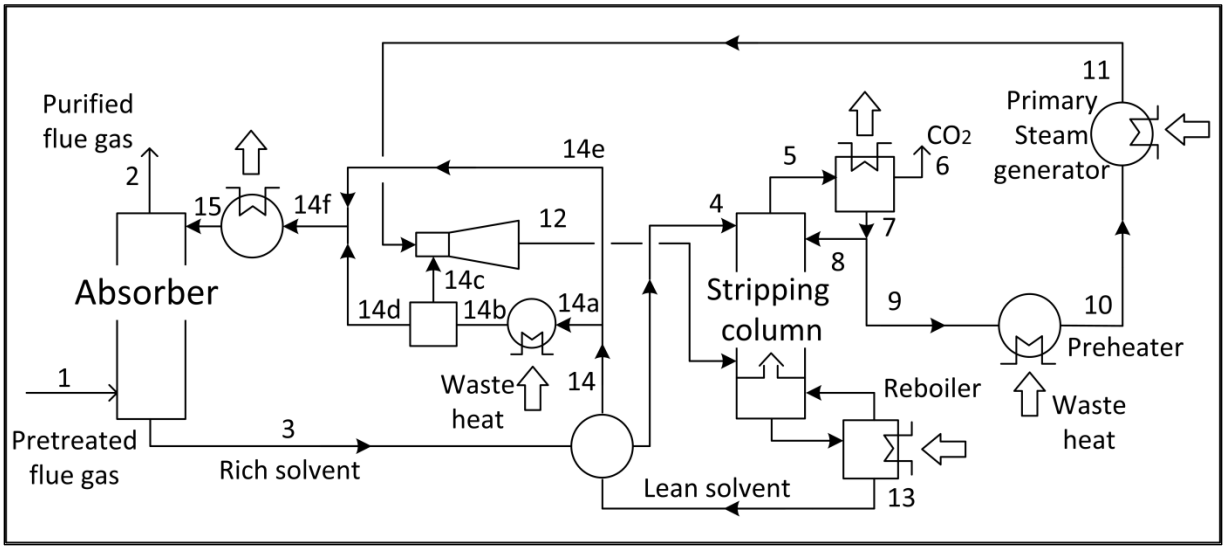

Fig. 5.5 Ejector on lean case

The ejector on rich case, shown in Fig. 5.6, creates the primary steam in the same way as the ejector on lean case of Fig. 5.5. The ejector secondary steam (Stream 3b) is produced by heating the rich solvent (Stream 3) with waste heat. Rather than connecting the ejector exit (Stream 12) with the stripping column, which has already been evaluated [89], the ejector exit is connected directly to a condenser, where the CO_2 (Stream 12b) is collected for long term storage and the condensate (Stream 12a) is available for reflux or water makeup.

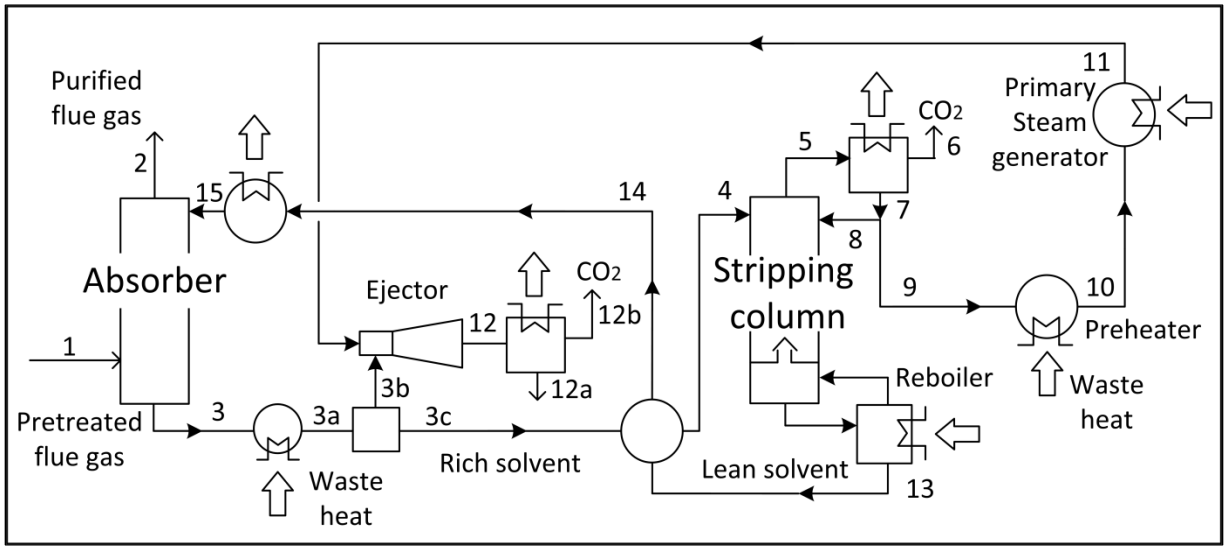

Fig. 5.6 Ejector on rich case; first stage of desorption

5.4.5 Rate-based simulation of the base case using AspenPlus

The assumed flue gas specifications for a 400 MWe power plant, shown in Table 5.2, are typical of pulverized coal-fired combustion [20]. For the purpose of allowing comparison with our earlier work, the solvent solution is 20% wt. MEA, the target CO_2 capture rate is 85%, and the flue gas characteristics are the same as in previous publications [89, 91]. Five pressures are evaluated for the stripping column, 126, 133, 140, 147 and 154 kPa, covering the range of 140 kPa +/- 10%. The CO_2 loading for the lean and rich streams are respectively 0.15 and 0.45 kmol CO_2/kmol MEA, again chosen to allow comparison with our previous publications. The goal of the base case simulation is to allow a basis for comparison with the simulations that incorporate the various strategies of ejector integration.

The starting point for our full scale conventional capture process is available sample code, part of the Aspen Plus package, and the accompanying documentation from Aspen Tech [85]. This code models the CO_2 capture pilot plant at the University of Kaiserslautern in Germany [72]. The available Aspen Plus model is well documented and calculates a reboiler duty of 5.05 GJ/tCO_2, very close to the experimental results of 5.01 GJ/tCO_2 [85].The sample code has several important differences in comparison with our target base case: the solvent solution is 29% wt. MEA, the CO_2 capture rate is 79.1%, the stripping column pressure is 200 kPa, and the lean

and rich stream loading are respectively 0.262 and 0.384 kmol CO_2/kmol MEA. It must be noted that the starting sample code models a flue gas stream of 72 kg/h, a factor of 28,000 times smaller than the target base case. Thus, the available pilot plant code must be dramatically scaled up for our purposes.

As part of the scale up of the pilot plant code, the original water wash features are removed from the absorber and stripping columns, the stripping tower condenser is modeled as a separate unit operation, and the cross heat exchanger is modeled as two interconnected heat exchangers. The water and MEA mass balances are assured by the use of makeup on the lean solvent line returning to the absorber. Table 5.2 presents the results of the scale up activity, showing a significant portion of the final parameter choices. Some changes are necessary to overcome flooding problems in the columns. Where possible, the pilot plant parameters are used in the full scale simulation. The base case tower diameters are larger than the more typical study range of 9-13 m [48]. For comparison purposes in this study the larger diameters were retained, although for design purposes the solution would be to divide the capture process into two or more process trains.

Table 5.2 Base case tower specifications

Specification	Absorber	Stripper
Number of stages	20	20
Operating pressure (kPa)	97.708	126, 133, 140, 147 or 154
Pressure drop (kPa)	1	1
Specification/Reactions/Holdups (m^3)	0.001	0.01
Tower diameter (m)	17	15
Packing type	IMTP, Norton, metal, 75mm	FLEXIPAC, Koch, metal, 250Y
Section packed height (m)	42	13
Mass transfer correlation	Onda et al. (1968)	Bravo et al. (1985)
Heat transfer correlation	Chilton and Colburn	Chilton and Colburn
Interfacial area method	Onda et al. (1968)	Bravo et al. (1985)
Flow model	Mixed	Mixed
Interfacial area factor	1	1
Additional discretization points	5	5
Holdups correlation	Stichlmair et al. (1989)	Stichlmair et al. (1989)
Film discretization ratio	5	5

The first step in describing the simulation of the absorption process concerns the column hydrodynamics, directly related to tower design. In the general equilibrium stage model, each stage is the equivalent of a distillation tower theoretical tray [109]. The liquid and gas streams leaving each stage are assumed to be in equilibrium. In rate-based modeling, in contrast, the number of stages defines the number of discretization points along the height of the tower. The hydrodynamic aspects of the simulation, predicting the column pressure drop and flooding tendency, are calculated based on user input of packing type, column height and diameter, as well as the chosen holdups correlation and flow model. The full scale model used the Stichlmair et al. 1989 correlation for the holdups correlation and flooding prediction, as did the pilot plant simulation [107]. Aspen Plus allows the user to choose among four "flow models", which

indicate how the bulk properties are calculated within each stage. The pilot plant simulation used the "Vplug" model, where stage outlet conditions are applied to the liquid and the stage average conditions are applied to the vapour. Following the example of Zhang et al. [124] and Léonard [52], our full scale simulation uses the "Mixed flow model", where the bulk properties are assumed to be at the same outlet conditions as the streams leaving the stage.

The second step in the absorption process description involves the liquid-vapour interface aspects of the simulation. These parameters control the implementation of the two-film theory [115], as well of the choice of the mass transfer correlation, the heat transfer correlation, the interfacial area method and the interfacial area factor. Approaching the liquid-vapour interface, the concentration gradient in the liquid and the partial pressure gradient in the gas phase provide the driving potential for diffusion within the respective films [115]. The associated parameters in the full scale model, such as the number of additional discretization points, are left unchanged from the pilot plant simulation. To overcome flooding problems in the absorber during scale up, the original structured packing "FLEXIPAC, Koch, 250Y" was changed to the random packing "IMTP, Norton, 75mm". Thus, the mass transfer correlation and interfacial area method "Bravo et al. (1985)" [13], appropriate for a structured packing, was changed to "Onda et al. (1968)" [78], suitable for random packing [52, 124]. Aspen Plus provides the "interfacial area factor" as a means of adjusting the interfacial area method for more precisely fitting the simulation results with available data. Zhang et al. 2009 [124] changed this parameter to 1.8 in their simulation using the random packing IMTP, 40mm, indicating that the "Onda et al. 1968" correlation was expected to under predict the interfacial area. Given that we do not have access to experimental data for our choice of IMTP 75 mm random packing, the "interfacial area factor" of 1 was retained, as was also done by Leonard [52]. The Chilton and Colburn correlation was kept for the heat transfer [17].

The third step in describing the simulation of the absorption process relates to the CO_2-MEA-H_2O solution chemistry. Part of the preliminary Aspen Plus setup of the capture process, already completed in the sample code, is the specification of the liquid and gas characteristics, as well as the heat and mass transport properties. The chemistry of the highly non-ideal solution of the CO_2-H_2O-MEA system is defined with the electrolyte non-random two liquid model (eNRTL), which accounts for the solution thermodynamics and chemical kinetics. The Aspen "true component" approach is used, calculating the material balance based on the calculated ionic

concentrations. The gas phase is defined by the Redlich-Kwong equation of state. Convergence difficulties during scale up required changing the absorber and stripping column liquid from "standard" to "strongly non-ideal", as well as upgrading the damping level from "standard" to "severe". It was found that the Broyden algorithm option gave more rapid and robust convergence for the overall process simulation, rather than the Wegstein default option [101, 126].

5.5 Results and discussion

Section 5.5.1 will present an overview of the base case and ejector results. Section 5.5.2 provides an explanation as to why waste heat was used to preheat the ejector primary fluid in the current study. Sections 5.5.3 and 5.5.4 present the ejector on condensate and lean cases, with varying reflux ratios. Section 5.5.5 discusses the ejector on rich case. In several sections the stripping column pressure is set to 126 kPa. The reason for this choice is that the optimal pressure for valuable energy savings occurs at lower stripping column pressure, as will be discussed in section 5.5.6. Section 5.5.7 summarizes the combined effects of the studied parameters. Finally, section 5.5.8 discusses how ejector heat integration and waste heat upgrading relate more generally to CO_2 capture process heat integration.

5.5.1 Base case

Typical published MEA based reference values for the specific heat duty required to recover the solvent are in the 4-5 GJ/tCO_2 range [82]. Table 5.3 presents the calculated base case results after the scale up, over a range of stripping column pressures. The calculated values may be lower than expected, given that the lean and rich CO_2 loadings and the solvent flow rate are not optimized. The use of 20% rather than 30% wt. MEA solution would be expected to increase

the specific reboiler duty, as would our target of an 85% capture rate, higher than the pilot plant model of 79.1%. On the other hand, the slightly over dimensioned columns, and the higher CO_2 level in the base case flue gas of 12%, rather than the pilot plant simulation of 5.4% [85], would tend to lower the valuable heat duty. For the purpose of allowing a comparison point for the ejector enhanced process flow plans, the Table 5.3 values are reasonable for the base case.

Table 5.3 Base case specific valuable duty

Stripping column pressure (kPa)	Valuable duty, Q_{VAL} (MW)	Specific valuable duty (GJ/tCO_2)	Lean solvent temperature, leaving stripping column (^oC)
126	487.5	5.59	107.8
133	466.0	5.34	109.3
140	448.4	5.14	110.8
147	434.1	4.97	112.2
154	422.5	4.84	113.5

In the base case and the ejector strategies using waste heat to preheat the primary fluid, an Aspen Plus "design specification" set the approach temperature at the hot end of the cross heat exchanger to 10 ^oC. In the base case, the actual minimum approach temperature of the cross heater exchanger was at the cold end, having a value of 9.0 to 9.2 ^oC for the Table 5.3 results. Manually and iteratively setting the rich stream temperature at the entrance of the stripping column to guarantee a true cross heat minimum approach temperature of 10 ^oC would have had the effect of slightly increasing the specific valuable duty for the base case. Thus the values in Table 5.3 are slightly lower than they should be for a minimum cross heat exchanger approach temperature of 10 ^oC, allowing a conservative estimation on any valuable energy savings that will be calculated in comparison with the ejector integration strategies.

Table 5.4 Base case stream parameters, stripping column 126 kPa

Equipment (-->)	Absorber	Absorber	Absorber	Absorber	Stripper	Stripper	Condenser
Stream (-->)	Fluegas	Gas out	Lean in	Rich out	Lean out	Gas out	CO_2 out
Stream number	1	2	15	3	13	5	6
Mass Frac							
MEA	0.0000	0.0003	0.1958	0.1879	0.2000	0.0000	0.0000
H_2O	0.0889	0.1068	0.7831	0.7514	0.7783	0.5288	0.0252
CO_2	0.1861	0.0334	0.0212	0.0607	0.0216	0.4708	0.9742
Flow (tonne/h)	1990	1678	7471	7782	7309	668	322
Temperature (^oC)	48.0	55.8	40.0	60.7	107.8	97.3	40.0
Pressure (kPa)	120	100	127	117	127	126	126
Vapour fraction	1	1	0	0	0	1	1
kmol CO_2/kmol MEA			0.1500	0.4484	0.1500		

As will be discussed in section 5.5.6, the optimal stripping column pressure for the range studied was 126 kPa. Table 5.4 lists the main stream process parameter values for the base case. Table 5.5 presents a comparison of the ejector case simulations, with an emphasis on showing the change in H_2O and CO_2 liquid and gas mass fractions before and after the flash tank. The "flash tank vapour out" column is also the ejector secondary fluid. The secondary fluid is essentially steam in the ejector on condensate case, contains a small amount of CO_2 in the ejector on lean case, and contains around 44% CO_2 by mass in the ejector on rich case.

Table 5.5 Ejector cases stream parameters, stripping column 126 kPa

Case	Equipment (-->)	Absorber	Stripper	Flash tank	Flash tank	Flash tank	Ejector
	Stream (-->)	Rich out	Lean out	Liquid in	Liquid out	Vapour out	Ejector out
Ejector on Condensate	Stream number	3	13	7a	n.a.	7c	12
	Mass Frac						
	MEA	0.1879	0.1960	0.0001		0.0001	0.0001
	H_2O	0.7514	0.7828	0.9985		0.9985	0.9985
	CO_2	0.0607	0.0212	0.0013		0.0013	0.0013
	Flow (tonne/h)	7782	7459	106		106	346
	Temperature (^oC)	60.7	107.8	40.0		90.0	115.1
	Pressure (kPa)	117	127	126		70	126
	Vapour fraction	0	0	0		1	1
	kmol CO_2/kmol MEA	0.4484	0.1500				
Ejector on Lean	Stream number	3	13	14a	14d	14c	12
	Mass Frac						
	MEA	0.1879	0.1921	0.1921	0.2143	0.0061	0.0020
	H_2O	0.7514	0.7871	0.7871	0.7649	0.9733	0.9908
	CO_2	0.0607	0.0208	0.0208	0.0208	0.0206	0.0073
	Flow (tonne/h)	7734	7571	1514	1353	161	526
	Temperature (^oC)	60.7	107.7	71.4	91.8	91.8	115.7
	Pressure (kPa)	117	127	127	70	70	126
	Vapour fraction	0	0	0	0	1	1
	kmol CO_2/kmol MEA	0.4481	0.1500	0.1500	0.1346		
Ejector on Rich	Stream number	3	13	3	3c	3b	12
	Mass Frac						
	MEA	0.1879	0.2013	0.1879	0.1896	0.0008	0.0003
	H_2O	0.7514	0.7769	0.7514	0.7532	0.5569	0.8632
	CO_2	0.0607	0.0218	0.0607	0.0572	0.4392	0.1356
	Flow (tonne/h)	7783	7263	7783	7712	70	229
	Temperature (^oC)	60.7	107.8	60.7	84.2	84.2	115.0
	Pressure (kPa)	117	127	117	70	70	126
	Vapour fraction	0	0	0	0	1	1
	kmol CO_2/kmol MEA	0.4484	0.1500	0.4484	0.4191		

5.5.2 Ejector on condensate: Primary preheat with waste heat versus heat integration

Two methods of preheating the ejector primary fluid were simulated and compared for the ejector on condensate case. In the "waste heat" method, the 100 ^{o}C waste heat stream preheats the ejector primary fluid (Stream 10 in Fig. 5.4) to 90 ^{o}C. In the "heat integration" method, shown in Fig. 5.7, rather than sending all of the lean solvent from the reboiler (Stream 13) to the cross heat exchanger (Stream 13c), some of this hot fluid is sent to the primary fluid preheater (Stream 13a). Heat integration offers the potential advantage of reducing the required surface area of the condenser and of the cooler at the absorber lean solvent entrance, as introducing less heat duty into the capture process implies lowering the need to remove this heat duty from the process. A second potential advantage of using heat integration is that the preheater exit temperature can be hotter, up to within 10 ^{o}C of that of the hot lean solvent temperature. Again we assume a temperature difference of 10 ^{o}C for heat transfer.

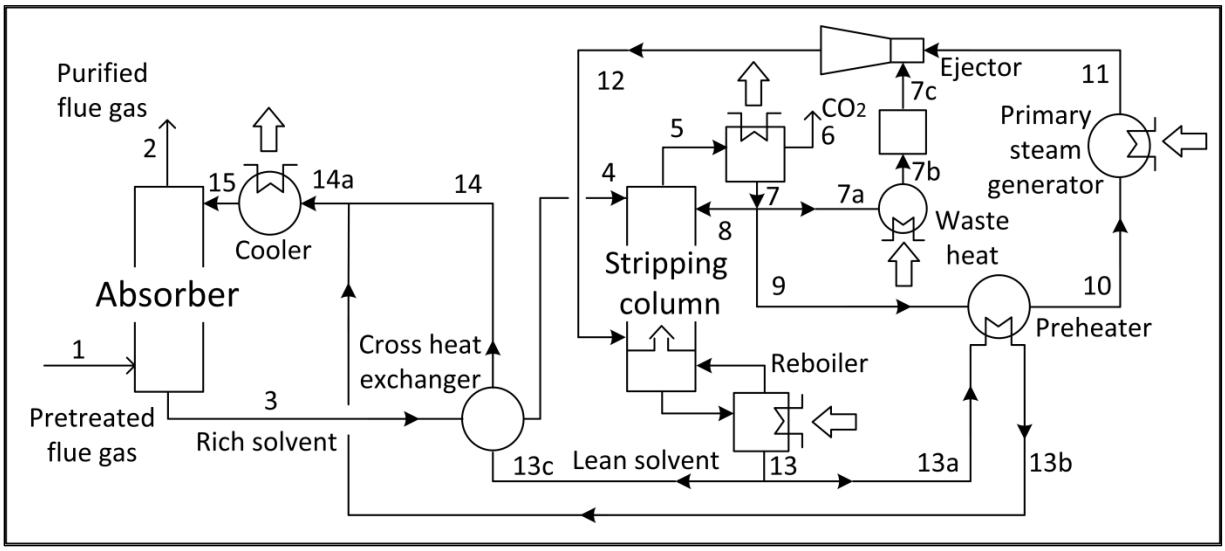

Fig. 5.7 Ejector on condensate case with heat integration

It is insightful to divide the comparison of the two preheating methods into two steps. First, a comparison will be made with the preheater exit temperature at 90 ^{o}C for both methods. In the second step, the preheater exit temperature of the "heat integration" method will be allowed to increase to within 10 ^{o}C of the temperature of the hot lean solvent. For comparison

purposes the stripping column pressure was operated at 126 kPa, corresponding to a lean solvent temperature of 107.8 ^{o}C, shown in Table 5.3. The reflux ratio was fixed at 0.1 in all cases. Thus, in this second step the preheater exit temperature was set to 98 ^{o}C for the "heat integration" method. A minimum approach temperature of 10 ^{o}C was carefully controlled for the cross heat exchanger for both preheating methods.

Table 5.6 Preheating comparison, with method and preheater exit temperature as parameters

	"waste heat", 90 ^{o}C	"heat integration", 90 ^{o}C	"heat integration", 98 ^{o}C
Rich solvent (stream 4) temp. (^{o}C)	97.8	97.0	96.9
Ejector output mass flow (tonne/h)	346	338	336
Q_{RB}, reboiler duty (MW)	283.5	289.1	290.4
Q_{SGEN}, steam generator (MW)	155.8	152.1	149.0
Q_{RB}+Q_{SGEN}, valuable heat duty (MW)	439.3	441.2	439.4
Specific valuable heat duty (GJ/tCO_2)	5.03	5.05	5.03

Referring to Table 5.6, three main points can be made by comparing the simulations. 1) There was no significant difference between the preheating methods in terms of the amount of specific valuable heat duty. 2) Given the same preheater exit temperature for both methods, the "waste heat" method offered a slight reduction in specific valuable heat duty. 3) The hotter preheater exit temperature can favour the "heat integration" case, but only if a sufficiently high exit temperature is reached.

For the "heat integration" method of Fig. 5.7, as more of the lean solvent (stream 13a) is directed toward the preheater, the temperature of the rich solvent (stream 4) entering the stripping column decreases as less heat is transferred in the cross heat exchanger. As a consequence, a lower amount of water vapour leaves the top of the column, resulting in a lower mass output from the ejector, corresponding to a lower steam generator duty, Q_{SGEN}. For the same preheater exit

temperature, the "waste heat" method is favoured because the slightly higher ejector output mass flow provides more upgraded heat to replace valuable reboiler heat when compared with the "heat integration" method. When the "heat integration" method preheater exit temperature is allowed to increase beyond 90 ^{o}C, there is a downward trend in the valuable specific heat duty. Fig. 5.8 shows the specific valuable duty as the preheater exit temperature is increased for the "heat integration" method. In this case the valuable steam generator duty, Q_{SGEN}, is being incrementally replaced by the higher quality heat from the hot lean solvent stream.

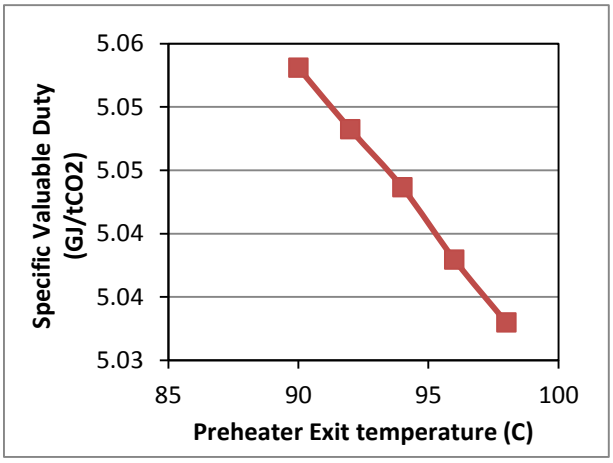

Fig. 5.8 Effect of preheater exit temperature on specific valuable heat, with heat integration

In the current study, the use of "waste heat" was chosen as the method of preheating the ejector primary fluid, as shown in Fig. 5.4, Fig. 5.5 and Fig. 5.6. The "waste heat" method offered a simplified process layout, and there was no significant specific valuable energy difference found in the ejector on condenser case. This choice also provided a pragmatic solution to the convergence problems encountered when attempting to apply the heat integration method to the ejector on lean case. In an actual application, the preferred choice would be based on both thermodynamic and economic considerations.

5.5.3 Ejector on condensate, for varying reflux ratio

In the base case simulation, with a stripping column pressure of 126 kPa, the valuable heat duty to regenerate the solvent was 487.5 MW, shown in Table 5.3. For the ejector on condensate case, reducing the reflux ratio from 0.5 to 0.1 reduced the valuable heat duty from 461.5 to 439.3 MW. As can be seen in Fig. 5.4, reducing the reflux ratio directly increases the mass flow leaving the ejector. As the reflux ratio decreased, shown in Fig. 5.9, the increasing consumption of valuable heat duty in the primary steam generator (SGEN) was more than offset by the decreasing heat duty of the reboiler (RB), resulting in a small net decrease in the valuable heat duty (VAL).

To avoid processing difficulties in operating a stripping column with no reflux [45], such as excessive solvent losses, the reflux ratio of 0.1 will be considered as optimal for the ejector on condensate case. Thus, in the current study the valuable energy savings is 9.9%. This result is lower than the value of 13.8% reported a previous study using the equilibrium model assumption for the Aspen Plus simulations of the absorber and stripping column [89]. The main reason for this difference is the overestimation of the water content leaving the top of the stripping column in the equilibrium model, thus making 2.4 times more water available for the ejector output mass flow. The ejector output mass flow of 346 tonne/h in the current study compares with 820 tonne/h in the previous study [89].

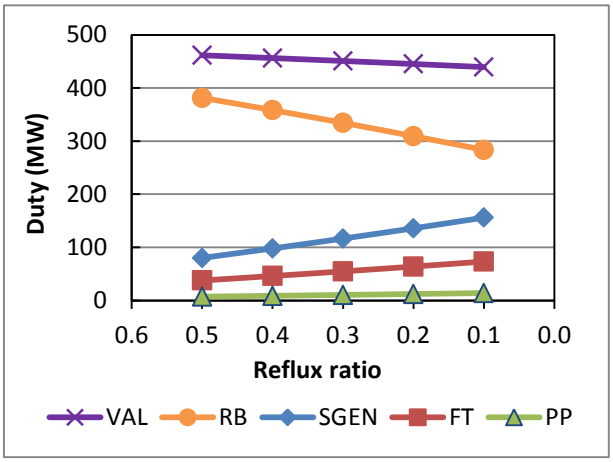

Fig. 5.9 Duties, ejector on condensate case, with stripping column pressure 126 kP

5.5.4 Ejector on lean, for varying reflux ratio

For the ejector on lean case, shown in Fig. 5.10, reducing the reflux ratio had the effect of reducing the valuable steam duty, as was found in the ejector on condensate case. The reduction in the reflux ratio from 0.5 to 0.1 caused a corresponding valuable heat duty (VAL) reduction from 452.5 MW to 421.5 MW. Again choosing a reasonable lower reflux ratio of 0.1, the ejector on lean valuable energy savings is 13.5%, lower than the result of 23% reported in the previous study [89]. The main source of the discrepancy, once again, is the consequence of changing to the more realistic rate-based model. In the current study the ejector outlet mass flow is 426 tonne/h, significantly lower than the 1,270 tonne/h in the corresponding equilibrium model study [89].

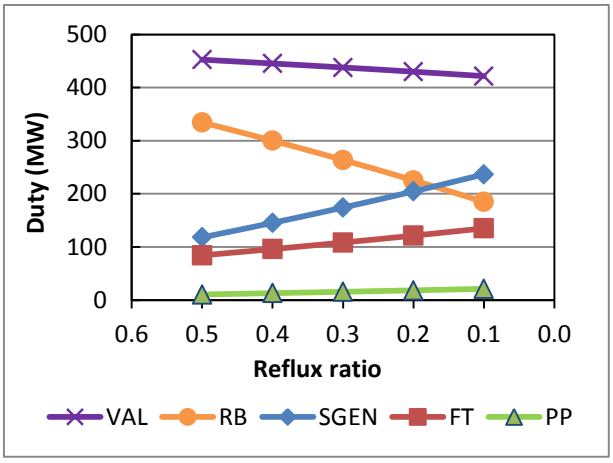

Fig. 5.10 Duties, ejector on lean case, split fraction 20%, with stripping column pressure 126 kPa

5.5.5 Ejector on rich

Comparing the specific valuable duty results of the ejector on rich case, shown in Table 5.7, with those of the base case, shown in Table 5.3, shows that the idea of using the ejector for a first stage of desorption did not generate valuable energy savings. The use of the ejector captured from 9.8 to 3.7% of the target CO_2 and reduced the reboiler duty by 3.6 MW and 2.0 MW, corresponding respectively to stripping column pressures of 126 and 154 kPa. The simulated ejector on rich case of Fig. 5.6, however, did not benefit from the key advantage of the ejector on condensate or ejector on lean cases. In those cases, part of the valuable reboiler duty is replaced by a combination of valuable steam generator duty and waste heat, due to the input of the ejector exit live steam into the stripping column. In the ejector on rich case, in contrast, the valuable steam generator duty, Q_{SGEN}, and entrained waste heat, Q_{FT}, are sent to a condenser. The slight reduction in the overall desorption load caused by the first stage of desorption, and thus the slight reduction in the reboiler duty, is not enough to offset the significant increase in the valuable steam generator duty required to produce the ejector primary steam.

Table 5.7 Ejector on rich results

Stripping column pressure (kPa)	CO_2 from ejector exit (tonne/h)	CO_2 from stripping column (tonne/h)	Reboiler duty QRB (MW)	Primary steam duty QSGEN (MW)	Specific valuable duty (GJ/tCO2)
126	31	283	483.9	103.3	6.73
133	24	290	463.0	92.9	6.37
140	19	295	445.8	84.5	6.08
147	15	299	431.8	77.6	5.84
154	12	302	420.5	72.2	5.65

5.5.6 Ejector on condensate versus ejector on lean, for varying stripping column pressure

In this section, the ejector on condensate and ejector on lean cases will be compared for similar operating parameters. The reflux ratio was fixed at the optimal value of 0.1, and the stripping column pressure was varied over the range of 126 kPa to 154 kPa. The metric "valuable energy savings" will be used to indicate the percent reduction in valuable heat duty in the indicated ejector case, "Condensate" or "Lean", in comparison with the base case capture process at the same stripping column pressure. As shown in Fig. 5.11, for the same stripping column pressure, the ejector on lean yields higher valuable energy savings than the ejector on condensate. In both cases, the lower stripping column pressure yielded the higher valuable energy savings.

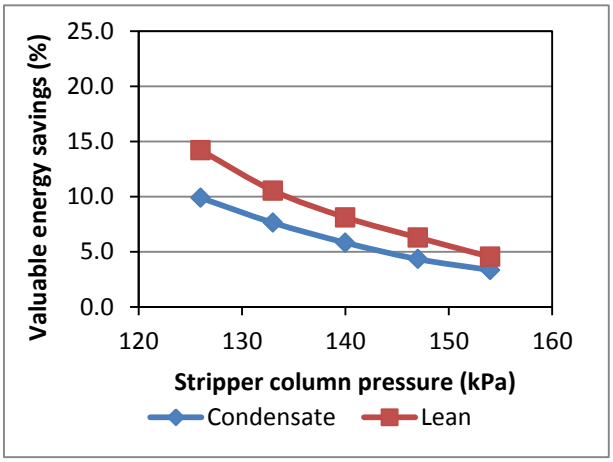

Fig. 5.11 Valuable energy savings as a function of ejector case and stripping column pressure

Fig. 5.12 and Fig. 5.13 again present the valuable energy savings for the same simulations, but consider different parameters for the abscissa. As the stripping column pressure increases so does the ejector compression ratio, which in turn is associated with a diminishing entrainment ratio, as was presented in Fig. 5.3. As the entrainment ratio increased, presented in Fig. 5.12, the valuable energy savings increased for both the ejector on condensate and ejector on lean cases.

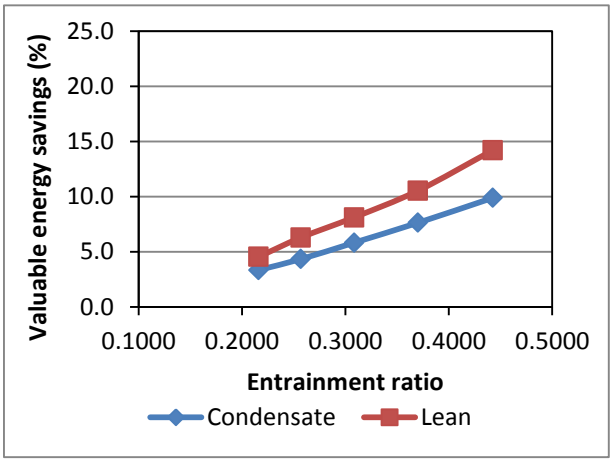

Fig. 5.12 Valuable energy savings as a function of ejector case and ejector entrainment ratio

Fig. 5.13 shows the effect of the rising ejector output mass flow rate on the valuable energy savings, corresponding to the decreasing stripping column pressure. For the same ejector exit mass flow rate the ejector on condensate provided a greater valuable energy savings. The reason for the slightly lower result in the case of the ejector on lean case is due to the presence of the small amount of CO_2 in the ejector secondary stream, of the order of 1% by mass, which slightly decreases the partial pressure driving force in the stripping column where the ejector steam is injected.

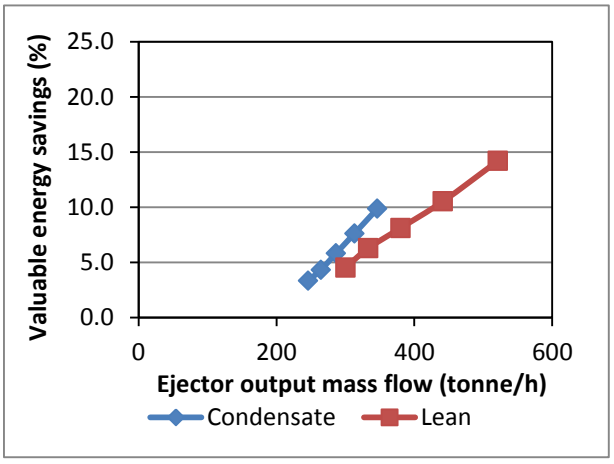

Fig. 5.13 Valuable energy savings as a function of ejector case and ejector exit mass flow

5.5.7 Ejector on condensate versus ejector on lean, varying stripping column pressure and reflux ratio

In this section the ejector on condensate and ejector on lean cases are compared, allowing variation of both the stripping column pressure and the reflux ratio. For the purpose of simplifying the graphical presentation, the pressure was set to 126, 140 or 154 kPa, while the reflux ratio was varied from 0.1 to 0.5, in increments of 0.1. Fig. 5.14 presents the combined results, including the associated base case values, and shows the valuable energy savings as a function of reboiler duty. For a given stripping column pressure, the reboiler duty values are almost collinear for the associated ejector on lean, ejector on condensate and the base case results. Fig. 5.14 is very similar in appearance to a corresponding figure in a previous study, Fig. 4.13, where the reboiler steam was gradually replaced by ejector steam [91]. The earlier simulations were based on thermo-physical properties rather than a commercial process simulator, although in that case the finite limit of the available amount of condensate for the ejector primary was not accounted for [91]. In the current study, the finite amount of stripping column condensate available to be redirected to the ejector limits the potential valuable energy savings that can be provided.

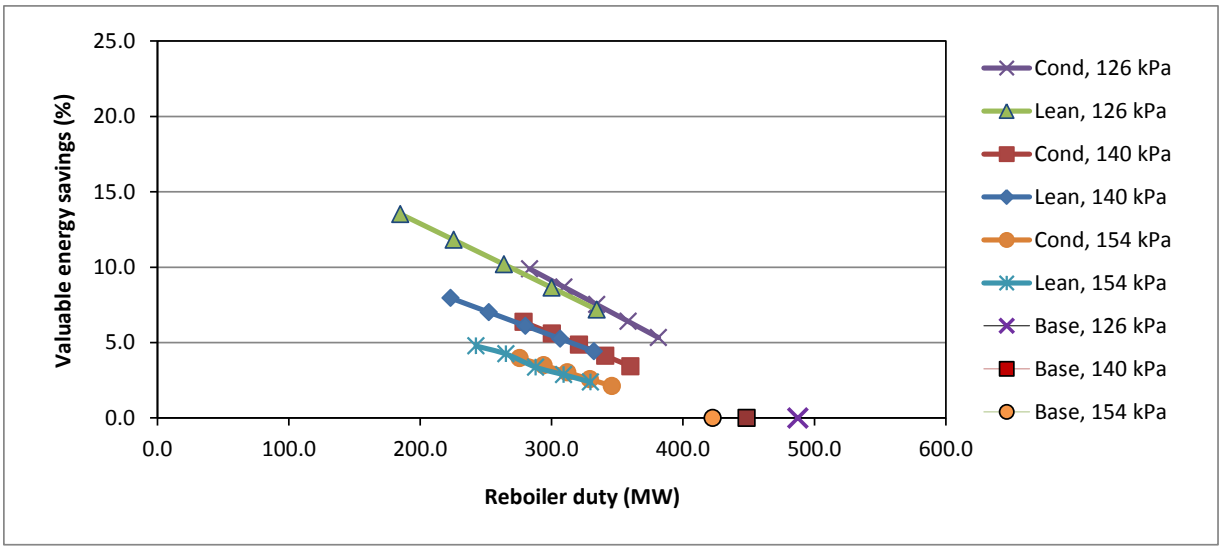

Fig. 5.14 Valuable energy savings as a function of ejector case, stripping column pressure, and reflux ratio

Raynal et el. [88] completed an economic study on a 630 MWe coal-fired plant, finding that the reboiler duty was 82% of the operating cost, where the operating cost was 72% of the total capture cost. The reboiler duty thus represents 59% of the total capture cost. If we assume an average mitigation cost of 50 US$/t$CO_2$ avoided [64], the potential economic benefit of the valuable energy savings of 9.9 to 13.5% is from 3 to 4 US$/t$CO_2$. Applying these figures to our 400 MWe coal-fired base plant, and assuming an 80% capacity factor, the annual economic benefit would be from 7 to 9 million US$.

5.5.8 Discussion: Post-combustion CO_2 capture and process integration

Yokayama et al. [118] describe how a flue gas cooler upstream of the carbon capture process uses flue gas heat to reduce the overall energy consumption within the CO_2 capture process. When CO_2 capture is required, the flue gas entering the absorption/desorption process must be cooled to around 50 ^oC. Although the ejector simulations began with the assumption of available 100 ^oC waste heat, for example from flue gas energy, the ejector application is more general in nature. Other sources of waste heat could include neighbouring industrial sites, or other intermediate hot gas streams. A different ejector design could also function with waste heat as low as 60 ^oC, although the overall benefit would have to be evaluated.

In the context of current fossil fuel based power production without CO_2 capture, the optimal use of flue gas energy is a subject of continuing research. For example, Gang Xu et al. studied four schemes of heat integration within the steam power cycle, and indicated that the flue gas temperature range is 120 ^oC to 150 ^oC [117]. Lukowicz and Kochaniewicz studied four layouts specifically for hard coal, with a flue gas temperature of 120 ^oC, and six for brown coal, having a flue gas temperature of 170 ^oC [110]. In the context of CO_2 capture, the most appropriate use of flue gas heat, and waste heat more generally, could be quite different from the current situation without CO_2 capture.

The absorption/desorption process can also be a source of heat to the steam power cycle, although the net transfer is clearly to the capture system. Sarunac et al. [100] studied returning heat from the CO_2 compression train, in combination with flue gas recovery, for improving the power plant Rankine cycle efficiency. Duan et al. studied thermal integration of the MEA-based capture process and the steam power cycle, incorporating the CO_2 compression heat and, for

example, an absorption heat pump [26]. Zhang et al. applied pinch analysis within the MEA capture process, finding that the best choice in terms of energy penalty reduction was to incorporate an absorption refrigerator [122]. Many other combinations of heat integration strategies are possible, with and without ejector enhancement.

In the current study ejectors have shown their potential in reducing the amount of valuable energy required for post-combustion power plant CO_2 capture. Their mechanical simplicity and long history in industrial applications are two reasons why they should be considered in related research. Their ability to upgrade waste heat is another reason for their continuing interest in the area of heat integration.

5.6 Conclusions

The integration of ejector technology into post-combustion carbon capture can help reduce the valuable energy consumption necessary to regenerate the solvent. The commercial chemical simulator Aspen Plus, was used to simulate a full scale capture process. The process targeted an 85% capture rate for the simulated 400 MW coal-fired power plant flue gases, using 20%wt MEA as the reference solvent. Three strategies of integrating the ejector into the layout were evaluated. Producing the ejector secondary steam from either the stripping column condensate or from the lean solvent were found to be viable options, showing respectively valuable energy savings of 10 and 14%. The current results are in agreement with typical specific heat consumption for the base case. Producing the ejector secondary steam from the rich stream does not offer any valuable energy reduction. In both of the viable cases the potential valuable energy reductions were limited by the finite amount of condensate available to create the ejector live steam.

The choice of preheating the ejector primary fluid by means of waste heat or by heat integration was discussed. In the context of the studied process configurations, preheating with waste heat was chosen. It was shown that in the case of producing the ejector secondary steam from condensate, there is no significant difference between the two preheating methods in terms of the valuable energy consumption. The waste heat method was chosen for all simulations as it provides both a simpler process layout and it avoided convergence problems that occurred when

evaluating preheater heat integration in the ejector on lean case. In general, economic evaluation must be applied on a case by case basis to determine the best choice.

Our study shows that the strategic use of ejector technology, by upgrading waste heat, can significantly reduce the valuable energy consumption in post-combustion carbon capture. Ejector integration allows some of the valuable stripping column heat duty to be replaced by upgraded waste heat. This paper thus makes a contribution to reducing the barrier to the implementation of full-scale deployment of carbon capture.

5.7 Acknowledgments

The first author would like to thank CanmetENERGY (Natural Resources Canada) for the financial support.

5.8 Nomenclature

Table 5.8 Chapter 5 nomenclature

Cr	ejector compression ratio
m	mass flow rate (tonne/h)
P	pressure (kPa)
Q	heat duty (MW)
Greek	
ω	ejector entrainment ratio
Subscript	
s	
exit	ejector exit
FT	flash tank
PP	primary preheater
prim	ejector primary
RB	reboiler
sec	ejector secondary
SGEN	primary steam generator
VAL	valuable

CHAPTER 6 THESIS CONCLUSION

This thesis evaluated the extent to which gas-gas ejectors might be able to reduce the huge amount of energy required to regenerate the solvent in post-combustion carbon capture. Three detailed simulation studies were completed, differing principally in the model used to represent the CO_2-MEA-H_2O mixture in the separation process. An empirical steam ejector model was created to represent the ejector behaviour in both simulation studies. An experimental program was completed to quantify the change in steam ejector behaviour when the secondary fluid contains a mixture of steam and CO_2. The experimental results were accounted for in the process simulations.

The experimental program first characterized the steam ejector over various primary pressures (350, 450 and 450 kPa) and secondary pressures (50, 70 and 90 kPa), for two primary nozzles. Using the same primary nozzles, of 4.60 mm and 4.23 mm diameter, the ejector was evaluated over a range of secondary fluid CO_2 levels, up to 42% by mass. For the tests with CO_2 the primary pressure was 450 kPa with 10 °C superheat and the secondary pressure was 70 kPa. It was found that the critical exit pressure did not change as the mass fraction of CO_2 in the secondary fluid increased. The entrainment ratio, however, increased approximately linearly over the experimental range. An improvement of 23% in the entrainment ratio, as compared with pure steam, was found when the secondary fluid contains 42% CO_2 by mass. This behaviour is in sharp contrast to the experimentally observed behaviour of a pure steam ejector, where an increase in entrainment ratio comes at the expense of a decrease in the ejector exit critical pressure.

Two peer-reviewed published journal articles evaluated various scenarios for the integration of a steam injector into a chemical absorption/desorption post-combustion capture process. Both studies assumed the same flue gas specifications of a 400 MWe coal-fired power plant. The chosen reference solvent was 20% wt. monoethanolamine (MEA), and the target CO_2 capture rate was 85%. The lean and rich stream CO_2 loading values were fixed respectively at 0.15 and 0.45 kmol CO_2/kmol MEA. Three principal configurations were studied, according to the choice of the liquid stream used to produce the ejector secondary fluid: ejector on condensate, ejector on lean or ejector on rich.

The first study focused on the desorption process and presented a shortcut method based on vapour liquid equilibrium data. The optimal position of the live steam injection was determined to be the base of the stripping column. The simulations revealed reductions in the required amount of valuable energy from 10 to 25%. These reductions were found for the cases where the flash tank is fed with the condensate or the lean solvent streams, corresponding respectively to CO_2 loadings of 0 and 0.15 kmol CO_2/kmol MEA. It was also demonstrated that feeding the flash tank with the rich stream (CO_2 loadings of 0.45 kmol CO_2/kmol MEA) is not a viable option.

The second publication used a commercial process simulator, Aspen Plus, and a more realistic rate-based model to evaluate configurations similar to those of the first publication. A study was included that compared preheating the primary steam with waste heat or by heat integration. The rate-based simulation found valuable energy savings of 10 to 14%, with the "ejector on condensate" and "ejector on lean" again being the advantageous scenarios.

The incorporation of ejector technology into post-combustion carbon capture can reduce the valuable energy consumption necessary to regenerate the solvent. More specifically, this thesis shows the potential energy advantages of combining the following concepts: the use of a gas-gas ejector; a post-combustion absorption/desorption CO_2 capture process; the upgrading of waste heat external to the capture process. Expressed in a different way, external waste heat, upgraded by means of an ejector, can be used to partially replace the valuable steam that would otherwise be taken from the valuable turbine steam in an electric power plant to drive the CO_2 capture process. This central conclusion is the result of three detailed simulation studies, and is supported by experimental ejector work on a custom test bench.

CHAPTER 7 CONCLUSION DE LA THÈSE

La thèse visait à évaluer le potentiel d'amélioration énergétique du système de captage postcombustion de carbone dans les centrales thermiques par l'intégration optimale des éjecteurs monophasiques. Un tel système de captage de carbone dans une station thermique de production d'électricité nécessite une quantité d'énergie très importante afin de régénérer le solvant qui capte le gaz carbonique. Trois études détaillées de simulation ont été complétées, différant principalement par le modèle choisi pour représenter le mélange CO_2-MEA-H_2O dans le procédé de séparation. Un modèle empirique de l'éjecteur à vapeur a été créé et a servi à représenter l'éjecteur à vapeur dans les études. Un programme d'expérimentation a été complété afin de quantifier le changement dans le comportement de l'éjecteur à vapeur lorsque le fluide secondaire comporte un mélange de vapeur d'eau et d'un gaz non-condensable, le CO_2.

Le programme expérimental a d'abord caractérisé l'éjecteur à vapeur sous plusieurs pressions primaires (350, 450 et 450 kPa) et pressions secondaires (50, 70 et 90 kPa), pour deux tuyères. Se servant des mêmes tuyères, de 4.60 mm et 4.23 mm de diamètre, l'éjecteur a été évalué sur une plage de niveaux de CO_2 dans le fluide secondaire, allant jusqu'à 42% par masse. Pour les tests avec CO_2 la pression primaire était de 450 kPa avec 10 °C de surchauffe et la pression du fluide secondaire était de 70 kPa. Il s'avère que la pression critique de sortie n'a pas changé à mesure que la fraction massique de CO_2 dans le secondaire augmentait. Le rapport d'entraînement, pourtant, augmentait de façon presque linéaire sur la plage expérimentale. Une amélioration de 23% dans l'entraînement par rapport à la vapeur pure s'est produite, lorsque le fluide secondaire contenait 42% CO_2 par masse. Ce comportement est en contraste net avec celui d'un éjecteur de vapeur pure, où une augmentation du rapport d'entraînement se fait au détriment d'une diminution dans la pression critique de l'éjecteur.

Deux publications de revue scientifique ont évalué divers scénarios quant à l'intégration d'un éjecteur à vapeur dans un procédé de captage postcombustion basé sur l'absorption/désorption chimique. Les deux études ont supposé les mêmes spécifications des gaz d'échappement d'une centrale thermique de charbon. Le solvant de référence choisi a été la monoéthanolamine (MEA) de 20% par masse, et la cible de taux de captage de CO_2 était de 85%. Les écoulements de CO_2, pauvre et riche, ont été fixés respectivement à 0.15 et à

0.45 kmol CO_2/kmol MEA. Trois configurations principales ont été étudiées, selon le choix de l'écoulement liquide servant à produire la vapeur secondaire de l'éjecteur : éjecteur sur condensat, éjecteur sur pauvre ou éjecteur sur riche.

Le premier article a focalisé sur le procédé de désorption et a présenté une méthode raccourcie basée sur les données vapeur/liquide à l'équilibre. Il a été déterminé que la position optimale du point d'injection de la vapeur est à la base du désorbeur. Les simulations ont montré une réduction dans la quantité d'énergie de haute qualité de 10 à 25%. Ces réductions sont pour les cas où le réservoir de détente est alimenté par le condensat ou le courant faible, correspondant respectivement à des charges de CO_2 de 0 et 0.15 kmol CO_2/kmol MEA. Il a été démontré que l'alimentation du réservoir de détente par le courant riche (charge de CO_2 de 0.45 kmol CO_2/kmol MEA) n'est pas une option viable.

Le deuxième article s'est servi d'un simulateur de procédé commercial, Aspen Plus, et d'un module cinétique *rate-base* plus réaliste afin d'évaluer des configurations semblables à celles de la première publication. Une étude faisant partie de l'article comparait deux façons de préchauffer le courant de la vapeur primaire : soit par les rejets thermiques, soit par l'intégration de la chaleur. Les simulations basées sur le module cinétique ont montré une réduction de la quantité d'énergie de haute qualité de 10 à 14%, où les cas «éjecteur sur condensat» et «éjecteur sur faible» sont encore avantageux.

En somme, l'incorporation de la technologie des éjecteurs dans un système de captage postcombustion de carbone peut réduire la quantité d'énergie de haute qualité nécessaire à régénérer le solvant. Spécifiquement, cette thèse démontre le potentiel d'amélioration énergétique de la combinaison stratégique des éléments suivants : l'utilisation d'un éjecteur monophasique ; un procédé de captage postcombustion de carbone basé sur l'absorption/désorption ; la revalorisation des rejets thermiques, externes au procédé de captage. En résumé, des rejets thermiques, revalorisés au moyen des éjecteurs, peuvent servir à remplacer partiellement de la vapeur de turbine à coût élevé, qui serait autrement prise de la centrale thermique pour générer de l'électricité. Cette conclusion principale est le résultat de trois études détaillées de simulation et est appuyée par un programme d'expérimentation effectué sur un banc d'essai conçu pour ce projet.

APPENDIX A. Instrumentation calibration

All of the resistance temperature detectors (RTDs) used on the APCCO2 test bench were calibrated to conform with the European standard DIN 1/10. This standard requires that the temperature uncertainty should be less than +/- 1/10*(0.3+0.005*t) °C, where t is the temperature measured in Celsius. For example, at 100 °C the uncertainty is +/- 0.08 °C, while at 130 °C the uncertainty is 0.095 °C. An in-house calibration procedure was completed to assure that each specific RTD and its associated acquisition circuit respect the DIN 1/10 standard over the target temperature range. Fig. A.1 shows the final calibration curve for RTD TE006, used to measure the secondary fluid temperature.

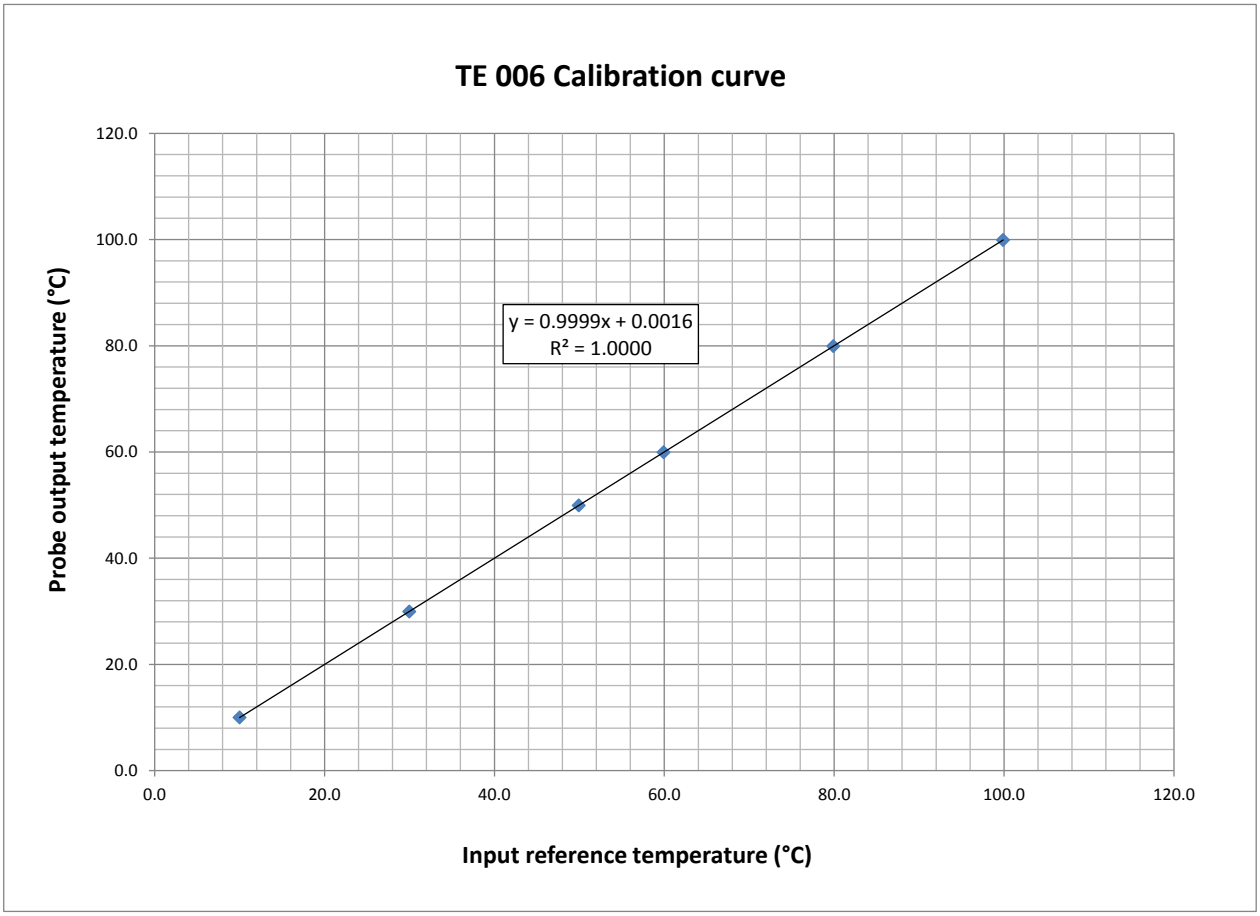

Fig. A.1 Typical in-house RTD calibration curve

Pressure sensors were supplied with a calibration certificate for at least one of sensors for each pressure range. Fig. A.2 shows a typical certificate for a 0-10 bar (150 psia) pressure sensor. In this case the relative uncertainty for measured pressures of 0.16, 5.1 and 10.2 bar was -0.0064, -0.0087 and -0.0005% respectively.

The flow sensors were also supplied with supplier calibration certificates in most cases. Fig. A.3, Fig. A.4 and Fig. A.5 show the three pages of the calibration certificate applicable both to flow meters GF001 and FT001 in Table 3.2. In this case the relative uncertainty at 30, 45 and 75% of the requested flow range was 0.51, 0.05 and -0.56 %. The flow meter was tested with saturated steam, which is noted in Fig. A.5

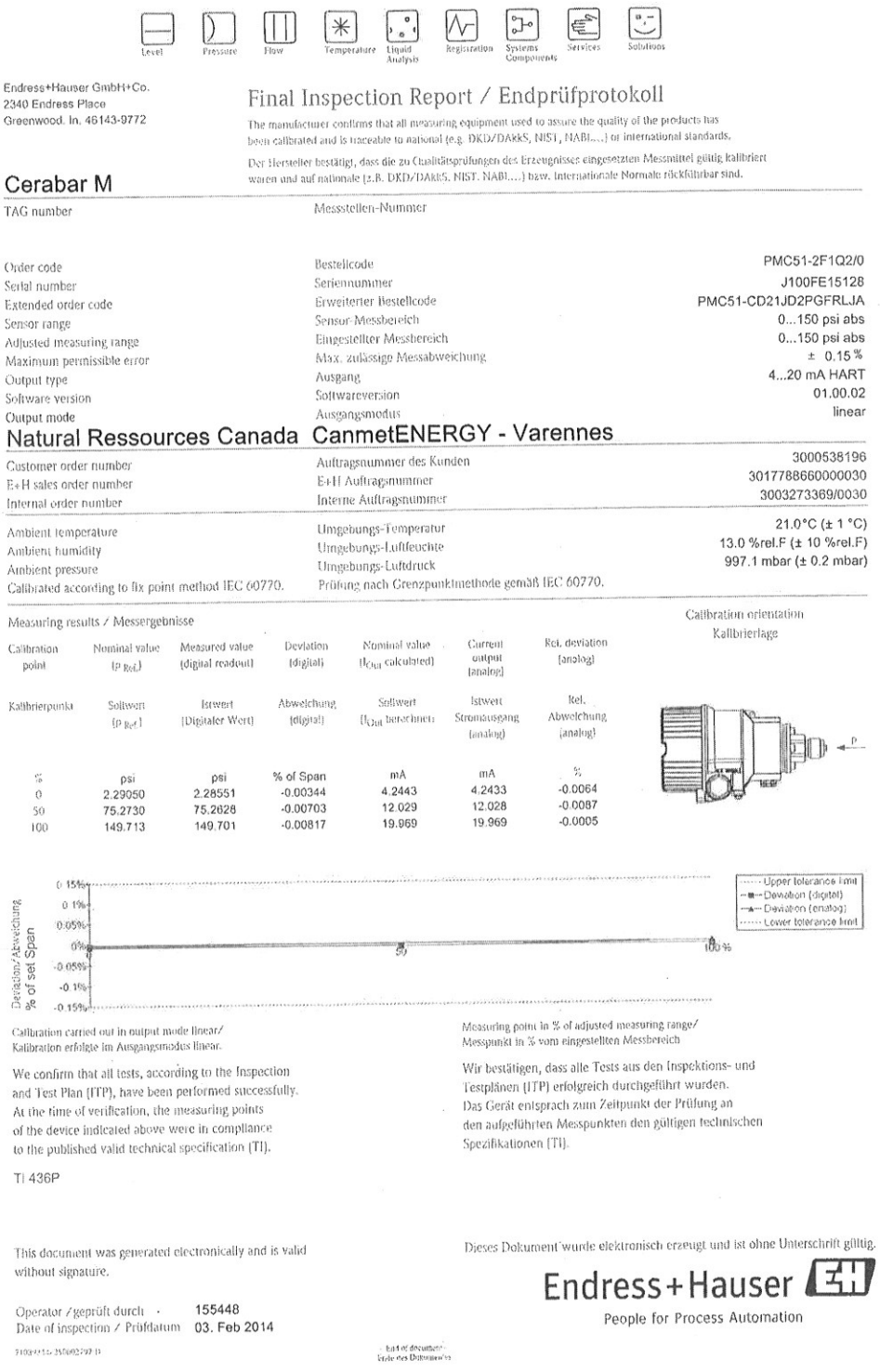
Level Pressure Flow Temperature Liquid Analysis Registration Systems Components Services Solutions

Endress+Hauser GmbH+Co.
2340 Endress Place
Greenwood, In, 46143-9772

Final Inspection Report / Endprüfprotokoll

The manufacturer confirms that all measuring equipment used to assure the quality of the products has been calibrated and is traceable to national (e.g. DKD/DAkkS, NIST, NABI,...) or international standards.

Der Hersteller bestätigt, dass die zu Qualitätsprüfungen des Erzeugnisses eingesetzten Messmittel gültig kalibriert waren und auf nationale (z.B. DKD/DAkkS, NIST, NABI,...) bzw. internationale Normale rückführbar sind.

Cerabar M

TAG number	Messstellen-Nummer	
Order code	Bestellcode	PMC51-2F1Q2/0
Serial number	Seriennummer	J100FE15128
Extended order code	Erweiterter Bestellcode	PMC51-CD21JD2PGFRLJA
Sensor range	Sensor-Messbereich	0...150 psi abs
Adjusted measuring range	Eingestellter Messbereich	0...150 psi abs
Maximum permissible error	Max. zulässige Messabweichung	± 0.15 %
Output type	Ausgang	4...20 mA HART
Software version	Softwareversion	01.00.02
Output mode	Ausgangsmodus	linear

Natural Ressources Canada CanmetENERGY - Varennes

Customer order number	Auftragsnummer des Kunden	3000538196
E+H sales order number	E+H Auftragsnummer	3017788660000030
Internal order number	Interne Auftragsnummer	3003273369/0030
Ambient temperature	Umgebungs-Temperatur	21.0°C (± 1 °C)
Ambient humidity	Umgebungs-Luftfeuchte	13.0 %rel.F (± 10 %rel.F)
Ambient pressure	Umgebungs-Luftdruck	997.1 mbar (± 0.2 mbar)
Calibrated according to fix point method IEC 60770.	Prüfung nach Grenzpunktmethode gemäß IEC 60770.	

Measuring results / Messergebnisse

Calibration orientation
Kalibrierlage

Calibration point	Nominal value ($p_{Ref.}$)	Measured value (digital readout)	Deviation (digital)	Nominal value (I_{Out} calculated)	Current output (analog)	Rel. deviation (analog)
Kalibrierpunkt	Sollwert ($p_{Ref.}$)	Istwert (Digitaler Wert)	Abweichung (digital)	Sollwert (I_{Out} berechnet)	Istwert Stromausgang (analog)	Rel. Abweichung (analog)
%	psi	psi	% of Span	mA	mA	%
0	2.29050	2.28551	-0.00344	4.2443	4.2433	-0.0064
50	75.2730	75.2628	-0.00703	12.029	12.028	-0.0087
100	149.713	149.701	-0.00817	19.969	19.969	-0.0005

Calibration carried out in output mode linear/
Kalibration erfolgte im Ausgangsmodus linear.

Measuring point in % of adjusted measuring range/
Messpunkt in % vom eingestellten Messbereich

We confirm that all tests, according to the Inspection and Test Plan (ITP), have been performed successfully. At the time of verification, the measuring points of the device indicated above were in compliance to the published valid technical specification (TI).

Wir bestätigen, dass alle Tests aus den Inspektions- und Testplänen (ITP) erfolgreich durchgeführt wurden. Das Gerät entsprach zum Zeitpunkt der Prüfung an den aufgeführten Messpunkten den gültigen technischen Spezifikationen (TI).

TI 436P

This document was generated electronically and is valid without signature.

Dieses Dokument wurde elektronisch erzeugt und ist ohne Unterschrift gültig.

Operator / geprüft durch · 155448
Date of inspection / Prüfdatum 03. Feb 2014

Endress+Hauser
People for Process Automation

End of document
Ende des Dokuments

Fig. A.2 Typical supplier pressure sensor calibration certificate

FE 002

Endress+Hauser

People for Process Automation

Flow Calibration with Adjustment

30223007-2711371

3003250628 Purchase order number	FCP-6.F Calibration rig
CA-3004784666-10 / Endress+Hauser Flowtec Order N°/Manufacturer	21.64712 us.gal/min (≙ 100%) Calibrated full scale
73F15-SK4AA5NAB4AW Order code	Service interface Calibrated output
PROWIRL 73 F 1/2" Transmitter/Sensor	371.76 Imp./dm³ Calibration factor
F10A0316000 Serial N°	79.8 °F Water temperature
– Tag N°	

Flow [%]	Flow [us.gal/min]	Duration [s]	V target [us.gal]	V meas. [us.gal]	Δ o.r.* [%]	Outp.** [mA]
30.4	6.58	50.2	5.5027	5.5305	0.51	8.89
45.1	9.76	35.2	5.7243	5.7272	0.05	11.22
75.5	16.3	30.2	8.2228	8.1770	-0.56	16.01
–	–	–	–	–	–	–
–	–	–	–	–	–	–
–	–	–	–	–	–	–
–	–	–	–	–	–	–
–	–	–	–	–	–	–
–	–	–	–	–	–	–
–	–	–	–	–	–	–

*o.r.: of rate

**Calculated value (4 - 20 mA)

Measured error % o.r.

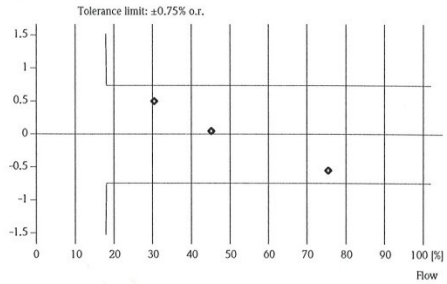

For detailed data concerning output specifications of the unit under test, see Technical Information (TI), chapter Performance characteristics.

The calibration is traceable to the N.I.S.T. through standards certified at preset intervals.

Endress+Hauser Flowtec operates ISO/IEC 17025 accredited calibration facilities in Reinach (CH), Cernay (FR), Greenwood (USA), Aurangabad (IN) and Suzhou (CN).

Leonard D. McGee

01-27-2012
Date of calibration

Endress+Hauser Flowtec, Division USA
2330 Endress Place
Greenwood, IN 46143

Leonard McGee
Operator

Certified acc. to
ISO 9001, Reg.-N° 030502.2
ISO 14001, Reg.-N° EMS561046

Page 1 / 1

Fig. A.3 Typical supplier flow meter calibration certificate, page 1 of 3

Endress+Hauser

People for Process Automation

Parameter Setting

30185690-2711371

3003250628	PROWIRL 73 F
Purchase order number	Transmitter/Sensor
3004784666-10 / Endress+Hauser Flowtec	1/2"
Order N°/Manufacturer	Nominal diameter
73F15-SK4AA5NAB4AW	–
Order code	Tag N°
F10A0316000	
Serial N°	

The below parameters are set according to your order.
Please refer to the Operating Manual for any parameters not mentioned.

Device software	V1.06.00
Communication type	HART
Device revision	Dev.6/DD.1 [ID 57(hex)]
Meter body type (MB)	310
Device address	0
Tag name	———
Tag description	———————
Units	
Unit volume flow	cu.ft/min
Unit mass flow	lb/min
Unit corrected volume flow	Sm^3/hr
Unit heat flow	kBtu/min
Unit density	lb/ft^3
Unit of length	Inch
Unit temperature	°F
Unit pressure	psi a

01-27-2012
Date

Endress+Hauser Flowtec, Division USA
2330 Endress Place
Greenwood, IN 46143

Fig. A.4 Typical supplier flow meter calibration certificate, page 2 of 3

Endress+Hauser
People for Process Automation

Parameter Setting

30185690-2711371

Totalizer	
Assign totalizer 1	Calculated mass flow
Unit volume totalizer 1	us.gal
Unit mass totalizer 1	lb
Unit corrected volume totalizer 1	Sm^3
Unit heat totalizer 1	kBtu
Assign totalizer 2	Heat flow
Unit volume totalizer 2	us.gal
Unit mass totalizer 2	lb
Unit corrected volume totalizer 2	Sm^3
Unit heat totalizer 2	kBtu
User interface	
Language	English
Assign line 1	Calculated mass flow
Assign line 2	Totalizer 1
Process parameters	
Fluid	Saturated steam
Operating pressure	145 psi a
Ambient pressure	14.5038 psi a
Error pressure	145.038 psi a
Reference pressure	14.6923 psi a
Error temperature	167 °F
Error temperature value	68 °F
Reference temperature	32 °F
Saturated steam calculation method	Temperature
Current output 1	
Assign current output	Calculated mass flow
Value 0/4 mA	0 lb/min
Value 20 mA	5 lb/min
Current span	4-20 mA HART US
Failsafe mode	Maximum current
Time constant	5 s

01-27-2012
Date

Endress+Hauser Flowtec, Division USA
2330 Endress Place
Greenwood, IN 46143

Fig. A.5 Typical supplier flow meter calibration certificate, page 3 of 3

LIST OF REFERENCES

[1] Abanades, J. C., Arias, B., Lyngfelt, A., Mattisson, T., Wiley, D. E., Li, H., Ho, M. T., Mangano, E. and Brandani, S. (2015). Emerging CO_2 capture systems. *International Journal of Greenhouse Gas Control,* volume 40, p. 126-66.

[2] Abdulateef, J. M., Sopian, K., Alghoul, M. A. and Sulaiman, M. Y. (2008). Review on solar-driven ejector refrigeration technologies. *Renewable and Sustainable Energy Reviews,* volume 13, number 6-7, p. 1338-1349.

[3] Aidoun, Z. and Ouzzane, M. (2004). The effect of operating conditions on the performance of a supersonic ejector for refrigeration. *International Journal of Refrigeration,* volume 27, number 8, p. 974-984.

[4] Alexis, G. K. and Rogdakis, E. D. (2002). Performance characteristics of two combined ejector-absorption cycles. *Applied Thermal Engineering,* volume 22, number 1, p. 97-106.

[5] Alexis, G. K. and Rogdakis, E. D. (2002). Performance of solar driven methanol-water combined ejector-absorption cycle in the Athens area. *Renewable Energy,* volume 25, number 2, p. 249-66.

[6] Alie, C., Backham, L., Croiset, E. and Douglas, P. L. (2005). Simulation of CO_2 capture using MEA scrubbing: A flowsheet decomposition method. *Energy Conversion and Management,* volume 46, number 3, p. 475-487.

[7] Ameur, K., Aidoun, Z. and Ouzzane, M. (2016). Modeling and numerical approach for the design and operation of two-phase ejectors. *Applied Thermal Engineering,* volume 109, p. 809-818.

[8] Bartosiewicz, Y., Aidoun, Z. and Mercadier, Y. (2006). Numerical assessment of ejector operation for refrigeration applications based on CFD. *Applied Thermal Engineering,* volume 26, number 5-6, p. 604-612.

[9] Bartosiewicz, Y., Aidoun, Z., Desevaux, P. and Mercadier, Y. (2005). Numerical and experimental investigations on supersonic ejectors. *International Journal of Heat and Fluid Flow,* volume 26, number 1, p. 56-70.

[10] Bergander, M. J. (2006). Refrigeration cycle with two-phase condensing ejector. In *11th International Refrigeration and Air Conditioning Conference at Purdue,* West Lafayette, IN, USA.

[11] Bernstein, L., Bosch, P., Canziani, O., Chen, Z., Christ, R., Davidson, O., Hare, W., Huq, S., Karoly, D. and Kattsov, V. (2007). *IPCC, 2007: climate change 2007: synthesis report. Contribution of working groups I* (Intergovernmental Panel on Climate Change (IPCC)). IPCC, Geneva, Switzerland.

[12] Bilir, N. and Ersoy, H. K. (2009). Performance improvement of the vapour compression refrigeration cycle by a two-phase constant area ejector. *International Journal of Energy Research,* volume 33, number 5, p. 469-480.

[13] Bravo, J. L., Rocha, J. A. and Fair, J. R. (1985). Mass transfer in gauze packings. *Hydrocarbon Processing,* volume 64, number 1, p. 91-95.

[14] Cardemil, J. M. and Colle, S. (2012). A general model for evaluation of vapor ejectors performance for application in refrigeration. *Energy Conversion and Management,* volume 64, p. 79-86.

[15] Chaiwongsa, P. and Wongwises, S. (2007). Effect of throat diameters of the ejector on the performance of the refrigeration cycle using a two-phase ejector as an expansion device. *International Journal of Refrigeration,* volume 30, number 4, p. 601-608.

[16] Chen, W., Liu, M., Chong, D., Yan, J., Little, A. B. and Bartosiewicz, Y. (2013). A 1D model to predict ejector performance at critical and sub-critical operational regimes. *International Journal of Refrigeration,* volume 36, number 6, p. 1750-1761.

[17] Chilton, T. H. and Colburn, A. P. (1934). Mass transfer (absorption) coefficients prediction from data on heat transfer and fluid friction. *Industrial & Engineering Chemistry,* volume 26, number 11, p. 1183-1187.

[18] Chunnanond,K., Aphornratana,S. (2004). Ejectors: Applications in refrigeration technology. *Renewable and Sustainable Energy Reviews,* volume 8, number 2, p. 129-155.

[19] Chunnanond, K. and Aphornratana, S. (2004). An experimental investigation of a steam ejector refrigerator: The analysis of the pressure profile along the ejector. *Applied Thermal Engineering,* volume 24, number 2-3, p. 311-322.

[20] Ciferno, J. P., DiPietro, P. and Tarka, T. (2005). An economic scoping study for CO_2 capture using aqueous ammonia. *Final Report, National Energy Technology Laboratory, US Department of Energy,* Pittsburgh, PA, USA.

[21] Cizungu, K., Groll, M. and Ling, Z. G. (2005). Modelling and optimization of two-phase ejectors for cooling systems. *Applied Thermal Engineering,* volume 25, number 13, p. 1979-1994.

[22] Croquer, S., Poncet, S. and Aidoun, Z. (2016). Turbulence modeling of a single-phase R134a supersonic ejector. Part 1: Numerical benchmark. *International Journal of Refrigeration,* volume 61, p. 140-152.

[23] Dahmani, A., Aidoun, Z. and Galanis, N. (2011). Optimum design of ejector refrigeration systems with environmentally benign fluids. *International Journal of Thermal Sciences,* volume 50, number 8, p. 1562-1572.

[24] DeFrate, L. and Hoerl, A. (1959). Optimum design of ejectors using digital computers. In *Chemical Engineering Progress Symposium Series,* , volume 55p. 43-51.

[25] Deng, J., Jiang, P., Lu, T. and Lu, W. (2007). Particular characteristics of transcritical CO_2 refrigeration cycle with an ejector. *Applied Thermal Engineering,* volume 27, number 2-3, p. 381-388.

[26] Duan, L., Zhao, M. and Yang, Y. (2012). Integration and optimization study on the coal-fired power plant with CO_2 capture using MEA. *Energy,* volume 45, number 1, p. 107-116.

[27] Eames, I. W., Aphornratana, S. and Haider, H. (1995). Theoretical and experimental study of a small-scale steam jet refrigerator. *International Journal of Refrigeration,* volume 18, number 6, p. 378-386.

[28] Elakhdar, M., Nehdi, E., Kairouani, L. and Tounsi, N. (2011). Simulation of an ejector used in refrigeration systems. *International Journal of Refrigeration,* volume 34, number 7, p. 1657-1667.

[29] Elbel, S. and Hrnjak, P. (2008). Experimental validation of a prototype ejector designed to reduce throttling losses encountered in transcritical R744 system operation. *International Journal of Refrigeration,* volume 31, number 3, p. 411-22.

[30] Elbel, S. (2011). Historical and present developments of ejector refrigeration systems with emphasis on transcritical carbon dioxide air-conditioning. *International Journal of Refrigeration,* volume 34, number 7, p. 1545-1561.

[31] El-Dessouky, H., Ettouney, H., Alatiqi, I. and Al-Nuwaibit, G. (2002). Evaluation of steam jet ejectors. *Chemical Engineering and Processing,* volume 41, number 6, p. 551-561.

[32] Galanis, N. and Sorin, M. (2016). Ejector design and performance prediction. *International Journal of Thermal Sciences,* volume 104, p. 315-329.

[33] Gaspar, J. and Cormos, A. (2012). Dynamic modeling and absorption capacity assessment of CO_2 capture process. *International Journal of Greenhouse Gas Control,* volume 8, p. 45-55.

[34] Harrell, G. S. and Kornhauser, A. A. (1995). Performance tests of a two phase ejector. In *Proceedings of 30th Intersociety Energy Conversion Engineering Conference,* , volume 3. ASME, New York, NY, USA, p. 49-53.

[35] He, S., Li, Y. and Wang, R. Z. (2009). Progress of mathematical modeling on ejectors. *Renewable and Sustainable Energy Reviews,* volume 13, number 8, p. 1760-1780.

[36] Hildbrand, C., Dind, P., Pons, M. and Buchter, F. (2004). A new solar powered adsorption refrigerator with high performance. *Solar Energy,* volume 77, number 3, p. 311-18.

[37] Holton, W. (1951). Effect of molecular weight of entrained fluid on the performance of steam-jet ejectors. *Transactions of the American Society of Mechanical Engineers,* volume 73, p. 905-910.

[38] Huang, B. J., Chang, J. M., Wang, C. P. and Petrenko, V. A. (1999). 1-D analysis of ejector performance. *International Journal of Refrigeration,* volume 22, number 5, p. 354-364.

[39] Idem, R., Tontiwachwuthikul, P., Gelowitz, D. and Wilson, M. (2011). Latest research on fundamental studies of CO_2 capture process technologies at the International Test Centre for CO_2 capture. *Energy Procedia,* volume 4, p. 1707-1712.

[40] Jassim, M. S. and Rochelle, G. T. (2006). Innovative absorber/stripper configurations for CO_2 capture by aqueous monoethanolamine. *Industrial & Engineering Chemistry Research,* volume 45, number 8, p. 2465-2472.

[41] Kairouani, L., Elakhdar, M., Nehdi, E. and Bouaziz, N. (2009). Use of ejectors in a multi-evaporator refrigeration system for performance enhancement. *International Journal of Refrigeration,* volume 32, number 6, p. 1173-1185.

[42] Keenan, J. H., Neumann, E. P. and Lustwerk, F. (1950). An Investigation of Ejector Design by Analysis and Experiment. *Americal Society of Mechanical Engineers Journal of Applied Mechanics,* number 72, p. 299-309.

[43] Keenan, J. and Neumann, E. (1942). A simple air ejector. *ASME Journal of Applied Mechanics,* volume 9, number 2, p. A75-A81.

[44] Khennich, M., Galanis, N. and Sorin, M. (2016). Effects of design conditions and irreversibilities on the dimensions of ejectors in refrigeration systems. *Applied Energy,* volume 179, p. 1020-1031.

[45] Kohl, A. and Nielsen, R. (1997). *Gas Purification*, 5 edition. Gulf Publishing Company, Houston, TX, USA, 1395 p.

[46] Kornhauser, A. A. (1990). The use of an ejector as a refrigerant expander. In *Proceedings of the 1990 USNC/IIR-Purdue Refrigeration Conference,* West Lafayette, IN, USA, p. 10-19.

[47] Kornhauser, A. A. (1990). The use of an ejector in a geothermal flash system. In *Proceedings of the 25th Intersociety Energy Conversion Engineering Conference, .* AIChE, New York, NY, USA, p. 79-84.

[48] Kothandaraman, A., Nord, L., Bolland, O., Herzog, H. J. and McRae, G. J. (2009). Comparison of solvents for post-combustion capture of CO_2 by chemical absorption. *Energy Procedia,* volume 1, number 1, p. 1373-1380.

[49] Lawal, A., Wang, M., Stephenson, P. and Obi, O. (2012). Demonstrating full-scale post-combustion CO_2 capture for coal-fired power plants through dynamic modelling and simulation. *Fuel,* volume 101, p. 115-128.

[50] Lawrence, N. and Elbel, S. (2012). Experimental and analytical investigation of automotive ejector air-conditioning cycles using low-pressure refrigerants. In *14th International Refrigeration and Air Conditioning Conference at Purdue,* West Lafayette, IN, USA.

[51] Leites, I. L., Sama, D. A. and Lior, N. (2003). The theory and practice of energy saving in the chemical industry: some methods for reducing thermodynamic irreversibility in chemical technology processes. *Energy,* volume 28, number 1, p. 55-97.

[52] Léonard, G. (2013). *Optimal design of a CO_2 capture unit with assessment of solvent degradation.* Doctoral thesis, Université de Liège, Liège, Belgique.

[53] Liang, Z., Fu, K., Idem, R. and Tontiwachwuthikul, P. (2016). Review on current advances, future challenges and consideration issues for post-combustion CO_2 capture using amine-based absorbents. *Chinese Journal of Chemical Engineering,* volume 24, number 2, p. 278-288.

[54] Liang, Z., Rongwong, W., Liu, H., Fu, K., Gao, H., Cao, F., Zhang, R., Sema, T., Henni, A., Sumon, K., Nath, D., Gelowitz, D., Srisang, W., Saiwan, C., Benamor, A., Al-Marri, M., Shi, H., Supap, T., Chan, C., Zhou, Q., Abu-Zahra, M., Wilson, M., Olson, W., Idem, R. and Tontiwachwuthikul, P. (2015). Recent progress and new developments in post-combustion carbon-capture technology with amine based solvents. *International Journal of Greenhouse Gas Control,* volume 40, p. 26-54.

[55] Lin, C., Cai, W., Li, Y., Yan, J. and Hu, Y. (2012). The characteristics of pressure recovery in an adjustable ejector multi-evaporator refrigeration system. *Energy,* volume 46, number 1, p. 148-155.

[56] Liu, F. and Groll, E. A. (2013). Study of ejector efficiencies in refrigeration cycles. *Applied Thermal Engineering,* volume 52, number 2, p. 360-370.

[57] Liu, F., Groll, E. A. and Li, D. (2012). Investigation on performance of variable geometry ejectors for CO_2 refrigeration cycles. *Energy,* volume 45, number 1, p. 829-839.

[58] Liu, F., Groll, E. A. and Li, D. (2012). Modeling study of an ejector expansion residential CO_2 air conditioning system. *Energy and Buildings,* volume 53, p. 127-136.

[59] Lu, F., Feng, X., Zhang, G., Tian, Y. and Xi, H. (2001). Optimization of the ejector flashing regeneration in Benfield carbon dioxide removal system. *Journal of Chemical Engineering of Japan,* volume 34, number 9, p. 1153-1158.

[60] Lucia, A., Roy, A. and Sorin, M. (2010). Energy efficient synthesis and design for carbon capture. In de Haan, A. B., Kooijman, H. and Gorak, A., *Distillation Absorption 2010, The 9th Distillation and Absoption Conference,* Eindhoven, The Netherlands.

[61] Martel, S. (janvier 2013). *Étude numérique d'un écoulement diphasique critique dans un convergent-divergent.* Thèse de doctorat, Université de Sherbrooke, Sherbrooke, Québec, Canada.

[62] Marynowski, T. (septembre 2007). *Étude expérimentale et numérique d'écoulements supersoniques en éjecteur avec et sans condensation.* Thèse de doctorat, Université de Sherbrooke, Sherbrooke, Québec, Canada.

[63] Menegay, P. and Kornhauser, A. A. (1996). Improvements to the ejector expansion refrigeration cycle. In *Proceedings of the 31st Intersociety Energy Conversion Engineering Conference,* . IECEC 96, volume 2. IEEE, New York, NY, USA, p. 702-6.

[64] Metz, B. (2005). *International Panel on Climate Change (IPCC). IPCC special report on carbon dioxide and storage.* (International Panel on Climate Change (IPCC)). Cambridge University Press, New York, NY.

[65] Meyer, A. J., Harms, T. M. and Dobson, R. T. (2009). Steam jet ejector cooling powered by waste or solar heat. *Renewable Energy,* volume 34, number 1, p. 297-306.

[66] Mores, P., Rodriguez, N., Scenna, N. and Mussati, S. (2012). CO_2 capture in power plants: Minimization of the investment and operating cost of the post-combustion process using MEA aqueous solution. *International Journal of Greenhouse Gas Control,* volume 10, p. 148-163.

[67] Mores, P., Scenna, N. and Mussati, S. (2012). CO_2 capture using monoethanolamine (MEA) aqueous solution: Modeling and optimization of the solvent regeneration and CO_2 desorption process. *Energy,* volume 45, number 1, p. 1042-1058.

[68] Munday, J. T. and Bagster, D. F. (1977). New ejector theory applied to steam jet refrigeration. *Industrial & Engineering Chemistry, Process Design and Development,* volume 16, number 4, p. 429-436.

[69] Nagy, T. and Mizsey, P. (2015). Model verification and analysis of the CO_2-MEA absorber-desorber system. *International Journal of Greenhouse Gas Control,* volume 39, p. 236-44.

[70] Nahdi, E., Champoussin, J., Hostache, G. and Chéron, J. (1993). Les paramètres géométriques optima d'un éjecto-compresseur frigorifique. *International Journal of Refrigeration,* volume 16, number 1, p. 67-72.

[71] Nehdi, E., Kairouani, L. and Bouzaina, M. (2007). Performance analysis of the vapour compression cycle using ejector as an expander. *International Journal of Energy Research,* volume 31, number 4, p. 364-375.

[72] Notz, R., Mangalapally, H. P. and Hasse, H. (2012). Post combustion CO_2 capture by reactive absorption: Pilot plant description and results of systematic studies with MEA. *International Journal of Greenhouse Gas Control,* volume 6, p. 84-112.

[73] Notz, R., Tonnies, I., Mangalapally, H. P., Hoch, S. and Hasse, H. (2011). A short-cut method for assessing absorbents for post-combustion carbon dioxide capture. *International Journal of Greenhouse Gas Control,* volume 5, number 3, p. 413-421.

[74] Ohashi, Y., Ogawa, T. and Egami, N. (2011). Development of carbon dioxide removal system from the flue gas of coal fired power plant. *Energy Procedia,* volume 4, p. 29-34.

[75] Oi, L. E. (2010). CO_2 removal by absorption: challenges in modelling. *Mathematical and Computer Modelling of Dynamical Systems,* volume 16, number 6, p. 511-533.

[76] Oi, L. E. (2007). Aspen HYSYS simulation of CO_2 removal by amine absorption from a gas based power plant. In *SIMS2007, The 48th Scandinavian Conference on Simulation and Modeling ,* Linköping, Sweden, p. 73-81.

[77] Olajire, A. A. (2010). CO_2 capture and separation technologies for end-of-pipe applications - A review. *Energy,* volume 35, number 6, p. 2610-2628.

[78] Onda, K., Takeuchi, H. and Okumoto, Y. (1968). Mass transfer coefficients between gas and liquid phases in packed columns. *Journal of Chemical Engineering of Japan,* volume 1, number 1, p. 56-62.

[79] Ouzzane, M. and Aidoun, Z. (2003). Model development and numerical procedure for detailed ejector analysis and design. *Applied Thermal Engineering,* volume 23, number 18, p. 2337-2351.

[80] Oyenekan, B. A. and Rochelle, G. T. (2007). Alternative stripper configurations for CO_2 capture by aqueous amines. *American Institute of Chemical Engineers Journal,* volume 53, number 12, p. 3144-3154.

[81] P.R.Arachchige, U. S. and Melaaen, M. C. (2012). Aspen Plus Simulation of CO_2 Removal from Coal and Gas Fired Power Plants. *Energy Procedia,* volume 23, number 0, p. 391-399.

[82] Pellegrini, G., Strube, R. and Manfrida, G. (2010). Comparative study of chemical absorbents in postcombustion CO_2 capture. *Energy,* volume 35, number 2, p. 851-7.

[83] Petrenko, V. O., Huang, B. J. and Ierin, V. O. (2011). Design-theoretical study of cascade CO_2 sub-critical mechanical compression/butane ejector cooling cycle. *International Journal of Refrigeration,* volume 34, number 7, p. 1649-1656.

[84] Petrenko, V. O. and Volovyk, O. S. (2011). Theoretical study and design of a low-grade heat-driven pilot ejector refrigeration machine operating with butane and isobutane and intended for cooling of gas transported in a gas-main pipeline. *International Journal of Refrigeration,* volume 34, number 7, p. 1699-1706.

[85] Plus, A. (2008). Rate Based model of the CO_2 capture process by MEA using Aspen Plus. *Aspen Technology Inc, Cambridge,* MA, USA.

[86] Power, R. B. (1994). *Steam jet ejectors for the process industries*. McGraw-Hill Inc., New York, NY, USA, 500 p.

[87] Power, R. B. (1994). Predicting unstable-mode performance of a steam jet ejector. *American Society of Mechanical Engineers, The Fluid Power and Systems Technology Division (Publication) FPST,* volume 1, p. 11-15.

[88] Raynal, L., Bouillon, P., Gomez, A. and Broutin, P. (2011). From MEA to demixing solvents and future steps, a roadmap for lowering the cost of post-combustion carbon capture. *Chemical Engineering Journal,* volume 171, number 3, p. 742-752.

[89] Reddick, C., Li, C., Sorin, M. and Sapoundjiev, H. (2014). Lowering the Energy Cost of Carbon Dioxide Capture using Ejectors for Waste Heat Upgrading. *Energy Procedia,* volume 63, p. 715-726.

[90] Reddick, C., Mercadier, Y. and Ouzzane, M. (2012). Experimental study of an ejector refrigeration system. In *14th International Refrigeration and Air Conditioning Conference at Purdue,* West Lafayette, IN, USA.

[91] Reddick, C., Sorin, M. and Rheault, F. (2014). Energy savings in CO_2 (carbon dioxide) capture using ejectors for waste heat upgrading. *Energy,* volume 65, p. 200-208.

[92] Reddick, C., Sorin, M., Sapoundjiev, H. and Aidoun, Z. (2016). Carbon capture simulation using ejectors for waste heat upgrading. *Energy,* volume 100, p. 251-261.

[93] Rochelle, G. T. (2009). Amine scrubbing for CO_2 capture. *Science,* volume 325, number 5948, p. 1652-1654.

[94] Rubin, E. S., Mantripragada, H., Marks, A., Versteeg, P. and Kitchin, J. (2012). The outlook for improved carbon capture technology. *Progress in Energy and Combustion Science,* volume 38, number 5, p. 630-671.

[95] Sag, N. B. and Ersoy, H. K. (2016). Experimental investigation on motive nozzle throat diameter for an ejector expansion refrigeration system. *Energy Conversion and Management,* volume 124, p. 1-12.

[96] Samake, O., Galanis, N. and Sorin, M. (2016). On the design and corresponding performance of steam jet ejectors. *Desalination,* volume 381, p. 15-25.

[97] Sarkar, J. (2010). Geometric parameter optimization of ejector-expansion refrigeration cycle with natural refrigerants. *International Journal of Energy Research,* volume 34, number 1, p. 84-94.

[98] Sarkar, J. (2008). Optimization of ejector-expansion transcritical CO_2 heat pump cycle. *Energy,* volume 33, number 9, p. 1399-406.

[99] Sarkar, J. (2012). Ejector enhanced vapor compression refrigeration and heat pump systems - A review. *Renewable and Sustainable Energy Reviews,* volume 16, number 9, p. 6647-6659.

[100] Sarunac, N., Romero, C. E. and Liebowitz, B. (2011). Use of waste heat and CO_2 compression heat to reduce penalty due to post-combustion CO_2 capture. In *28th Annual International Pittsburgh Coal Conference 2011,* , volume 3, Pittsburgh, PA, USA, p. 2082-2095.

[101] Schefflan, R. *Teach yourself the basics of Aspen Plus*. John Wiley & Sons, Hoboken, New Jersey, USA, 216 p.

[102] Scott, D., Aidoun, Z. and Ouzzane, M. (2011). An experimental investigation of an ejector for validating numerical simulations. *International Journal of Refrigeration,* volume 34, number 7, p. 1717-1723.

[103] Selvaraju, A. and Mani, A. (2004). Analysis of a vapour ejector refrigeration system with environment friendly refrigerants. *International Journal of Thermal Sciences,* volume 43, number 9, p. 915-921.

[104] Semenova, T. A. and Leites, I. L. (1977). *Purification of industrial gases*, 2 edition. Chimia, Moscow, 487 p.

[105] Shepherd, D. G. (1956). *Principles of turbomachinery*. Macmillan, New York, NY, USA, 463 p.

[106] Sirwan, R., Alghoul, M. A., Sopian, K. and Ali, Y. (2013). Thermodynamic analysis of an ejector-flash tank-absorption cooling system. *Applied Thermal Engineering,* volume 58, number 1-2, p. 85-97.

[107] Stichlmair, J., Bravo, J. and Fair, J. (1989). General model for prediction of pressure drop and capacity of countercurrent gas/liquid packed columns. *Gas Separation & Purification,* volume 3, number 1, p. 19-28.

[108] Sumeru, K., Nasution, H. and Ani, F. N. (2012). A review on two-phase ejector as an expansion device in vapor compression refrigeration cycle. *Renewable and Sustainable Energy Reviews,* volume 16, number 7, p. 4927-4937.

[109] Taylor, R., Krishna, R. and Kooijman, H. (2003). Real-world modeling of distillation. *Chemical Engineering Progress,* volume 99, number 7, p. 28-39.

[110] Tukowicz, H. and Kochaniewicz, A. (2013). Analysis of the use of waste heat in the turbine regeneration system of a 900 MW supercritical coal-fired power unit. *Energetyka,* number 11, p. 790-4.

[111] Van Ham, J., Reeve, D. (2008). *CCTRM, Canada's clean coal technology roadmap, CETC, CANMET Energy Technology Centre (www.cleancoaltrm.gc.ca).*

[112] Van Wagener, D. H. and Rochelle, G. T. (2011). Stripper configurations for CO_2 capture by aqueous monoethanolamine. *Chemical Engineering Research & Design,* volume 89, number 9, p. 1639-46.

[113] Varga, S., Oliveira, A. C. and Diaconu, B. (2009). Influence of geometrical factors on steam ejector performance: a numerical assessment. *International Journal of Refrigeration,* volume 32, number 7, p. 1694-701.

[114] Varga, S., Oliveira, A. C., Ma, X., Omer, S. A., Zhang, W. and Riffat, S. B. (2011). Experimental and numerical analysis of a variable area ratio steam ejector. *International Journal of Refrigeration,* volume 34, number 7, p. 1668-75.

[115] Whitman, W. G. (1923). A preliminary experimental confirmation of the two-film theory of gas absorption. *Chemical and Metallurgical Engineering,* volume 29, number 4, p. 146-148.

[116] Work, L. T. and Haedrich, V. W. (1939). Performance of Ejectors as a Function of the Molecular Weights of Vapors. *Industrial & Engineering Chemistry,* volume 31, number 4, p. 464-477.

[117] Xu, G., Huang, S., Yang, Y., Wu, Y., Zhang, K. and Xu, C. (2013). Techno-economic analysis and optimization of the heat recovery of utility boiler flue gas. *Applied Energy,* volume 112, p. 907-17.

[118] Yokoyama, K., Takamoto, S., Kikkawa, H., Katsube, T., Nakamoto, T., Oda, N., Kawasaki, T., Sugiura, T., Wu, S., Eswaran, S., Schreier, W., Heberle, A. and Pavlish, B. (2011). Hitachi's carbon dioxide scrubbing technology with new absorbent for coal fired power plants. *Energy Procedia,* volume 4, p. 245-252.

[119] Yokoyama, T. (2012). Analysis of reboiler heat duty in MEA process for CO_2 capture using equilibrium-staged model. *Separation and Purification Technology,* volume 94, p. 97-103.

[120] Yu, Y. S., Li, Y., Li, Q., Jiang, J. and Zhang, Z. X. (2009). An innovative process for simultaneous removal of CO_2 and SO_2 from flue gas of a power plant by energy integration. *Energy Conversion and Management,* volume 50, number 12, p. 2885-2892.

[121] Zhang, K., Liu, Z., Wang, Y., Li, Y., Li, Q., Zhang, J. and Liu, H. (2014). Flash evaporation and thermal vapor compression aided energy saving CO_2 capture systems in coal-fired power plant. *Energy,* volume 66, p. 556-568.

[122] Zhang, K., Liu, Z., Huang, S. and Li, Y. (2015). Process integration analysis and improved options for an MEA CO_2 capture system based on the pinch analysis. *Applied Thermal Engineering,* volume 85, p. 214-24.

[123] Zhang, K., Shen, S., Yang, Y. and Tian, X. (2012). Experimental investigation of adjustable ejector performance. *Journal of Energy Engineering,* volume 138, number 3, p. 125-129.

[124] Zhang, Y., Chen, H., Chen, C., Plaza, J. M., Dugas, R. and Rochelle, G. T. (2009). Rate-based process modeling study of CO_2 Capture with aqueous monoethanolamine solution. *Industrial and Engineering Chemistry Research,* volume 48, number 20, p. 9233-9246.

[125] Zhu, Y. and Li, Y. (2009). Novel ejector model for performance evaluation on both dry and wet vapors ejectors. *International Journal of Refrigeration,* volume 32, number 1, p. 21-31.

[126] Ziad, H. (2014). *Ejector optimization in absorption based CO_2 capture process.* Master of Engineering Design, Université de Sherbrooke, Sherbrooke, Québec, Canada.